TOUGHENING OF CARBON FIBER-REINFORCED EPOXY POLYMER COMPOSITES VIA COPOLYMERS AND GRAPHENE NANO-PLATELETS

By

Markus A. Downey

A DISSERTATION

Submitted to
Michigan State University
in partial fulfillment of the requirements
for the degree of

Chemical Engineering - Doctor of Philosophy

2016

ABSTRACT

TOUGHENING OF CARBON FIBER-REINFORCED EPOXY POLYMER COMPOSITES VIA COPOLYMERS AND GRAPHENE NANO-PLATELETS

By

Markus A. Downey

Carbon fiber-reinforced epoxy composites currently play a significant role in many different industries. Due to their high cross-link density, aromatic epoxy polymers used as the matrix in composite materials are very strong and stiff however they lack toughness. This dissertation investigates three areas of the carbon fiber-reinforced composite, which have the potential to increase toughness: the carbon fiber surface; the fiber/matrix interphase; and the matrix material. Approaches to improving each area are presented which lead to enhancing the overall composite toughness without reducing other composite mechanical properties.

The toughening of the base matrix material, DGEBA/mPDA, was accomplished by two methods: first, using low concentrations of aliphatic copolymers to enhance energy absorption and second by adding graphene nano-platelets (GnP) to act as crack deflection agents. 1wt% copolymer concentration was determined to substantially increase the notched Izod impact strength without reducing other static-mechanical properties. Toughening of DGEBA/mPDA using 3wt% GnP was found to be dependent on the aspect ratio of GnP and treatment of GnP with tetraethylenepentamine (TEPA). GnP C750 enhanced flexural properties but not fracture toughness because the small aspect ratio cannot effectively deflect cracks. TEPA-grafting enhanced GnP/matrix bonding. Larger aspect ratio GnP M5 and M25 showed significant increases in fracture toughness due to better crack deflection but also decreased flexural strength based on

limited GnP/matrix bonding. TEPA-grafting mitigated some of the flexural strength reductions for GnP M5, due to enhanced GnP/matrix adhesion.

In the high-fiber volume fraction composite, the fiber/matrix bonding was enhanced with UV-ozone surface treatment by reducing a weak fiber surface boundary layer and increasing the concentration of reactive oxygen groups on the fiber surface. Further increases in Mode I fracture toughness were seen with the addition of an epoxy fiber sizing: aromatic epoxy increased the modulus and aliphatic epoxy increase the shear-strain to failure and toughness at the fiber/matrix interphase. All improvements were made without reducing other static-mechanical properties.

Combining the above surface treatments with a 1wt% aliphatically toughened matrix increase Mode I fracture toughness without reducing other static-mechanical properties. The fracture toughness enhancement was more pronounced in composites with low fiber/matrix adhesion. Due to reduced diffusion of the aliphatic epoxy away from the fiber surface with the addition of 1wt% aliphatic to the matrix, leading to a more compliant interphase, the aliphatic fiber sizing composite showed reductions in flexural properties and Mode I fracture toughness.

The addition of GnP M5 to the aromatic fiber sizing enhanced the Mode I fracture toughness substantially by defecting cracks away from the fiber/matrix interphase. All flexural properties were similar with heat-treated GnP and better with TEPA-grafted GnP. Aliphatic fiber sizing with TEPA-grafted GnP reduced flexural properties with no change in fracture toughness by an enrichment of aliphatic epoxy at the fiber surface leading to a more compliant interphase.

Dedicated to my parent, my sister, my niece, and my nephew

ACKNOWLEDGEMENTS

Even though earning a PhD is very much an individual effort, there are many people I need to express my deepest gratitude to. Without you, I would have not made it through this phase of my life's journey.

I am indebted to my advisor, Dr Lawrence Drzal, who took me into his research group and allowed me to learn from his vast knowledge. For allowing me to forge my own direction in the work that I did but was always available to guide me in uncertain times.

Thanks to my dissertation committee Dr Mahmoodul Haq, Dr K. Jayaraman, and Dr Alfred Loos for their willingness to test and guide me.

The CMSC staff, who were instrumental in my education and development: Per Askeland, Ed Drown, Brian Rook, and Mike Rich. The CMSC would be a poorer place to work without each of your every individual personalities and contributions.

Many thanks to GE Aviation, who financially supported my doctoral studies. Thanks to Greg Gemeinhardt for his guidance and support over the years.

My lab mates who were present in an ever changing surrounding: Pat, Dee, Yan, Keith, Nick, Zhang, and Mariana. Some have already moved on and can call themselves Doctor while others will follow later. I have been fortunate to meet and work with so many interesting and talented individuals.

To Carolyn, Daniel, Jake, and Keith, without whom I would have probably not made it through my first semester, go my deep thanks for the support in those trying time.

And last but defiantly not least my heart-felt thanks go to my family, my parents Sabine and William and my sister Rebecca: you have been there to encourage me throughout the years. I always knew I could count on your support and love.

TABLE OF CONTENTS

LIST OF TABLES

LIST OF FIGURES

Chapter 1: Introduction

1.1 Project Background

Already widely used in the aerospace in industry, composite materials represent a path to reducing weight and increasing fuel efficiency. Starting in the 1970's composite materials were introduced to secondary structures in commercial aircraft. [1] Modern jet liners such as the Boeing 787 and Airbus A350XWB are made of up to 50% composite materials. [2]

Looking at a wider industry, the growing number of vehicles on the road today have also put a strain the environment, triggering new emissions legislation. The US EPA CAFÉ standards mandate a fleet average fuel consumption of 54.5 miles per gallon by the year 2025. [3] With many engine efficiency and aerodynamic improvements already implemented and only marginal efficiency gains expected, manufacturers are turning to weight reduction strategies, known as lightweighting. Many different materials are being used for lightweighting, including alloys of aluminum, magnesium, advanced steel, and fiber reinforced polymer composites. The used of fiber reinforced composite materials, while traditionally used in the high-performance vehicle market, are also being introduced into the large volume vehicle market. While still produced at moderate volumes of close to 30,000 vehicles in 2015, the BMW i3 and i8 are good examples of application of substantial amounts of carbon fiber, as the chassis of both vehicle is made of carbon fiber-reinforced polymer composite. [4] Major efforts are currently being undertaken to reduce the production cost of fiber-reinforced composites in order to make them more available to the large-volume market. Currently

the sales volume of composite materials is projected to be around $90 billion by the year 2020, [5] making this a very lucrative market.

1.2 Composite Material Classification

A composite is a material composed of two or more constituents that remain separate and distinct after production and give the resulting material properties that cannot be attained by the individual components. [6] Wood is an example of nature making a composite material with cellulosic fibrils as the reinforcing fiber and hemicellulose and lignin as the matrix material. [7] Based on this definition, many different kinds of composite materials exist, with most composites consisting of two constituents that are the matrix and the reinforcing phase. They can be classified by their matrix material and the nature of the reinforcement. Schemes of classifying composite materials by the nature of their matrix is shown in Figure 1.1 and by reinforcing constituent is shown in Figure 1.2:

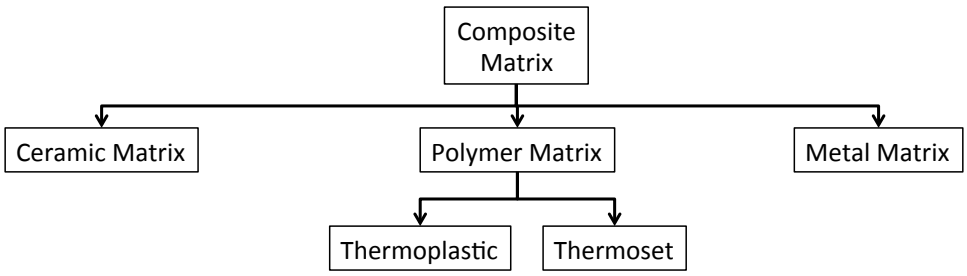

Figure 1.1: Classification of composite materials based on matrix [8]

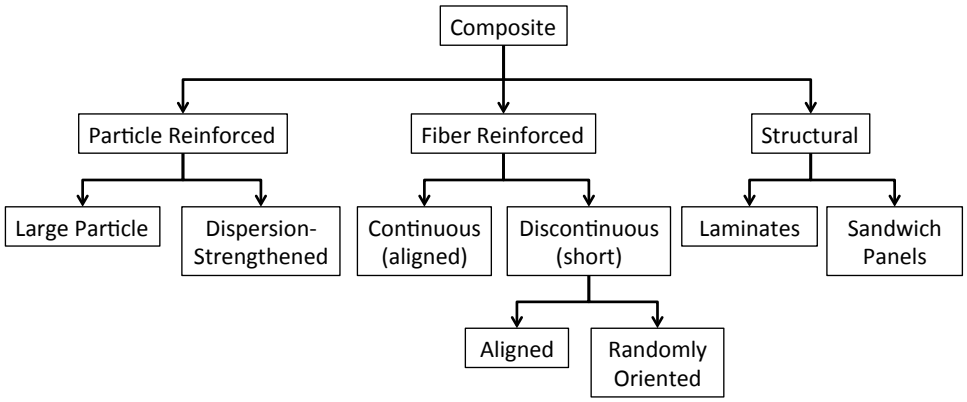

Figure 1.2: Classification of composite materials based on reinforcement [6]

As shown in Figure 1.1, the composite matrix can be divided into polymer, metal, and ceramic materials. Metal and ceramic matrix composites are used in high temperature and high wear applications. Polymer composites that will be the focus of this dissertation have the largest penetration of different markets and applications. For polymer matrix composites, there can be a further distinction of thermoplastic and thermosetting polymers. For high-performance structural applications, thermosetting polymers are largely the matrix of choice based on their high stiffness and strength as well as flexibility in manufacturing techniques.

Figure 1.2 shows the different confirmations that the reinforcing phase can take on. Particle reinforced composites use solid particles, such as clay, aluminum oxide, dispersed throughout the matrix as reinforcing agents. Large particle reinforcement refers to particle/matrix interactions that are not on the molecular level. Concrete is an example of large particle reinforced composite. In dispersion-strengthened composites, the size range of the reinforcing phase is in the tens of nanometers and strengthening happens on the molecular level, as in metal alloys. Structural composites are subdivided into laminates and sandwich panels. Laminates combine layers having directions of high strength. Varying the orientation of the layers yields a composite with

good strength in many directions, as in plywood. Sandwich panels usually consist of outer layers such as aluminum laminated to a honeycomb core to provide reduced weight combined with rigidity.

Fiber reinforced composites can further be classified as continuous and discontinuous fiber composites. In discontinuous fiber composites, the reinforcing fibers are relatively short compared to the dimensions of the composite and do not span the whole length or width of the composite part. The fibers in a discontinuous fiber composite can be either oriented or distributed randomly. The processing of the composite, where extrusion or additive manufacturing processes will lead to a higher degree of orientation, mainly influences the distribution of the fibers. Since the reinforcing effect is not as strong as with a continuous fiber, discontinuous fiber composites are used mainly in non-structural applications. However, the advantage is that recycled fibers can be used.

Structural application of composites requires the use of continuous reinforcing fibers, where the fibers run the length and width of the composite part. Since each composite layer is very strong along the axis of the fiber (longitudinal) and significantly weaker across the fiber direction (transverse), the layers are arranged in well-defined orientations to tailor the properties to the application requirements. [9]

The research discussed in this dissertation will relate to thermosetting polymer matrix composites with continuous carbon-based reinforcing fibers.

1.3 Carbon Fiber-Reinforced Polymer Composites

Carbon fiber-reinforced polymer (CFRP) composites are an important material for high-performance structural applications. CFRP composites are broadly speaking made of three different components as shown in the schematic example of a unidirectional CFRP composite in Figure 1.3:

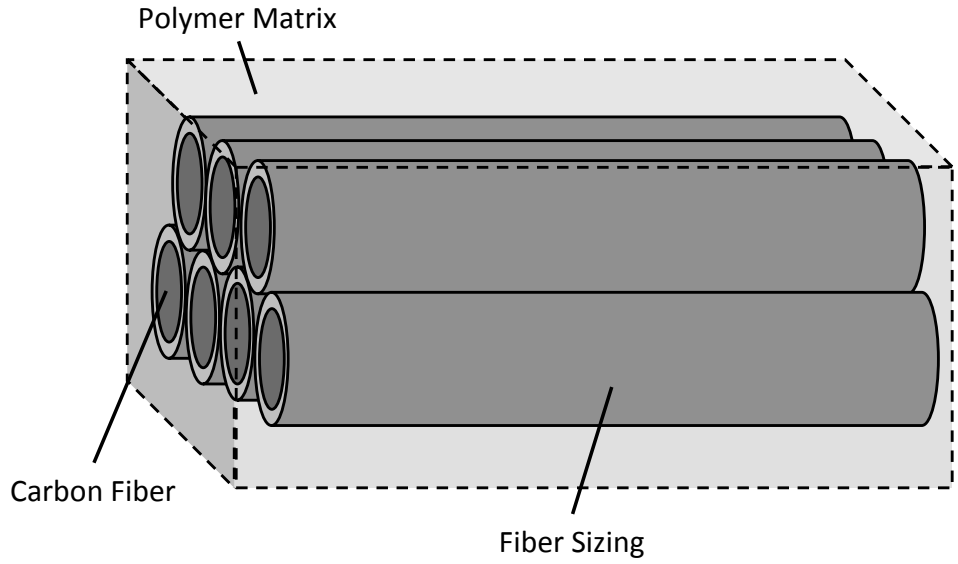

Figure 1.3: Components of a carbon fiber-reinforced composite

The first component is the reinforcing carbon fibers with a fiber diameter around 7μm. The fibers are the load-bearing component of the composite, having high strength and stiffness. The second component is the polymer matrix. The matrix serves several functions including keeping the fibers together, transferring the load between fibers and giving the part its final shape. The third and final component is the fiber surface treatment and fiber sizing. The fiber sizing is a very thin coating (50-100nm) applied to the fiber surface. For carbon fibers this sizing is often an epoxy but could consist of other components as well. The area where the fiber and matrix join, referred to as the fiber/matrix interphase, is a frequently overlooked part of the composite that has

significant importance to composite toughness since it directly affects the bonding between the fiber and the matrix. Since everything is more than the sum of its parts, a strong fiber and a tough matrix alone are not sufficient if they are not strongly bonded. Good fiber/matrix adhesion is needed to yield a tough composite. [10] Engineering the fiber/matrix interphase by improving the fiber/matrix adhesion can have a profound effect on composite toughness, a materials ability to absorb energy prior to fracture. [6]

The previous paragraph listed several areas in the composite that can be optimized to enhance overall toughness. The largest issue is the brittle nature of the epoxy matrix. [11], [12] Without a natural crack retention mechanism, any crack formed in the epoxy material will propagate without impediment. After discussing the mechanism underlying the formation of the highly cross-linked epoxy-amine network, several toughening approaches will be discussed in the following chapters.

1.4 Epoxy-Amine Reaction

Epoxy-based polymers have a long history and a very wide field of applications. [13] Named for the reactive epoxy group, epoxies can have one or more reactive epoxy groups on each molecule. Di- and higher functional epoxies have the ability to form large, highly cross-linked networks since each polymer molecule can form two or more bonds. With an amine-based curing agent, each amine group has two hydrogen atoms that can potentially react with an epoxy group via an addition reaction, giving each amine group the ability to react with two epoxy groups. The nucleophilic attack of the primary amine happens at the less steric hindered methylene group, resulting the conversion of the epoxide oxygen into a hydroxyl group. This hydroxyl group has been

reported to function as a catalyst, making the epoxy/amine reaction auto-catalytic. [14] The primary amine converts into a secondary amine during this reaction. [15]-[18] A second nucleophilic attack of an epoxy group is possible by the secondary amine but due to steric hindrance and reductions in molecular mobility due to cross-link formation, the reaction of a secondary amine is usually slower. The third possible reaction is an etherification reaction of an epoxy group with the hydroxyl group, which is considered to happen predominantly at elevated temperatures or in the presence of a catalyst. [19], [20] The schematic of the three reaction pathways is shown in Figure 1.4 [15]:

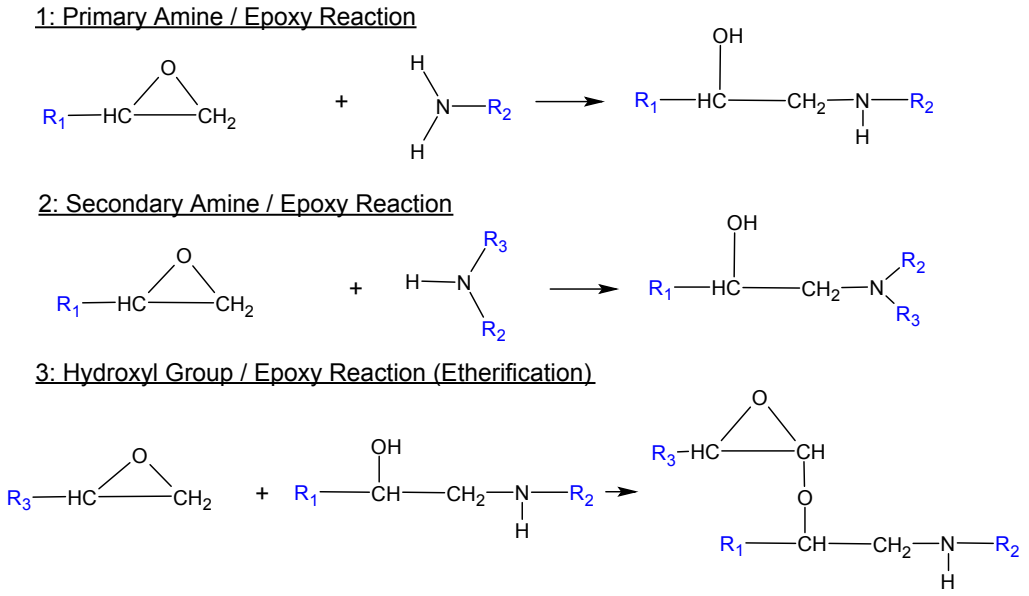

Figure 1.4: Reaction pathways in epoxy/amine system

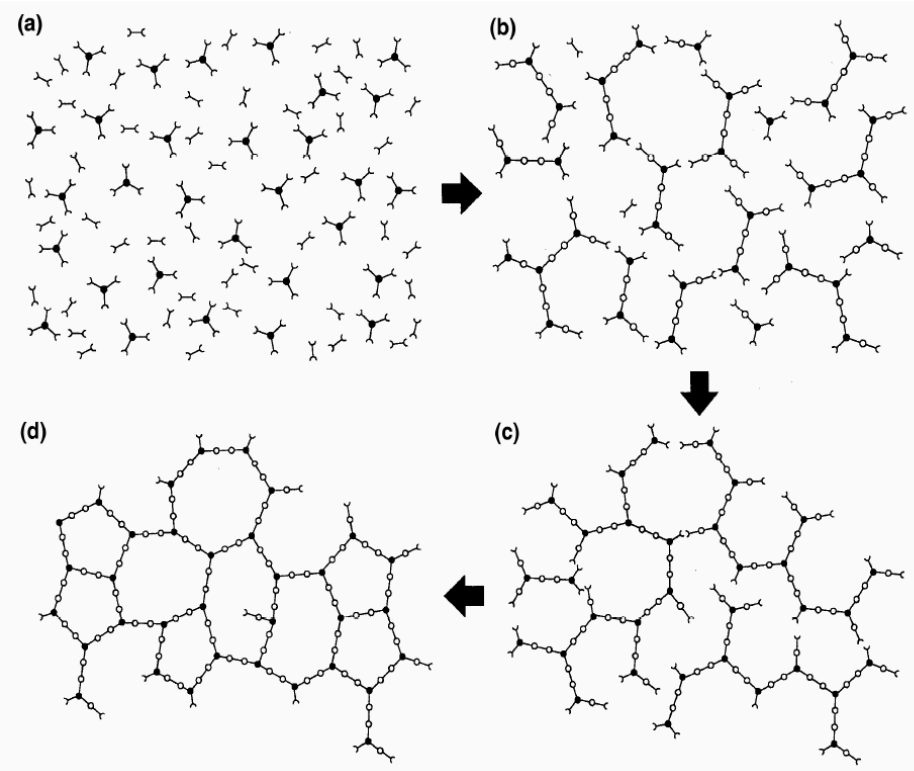

Figure 1.5: Stages of thermoset curing. (a): Uncured epoxy monomers and curing agent (A-stage), (b): formation and growth of linear polymer chains and branching below gel point (B-stage), (c) gelation and incomplete network formation, (d) fully cured network (C-stage) [21]

While higher molecular weight epoxies may be solid, many epoxy monomers are liquids at room temperature. This makes their handling and processing fairly straightforward. During initial curing the epoxy/amine system will form linear as well as branching molecules. As the curing continues to advance, the molecular weight of the molecules will increase until several chains become linked together and the system changes from a liquid to a rubbery state, called the gelation. [21]-[23] Above the gel point, the epoxy network looses its ability to flow. As curing further proceeds, the system will further cross-link and transition from a rubbery to a glassy state.

As mentioned above, the epoxy nomenclature comes from the reactive groups on the polymer molecule. Another parameter that will significantly affect the mechanical

properties of the cured epoxy is the molecular chain that connects the epoxy groups. The bulk and flexibility of the molecular chain is going influence the modulus and strength of the resulting material. One of the most studied di-functional epoxies is the diglycidyl ether of bisphenol A (DGEBA) has an aromatic backbone containing bulky benzene rings. The cured epoxy polymer exhibits high strength and stiffness but is also a brittle material with limited toughness. Energy absorption within the cross-linked network comes from polymer chain movements and for DGEBA the bulky polymer chain makes chain motion difficult. By contrast, aliphatic epoxies have more linear, flexible aliphatic backbone that allow for more energy absorption. The flexibility of the aliphatic epoxy does not give it the same rigidity and stiffness of the aromatic epoxy. For samples of di-functional aromatic (DGEBA) and di-functional aliphatic (PDGE 380) epoxy cured under identical conditions, the aliphatic epoxy exhibits a notched Izod impact strength that is 19-fold higher than the aromatic epoxy. However, the flexural modulus and strength of the aliphatic epoxy is more than two orders of magnitude lower than the aromatic epoxy. The amount of aliphatic epoxy can be tailored to achieve the desired mechanical properties within the limits of reduction in other properties is acceptable.

Similarly, the curing agent that is used to cross-link the epoxy monomers will have a significant impact on the mechanical properties of the cured epoxy. Amine curing agents where discussed in Chapter 1.4 . Di- and higher functional amines are used to create a highly cross-linked epoxy network. The molecular chain that connects the amine groups, depending on if it is aromatic or aliphatic, will change the mechanical properties. An aliphatic amine curing agent will in general yield a cured epoxy with

higher toughness but lower static-mechanical properties than an epoxy cured with a comparable aromatic curing agent. [24] The use of amine-based curing agents is a common approach for toughening of epoxy polymers. One drawback to the use of amine-based curing agents is that the amount of curing agent needed to cure the epoxy is dictated by stoichiometry. Stoichiometry is the amount of curing agent needed to fully cure the epoxy and is based on the functionalities and molecular weights of the epoxy and amine molecules involved in the reaction. This fixes the amount of aliphatic amine used in the cured epoxy and its impact on the mechanical properties. In contrast, the use of aliphatic epoxies does not have this limitation.

1.5 Toughening of Epoxy Polymer Matrix Materials

Toughening of epoxy polymer matrix materials has been the subject of many publications. Surveying the literature, researchers have taken many different approaches to enhancing toughness. The brittle nature of epoxy polymers is due to their lack of crack propagation resistance. Metals have a natural crack retention mechanism in the grain boundaries that are present. A crack will quickly encounter a grain boundary that will slow or blunt its growth. [25] In an epoxy there is no such mechanism. Once a crack has formed, it will propagate through the epoxy material uninhibited. Two main approached can be taken when toughening the matrix material: First, the amount of energy that can be absorbed by the matrix prior to fracture can be increased; second, filler materials can be added to act as crack arresting agents.

In pursuit of the former, more flexible aliphatic epoxy copolymers, having the same functional epoxy groups can be used. These copolymers will undergo the same

reaction with the curing agent as the aromatic epoxy to form a highly cross-linked network. The main difference between the molecules is the flexibility of the chain segments between the functional groups. Aromatic epoxies, like diglycidyl ether of bisphenol A (DGEBA), have large, stiff backbone chains that contain large benzene rings. This gives them the desired stiffness properties. Aliphatic epoxies on the other hand have more flexible aliphatic backbone chains that allow for more chain movement. Traditionally used as viscosity reducers, di- and tri-functional aliphatic epoxies have also been investigated as toughening agents by several researchers. [26]-[28] While their findings will be discussed in more detail in Chapter 2, good improvements in toughness were achieved but at the expense of modulus and glass transition temperature.

Several different mechanisms of how micro and nano-scale particles toughen epoxies have been proposed in the literature. (Figure 1.6) [29] Three of the proposed mechanisms are considered more significant: particle bridging, where a particle spans both faces of the propagating crack, reducing the stress concentration at the crack tip, slowing crack propagation; second is crack pinning, where the filler particle acts as an obstacle to the crack. The crack is required to move around the particle, increasing the energy required for propagation. In crack deflection, the crack is forced to deviate out from its original plane of growth, decreasing the Mode I character and increasing the surface area and energy needed for propagation.

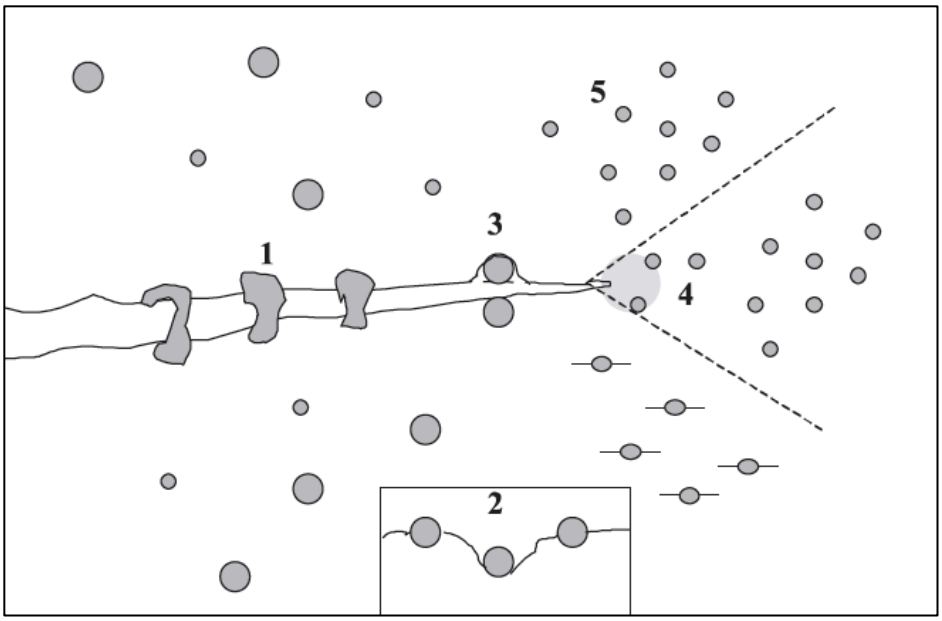

Figure 1.6: Proposed toughening mechanisms for thermoplastic-modified epoxies: (1) particle bridging, (2) crack pinning, (3) crack path deflection, (4) particle yielding-induced shear banding, (5) particle yielding (figure from [30], adapted from [29])

The use of nano-scale fillers is that they can enhance material properties at low filler loadings. (< 0.3wt%) On a per volume basis, nano-fillers will have much larger surface area than fillers on the micro-scale. [31] Nano-scale fillers also allow for much finer dispersion of the filler in the matrix. Assuming a homogeneous distribution of the filler particles, a crack is much more likely to intersect a nano-filler particle. Three different cases are generally considered in filler-matrix interactions (Figure 1.7): immiscible, intercalated and exfoliated [32]-[34]:

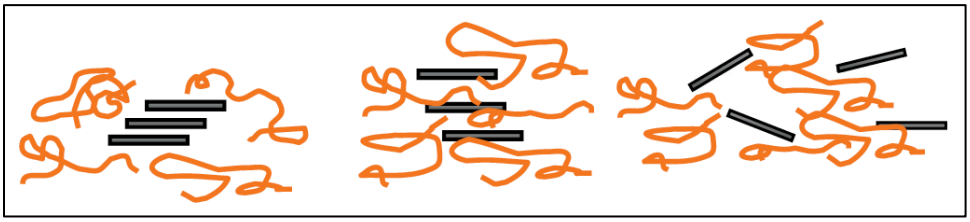
Figure 1.7: Different cases of filler particle-polymer matrix interactions: Immiscible (left), intercalated (center) and exfoliated (right) [32]

When the filler is immiscible, it is present in the matrix as agglomerations, without the any matrix material being present between the individual filler particles. While this is the natural state of most nano-filler materials, it is undesirable for the enhancement of mechanical properties. During intercalation some matrix material is present between the filler particles, forcing these to take on a greater distance between the particles. Agglomerations of filler particles can still exist in the intercalated state. In the exfoliated case, all the filler particles are separated and completely surrounded by matrix material. The exfoliated case is the ideal case for the dispersion of filler particles when looking at toughening. The exfoliated filler particles will be well distributed throughout the matrix and in intimate contact with the matrix material.

Elastomeric toughening and thermoplastic toughening and are two common approaches to enhance epoxy polymers. Copolymerization is another important route of toughening epoxy materials. The general goal is to form interpenetrated networks (IPNs), where both polymers form interweaved networks without being cross-linked. [35], [36]

In the first method, a rubber copolymer (usually butadiene acrylonitrile rubber) is functionalized at both ends of the chain with carboxyl, [37]-[39] hydroxyl [40], [41] or amine [11], [42] groups. The rubber is added to the epoxy resin as a liquid prior to curing, leading to a second network or phase being formed in a process known as phase separation during the curing process. [39] The particle size in this second phase has a profound impact on the improvement of the mechanical properties, with the best results being achieved when the particle size is on the nanometer scale. The concentration of rubber added, the curing time and schedule play paramount roles.

While providing improvements in the toughness of the epoxy, other mechanical properties such as the modulus (tensile and flexural) tend to decrease with this method, making their use in high-performance applications challenging.

The second class of copolymer used is thermoplastics, where a thermoplastic polymer is dispersed within the thermoset polymer, without being cross-linked into it. [43] The mechanism in thermoplastic toughening is the formation of interpenetrated networks as mentioned above. Similar to other nano-fillers, the particle size of thermoplastic particles in the epoxy matrix needs to be on the nano-scale. Good property enhancements have been reported with particle sizes in the range of 0.2 to 2 μm. A downside to thermoplastic toughening is the need for relatively high concentrations of thermoplastic co-polymer. Good enhancements of the mechanical properties have been reported, however these were achieved at concentrations of 30 to 50 phr of thermoplastic copolymer, far higher that those of other nano-scale filler materials as discussed above.

Nano-fillers can be roughly divided into two categories: inorganic and organic. The inorganic nano fillers include clays and alumina; organic are carbon based, including graphene and carbon nanotubes, which have garnered much of the current research effort in the past decade.

Nano-clays were the first nano-filler materials to be investigated in detail. In nano-clays, silicon atoms are in a tetrahedral arrangement, bonded between octahedral sheet of Al and/or Mg hydroxide to form sheets with a layer thickness of around 1nm. [44] While naturally existing in stacks of several layers, the ability of these nano-clays to form individual layers make them appealing for the use in nano composites. [32] Toyota

Research Labs published studies on a nano-composite consisting of nylon-6 and a clay filler material in 1992, showing improvements in tensile and flexural modulus and strength. [45], [46]

Alumina (Al2O3) nano-particles have been investigated as another inorganic nano-filler material. Mainly used as spherical particles they have a surface area around 100 m^2/g. [47] Strong Van de Waals forces lead to agglomerations of the alumina particles. Modification of epoxy polymers with alumina was seen to yield a considerable improvement in the stiffness and impact strength at low alumina concentrations. [48], [49] Surface modification, which yields a strong interface between filler and matrix, is needed for both silica and alumina nano-fillers to achieve the reported property improvements. [50]

Carbon based nano-fillers have garnered the bulk of the research interest for polymer toughening in the past decade. [51] Several allotropes of carbon used as toughening agents are shown in Figure 1.8:

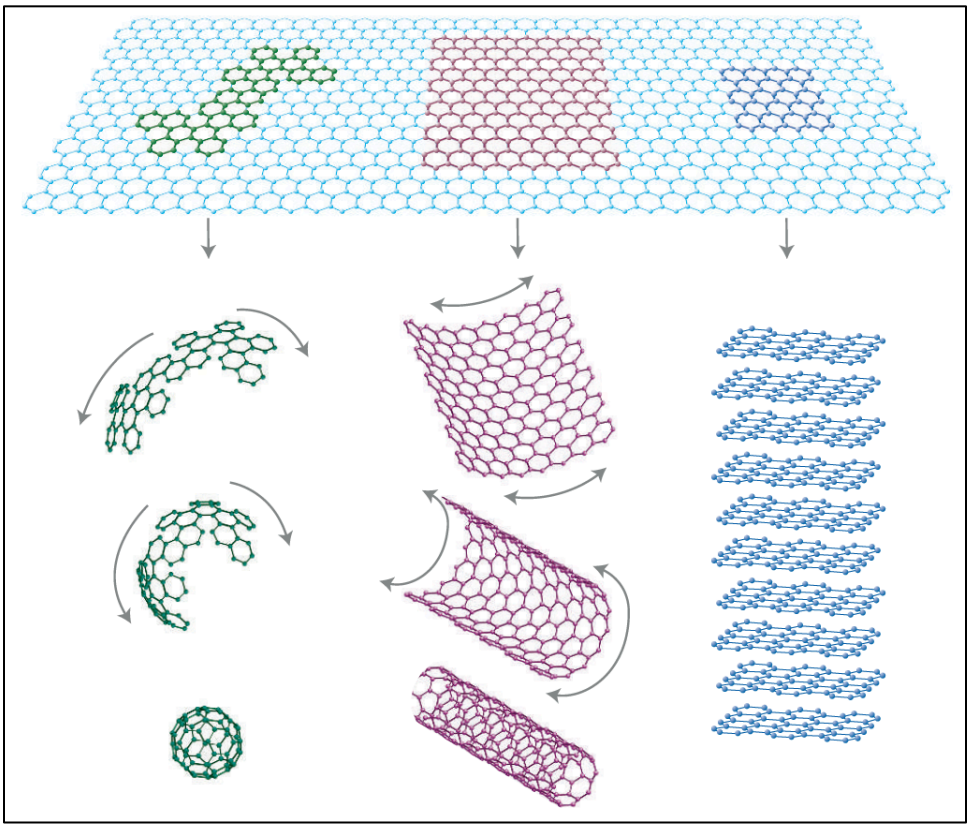

Figure 1.8: Different allotropes of carbon investigates as nano-fillers: Graphene (right), single-walled carbon nano tube (middle), Buckey ball C60 (left) [52]

Carbon nanotubes (CNTs), both single and multi-walled, have shown great potential for toughening polymer materials. [53], [54] CNT are in fact often used as a benchmark for other nano-filler materials. Single-walled CNT are a rolled-up sheet of single carbon atoms, where as multi-walled CNT consist several concentric single-walled tubes. CNT are considered a 1-dimensional filler material with tube lengths on the micron-scale and diameters on the nano-scale. Their aspect ratios, which are in the range of 1000 or more, makes it easy for CNT to toughen materials by crack bridging as discussed above. Their mechanical properties are quite impressive with tensile strength and tensile modulus in the gigapascal and terrapascal respectively. [55] While providing significant improvements in mechanical properties, the intricate production methods and

associated production cost of CNT require a critical assessment of their large scale application. [56]

Some research work in carbon nano-fillers has even investigated the used of fullerenes (C60) for toughening of polymers. [57] An increase in the tensile modulus without decreasing the tensile strength and a three-fold increase in fracture strength was found with filler loading in the range of 0.1 wt%. Similar issues of cost and manufacturing as with carbon nano tubes also apply to C60.

Graphene, which was first reported 2004 [58] and won the Noble Prize in physics a mere six years later [59], consists of a single layer of sp2-hybridized carbon atoms. In the single layer form, graphene has some of the highest mechanical properties ever measured for any material. [60] However in its single layer form, graphene is challenging to use based on production cost and processing. Graphene nanoplatelets (GnP) are stacks of graphene layers and is a material that can be commercially made at a reasonable cost compared to other carbon-based fillers like single-walled carbon nanotubes. [56], [61] The use of GnP is also beneficial on the basis of their platelet-type structure. This structure has two-dimensions (2D) on the micrometer scale with a third on the nanometer scale. The high aspect ratio of 2D nano-fillers occupy a large area and are superior at intersecting cracks compared to 1D nano-fillers such as carbon nano tubes. [62] Chong *et al.* recently showed that an increasing GnP aspect ratio increased the enhancement of fracture toughness of an epoxy polymer. [63] SEM micrographs of GnP M5, with a nominal platelet diameter of 5μm and a surface area of 120-150 m^2/g of surface area [64], are show in Figure 1.9. The platelet-like structure is clearly visible in these images:

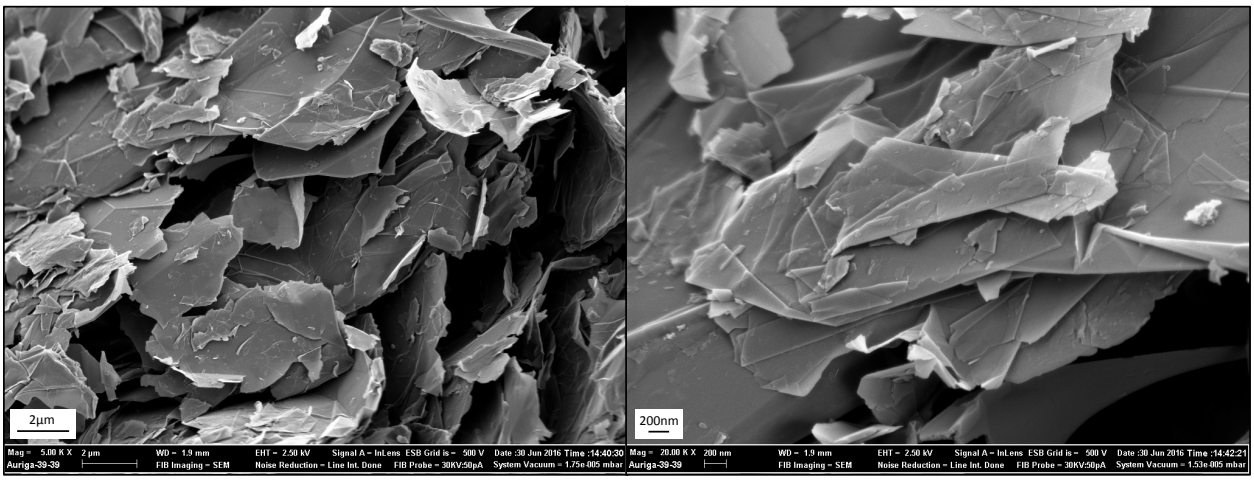

Figure 1.9: SEM micrographs of GnP M5 with 5µm nominal platelet diameter

A key aspect of enhancing the mechanical properties of a polymer using a nano-filler material is the compatibility and adhesion between the polymer matrix and the filler material. [38], [48], [49], [51], [65] Stresses applied to the polymer matrix by an external force can only be effectively transferred from the matrix to the filler material if these are in intimate contact and strongly bonded. [66] Weak bonding can make the filler materials act as voids and stress concentrators within the matrix and will lead to a reduction in the mechanical properties.

A common route to make the filler materials more compatible is functionalization, which involves the addition of functional groups to the surface of the filler particles. [65], [67] Most of these routes add aldehyde, carboxyl or amino groups, which are compatible with the epoxy matrix. In the case of the amino groups, the functional groups can take part in the cross-linking reaction during the cure of an epoxy. [67] Functionalization can occur either via non-covalent or covalent bonding. Non-covalent functionalization can occur via a number of different forces, including Van der Waals and π-π stacking interactions. [68] Pyrenes, which have large aromatic structures, are

an example of using π-π stacking for functionalization. A functional group is attached to the pyrene, whose π-orbitals interact with those on the basal plane of the GnP platelets. This has a two-fold effect: First, the pyrene attached to the GnP will impede the GnP platelets from re-agglomerating; second, the attached functional group will interact with the matrix, increasing compatibility of the GnP and can be cross-linked into the matrix. However, the non-covalent bonding forces are considered not to be as strong as those of covalent bonds.

Covalent functionalization involves covalently bonding of the functional groups. In the case of GnP, the functionalization can occur either on the basal plane or the platelet edge. A plethora of approaches have been studied. Many methods for covalent functionalization involve the intermediate step of producing graphene oxide (GO). Since GO is readily soluble in aqueous solutions, dispersion of GO is addressed. Functionalization and reduction back to graphene are subsequent steps. However, functionalization through GO has the issues of introducing defects into the graphene structure [69], potentially effecting the mechanical an electrical properties. Plasma induced covalent functionalization has been shown to add hydrogen, fluorine or chlorine atoms to the GnP and is appealing due to the simple processing. [70] Work by Ma *et al.* in covalent modification has grafted epoxy monomer molecules onto the surface of the GnP. [71] This will allow the GnP to be cross-linked directly into the matrix. Many of the covalent functionalization routes involve strong, harsh chemicals and very long, tedious processing. The scalability and cost-effectiveness of these routes need to be carefully examined, as they dictate the future use of the functionalization in any large-scale commercial applications

1.6 Problem Statement

The research work in this dissertation focuses on the toughening of carbon fiber-reinforced epoxy composites by engineering the fiber/matrix interphase and enhancing the matrix toughness. Copolymers and graphene nanoplatelets will be used for the for both fiber/matrix interphase and matrix. The increase in toughness should not be attained at the expense of other static-mechanical properties, such as flexural strength and modulus or glass transition temperature. Furthermore, it is desired to use commodity chemical and not to change the manufacturing process significantly, in order to keep the cost of applying these approaches as low as possible.

1.7 Dissertation Outline

This dissertation is divided up into five main research chapters that build on one another and provide a systematic look at composite toughening by engineering of the fiber/matrix interphase. Chapter 2 looks at the benefits of using low concentrations of aliphatic copolymers, both di- and tri-functional, to toughen aromatic epoxy without reducing static-mechanical properties. Chapter 3 looks at enhancing toughness of carbon fiber-reinforced epoxy composite by engineering the fiber/matrix interphase with fiber surface treatment and fibersizing with aromatic and aliphatic epoxy. Chapter 4 combines the lessons learned from chapters two and three by combining the engineered interphase with the approach using a low concentration of aliphatic copolymers to toughen the epoxy matrix. Chapter 5 discusses toughening of the epoxy matrix material with the dispersion of different grades of graphene nanoplatelets.

Improving the filler/matrix adhesion by grafting amine groups to the graphene nanoplatelets is also illuminated. Chapter 6 applies the toughening approach from Chapter 5 to the fibersizing of a carbon fiber-reinforced composite. The addition of graphene nanoplatelets to the interphase of the composite will toughen the composite as a whole.

BIBLIOGRAPHY

BIBLIOGRAPHY

[1] J. T. Quinlivan and H. R. Fenbert, “Composite Applications in Commercial Transport Aircraft,” *Polymers and Other Advanced Materials*, 1995.

[2] G. Marsh, “Airbus takes on Boeing with reinforced plastic A350 XWB,” *Reinforced Plastics*, vol. 51, no. 11, pp. 26–29, Dec. 2007.

[3] U. S. EPA, OAR, O. O. T. A. A. Quality, and A. A. S. Division, “EPA and NHTSA Set Standards to Reduce Greenhouse Gases and Improve Fuel Economy for Model Years 2017-2025 Cars and Light Trucks,” pp. 1–10, Aug. 2012.

[4] E. Begley, “BMW Group achieves fifth consecutive record sales year,” vol. 80788, no. 49. BMW Group Corporate Communications, Detroit/Munich, pp. 1–5, 11-Jan-2016.

[5] R. SALGARKAR, “Composites Market worth $ 90 Billion by 2020,” *Markets And Markets*, 20-Mar-2015. [Online]. Available: http://www.marketsandmarkets.com/PressReleases/composite.asp. [Accessed: 16-Apr-2016].

[6] W. Callister, *Materials Science and Engineering An Introduction*, 4 ed. New York: John Wiley & Sons, Inc., 1997.

[7] D. H. Page, “A note on the cell-wall structure of softwood tracheids,” *Wood and Fiber Science*, vol. 7, no. 4, pp. 246–248, Jan. 1976.

[8] N. B. Singh, R. Sarita, and A. Sonal, “Polymer Nanocomposites and Cr (VI) Removal from Water,” *Nanosci Technol*, 2014.

[9] M. W. Hyer, *Stress Analysis of Fiber-reinforced Composite Materials*. DEStech Publications, Inc, 2009.

[10] S. Dong and R. Gauvin, “Application of dynamic mechanical analysis for the study of the interfacial region in carbon fiber/epoxy composite materials,” *Polym. Compos.*, vol. 14, no. 5, pp. 414–420, 1993.

[11] Le Hoang Sinh, B. T. Son, N. N. Trung, D.-G. Lim, S. Shin, and J.-Y. Bae,

"Improvements in thermal, mechanical, and dielectric properties of epoxy resin by chemical modification with a novel amino-terminated liquid-crystalline copoly(ester amide)," *REACTIVE AND FUNCTIONAL POLYMERS*, vol. 72, no. 8, pp. 542–548, Aug. 2012.

[12] A. C. Garg and Y.-W. Mai, "Failure mechanisms in toughened epoxy resins—A review," *Composites Science and Technology*, vol. 31, no. 3, pp. 179–223, Jan. 1988.

[13] M. H. Irfan, *Chemistry and Technology of Thermosetting Polymers in Construction Applications*. Springer Science & Business Media, 2012.

[14] P. I. Karkanas and I. K. Partridge, "Cure modeling and monitoring of epoxy/amine resin systems. I. Cure kinetics modeling," *J. Appl. Polym. Sci.*, 2000.

[15] O. Ansong, "Anomalous but useful behavior of epoxy adhesive system," *International Journal of Adhesion and Adhesives*, vol. 31, no. 7, pp. 620–628, Oct. 2011.

[16] I. T. Smith, "The mechanism of the crosslinking of epoxide resins by amines," *Polymer*, 1961.

[17] H. Liu, A. Uhlherr, R. J. Varley, and M. K. Bannister, "Influence of substituents on the kinetics of epoxy/aromatic diamine resin systems," *J. Polym. Sci. A Polym. Chem.*, vol. 42, no. 13, pp. 3143–3156, 2004.

[18] H. Liu, A. Uhlherr, and M. K. Bannister, "Quantitative structure–property relationships for composites: prediction of glass transition temperatures for epoxy resins," *Polymer*, vol. 45, no. 6, pp. 2051–2060, Mar. 2004.

[19] J. Mijovic and J. Wijaya, "Reaction Kinetics of Epoxy/Amine Model Systems. The Effect of Electrophilicity of Amine Molecule," *Macromolecules*, vol. 27, pp. 7589–7600, Dec. 1994.

[20] Y. Zhang and S. Vyazovkin, "Effect of Substituents in Aromatic Amines on the Activation Energy of Epoxy−Amine Reaction," *J. Phys. Chem. B*, vol. 111, no. 25, pp. 7098–7104, Jun. 2007.

[21] R. B. Prime, “Chapter 1: Thermosets,” in *Thermal characterization of polymeric materials*, 2nd ed., vol. 2, E. A. Turi, Ed. New York: Academic Press, 1997, pp. 1380–1744.

[22] J. D. Menczel and R. B. Prime, “Chapter 2,” in *Thermal analysis of polymers : fundamentals and applications*, Hoboken, New Jersey: John Wiley & Sons, Inc., 2009.

[23] P. I. Karkanas and I. K. Partridge, “Cure modeling and monitoring of epoxy/amine resin systems. II. Network formation and chemoviscosity modeling,” *J. Appl. Polym. Sci.*, 2000.

[24] F. G. Garcia, B. G. Soares, V. J. R. R. Pita, R. Sánchez, and J. Rieumont, “Mechanical properties of epoxy networks based on DGEBA and aliphatic amines,” *J. Appl. Polym. Sci.*, vol. 106, no. 3, pp. 2047–2055, 2007.

[25] R. PIPPAN, C. ZELGER, E. GACH, C. BICHLER, and H. WEINHANDL, “On the mechanism of fatigue crack propagation in ductile metallic materials,” *Fatigue & Fracture of Engineering Materials & Structures*, vol. 34, no. 1, pp. 1–16, Aug. 2010.

[26] C. H. Zhang, H. G. Wei, Y. Y. Liu, H. F. Tan, and Z. Guo, “Enhanced toughness and shape memory behaviors of toughed epoxy resin,” *High Performance Polymers*, vol. 24, no. 8, pp. 702–709, Nov. 2012.

[27] T. Misaki, T. Hirohata, M. Yoshii, and T. Hamasaki, “Properties of networks obtained by internal plasticization of epoxy resin with aromatic and aliphatic glycidyl compounds,” *J. Appl. Polym. Sci.*, vol. 37, no. 9, pp. 2617–2625, 1989.

[28] S.-J. Park, T.-J. Kim, and J.-R. Lee, “Cure behavior of diglycidylether of bisphenol A/trimethylolpropane triglycidylether epoxy blends initiated by thermal latent catalyst,” *J. Polym. Sci. B Polym. Phys.*, vol. 38, pp. 2114–2123, Aug. 2000.

[29] R. A. Pearson and A. F. Yee, “Toughening mechanisms in thermoplastic-modified epoxies: 1. Modification using poly (phenylene oxide),” *Polymer*, vol. 34, no. 17, pp. 3658–3670, 1993.

[30] M. Rutnakornpituk, “Thermoplastic toughened epoxy networks and their toughening mechanisms in some systems,” *Naresuan university Journal*, vol. 13,

no. 1, pp. 73–83, 2005.

[31] B. Wetzel, F. Haupert, K. Friedrich, M. Q. Zhang, and M. Z. Rong, “Impact and wear resistance of polymer nanocomposites at low filler content,” *Polym Eng Sci*, vol. 42, no. 9, pp. 1919–1927, 2004.

[32] D. R. Paul and L. M. Robeson, “Polymer nanotechnology: Nanocomposites,” *Polymer*, vol. 49, no. 15, pp. 3187–3204, Jul. 2008.

[33] V. V. Ginzburg, J. D. Weinhold, P. K. Jog, and R. Srivastava, “Thermodynamics of Polymer−Clay Nanocomposites Revisited: Compressible Self-Consistent Field Theory Modeling of Melt-Intercalated Organoclays,” *Macromolecules*, vol. 42, no. 22, pp. 9089–9095, Nov. 2009.

[34] G. Choudalakis and A. D. Gotsis, “Permeability of polymer/clay nanocomposites: A review,” *European Polymer Journal*, vol. 45, no. 4, pp. 967–984, Apr. 2009.

[35] Y.-G. Hsu and C.-W. Liang, “Properties and behavior of CTBN-modified epoxy with IPN structure,” *J. Appl. Polym. Sci.*, vol. 106, no. 3, pp. 1576–1584, 2007.

[36] T. C. Mauldin and M. R. Kessler, “Self-healing polymers and composites,” *int. mat. rev.*, vol. 55, no. 6, pp. 317–346, Nov. 2010.

[37] H. Kishi, A. Nagao, Y. Kobayashi, S. Matsuda, T. Asami, and A. Murakami, “Carboxyl-terminated butadiene acrylonitrile rubber/epoxy polymer alloys as damping adhesives and energy absorbable resins,” *J. Appl. Polym. Sci.*, vol. 105, no. 4, pp. 1817–1824, 2007.

[38] Y. T. Wang, “Carboxyl-terminated butadiene-acrylonitrile-toughened epoxy/carboxyl-modified carbon nanotube nanocomposites: Thermal and mechanical properties,” *expresspolymlett*, vol. 6, no. 9, pp. 719–728, Jul. 2012.

[39] N. T. Kamar and L. T. Drzal, “Micron and nanostructured rubber toughened epoxy: A direct comparison of mechanical, thermomechanical and fracture properties,” *Polymer*, vol. 92, no. C, pp. 114–124, Jun. 2016.

[40] V. D. Ramos, H. M. da Costa, V. L. P. Soares, and R. S. V. Nascimento, “Modification of epoxy resin: a comparison of different types of elastomer,” *Polymer Testing*, vol. 24, no. 3, pp. 387–394, May 2005.

[41] W. Chonkaew and N. Sombatsompop, “Mechanical and tribological properties of epoxy modified by liquid carboxyl terminated poly(butadiene-co-acrylonitrile) rubber,” *J. Appl. Polym. Sci.*, vol. 125, no. 1, pp. 361–369, Dec. 2011.

[42] S. Park and D. S. Kim, “Preparation and physical properties of an epoxy nanocomposite with amine-functionalized graphenes,” *Polym Eng Sci*, vol. 54, no. 5, pp. n/a–n/a, Nov. 2012.

[43] J. H. Hodgkin and G. P. Simon, “Thermoplastic toughening of epoxy resins: a critical review,” *Polymers for Advanced …*, 1998.

[44] S. Sinha Ray and M. Okamoto, “Polymer/layered silicate nanocomposites: a review from preparation to processing,” *Progress in Polymer Science*, vol. 28, no. 11, pp. 1539–1641, Nov. 2003.

[45] A. Usuki, Y. Kojima, M. Kawasumi, A. Okada, Y. Fukushima, T. Kurauchi, and O. Kamigaito, “Synthesis of nylon 6-clay hybrid,” *J. Mater. Res.*, vol. 8, no. 5, pp. 1179–1184, May 1993.

[46] Y. Kojima, A. Usuki, M. Kawasumi, A. Okada, Y. Fukushima, T. Kurauchi, and O. Kamigaito, “Mechanical properties of nylon 6-clay hybrid,” *J. Mater. Res.*, vol. 8, no. 5, pp. 1185–1189, May 1993.

[47] B. Wetzel, F. Haupert, and M. Qiu Zhang, “Epoxy nanocomposites with high mechanical and tribological performance,” *Composites Science and Technology*, vol. 63, no. 14, pp. 2055–2067, Nov. 2003.

[48] S. Zhao, L. S. Schadler, R. Duncan, H. Hillborg, and T. Auletta, “Mechanisms leading to improved mechanical performance in nanoscale alumina filled epoxy,” *Composites Science and Technology*, vol. 68, no. 14, pp. 2965–2975, Nov. 2008.

[49] S. Zhao, L. S. Schadler, H. Hillborg, and T. Auletta, “Improvements and mechanisms of fracture and fatigue properties of well-dispersed alumina/epoxy nanocomposites,” *Composites Science and Technology*, vol. 68, no. 14, pp. 2976–2982, Nov. 2008.

[50] H. Y. Kang, “A Review of the Emerging Nanotechnology Industry: Materials, Fabrications, and Applications,” *Department of Toxic Substances Control,[online] Sep*, 2010.

[51] N. Domun, H. Hadavinia, T. Zhang, T. Sainsbury, G. H. Liaghat, and S. Vahid, “Improving the fracture toughness and the strength of epoxy using nanomaterials – a review of the current status,” *Nanoscale*, vol. 7, no. 23, pp. 10294–10329, 2015.

[52] A. K. Geim and K. S. Novoselov, “The rise of graphene.,” *Nat Mater*, vol. 6, no. 3, pp. 183–191, Mar. 2007.

[53] J. N. Coleman, U. Khan, W. J. Blau, and Y. K. Gun’ko, “Small but strong: A review of the mechanical properties of carbon nanotube–polymer composites,” *Carbon*, vol. 44, no. 9, pp. 1624–1652, Aug. 2006.

[54] E. THOSTENSON, C. LI, and T. CHOU, “Nanocomposites in context,” *Composites Science and Technology*, vol. 65, no. 3, pp. 491–516, Mar. 2005.

[55] X. XIE, Y. MAI, and X. ZHOU, “Dispersion and alignment of carbon nanotubes in polymer matrix: A review,” *Materials Science and Engineering: R: Reports*, vol. 49, no. 4, pp. 89–112, May 2005.

[56] Y. Li, J. Zhu, S. Wei, J. Ryu, L. Sun, and Z. Guo, “Poly(propylene)/Graphene Nanoplatelet Nanocomposites: Melt Rheological Behavior and Thermal, Electrical, and Electronic Properties,” *Macromol. Chem. Phys.*, vol. 212, no. 18, pp. 1951–1959, Jul. 2011.

[57] V. V. Zuev, “The mechanisms and mechanics of the toughening of epoxy polymers modified with fullerene C 60,” *Polym Eng Sci*, vol. 52, no. 12, pp. 2518–2522, May 2012.

[58] A. H. Castro Neto, “Drawing Conclusions from Graphene,” *American Physical Society*, p. 1002, Oct. 2007.

[59] “Scientific Background on the Nobel Prize in Physics 2010 - GRAPHENE,” *Royal Swedish Academy of Sciences*, pp. 1–11, Oct. 2010.

[60] C. Lee, X. Wei, J. W. Kysar, and J. Hone, “Measurement of the Elastic Properties and Intrinsic Strength of Monolayer Graphene,” *Science*, vol. 321, no. 5887, pp. 385–388, Jul. 2008.

[61] K. Kalaitzidou, H. Fukushima, and L. T. Drzal, “Multifunctional polypropylene

composites produced by incorporation of exfoliated graphite nanoplatelets," *Carbon*, vol. 45, no. 7, pp. 1446–1452, Jun. 2007.

[62] M. A. Rafiee, J. Rafiee, Z. Wang, H. Song, Z.-Z. Yu, and N. Koratkar, "Enhanced Mechanical Properties of Nanocomposites at Low Graphene Content," *ACS Nano*, vol. 3, no. 12, pp. 3884–3890, Dec. 2009.

[63] H. M. Chong, S. J. Hinder, and A. C. Taylor, "Graphene nanoplatelet-modified epoxy: effect of aspect ratio and surface functionality on mechanical properties and toughening mechanisms," *J Mater Sci*, vol. 51, no. 19, pp. 8764–8790, Jul. 2016.

[64] X. G. Sciences, "xGnP Graphene Nanoplatelets - Grade M - Technical Data Sheet," pp. 1–1, Apr. 2011.

[65] T. Ramanathan, A. A. Abdala, S. Stankovich, D. A. Dikin, M. Herrera-Alonso, R. D. Piner, D. H. Adamson, H. C. Schniepp, X. Chen, R. S. Ruoff, S. T. Nguyen, I. A. Aksay, R. K. Prud'Homme, and L. C. Brinson, "Functionalized graphene sheets for polymer nanocomposites," *Nature Nanotech*, vol. 3, no. 6, pp. 327–331, May 2008.

[66] P.-C. Ma, Q.-B. Zheng, E. Mäder, and J.-K. Kim, "Behavior of load transfer in functionalized carbon nanotube/epoxy nanocomposites," *Polymer*, vol. 53, no. 26, pp. 6081–6088, Dec. 2012.

[67] K.-S. Kim, I.-Y. Jeon, S.-N. Ahn, Y.-D. Kwon, and J.-B. Baek, "Edge-functionalized graphene-like platelets as a co-curing agent and a nanoscale additive to epoxy resin," *J. Mater. Chem.*, vol. 21, no. 20, p. 7337, 2011.

[68] J. Liu, J. Tang, and J. J. Gooding, "Strategies for chemical modification of graphene and applications of chemically modified graphene," *J. Mater. Chem.*, vol. 22, no. 25, p. 12435, 2012.

[69] V. Singh, D. Joung, L. Zhai, S. Das, S. I. Khondaker, and S. Seal, "Graphene based materials: Past, present and future," *Progress in Materials Science*, vol. 56, no. 8, pp. 1178–1271, Oct. 2011.

[70] T. S. Sreeprasad and V. Berry, "How Do the Electrical Properties of Graphene Change with its Functionalization?," *Small*, vol. 9, no. 3, pp. 341–350, Nov. 2012.

[71] J. Ma, Q. Meng, A. Michelmore, N. Kawashima, Z. Izzuddin, C. Bengtsson, and H.-C. Kuan, “Covalently bonded interfaces for polymer/graphene composites,” *J. Mater. Chem. A*, vol. 1, no. 13, p. 4255, 2013.

Chapter 2: Toughening of Aromatic Epoxy Polymers via Aliphatic Copolymers

The material in this chapter was published in the journal Polymer in December 2014 under the title *Toughening of aromatic epoxy via aliphatic epoxy copolymers*. (10.1016/j.polymer.2014.10.052)

2.1 Introduction

Light-weighting is a concept that replaces traditional materials of construction such as steel and aluminum with advanced metal alloys and composites to achieve the goals of weight reduction and reduced energy use. Fiber-reinforced composites play an important part in many light-weighting strategies. The aviation industry, both airframe and turbine engine, has been implementing composite materials on their products in an effort to reduce weight and increase efficiency. The modern airliners, such as the Boeing 787 and Airbus A350 XWB, are comprised of more than 50% composite materials [1].

The appeal of thermosetting epoxy resins used as the matrix material in fiber-reinforced composites for high-performance structural applications is their high strength-to-weight ratio, good stiffness and high corrosion resistance. One of the drawbacks is the brittle nature of the highly cross-linked epoxy system, i.e. their lack of toughness [2]. Once formed in an epoxy material, a crack will propagate through the material uninhibited. Unlike metals, where the crack propagation will be quickly impeded by intersection of a grain boundary [3], no such mechanism exists in epoxies.

Much research effort has already been put into the toughening of epoxy polymers as has been recently summarized by P. Mohan [4]. Two general approaches can be taken to enhance the toughening of an epoxy polymer: first, adding filler materials as a crack arresting mechanism and second enhancing the amount of energy that can be adsorbed before a fracture occurs by addition of a more flexible aliphatic co-polymer. In pursuit of the former, nano-scale filler materials have been shown to have toughening benefits at low filler loadings (< 0.3 wt%) [5], [6]. Many different nano-fillers have been investigated, including thermoplastic co-polymers [7], [8], inorganic nano-fillers [9], [10] and organic nano-fillers [11]-[13]. All of these filler materials have shown promise in enhancing the toughness of epoxy polymers via different toughening mechanisms, such as crack bridging, crack pinning and crack deflection which have been proposed in the literature [5]. Other approaches that have shown toughening of epoxies include the use of micro-scale particles filled with healing agent to impart some self-healing properties [14]. As with any filler based toughening mechanism, the suspension of particulates in the matrix phase can pose a challenge when these toughening approaches are applied to production methods using liquid molding processing. For example, resin transfer molding (RTM) and vacuum-assisted resin transfer molding (VARTM) inject the epoxy resin matrix material under pressure into a layup of reinforcing fibers [15]. Particulates that are suspended in the liquid matrix material can be filtered out by the weave of reinforcing fibers, resulting in an uneven distribution of nano-filler material. Since a uniform distribution of the nano-filler is essential, this would negate any potential toughening benefits.

The second approach of adding a more flexible aliphatic epoxy copolymer would address the issue of processability, provided that the epoxy copolymers are miscible. Having the same functional epoxy groups, the copolymers will undergo the same reaction with the diamine curing agent to form a highly cross-linked network. The main difference between the molecules is the flexibility of the chain segments between the functional groups. The higher flexible aliphatic chains should be able to absorb more impact energy prior to fracturing. Misaki et. al. [16] showed increases of toughness of several different aliphatic epoxies at a constant concentration of 30 wt%. The increased toughness was associated with decreases in tensile modulus and glass transition temperature. Zhang et. al. [17] looked at different concentrations of a di-functional aliphatic epoxy in the range of 7 to 15 wt% which showed substantial increases in impact strength. However, these were also associated with substantial decreases in modulus and glass transition temperature. A survey of the current literature indicates that the toughening of aromatic epoxies with low concentrations (< 5 wt%) of aliphatic epoxies has not been systematically investigated. This study includes this lower concentration range.

As with any toughening approach, the optimization of a single parameter is straightforward. However, a substantial increase in toughness is mostly done to the detriment of other material properties such as modulus or glass transition temperature. Both parameters are essential for structural applications. A balanced approach of enhancing impact toughness without detrimentally affecting the other system properties is desirable and presented in this work.

2.2 Materials and Methods

The aromatic epoxy, diglycidyl ether of bisphenol A (DGEBA, Epon 828,Figure 2.1), with an epoxy equivalent weight (EEW) of 185-195, as well as the tri-functional aliphatic epoxy, trimethyolpropane triglycidyl ether (Heloxy 48, Figure 2.2) with an EEW of 138 were purchased from Momentive Specialty Chemicals Inc. The di-functional aliphatic epoxy, polypropylene glycol diglycidyl ether (PDGE, Figure 2.3) with an EEW of 190 (Mn 380), as well as the curing agent meta-phenylenediamine (m-PDA, Figure 2.4) were purchased from Sigma-Aldrich. All chemicals were used as received.

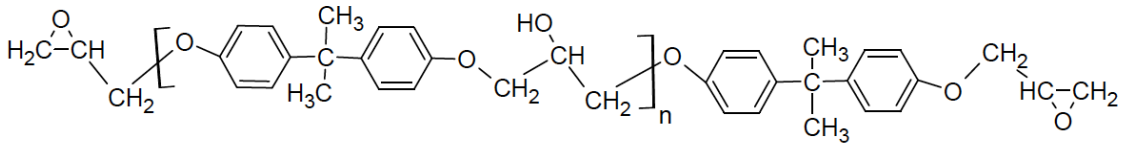

Figure 2.1: Diglycidyl ether of bisphenol A (DGEBA)

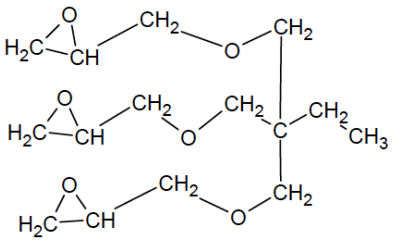

Figure 2.2: Trimethyolpropane triglycidyl ether (tri-functional aliphatic)

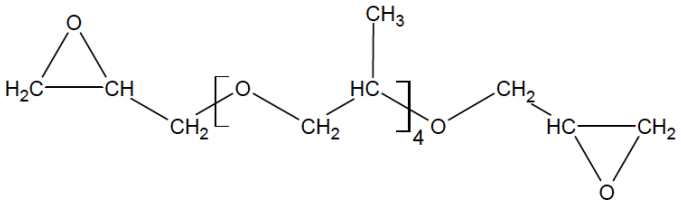

Figure 2.3: Polypropylene glycol diglycidyl ether (di-functional aliphatic)

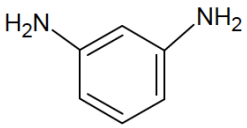

Figure 2.4: Meta-Phenylenediamine

The DGEBA was weighed out in a glass beaker and the appropriate amount of aliphatic epoxy (either di- or tri-functional) was added. The mixture was then placed on a stir plate and heated to about 70˚C under agitation with a magnetic stir bar. The heating of the epoxy mixture was primarily done in an effort to reduce the viscosity during mixing, degasing and casting of the material into the molds. A stoichiometric amount of m-PDA was melted in an oven. In the case of di-functional aliphatic, the stoichiometry was constant at 14.5 phr based on the similar EEW of the two epoxies. The stoichiometry for the tri-functional aliphatic, needed to be adjusted for each tri-functional aliphatic epoxy concentration and ranged from 14.6 to 15.5 phr. After addition of the liquefied curing agent and homogenizing the DGEBA/aliphatic epoxy/mPDA mixture by hand, the mixture was degassed in a vacuum oven for about 5 min to eliminate trapped gas bubbles. After degassing, the mixture was poured into silicone molds for the appropriate sample configuration and placed in a convection oven. The samples were cured at 75˚C for 2h and post-cured at 125˚C for 2h. The cured samples were polished on a Struers Abramin polisher with 320, 600, 1200 and 4000 grit paper to yield a smooth sided sample prior to mechanical testing. Neat DGEBA/mPDA samples were made without the addition of any aliphatic epoxy copolymer to serve as a baseline. All mechanical properties were tested on the bases of at least two replicates at each aliphatic co-polymer concentration, with each replicate consisting of at least 4 samples. The flexural properties were determined on the basis of ASTM D790 using a United Testing Systems SFM-20 load frame with a 100lbf load cell. The flexural samples had dimensions of 75x12.5x3mm. The support span width to thickness ratio was taken at 16:1 and the crosshead speed was calculated per ASTM D790-10. The notched Izod

impact properties were determined using a TMI pendulum impact tester on the basis of ASTM D256 using a 1 ft-lbf hammer. The notched Izod impact samples used a molded pre-notch and had dimensions of 63.5x12.5x12.5mm. The thermo-mechanical properties were determined using a TA Instruments Q800 dynamic mechanical analysis (DMA) instrument using a single-cantilever beam setup in air from room temperature to 250˚C at a ramp rate of 3˚C/min and a TA Instruments Q2000 differential scanning calorimeter (DSC) using a modulated DSC at from 25 to 250 ˚C at 3 ˚C/min and a modulation of +/- 2˚C.

Fracture surfaces were investigated using a Zeiss EVO LS25 scanning electron microscope under high-vacuum. Samples were coated with a 3 nm thick layer of tungsten prior to observation.

2.3 Results and Discussion

The aromatic and aliphatic epoxies were found to be completely miscible in the concentration ranges investigated in this study (up to 20 wt%). Simple mechanical mixing was sufficient to achieve a homogenous mixture. Figure 2.5 shows representative tand curves for the different di- and tri-functional aliphatically toughened DGEBA. Tan δ also referred to as the material loss factor is the ratio of the loss to the storage modulus of a material [18] and the maximum of the tan δ peak represents one measure of the glass transition temperature, which will be shown later in this paper. The single a transition is further indication of the homogenous structure that is formed between the two epoxies during curing. This bodes well for applying aliphatic

toughening to current production methods, such as pre-preg production and resin transfer type processes.

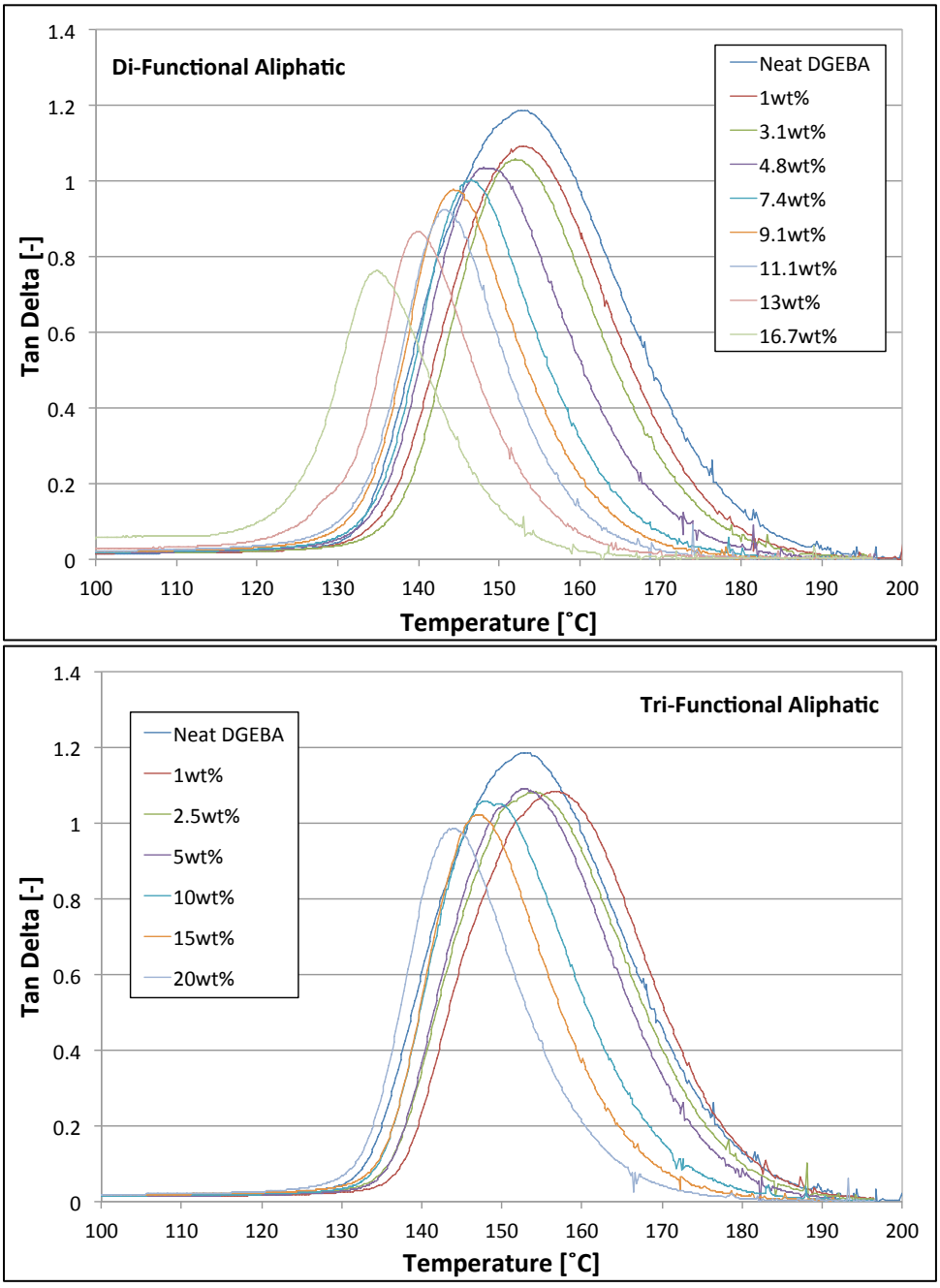

Figure 2.5: Tan δ function of DGEBA toughened with di-functional (top) and tri-functional (bottom) aliphatic epoxy determined by DMA

Figure 2.6 shows representative curves of the storage modulus, which is related to the stiffness of the material, of the di- and tri-functionally toughened DGEBA. At lower temperature, the storage moduli are similar for all aliphatic copolymer concentrations. This behavior is consistent with that seen in the flexural modulus as shown in figure 6. As the temperature increases, the storage modulus decreases. The temperature at which the storage modulus decreases substantially (onset temperature), decreases with increasing aliphatic epoxy concentration. The temperature decreases are not as large for the tri-functional aliphatically toughened samples as can be seen from narrower temperature band, which all curves fall into. The 1wt% toughened samples, both the di- and tri-functional, show very similar behavior to the neat DGEBA.

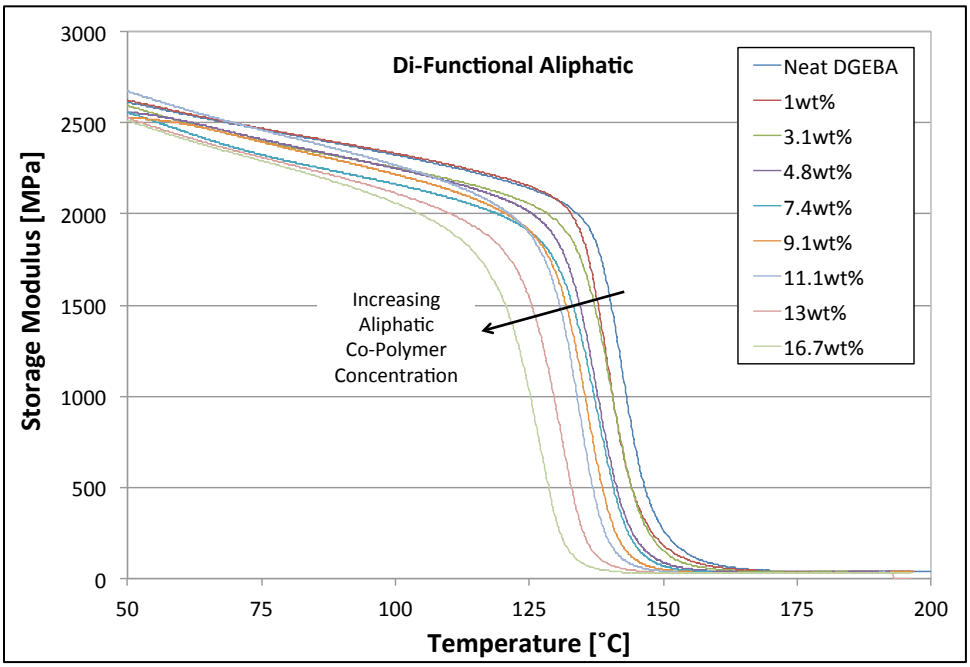

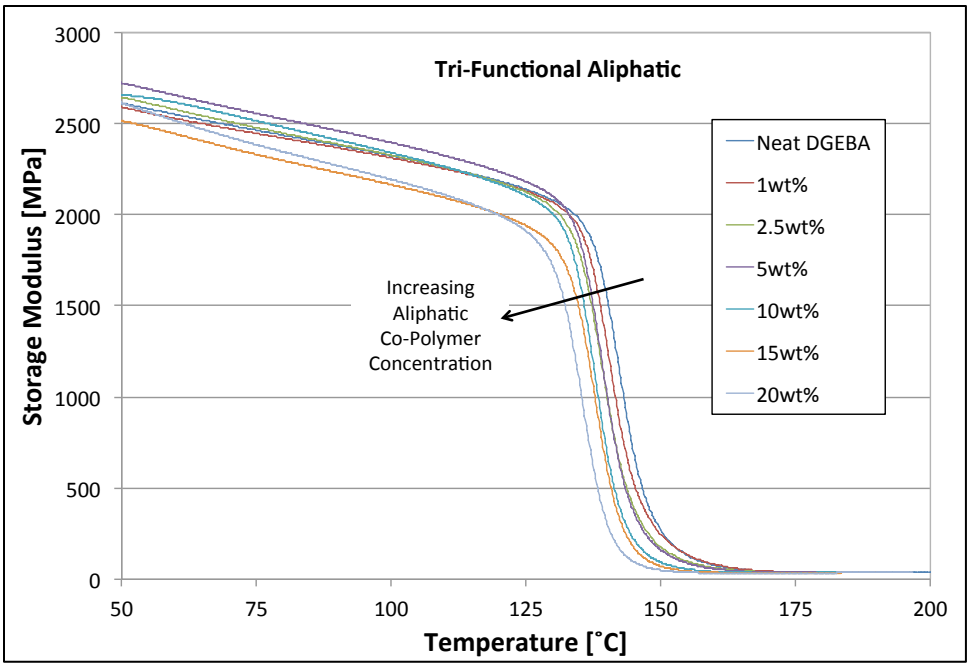

Figure 2.6: Storage Modulus of DGEBA toughened with di-functional (top) and tri-functional (bottom) aliphatic epoxy determined by DMA

The flexural modulus as shown in Figure 2.7 was found to be independent of aliphatic epoxy concentration within the investigated concentration range. This is true for both the di- and tri-functional aliphatic epoxies. Since the tensile and flexural

properties tend to mirror each other, the flexural behavior is consistent with previously published work by Zhang et. al. [17] where the Young's modulus was found to be constant up to 5 wt% of a di-functional aliphatic epoxy concentration. The flexural test is conducted at a slow loading rate so the polymer chains have a chance to rearrange to accommodate the load and the enhanced flexibility of the aliphatic epoxy chains does not come into play. Hence, there are no measureable differences in these slow loading rate properties between the samples with different aliphatic epoxy concentrations.

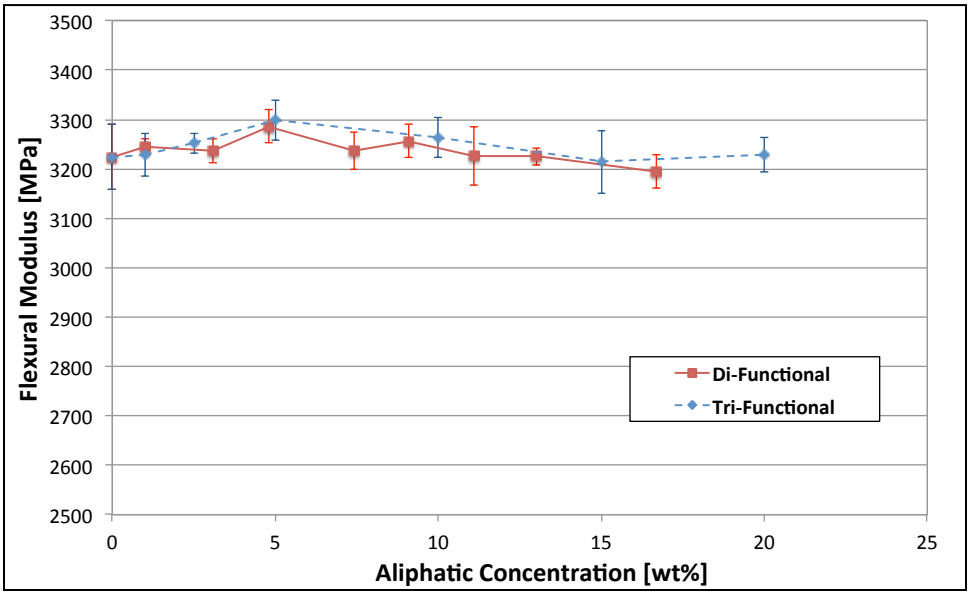

Figure 2.7: Flexural modulus of di- and tri-functionally toughened DGEBA/mPDA

The flexural strength shown in Figure 2.8 exhibited different behaviors for the di-functional and tri-functional aliphatic epoxies. For the di-functional aliphatic, the flexural strength is comparable with neat DGEBA up to a concentration of about 5 wt%. Above this concentration the flexural strength decreases. At a concentration of ~17 wt% the flexural strength drops by about 7% compared to the neat DGEBA. The tri-functional aliphatic on the other hand shows a flexural strength that is comparable to neat DGEBA

up to a concentration of about 10 wt%. Above 10 wt% the flexural strength decreases with a reduction of about 6% at 20 wt% tri-functional aliphatic. The trend of flexural strength decreasing with increased addition of aliphatic epoxy concentrations is again consistent with the results from Zhang et. al. [17], which found a reduction in upper yield stress with increasing aliphatic epoxy concentrations. The reason cited for this behavior is the enhanced flexibility of the aliphatic chain segments relative to the rigid aromatic chain segments of the DGEBA. The constant flexural strength up to a higher concentration of tri-functional aliphatic when compared to the di-functional aliphatic is probably due to the formation of a network with shorter distances between crosslinks of the tri-functional aliphatic resulting in a higher crosslink density.

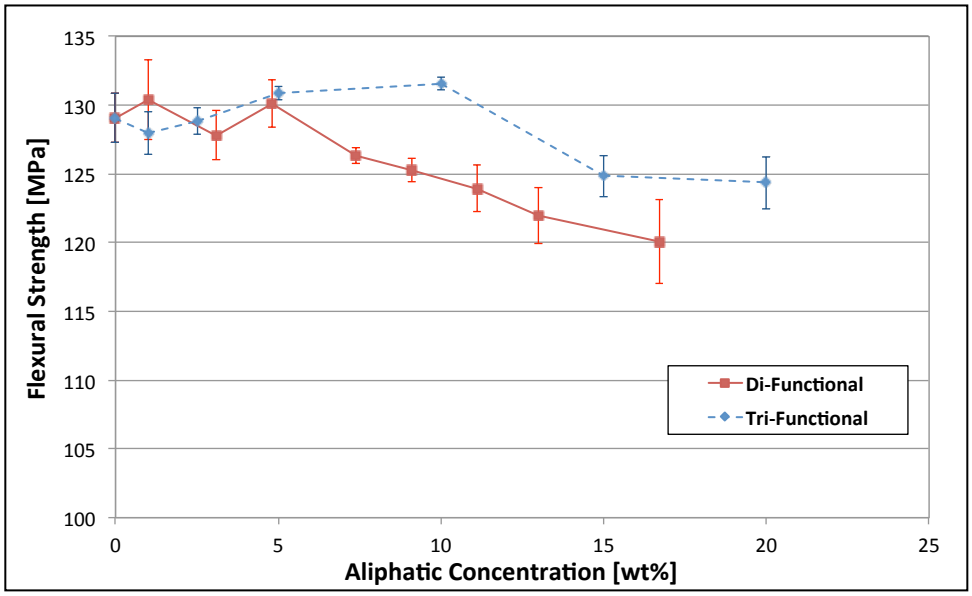

Figure 2.8: Flexural strength of di- and tri-functionally toughened DGEBA/mPDA

As shown in Figure 2.9, the notched Izod impact strength increases significantly with the addition of aliphatic epoxies. Even low concentrations of aliphatic epoxy increased the notched Izod impact strength considerably. The di-functional aliphatic

increases the impact strength by 56% over the neat DGEBA at 1 wt%. The impact strength further increases with increasing concentration up to about 77% at an aliphatic concentration of 10 wt%. No further increase is seen above this concentration. The tri-functional aliphatic shows a greater increase of 77% at 1 wt% concentration. Above 1 wt%, the impact strength is approximately constant with increasing tri-functional aliphatic concentration. In contrast to the slow loading rate of the flexural test, the notched Izod impact test is done under a high loading rate as the pendulum strikes the sample. The higher flexibility of the aliphatic chains enables energy to be absorbed during impact. As Misaki et. al. [16] postulated, the more flexible materials will fracture with crack branching, leading to a more uneven fracture surface that requires additional energy for fracture. These findings are supported by the fracture surfaces as shown in Figure 2.10. The fracture surface of the neat DGEBA sample exhibits the characteristic smooth surface of a brittle fracture. The featureless mirror region covers most of the failure initiation region. With the addition of the aliphatic copolymer at concentrations of 1, 5 & 15 wt%, hackle features begin to appear in the mirror region. As the aliphatic concentration is increased, the rough hackle features increase in frequency and the smooth mirror region becomes less evident. At 15 wt% tri-functional aliphatic, the mirror region has mostly disappeared. The rougher surface is associated with a higher crack velocity and indicates crack branching [19]. With higher energy dissipation rates, the rough morphology coincides with increased impact toughness.

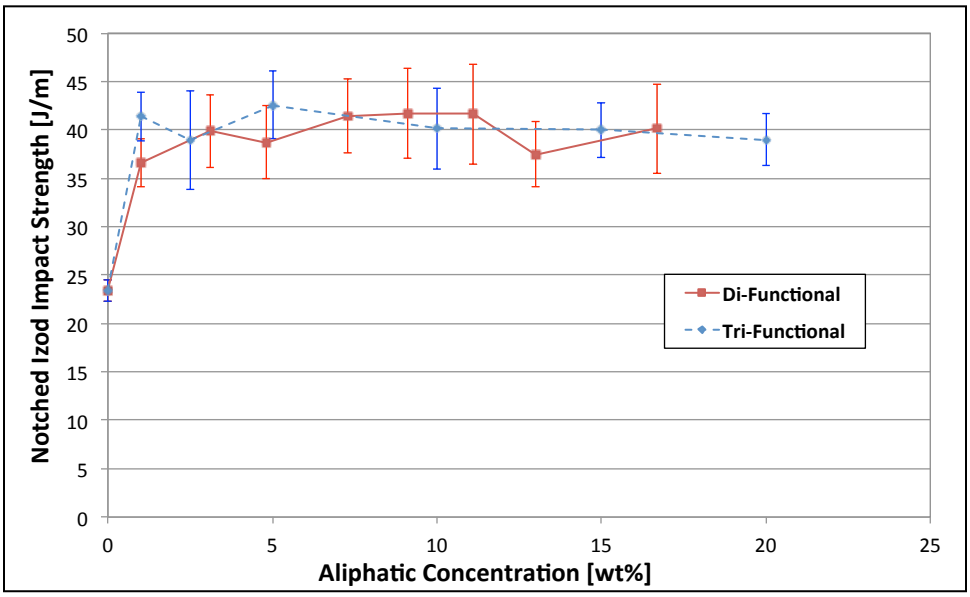

Figure 2.9: Notched Izod impact strength of di- and tri-functionally toughened DGEBA/mPDA

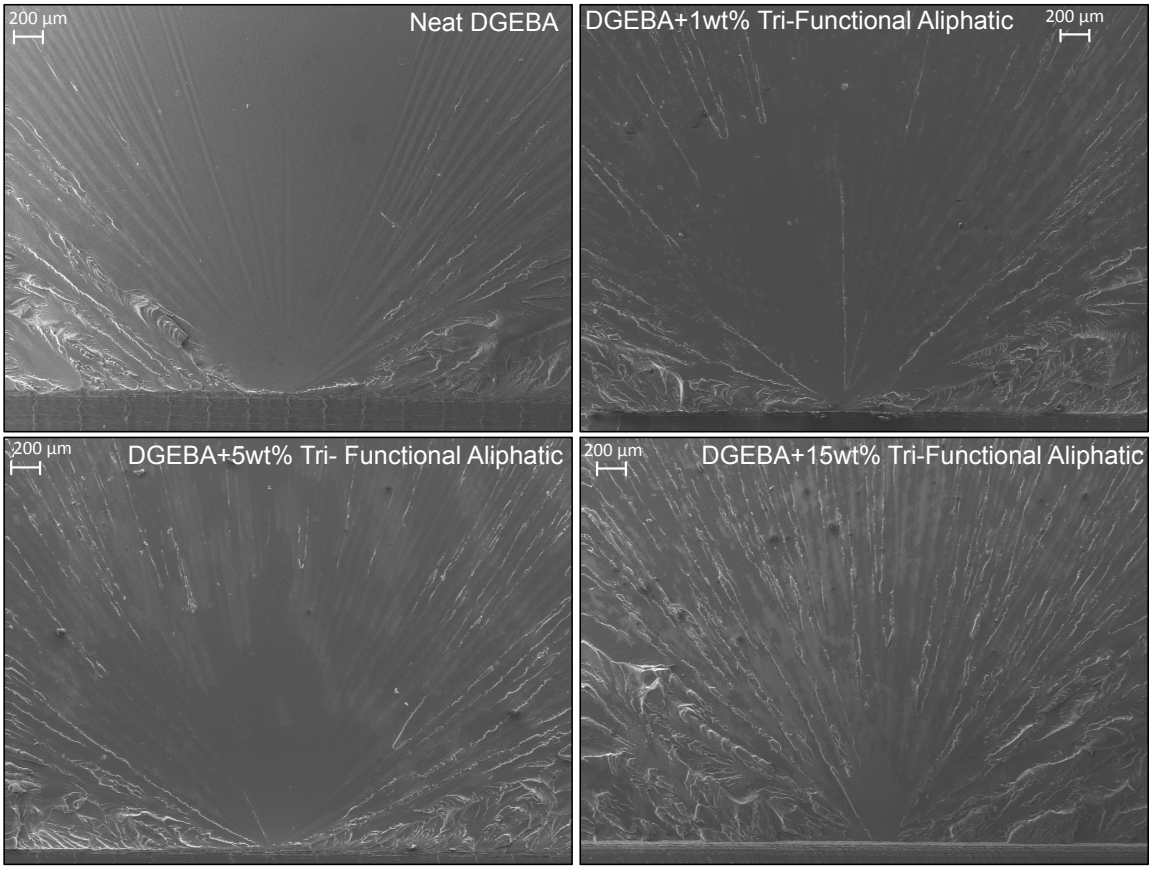

Figure 2.10: SEM micrograph of the fracture surface of notch Izod impact samples. Neat DGEBA (top, left) and DGEBA toughened with tri-functional aliphatic epoxy: 1 wt% (top, right), 5 wt% (bottom, left), 15 wt% (bottom right)

The impact of the addition of aliphatic epoxies on the glass transition temperature (T_g) is shown in Figure 2.11. At low concentrations (1 wt%) of di-functional aliphatic, the T_g is constant. Above that concentration, the T_g decreases with increasing di-functional aliphatic concentration. The maximum reduction is around 10% at ~17 wt% di-functional aliphatic. At 1 wt% tri -functional aliphatic, the T_g has an increase of about 2%. Up to a concentration of 5 wt% tri-functional aliphatic, the T_g is comparable to neat DGEBA. Above a concentration of 5 wt%, the T_g decreases with a maximum reduction of 6% at 20 wt% tri-functional aliphatic. For a given concentration the reduction in T_g for the tri-functional aliphatic epoxy is smaller when compared to the di-functional aliphatic epoxy.

This can be attributed to the different network formation of the tri-functional epoxy. The lower EEW of the tri-functional aliphatic implies a shorter distance between cross-links and a higher cross-link density. Representative curves of the reversible heat flow from the modulated DSC measurements are shown in Figure 2.12. The DSC measurements confirm the trends in the glass transition temperature that were seen in the measurements from the DMA.

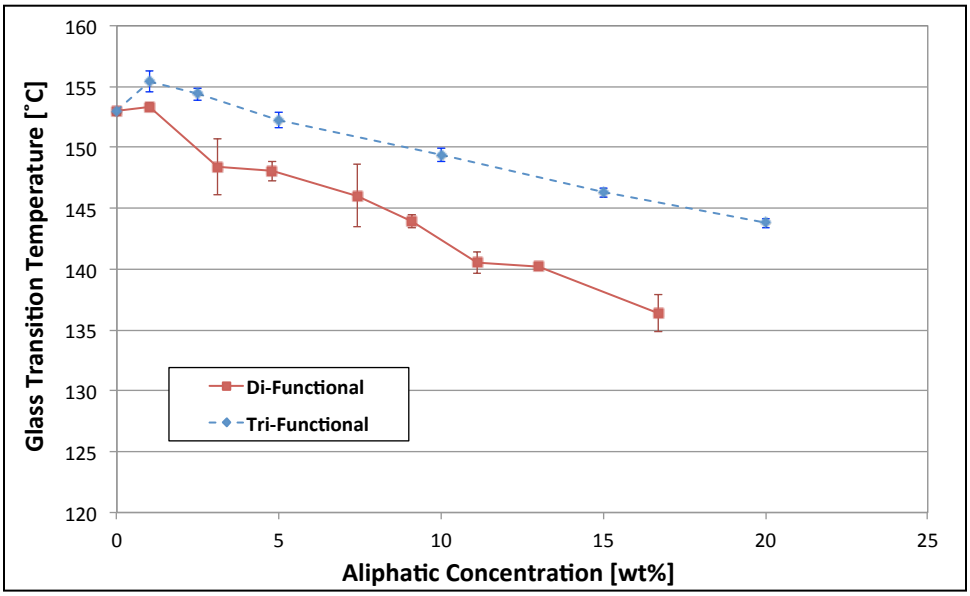

Figure 2.11: Glass transition temperature of di- and tri-functionally toughened DGEBA/mPDA determined from maxima of tan δ curve

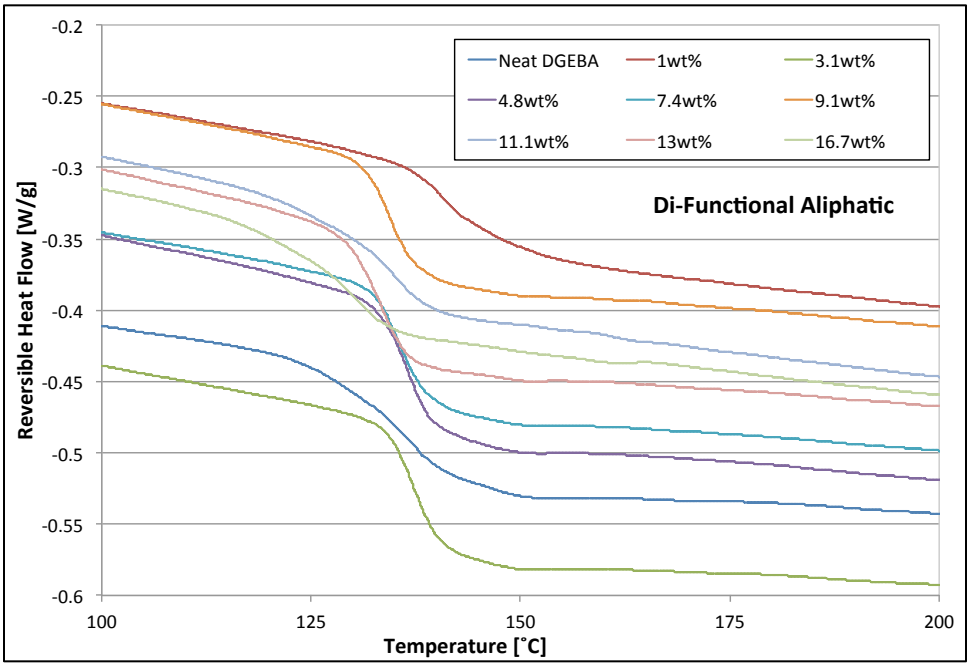

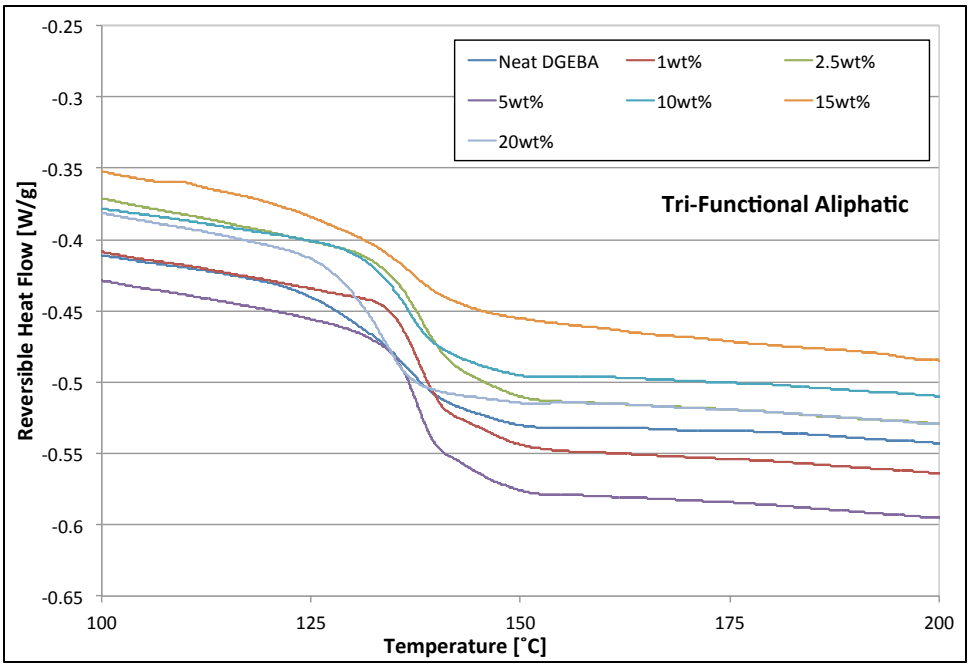

Figure 2.12: Reversible heat flow of di-functionally (left) and tri-functionally (right) toughened DGEBA/mPDA determined from modulated DSC measurements

The application of the presented toughening mechanism to fiber-reinforced composites needs to be confirmed and will be presented in a follow-up publication. As has been shown in the literature, the effectiveness of toughening mechanisms can be less pronounced in a system that includes reinforcing fibers. Hunston et.al. [20], [21]

showed that for brittle matrix materials, the increase in toughness can be more pronounced in the fiber-reinforced composite than the base matrix. This increase effect in the fiber-reinforced composite is attributed to the additional energy expended for fracturing of reinforcing fibers, fiber pullout and crack deflection. With highly toughened resins however, the toughening effect was reduced by as much as one-third. The toughening mechanisms that rely on the formation of large crack-tip deformation zones can have these deformation zone constrained between reinforcing fibers, reducing the effectiveness. Since the proposed aliphatic toughening mechanism relies on the cross-linking of more flexible chains into the epoxy network, the transfer to the fiber-reinforced composite is expected to be good.

2.4 Conclusion

The results presented here highlight an approach to enhance the impact toughness of an aromatic DGEBA/mPDA epoxy system by the addition of di- and tri-functional epoxy copolymers. At low aliphatic epoxy concentrations (1 wt%) the impact toughness can be significantly enhanced (57 to 77%) without reductions in the flexural properties or glass transition temperature. The excellent miscibility of the epoxy copolymers makes the application of this toughening mechanism directly implementable for current fiber-reinforced epoxy composite production methods.

BIBLIOGRAPHY

BIBLIOGRAPHY

[1] G. Marsh, “Airbus takes on Boeing with reinforced plastic A350 XWB,” *Reinforced Plastics*, vol. 51, no. 11, pp. 26–29, Dec. 2007.

[2] Le Hoang Sinh, B. T. Son, N. N. Trung, D.-G. Lim, S. Shin, and J.-Y. Bae, “Improvements in thermal, mechanical, and dielectric properties of epoxy resin by chemical modification with a novel amino-terminated liquid-crystalline copoly(ester amide),” *REACTIVE AND FUNCTIONAL POLYMERS*, vol. 72, no. 8, pp. 542–548, Aug. 2012.

[3] J. C. Newman and B. S. Annigeri, “Fatigue-Life Prediction Method Based on Small-Crack Theory in an Engine Material,” *J. Eng. Gas Turbines Power*, vol. 134, no. 3, p. 032501, 2012.

[4] P. Mohan, “A Critical Review: The Modification, Properties, and Applications of Epoxy Resins,” *Polymer-Plastics Technology and Engineering*, vol. 52, no. 2, pp. 107–125, 2013.

[5] M. Rutnakornpituk, “Thermoplastic toughened epoxy networks and their toughening mechanisms in some systems,” *Naresuan university Journal*, vol. 13, no. 1, pp. 73–83, 2005.

[6] F. Yavari, M. A. Rafiee, J. Rafiee, Z.-Z. Yu, and N. Koratkar, “Dramatic increase in fatigue life in hierarchical graphene composites.,” *ACS Appl. Mater. Interfaces*, vol. 2, no. 10, pp. 2738–2743, Oct. 2010.

[7] Y.-G. Hsu and C.-W. Liang, “Properties and behavior of CTBN-modified epoxy with IPN structure,” *J. Appl. Polym. Sci.*, vol. 106, no. 3, pp. 1576–1584, 2007.

[8] T. C. Mauldin and M. R. Kessler, “Self-healing polymers and composites,” *int. mat. rev.*, vol. 55, no. 6, pp. 317–346, Nov. 2010.

[9] A. Usuki, Y. Kojima, M. Kawasumi, A. Okada, Y. Fukushima, T. Kurauchi, and O. Kamigaito, “Synthesis of nylon 6-clay hybrid,” *J. Mater. Res.*, vol. 8, no. 5, pp. 1179–1184, May 1993.

[10] S. Zhao, L. S. Schadler, R. Duncan, H. Hillborg, and T. Auletta, “Mechanisms

leading to improved mechanical performance in nanoscale alumina filled epoxy," *Composites Science and Technology*, vol. 68, no. 14, pp. 2965–2975, Nov. 2008.

[11] J. N. Coleman, U. Khan, W. J. Blau, and Y. K. Gun'ko, "Small but strong: A review of the mechanical properties of carbon nanotube–polymer composites," *Carbon*, vol. 44, no. 9, pp. 1624–1652, Aug. 2006.

[12] R. Sengupta, M. Bhattacharya, S. Bandyopadhyay, and A. K. Bhowmick, "A review on the mechanical and electrical properties of graphite and modified graphite reinforced polymer composites," *Progress in Polymer Science*, vol. 36, no. 5, pp. 638–670, May 2011.

[13] J. R. Potts, D. R. Dreyer, C. W. Bielawski, and R. S. Ruoff, "Graphene-based polymer nanocomposites," *Polymer*, vol. 52, no. 1, pp. 5–25, Jan. 2011.

[14] E. N. Brown, S. R. White, and N. R. Sottos, "Microcapsule induced toughening in a self-healing polymer composite," *J Mater Sci*, vol. 39, no. 5, pp. 1703–1710, 2004.

[15] V. V. Vasiliev and E. V. Morozov, *Fundamentals of mechanics*, Third Edition. Elsevier, 2013, pp. 29–51.

[16] T. Misaki, T. Hirohata, M. Yoshii, and T. Hamasaki, "Properties of networks obtained by internal plasticization of epoxy resin with aromatic and aliphatic glycidyl compounds," *J. Appl. Polym. Sci.*, vol. 37, no. 9, pp. 2617–2625, 1989.

[17] C. H. Zhang, H. G. Wei, Y. Y. Liu, H. F. Tan, and Z. Guo, "Enhanced toughness and shape memory behaviors of toughed epoxy resin," *High Performance Polymers*, vol. 24, no. 8, pp. 702–709, Nov. 2012.

[18] R. P. Chartoff, J. D. Menczel, and S. H. Dillman, "Dynamic mechanical analysis (DMA)," *Thermal analysis of polymers: fundamentals and applications. San Jose: Wiley*, pp. 387–496, 2009.

[19] W. T. Becker, R. J. Shipley, and A. I. H. Committee, *Failure analysis and prevention, Vol 11*. ASM International, 2002, pp. 650–661.

[20] D. L. Hunston, "Composite interlaminar fracture-Effect of matrix fracture energy," *Journal of Composites, Technology and Research*, vol. 6, no. 4, Dec. 1984.

[21] D. L. Hunston, R. J. Moulton, N. J. Johnston, and W. Bascom, “Matrix resin effects in composite delamination: mode I fracture aspects,” *Toughened Composites, ASTM STP*, vol. 937, pp. 74–94, 1987.

Chapter 3: Toughening of Carbon Fiber-Reinforced Epoxy Polymer Composites via Fiber Surface Treatment and Epoxy Fiber Sizing

Most of the material of this chapter was published in Composites Part A under the title "*Toughening of Carbon Fiber-Reinforced Epoxy Polymer Composites Utilizing Fiber Surface Treatment and Sizing*" (10.1016/j.compositesa.2016.09.005) on September 3rd, 2016

3.1 Abstract

Toughening of fiber-reinforced epoxy composites while maintaining other mechanical properties represents a significant challenge. This paper presents an approach of enhancing the toughness of a DGEBA/mPDA-based carbon fiber-reinforced epoxy composite, without significantly reducing the static-mechanical properties such as flexural properties and glass transition temperature. The impact of combining an UV-ozone fiber surface treatment with an aromatic and aliphatic epoxy fiber sizing on composite toughness is investigated. Carbon fiber-epoxy adhesion was increased as measured by the single fiber interfacial shear test. The Mode I composite fracture toughness was enhanced by 23% for the UV-ozone fiber surface treatment alone. With the addition of an aromatic and aliphatic fiber sizing, the composite fracture toughness was further increased to 50% and 84% respectively over the as-received, unsized fiber. The increased fiber/matrix adhesion also improved the transverse flexural strength.

3.2 Introduction

The reduction of vehicle weight, in an effort to improve fuel efficiency and reduce emissions, is becoming the focus of many industries in the transportation sector, including the aerospace and automotive industries. Modern airliners, such as the Boeing 787 and Airbus A350, are being made with increasingly larger percentages of composites materials. The automotive industry is looking to lightweighting approaches using carbon fiber-reinforced composite to meet the US EPA CAFÉ standards by 2025 [1].

Carbon fiber-reinforced composites usually consist of two major components: First is the reinforcing fiber, which is the load bearing component; second is the epoxy matrix that holds the carbon fibers together, transfers the applied load between the fibers and gives the part its final shape. An important, but often overlooked third component, is the fiber-matrix interphase which consists of a fiber surface treatment and a very thin 30-100 nm sizing (coating) applied to the fiber for adhesion enhancement and fiber handling purposes. As everything is more than the sum of its parts, a strong fiber and tough matrix alone are insufficient if they are not strongly bonded. Good fiber/matrix adhesion is needed to yield a tough composite [2]-[4]. This paper focuses on toughening the composite by enhancing the fiber/matrix adhesion and toughening of the fiber/matrix interphase. Two approaches of enhanced fiber/matrix adhesion are investigated: First, a UV-ozone fiber surface treatment, which increases the fiber surface oxygen concentration, while simultaneously removing some surface material, providing for robust fiber/matrix bonding; and second, a specially formulated epoxy fiber sizing containing either aromatic or aliphatic epoxies.

Fiber surface treatment has been investigated in an effort to enhance fiber/matrix adhesion, taking the form of 'wet' (chemical and electrochemical) and 'dry' (plasma and thermal) treatments as recently reviewed by Sharma *et al* [5]. The main objective of the surface treatment is to increase the amount of reactive groups on the fiber surface and reducing the number of defects on the fiber surface [2], [4]. The UV-ozone (UVO) surface treatment is a 'dry' surface treatment that exposes the fiber to short wavelength UV in air in a continuous process. The fiber tow is treated simultaneously with atomic oxygen and ozone in presence of energetic UV photons. Some surface is removed through the gas phase creating a reactive surface to which surface oxygen groups are chemically attached to the surface of the fiber. The resulting treated surface can then react with the surrounding matrix or the fiber sizing [6]. Increasing the surface oxygen groups will yield better fiber/matrix adhesion. The UVO-treatment has also been reported to reduce the amount of defects on the fiber surface [2]-[4]. The UVO treatment process is a continuous process with a residence time of the fiber tow around 90s, making it is a very scalable process. More details about the UVO treatment process have been published [2].

Fiber sizing has historically been utilized to improve the handling of the fiber tow during processing, fiber surface protection and adhesion purposes [7]. For carbon fibers the sizing often consists of a thin layer of epoxy that is coated onto the fiber surface [6], [8]. In this investigation, the sizing consists of an epoxy monomer with an under-stoichiometric amount of curing agent, about 60% of stoichiometry, allowing the sizing to be vitrified at low temperature for better handling during production. During the curing cycle and consolidation of the composite, ideally as the temperature increases, the

sizing can swell and diffuse away from the fiber surface. This can also lead to a locally toughened system, depending on the constituents of the fiber sizing. One model of the fiber/matrix interface was proposed by Cox [9], who considered an elastic fiber and elastic matrix with the matrix under a general strain. Cox furthermore assumed perfect bonding between fiber and matrix and equal lateral contraction of the fiber and matrix [10]. Assuming that the material close to the interface has the same composition as the bulk matrix, an infinitesimally thin interface, and a fiber arrangement in a repeating array the following equation has been derived to predict the interfacial shear strength [11]:

$$\tau = E_f \epsilon_m \left(\frac{G_m}{2E_f \ln\left(\frac{R}{r}\right)} \right)^{0.5} \frac{sinh\beta(0.5L - x)}{cosh\beta\left(\frac{L}{2}\right)} \quad (1)$$

where,

τ: Interfacial shear strength at fixed point

E_f: Tensile modulus of fiber

ε_m: Strain in the matrix

G_m: Shear modulus of matrix

R: Interfiber spacing

r: Radius of fiber

β: Scaling Factor $\left(\left[\frac{2G_m}{2E_f ln\left(\frac{R}{r}\right)} \right]^{0.5} \right)$

L: Length of fiber fragment

x: Radial distance outward

Equation 1 contains many geometric and fiber-related quantities (subscript f). Since these fiber related quantities are constant, the equation states that the fiber/matrix bond strength is influenced mainly by shear strain-to-failure (ε_m) and shear modulus

(G_m) at the fiber matrix interface. Improving either of these properties should enhance the fiber/matrix bond strength. Under-stoichiometric amounts of curing agent have been shown by Gupta *et al.* to increase the modulus of the DGEBA/mPDA system due to steric hindrance of unreacted epoxy molecules in the glassy state [12], which should lead to enhanced fiber/matrix bond strength according to Equation 1. The approach of a vitrified epoxy sizing can also be used as a vehicle for the introduction of nano-particles such as carbon nanotubes [13] or graphene nano-platelets [14] at the fiber surface. Two different di-functional epoxies were investigated, aromatic and aliphatic (Figure 3.1).

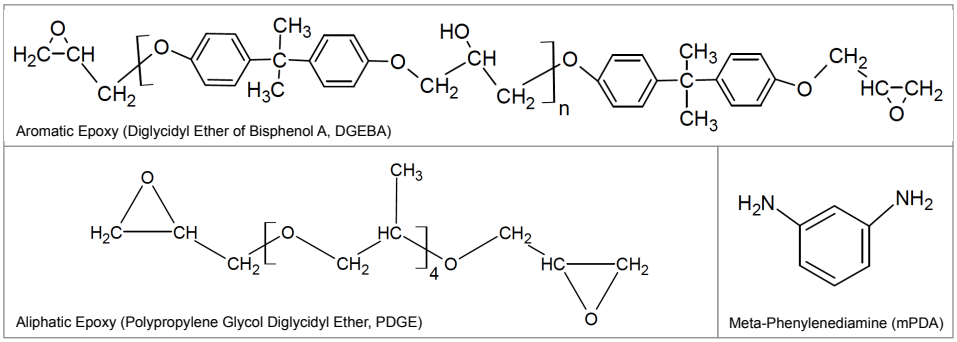

Figure 3.1: Structure of aromatic and aliphatic epoxies as well as curing agent

The aromatic sizing is the same epoxy as the matrix material, diglycidyl ether of bisphenol A (DGEBA), and should enhance the compatibility between the sizing and matrix. Since an under-stoichiometric amount of curing agent is used in the sizing, a stoichiometry gradient should be established from the fiber surface (60% stoichiometry) to the bulk matrix (100% stoichiometry), as has been proposed by Drzal, *et al* [7]. In the case of the aliphatic epoxy (polypropylene glycol diglycidyl ether (PDGE)) as the main component of the sizing, a concentration gradient of aliphatic epoxy can be established by the diffusion of the sizing, leading to an aliphatically toughened aromatic system. The addition of aliphatic copolymers to aromatic epoxies has been established to toughen

the DGEBA/mPDA system [15]-[17]. At low concentrations of aliphatic epoxy copolymer, the toughening can be done without detrimentally affecting other static-mechanical properties [18].

When applying any toughening approach, the composite properties need to be viewed as a whole. The optimization of a single property is usually fairly straightforward but may result in a reduction of other mechanical properties, e.g. increasing strength but decreasing toughness. This paper will identify a path to 'engineer' the interphase so that the toughness of the composite (Mode I fracture toughness) can be increased while not significantly reducing static-mechanical properties (flexural properties and glass transition temperature).

3.3 Materials and Methods

The aromatic epoxy, diglycidyl ether of bisphenol A (Epon 828, DGEBA), with an epoxy equivalent weight (EEW) of 185-195, was purchased from Hexion Inc. The di-functional aliphatic epoxy, polypropylene glycol diglycidyl ether (PDGE) with an EEW of 190 (Mn: 380) was purchased from Sigma-Aldrich. The curing agent meta-Phenylenediamine (mPDA) was purchased from Acros Organics. The structures of the epoxies and curing agent are shown in Figure 3.1. The ACS-grade 2-propanol (IPA) was purchased from J.T. Baker. All chemicals were used as received. The AS4-12k, unsized carbon fiber was purchased from Hexcel and was used either as-received or UV-ozone treated for 90s prior to use to further enhance the fiber surface (UVO-treated). Details on the UVO treatment have been published in other sources [2].

3.3.1 Single Fiber Sizing

A solution of 1wt% concentration of epoxy (aromatic or aliphatic) plus curing agent (mPDA) was made on the basis of total solution. The appropriate amount of epoxy was dissolved in IPA. Curing agent for a concentration of 9phr (60% of full stoichiometry) was dissolved in the epoxy/IPA solution. The sizing solution was mechanically stirred for 1h prior to use.

To size the fiber for the single-fiber fragmentation test (SFFT), the fiber tow was hand-dipped into the sizing solution for 10s. The excess solution was allowed to run off the tow before suspending the tow horizontally for drying. The fiber tow was dried in a convection oven for 3h at 60˚C to drive off residual solvent. Dog-bone specimens for the SFFT were made by suspending an individual carbon fiber in a silicone mold and surrounding it with DGEBA+14.5phr mPDA matrix material. The samples were then cured in a Precision Scientific EM18 mechanical convection oven at 75˚C for 2h and 125˚C for 2h. A rectangular cross-section was achieved by polishing the cured samples on a Stuers Abramin polisher with 320, 600, 1200 and 4000 grit polishing paper.

3.3.2 Adhesion-Interfacial Shear Strength

The fiber diameters were determined as an average of three measurements along the fiber length using an Olympus BH-2 optical microscope attached to an Olympus Cue-Micro 300 video caliper. The dog-bone samples were then mounted in a custom-built tensioning device with a Starrett dial gauge extensometer. The extension was increased at prescribed intervals and the number of fractures within a fixed length determined under polarized light. When the length of the fiber fragments becomes too

short to effectively transfer load from the matrix, the number of fractures will no longer increase with increasing stress (saturation point). The number of fractures was used to calculate the critical fracture length and interfacial shear strength using the following equations [19]:

$$\tau = \frac{\delta_f d}{2 l_c} \quad (2)$$

$$l_c = \frac{4}{3} l_{average} \quad (3)$$

where,

τ: Interfacial shear strength [MPa]

δ_f: Fiber tensile strength [MPa]

d: Fiber diameter [m]

l_c: Critical fiber length [m]

$l_{average}$: Average fiber length [m]

6 to 8 samples were measured for each composition. The birefringence pattern of the fiber fracture was characterized to determine the fracture type.

3.3.3 Fiber Tow Sizing

For the full composite, the sizing was applied to the fiber tow using a continuous fiber sizing tower system (Figure 3.2 & Figure 3.3). The fiber tow was drawn through the sizing bath containing the 1wt% epoxy/mPDA in IPA solution described above. The tow then passed through two drying towers that were at a temperature of 75˚C. The fiber tow pull speed was regulated at about 40 m/h. A recirculation system for the sizing solution was used to keep the epoxy concentration constant during the sizing operation.

After sizing, the fibers were dried at 60˚C for 3h in a convection oven to drive off residual IPA solvent.

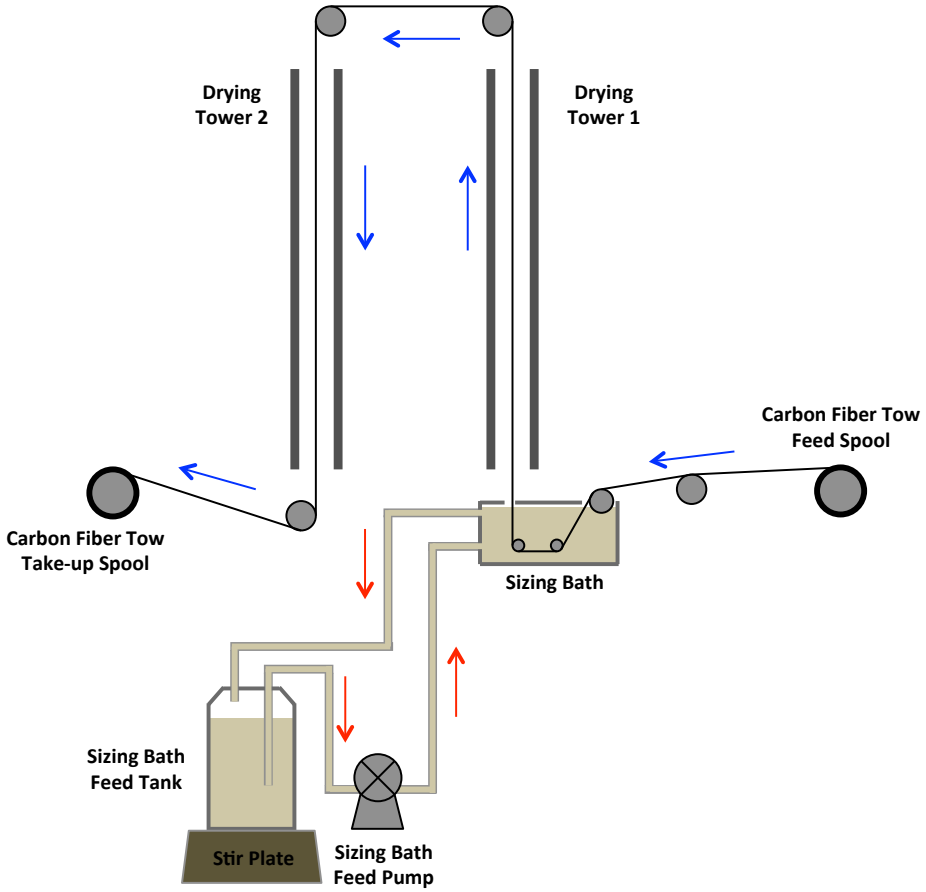

Figure 3.2: Schematic of fibersizing tower system with recirculation system for sizing solution

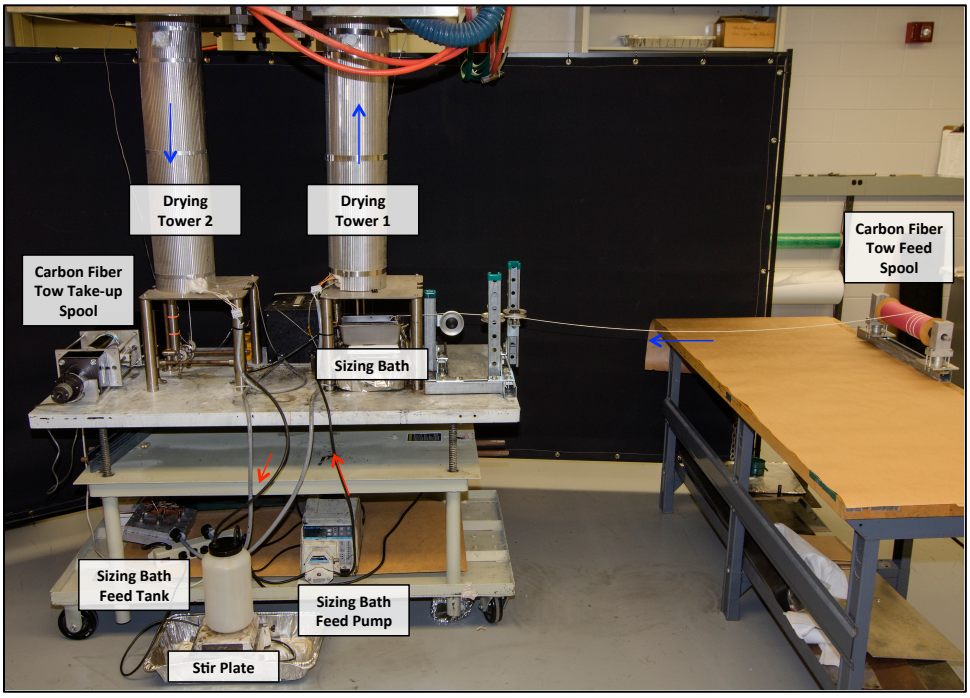

Figure 3.3: Photo of Fibersizing Tower System

The sizing mass was determined by measuring the differential mass of the fiber tow before and after an overnight soak in acetone under agitation and a drying for 3h at 60˚C. This determination was done for both hand and tower sized fiber tows.

3.3.4 Composite Prepregging

The sized fibers were processed into a pre-preg tape using a Research Tool Corporation Model 30 Research hot melt pre-pregger (Figure 3.4). The appropriate matrix material was prepared by weighing out the DGEBA. The stoichiometric amount (14.5phr) of mPDA curing agent was melted in a convection oven and mechanically mixed with the epoxy. Resin bath and other pre-pregger components were held at 107˚C to keep the viscosity of the matrix resin low during processing. The fiber tow was pulled through the resin bath at a speed of about 3.8 m/min and laid onto the pre-

pregger drum yielding a 1930x304mm pre-preg tape. Two pre-pregs were made from the sized fiber spool: one for Mode I fracture toughness (18-ply) and one for flexural and short beam shear samples (12-ply).

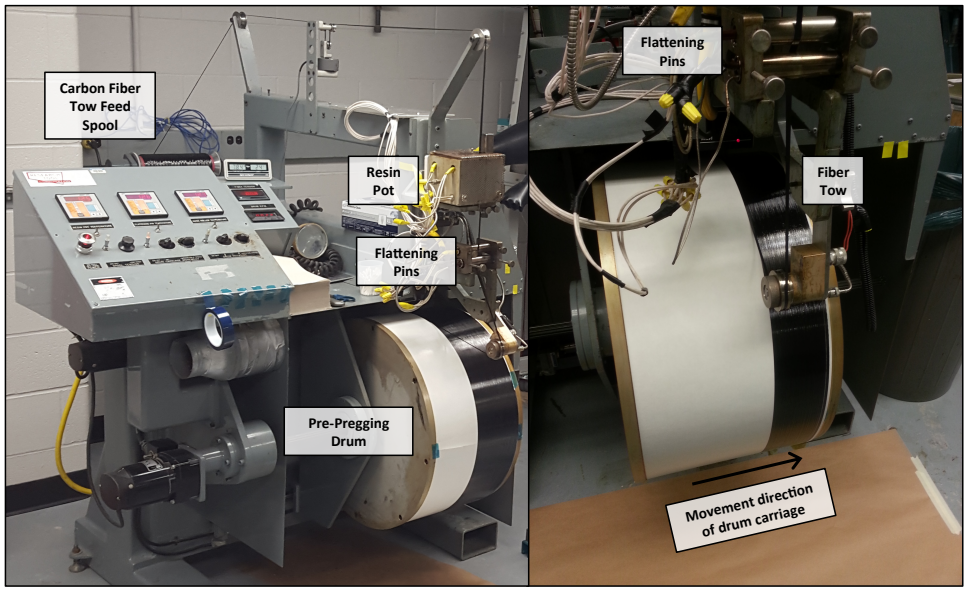

Figure 3.4: Research Tool Corporation Model 30 Research hot melt pre-pregger

3.3.5 Composite Mechanical Properties

For the Mode I fracture toughness samples the pre-preg tape was cut into 152 x 152mm plies and laid up as a unidirectional, 18-ply composite. On one end, a 55mm wide Teflon™ peel ply was inserted across the composite layup in the middle of the composite thickness between plies 9 and 10. This constitutes the starter crack for the Mode I fracture toughness samples. For the flexural and short beam shear samples, the pre-preg tape was cut into 304 x 152mm plies and laid up as a unidirectional, 12-ply composite. For both the 12- and 18-ply composites, the layup was sealed in a vacuum bag and processed in a United McGill Minibonder autoclave. (Figure 3.5) The thermal

cycle was 75˚C and 125˚C for 2h with ramp rates of 3˚C/min. The autoclave was pressurized to 5.8 atm during the thermal cycle. A vacuum of 0.82 atm was applied during the initial ramp up and 30 min into the 75˚C hold to remove any trapped gases. After that the vacuum bag was vented to atmospheric pressure. After cooling to room temperature the composite was cut into the appropriate sample sizes using a 41-AR Felker water-cooled tile saw.

Figure 3.5: United McGill Minibonder autoclave

All mechanical properties were measured on at least 4 samples. The flexural properties of both the 0˚ and 90˚ directions were determined on the basis of ASTM D790 using a United Testing Systems SFM-20 load frame with a 445 N (90˚ samples) or 4450 N (0˚ samples) load cell. The flexural samples had dimensions of 114x12.5x3 mm.

The support span width to thickness ratio was taken at 32:1 and the crosshead speed was calculated per ASTM D790. The Mode I fracture toughness was determined on the basis of ASTM D5528 using a United Testing Systems SFM-20 load frame with a 445 N load cell. The crosshead speed was 2 mm/min. The tests were recorded with a digital video camera and correlated to the load curve via time stamp. The crack propagation was measured using image-editing software (Adobe Photoshop CS6). The interlaminar shear strength was determined on the basis of ASTM D2344 using a United Testing Systems SFM-20 load frame with a 4450 N load cell. The composite density that was determined on the basis of ASTM D792. From the determined density, the fiber volume fraction was determined using the rule of mixtures and the nominal densities of matrix (1.20 g/cm^3) and carbon fiber (1.79 g/cm^3).

3.3.6 Glass Transition Temperature

The glass transition temperature, also called alpha-relaxation, was determined from the maximum of the Tan δ curve from a dynamic mechanical analysis (DMA) measurement done by single cantilever beam on a TA Instruments 800 instrument, with an amplitude of 20μm, a frequency of 1Hz, and a temperature ramp rate of 3˚C/min using samples with 90˚ fiber orientation.

3.3.7 Fracture Surfaces

The scanning electron microscopy investigation of the Mode I fracture surfaces were done using a Zeiss Auriga FIB SEM under high vacuum. The samples were sputter coated with a 1nm thick layer of tungsten prior to observation.

3.3.8 Surface Chemical Analysis

Surface analysis by XPS was conducted using a Physical Electronics PHI 5400 ESCA system. Samples were pumped to a pressure of less than 10^{-7} Torr and irradiated with a non-monochromatic Mg X-Ray with K-alpha 1,2 combined at an energy of 1254.6 eV. The take-off angle was 45 deg. Data analysis was performed using the Multipak version 8.0 by Physical Electronics.

3.4 Results and Discussion

3.4.1 Optimization of Composite Parameters Using Taguchi Design of Experiments Method

When faced with an experimental space of parameter combination, the issue arises how to most effectively take a systematic look. Even with a relatively small number of parameters, investigated at a small number of values (levels), the experimental effort becomes prohibitive due to cost and effort. For three parameters at three levels, an investigation of all possible combinations (full factorial design) requires 27 individual experiments (3^3 experiments). One approach to reducing the experimental effort is to use Design of Experiments (DOE) methodology. By designing the appropriate experiments, the whole design space can be investigated with a reduced

experimental effort. For this work, an orthogonal array first developed by Taguchi in the late 1970's was utilized. [20] Orthogonally refers to the fact that the properties can be evaluated independently of one another, provided that the experimental plan is balanced, meaning that here is the same number of samples under various experimental conditions. [21] A level 9, 3x3 Taguchi array was chosen to determine the composite parameters that would yield the maximum interfacial shear strength (IFSS) as determined by the single fiber fragmentation test. The three parameters chosen as critical for the IFSS were the curing agent stoichiometry of matrix and fibersizing as well as the concentration of DGEBA/mPDA in the sizing bath. Minitab 16 software was used to design the combinations for the nine experiments and analyze the results. The experimental combinations are shown in Table 3-1:

Table 3-1: Experimental combinations of L9, 3x3 Taguchi DOE for single fiber fragmentation test as determined by Minitab to optimize interfacial shear strength

Experiment Number	Matrix Stoichometry [phr]	Sizing Stoichiometry [phr]	DGEBA Concentration in Sizing Bath [wt%]
1	14.5	7.5	0.5
2	14.5	9	1
3	14.5	11	2
4	18	7.5	1
5	18	9	2
6	18	11	0.5
7	21	7.5	2
8	21	9	0.5
9	21	11	1

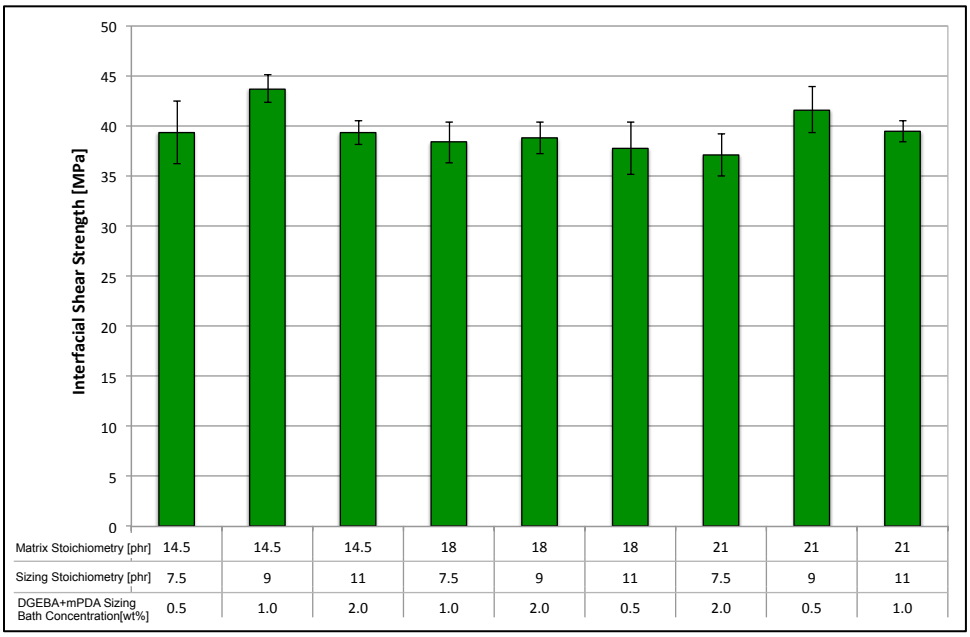

Figure 3.6: Interfacial shear strength of AS4, UVO-treated carbon fiber samples from level 9, 3x3 Taguchi DOE

The interfacial shear strength results from the Taguchi DOE experiments are shown in Figure 3.6 above. As the IFSS results show, the differences between most combinations are minor and in most cases the values are similar within the scatter of the data. The combination of 1wt% (DGEBA+9phr mPDA) sizing and 14.5phr matrix stoichiometry (experiment 2) is statistically higher than the other combinations. To deconvolute the influence of the individual parameters, the results from all of the nine experiments were evaluated using Minitab 16 software and the results are shown in Figure 3.7:

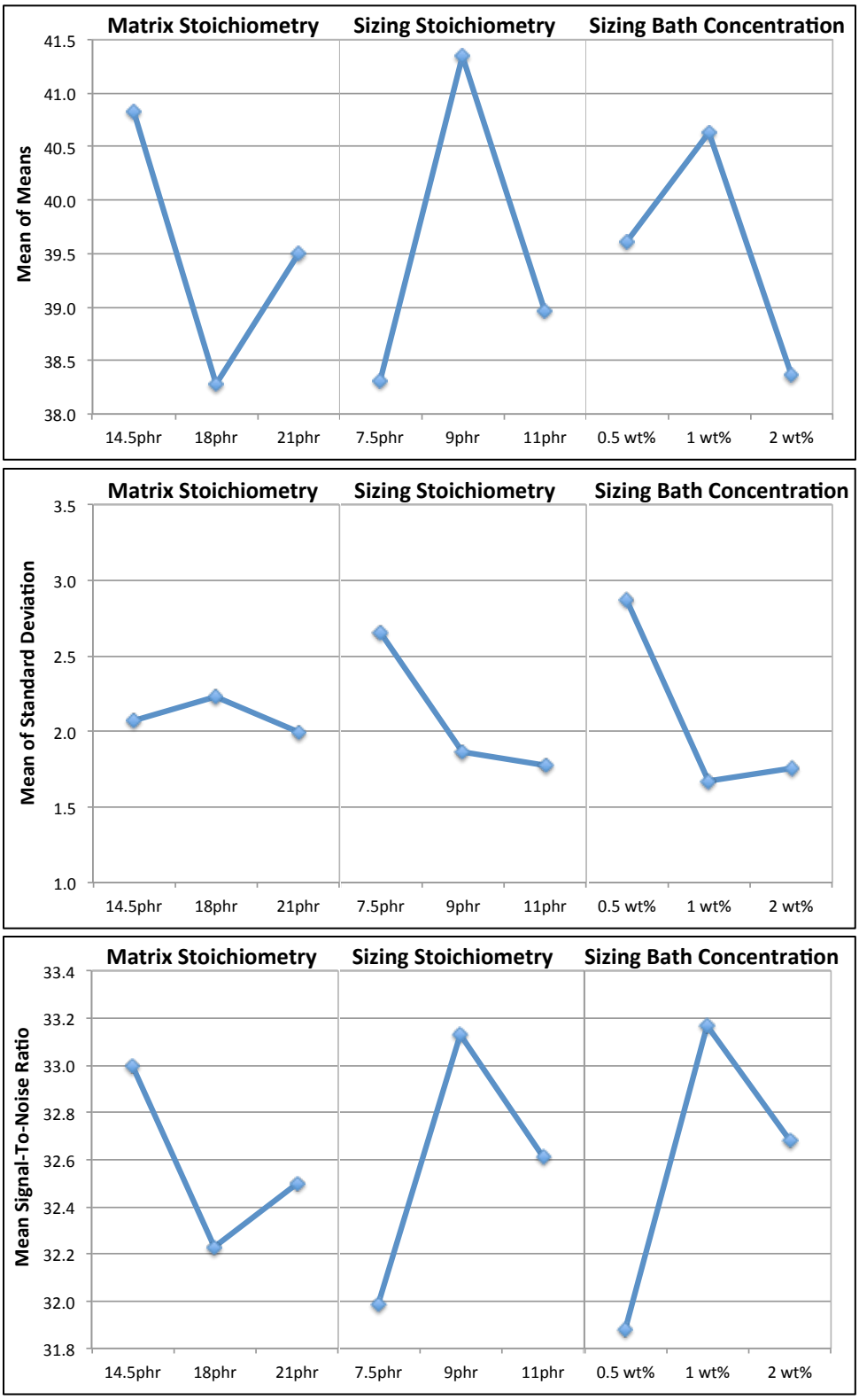

Figure 3.7: Effects plots of interfacial shear strength from Taguchi DOE. Top: mean of means, middle: mean of standard deviations, bottom: mean of signal-to-noise ratio

The top plot in Figure 3.7 shows the mean IFSS achieved in each experimental combination. The higher the mean value at each parameter is, the higher the influence on the IFSS will be. The results shown in Figure 3.6 are confirmed by, with the combination of 14.5phr matrix stoichiometry, 9phr sizing stoichiometry and 1wt% DGEBA/mPDA sizing bath concentration are the levels that yield the highest IFSS. The middle plot in Figure 3.7 shows the mean of standard deviation, which shows that the scatter of data at all parameters is at the lower end. Finally, the bottom plot of Figure 3.7 shows the mean of signal-to-noise ratio (SNR). A higher SNR indicates that the value of a parameter has a larger influence on the IFSS. For the purpose of maximizing the IFSS, the SNR values should be as high as possible. This again confirms the combination with the highest IFSS as shown in Figure 3.6.

The IFSS of the optimum combination, 1wt% (DGEBA+9phr mPDA) sizing and 14.5phr matrix stoichiometry, was tested in a follow-up SFFT experiments and was shown to be consistent and repeatable.

3.4.2 UVO-Surface Treatment

The concentration of oxygen, nitrogen and carbon as well as the identitiy of the surface oxygen groups on the surface of the AS4-12k carbon fiber before and after the 90s UVO treatment as determined by XPS is shown in Figure 3.8:

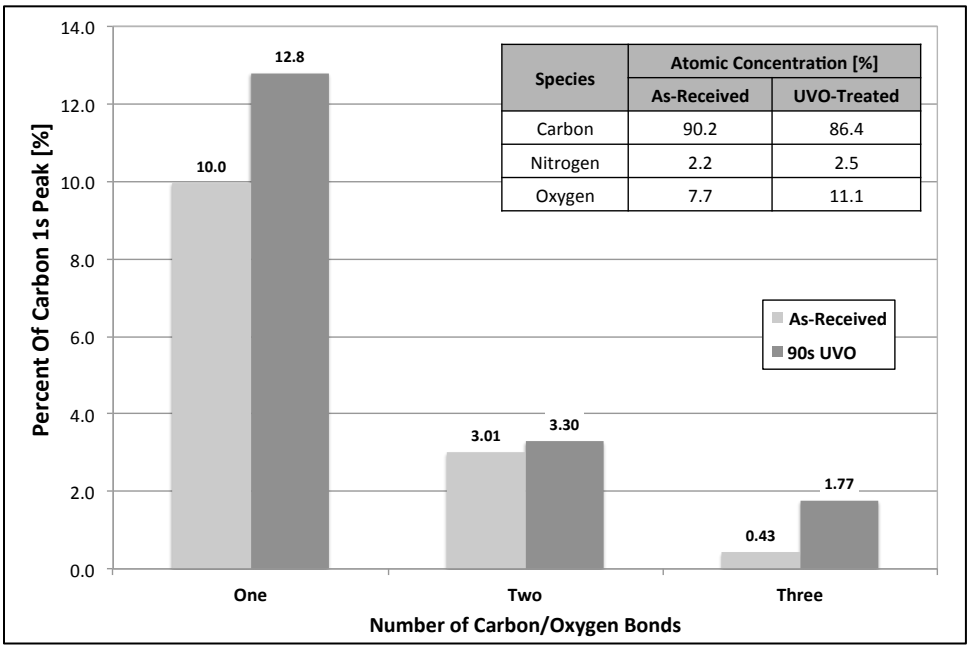

Figure 3.8: XPS analysis of atomic concentrations (table) and functional groups on surface of AS4-12k carbon fiber in as-received and 90s UV-ozone treated condition

Considerable changes are detected. The surface oxygen concentration is increased by about 45%, with an increase of about 17% in surface nitrogen. The surface oxygen groups have the ability to react with the matrix or sizing material, which should enhance the fiber/matrix adhesion. The nature of the surface oxygen groups is also essential, as the reactions of the oxygen groups with the epoxy groups or the amine groups on the curing agent will depend on the bonding state [6]. The XPS results shown in Figure 4 indicate a 29% increase in carbon atoms with one bond to oxygen atom (hydroxyl and ether groups), a 10% increase in carbon with two bonds to oxygen atoms (ketone and aldehyde groups) and a 312% increase in carbon with three bonds to oxygen atoms (carboxylic acid and ester groups).

3.4.3 Interfacial Shear Strength

The influence of fiber surface treatment and fiber sizing on the interfacial shear strength (IFSS) as determined by single-fiber fragmentation test is shown in Figure 3.9:

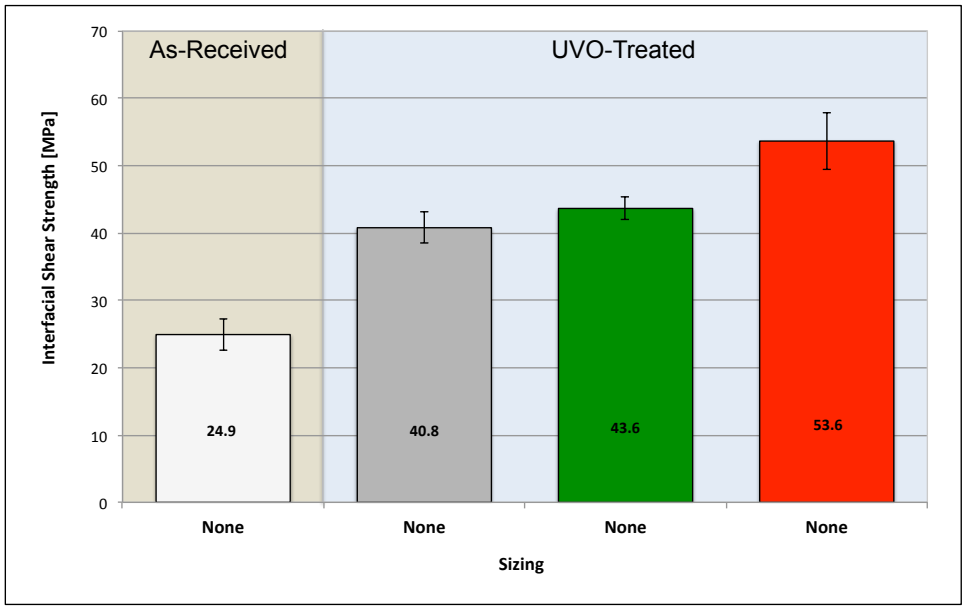

Figure 3.9: Interfacial shear strength of AS4 carbon fiber with different fiber surface treatments and fiber sizing as determined by single fiber fragmentation test

An increase of 64% in interfacial shear strength is seen when the fiber surface is treated via the UVO process. These results agree well with IFSS enhancements previously published [2], [22]. Since no sizing is present on these samples, the additional reactive oxygen groups and reduction of defects on the fiber surface are believed to be responsible for the increase in fiber/matrix adhesion [2], [4]. The addition of an aromatic fiber sizing to the UVO-treated fiber further enhances the IFSS by about 7%, which is 75% over the as-received baseline sample. The small enhancement of the IFSS from the aromatic fiber sizing may be rooted in the higher modulus of the under-stoichiometric sizing that is one of the factors affecting the fiber/matrix bond strength in the Cox equation, as explained in the introduction. As shown in Figure 3.10, the under-

stoichiometric epoxy/m-PDA mixture vitrifies during fiber sizing. When this sizing is immersed into the stoichiometric epoxy/m-PDA mixture, the sizing softens, swells and then starts to dissolve. Simultaneously m-PDA diffuses from the bulk toward the interphase. As the m-PDA reacts, diffusion slows and ultimately a gradient in modulus is formed which increase going towards the fiber surface. Experiments with DGEBA bulk matrix samples at varying mPDA stoichiometry have shown that the flexural modulus at 9phr mPDA stoichiometry is about 27% higher than at full stoichiometry of 14.5phr mPDA as also reported by Gupta *et al* [12].

A much larger increase in IFSS of 32% over that obtained with the UVO-treated, unsized fiber and 115% over the as-received, unsized fiber is achieved using the aliphatic fiber sizing. Again the Cox equation, states that the fiber/matrix bond strength is influenced mainly by the shear strain-to-failure and modulus as the fiber matrix interface. Since a significant different in modulus between the aromatic and aliphatic epoxy (3200 vs 8 MPa at full stoichiometry) would predict a lower fiber/matrix bond strength, the shear strain-to-failure appears to dominate the fiber/matrix bond strength in this case. Additionally, as the under-stoichiometric amount of curing agent is used during fiber sizing, allowing the sizing to swell and diffuse during curing, a concentration gradient of aliphatic epoxy at the fiber/matrix interface should be established (Figure 3.10). Toughening of this same aromatic epoxy/m-PDA with low concentrations of aliphatic epoxy, has been recently reported [18] and should enhance the IFSS.

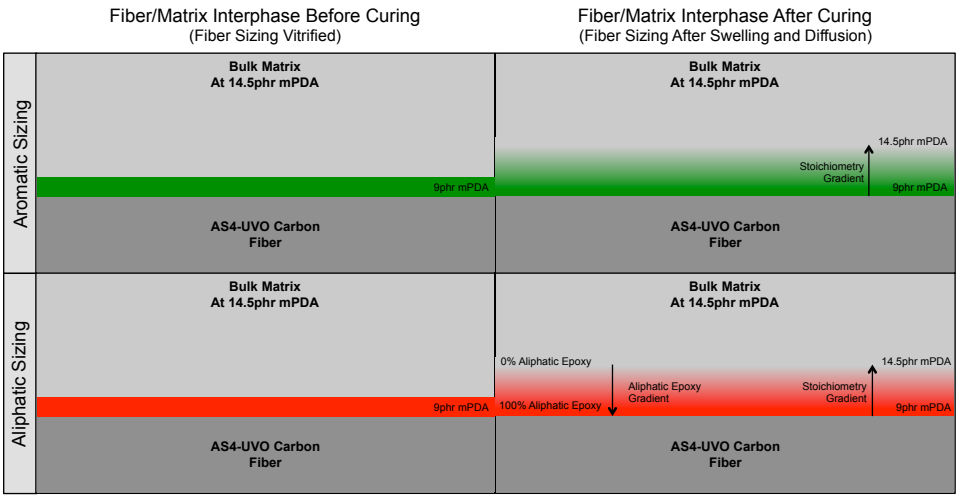

Figure 3.10: Schematic of swelling and diffusion of fiber sizing at 60% stoichiometry during composite curing. Aromatic sizing (top): Curing agent diffuses from bulk matrix to the fiber surface. Aliphatic sizing (bottom): Curing agent diffuses from bulk matrix to the fiber surface and aliphatic epoxy sizing will diffuse from fiber surface into bulk matrix

The IFSS results are supported by the birefringence patters from the single fiber fragmentation test as shown in Figure 3.11:

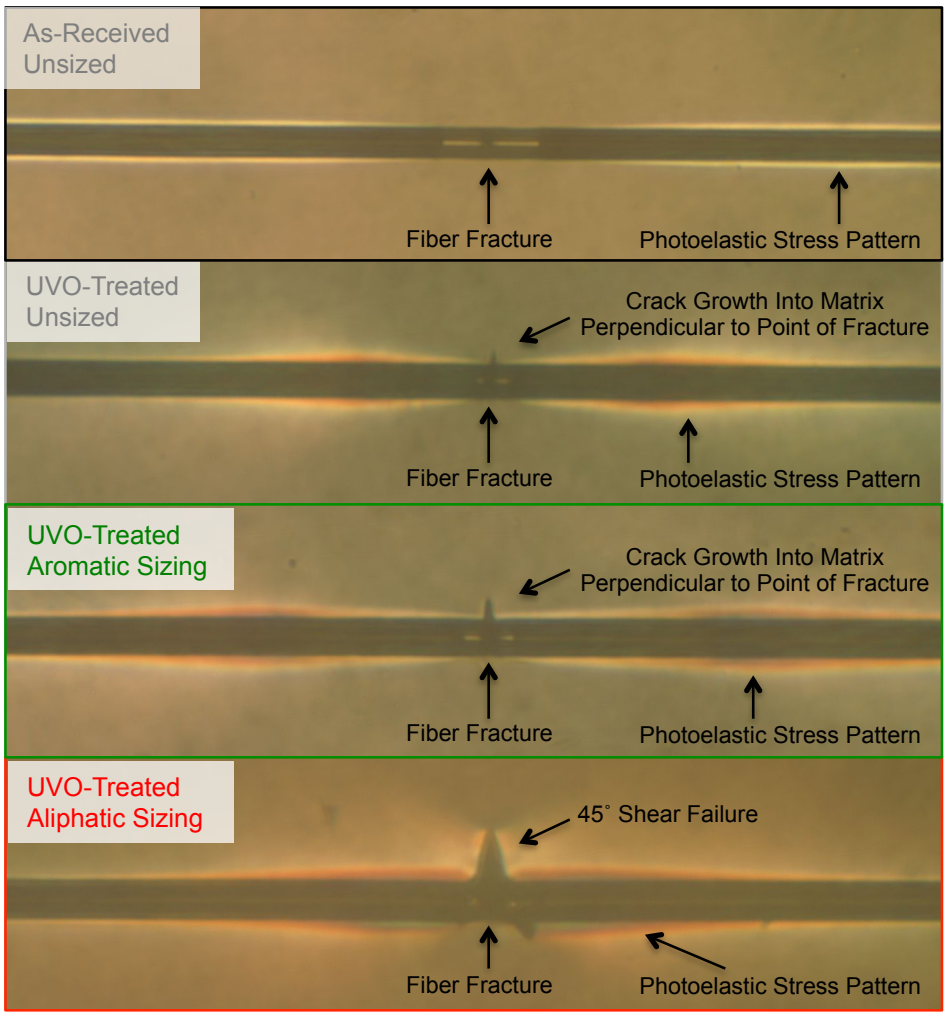

Figure 3.11: Birefringence patters with photoelastic stress patterns of AS4 carbon fiber with different fiber surface treatments and fiber sizing

The as-received fiber sample shows interfacial debonding emanating from the fiber break. This is a typical indication of low fiber/matrix adhesion. After fracture the debonded portion of the fiber slides inside the matrix rather than further transferring the applied load into the matrix. A clear change in birefringence pattern can be seen with UVO-treatment of the fiber. The fracture morphology has shifted to an intermediate strength failure. The photoelastic stress pattern is concentrated around the fiber fracture. Crack growth into the matrix is present which is an indicator of higher levels of load transfer that leads to perpendicular crack growth into the matrix at the point of fiber

fracture. Similar fracture morphology is seen with the addition of aromatic sizing. A more pronounced matrix crack is present as would be expected based on the slightly higher IFSS. The fracture morphology that is seen with the aliphatic fiber sizing is very different which is consistent with high levels of fiber/matrix adhesion. Shear failure at the 45˚ in the interphase is present, along with significantly larger matrix cracking. The photoelastic stress pattern is more intense and emanates from the ends of the fiber fracture. Based on the strong fiber/matrix adhesion, the failure mode has shifted from interfacial to matrix

3.4.4 Mechanical Properties of Full Composite

The fiber volume fraction (V_f) of the unidirectional fiber composites is shown in Figure 3.12:

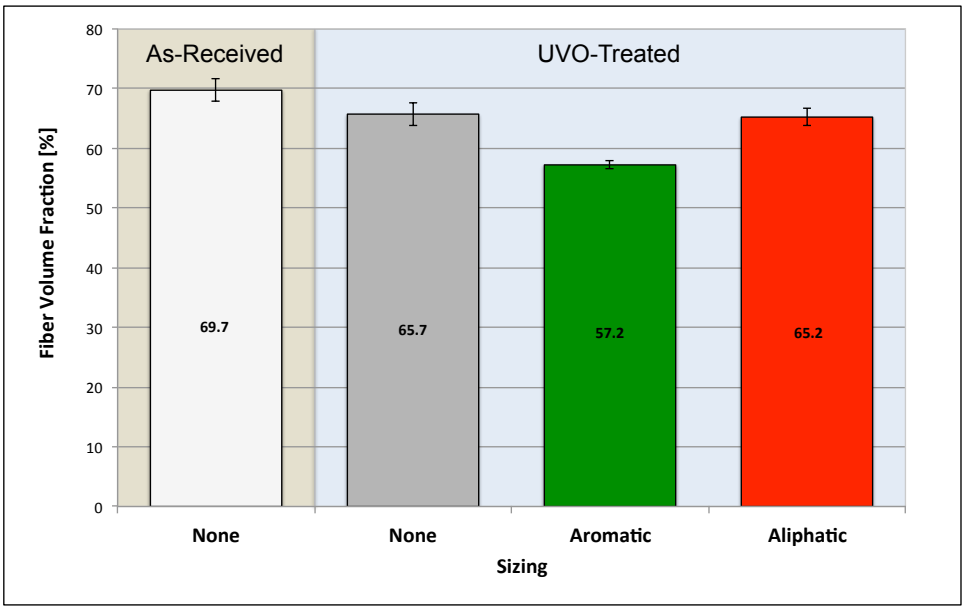

Figure 3.12: Fiber volume fraction of unidirectional AS4-12k carbon fiber composites with different fiber surface treatments and fiber sizing

The UVO-treated unsized, composites show a slightly lower (-6%) fiber volume fraction than the as-received, unsized composite. This may be due to the better fiber/matrix adhesion of the UVO-treated fibers as discussed above. The addition of the aromatic sizing to the UVO-treated fiber reduces the by about 13% over the UVO-treated, unsized composite. At a sizing level of 0.65wt%, the sizing thickness estimated on the basis of epoxy/mPDA density and nominal fiber surface area is 18nm, which would increase the apparent fiber diameter and fiber spacing. Larger spacing between the fibers would lead to a lower V_f as the fibers cannot be packed as tightly. The V_f of the UVO-treated, aliphatically sized composite is very similar (-1%) to the UVO-treated, unsized composite. Here the sizing level of 0.67wt% results in an estimated sizing thickness of 19nm. The fact that the aliphatic sizing at a similar sizing level and thickness does not seem to reduce the V_f as seen with the aromatic sizing may indicate that the aliphatic sizing swells and diffuses from the fiber surface at an earlier time in the consolidation processes than the aromatic sizing. If a majority of the aliphatic sizing has diffused away from the fiber surface before the matrix material has sufficiently vitrified, further consolidation could take place, reducing the inter-fiber spacing and increasing the fiber volume fraction.

To address the varying V_f of the different composites, all flexural and interlaminar shear strength properties were normalized to a V_f of 65%. The following equation was applied [23]:

$$Normalized\ Value = (Test\ Value) \times \frac{(FV_{Normalizing})}{(FV_{Speciment})} \quad (4)$$

where,

Normalized Value:	Test value adjusted for common fiber volume fraction
Test Value:	Measured test value
$FV_{Normalization}$:	Common fiber volume fraction [%]
$FV_{Speciment}$:	Actual fiber volume fraction [%]

This normalization is based on the concept that the mechanical properties of the composite lie somewhere between those of the matrix (V_f=0%) and those of the carbon fiber (V_f=100%). Over a range of fiber volume fractions above 50%, this dependence is expected to be linear [23] and the test values can be scaled according to Equation 4.

The void volume of all composites was determined from SEM micrographs using digital image editing software (Adobe Photoshop CS6). The void volume was well below the 1% threshold as has been established in the literature, below which no effect on mechanical properties is expected [24].

The flexural properties of the unidirectional composite were investigated in both the longitudinal (0˚) and the transverse (90˚) fiber direction. The longitudinal direction is dominated by the fiber properties, while the transverse direction is more sensitive to fiber/matrix adhesion. The flexural modulus, both longitudinal and transverse, is shown in Figure 3.13:

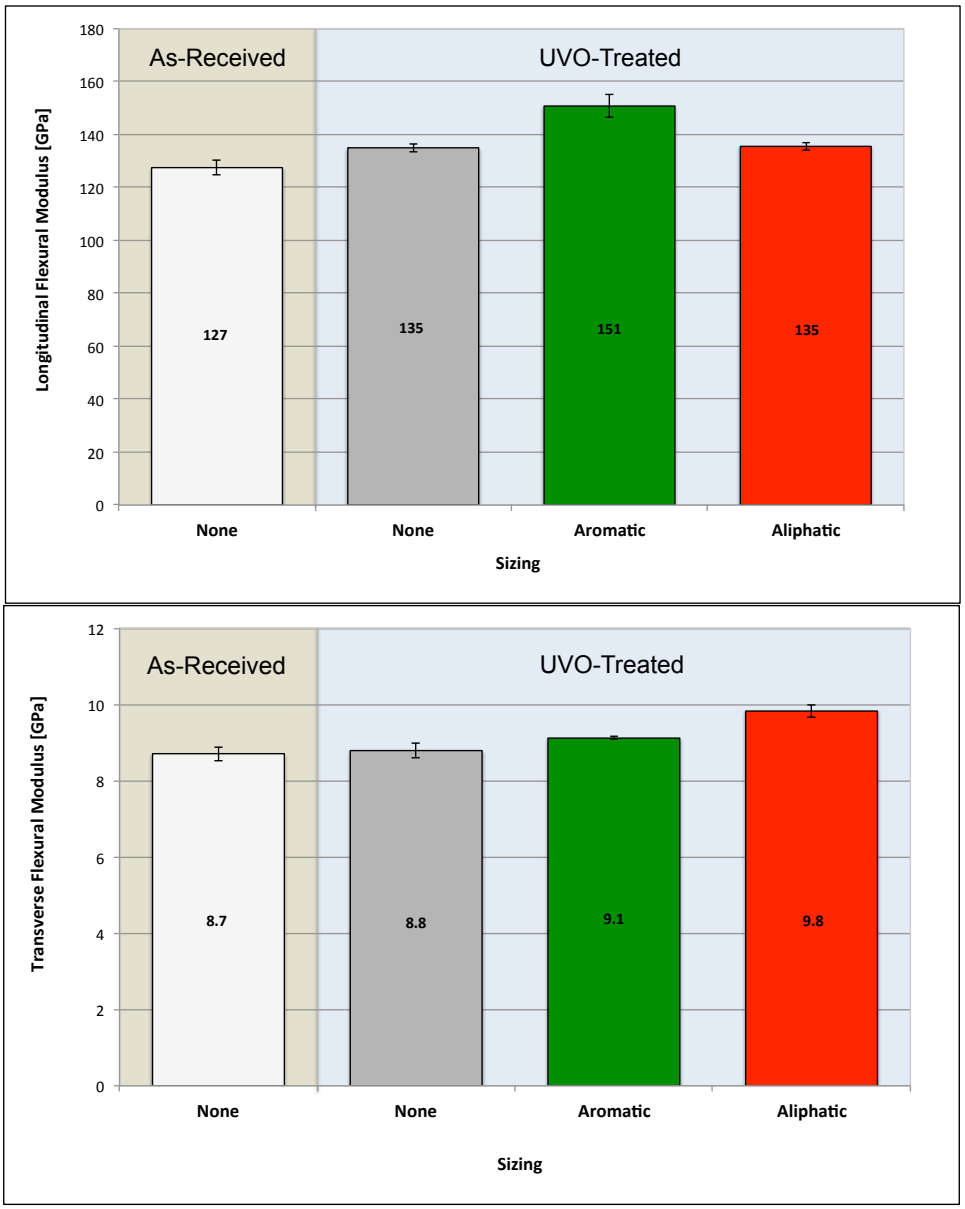

Figure 3.13: Flexural modulus (top: longitudinal; bottom: transverse) of unidirectional AS4-12k carbon fiber composites with different fiber surface treatments and fiber sizing

The longitudinal modulus for the unsized fiber composites is slightly higher for the UVO-treated fiber (+6%). This may be an indication of the improved fiber matrix adhesion. The aromatic sized, UVO-treated fiber composite shows a significant improvement over the UVO-treated unsized (+12%). As discussed in the section on the single fiber fragmentation test, the stiffer fiber/matrix interphase may be increasing the

global modulus of the composite. The improvement may also be somewhat inflated based on the normalization of the fiber volume fraction that is largest for the aromatic sized, UVO-treated fiber composite. The aliphatically sized UVO-treated fiber composite shows similar longitudinal flexural modulus to the UVO-treated unsized fiber. The transverse flexural modulus is similar for the unsized fiber composites both as-received and UVO-treated. Both of the UVO-treated, sized composites show higher transverse flexural modulus compared to the UVO-treated, unsized composite, +5% for the aromatic sized and +13% for the aliphatic sized composites. Both may indicate improved fiber/matrix adhesion.

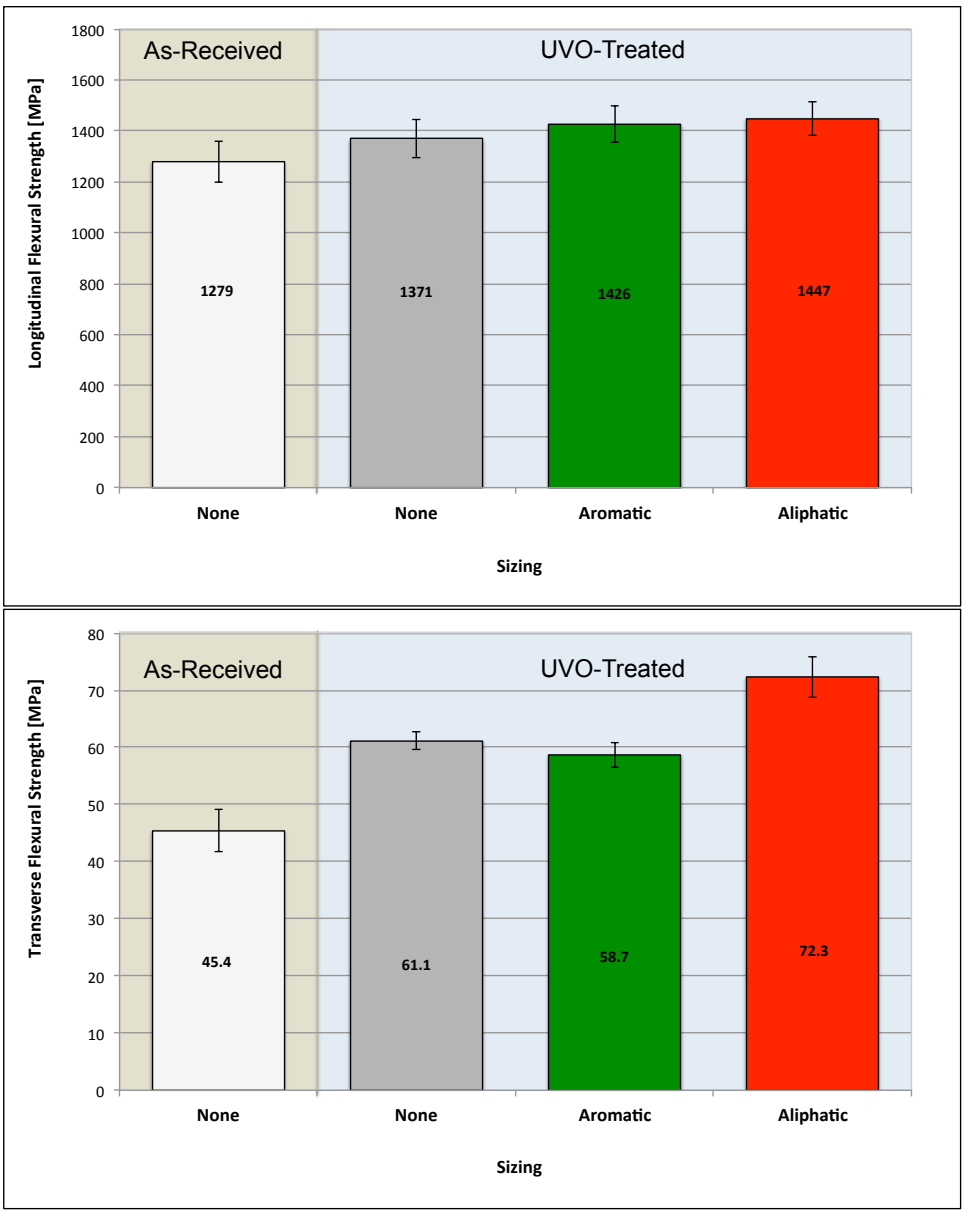

Figure 3.14: Flexural strength (top: longitudinal; bottom: transverse) of unidirectional AS4-12k carbon fiber composites with different fiber surface treatments and fiber sizing

The flexural strength, both longitudinal and transverse, is shown in Figure 3.14. In the longitudinal direction, which is dominated by the reinforcing fiber, the strength of the unsized fiber composites increase with UVO-treatment (+7%). Both of the sized fiber composites, have similar flexural strength, which are slightly above the UVO-treated, unsized composite (aromatic: +4%; aliphatic: +6%). Within error, the longitudinal flexural

strengths of all the UVO-treated fiber composites are similar. In the transverse direction, which is dominated by fiber/matrix adhesion, all the UVO-treated fiber composites show a significantly higher strength than the as-received fiber composite. For the unsized fiber composite the UVO-treated fiber has a 35% higher transverse strength. This further supports the interfacial shear strength results discussed in the previous section. The transverse strength of the aromatic sized fiber composite is slightly lower (-4%) compared to the UVO-treated, unsized fiber composite. However, the scatter of the two sample sets does overlap. The aliphatic sized fiber composite shows the greatest improvement in transverse strength with a 59% increase over the as-received baseline unsized fiber composite and 18% over the UVO-treated, unsized composite. This again supports the single fiber fragmentation results, that the enhanced strain to failure at the fiber matrix interface enhances the fiber/matrix bond strength.

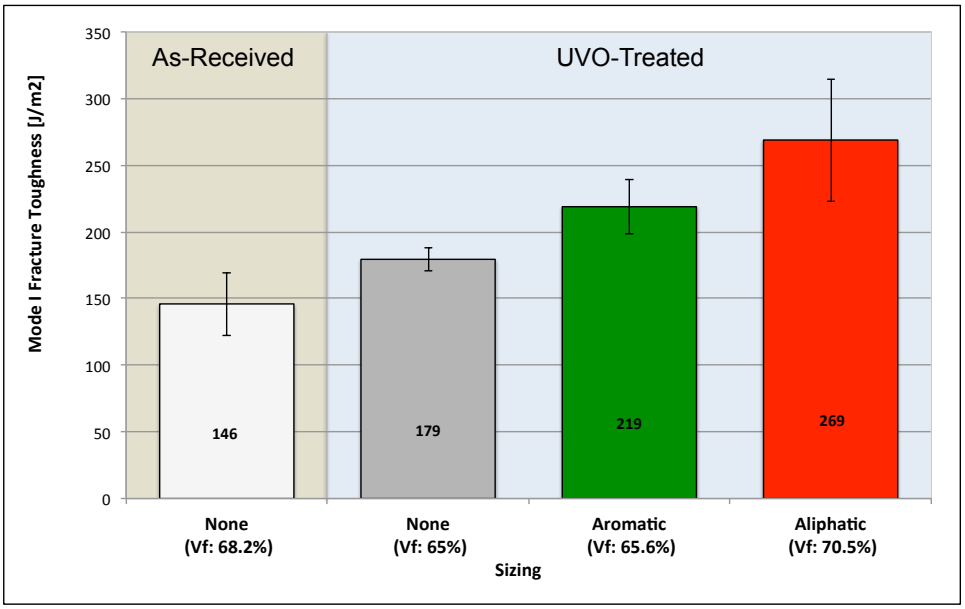

Figure 3.15: Mode I fracture toughness of unidirectional AS4-12k carbon fiber composites with different fiber surface treatments and fiber sizing

The improvements in fiber/matrix adhesion and their dependence on the surface treatment/sizing combination are clearly seen in the Mode I fracture toughness as shown in Figure 3.15. The UVO-treatment increases the Mode I fracture toughness by 23%, which can be attributed to the enhanced fiber/matrix adhesion. These results mirror the interfacial shear strength results but at a lower level, which is consistent as the IFSS represents an upper estimate of the fiber/matrix adhesion. The addition of aromatic fiber sizing further enhances the fracture toughness by 50% and the aliphatic sizing by 84% over the as-received, unsized fiber composite. The aromatic fiber sizing enhances the fiber/matrix adhesion due to the beneficial stoichiometry gradient as previously discussed. The enhancement due to the presence of the aliphatic sizing is probably due to the matrix toughening effect that has been previously discussed [18]. As the aliphatic sizing swells and diffuses away from the fiber a localized toughening of the matrix could take place, increasing the energy required to fracture the matrix during crack propagation.

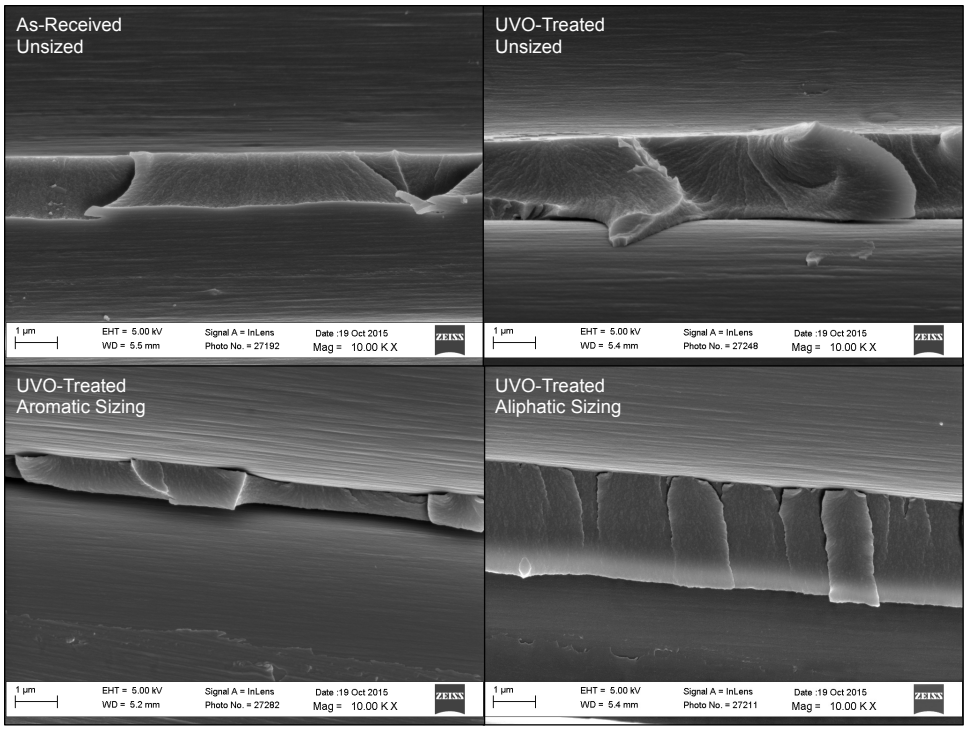

Figure 3.16: Scanning electron micrographs of Mode I fracture toughness fracture surfaces of unidirectional AS4-12k carbon fiber composites with different fiber surface treatments and fiber sizing. Direction of fracture is left to right across image

These results are supported by the scanning electron microscope images of the Mode I fracture surfaces shown in Figure 3.16. Both of the sized fiber composites (aromatic and aliphatic) show indications of residual matrix on the fiber surface (bottom of images) when compared to unsized fiber composites. When looking at the matrix area between the fibers, the fracture surface of the aliphatically sized fiber composite shows different fracture morphology compared to the other composites. The hackle pattern is finer and runs across the direction of fracture, indicating higher amounts of energy needed to fracture the matrix, in turn increasing the fracture toughness.

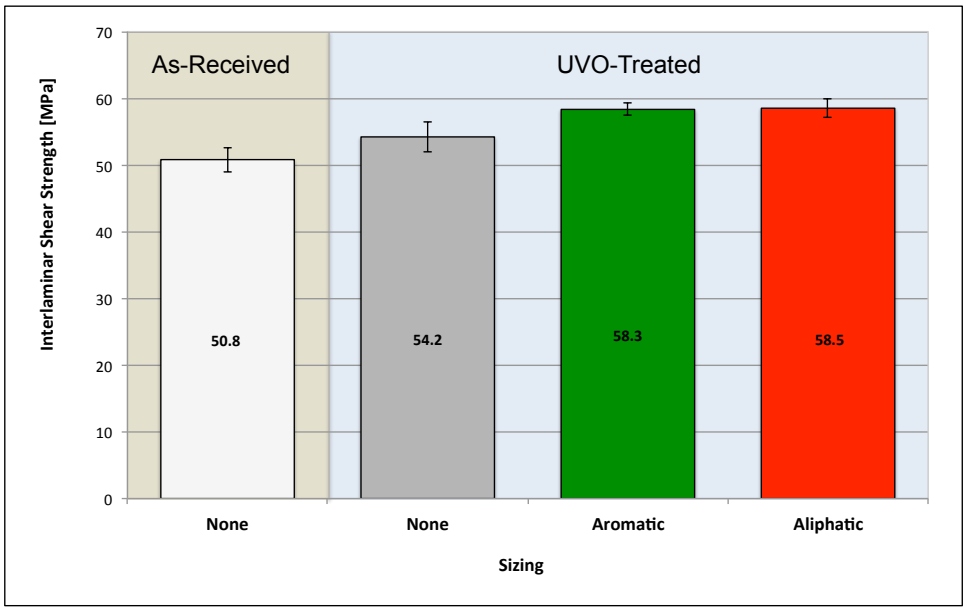

Figure 3.17: Interlaminar shear strength of unidirectional AS4-12k carbon fiber composites with different fiber surface treatments and fiber sizing as determined by the short beam shear test

The interlaminar shear strength (ILSS) as determined by the short beam shear test is shown in Figure 3.17. All samples failed in the same mode, by interlaminar shear between multiple plies. The unsized fiber composites, as-received and UVO-treated, have similar ILSS. The average value of the UVO-treated fiber composite is about 7% higher but the scatter of the data overlaps the error bars. Without any chemical modifications to fiber/matrix interface, similar ILSS of the samples would be expected. The ILSS of both of the sized fiber composites is the aromatic sized fiber composite is about 15% higher. This higher ILSS may be due to the modifications at the fiber/matrix interphase from the sizing. While not effecting the bulk matrix properties, the stoichiometry gradient of the aromatic sized composite and the toughening from the aliphatic sized composite may be enhancing the ILSS.

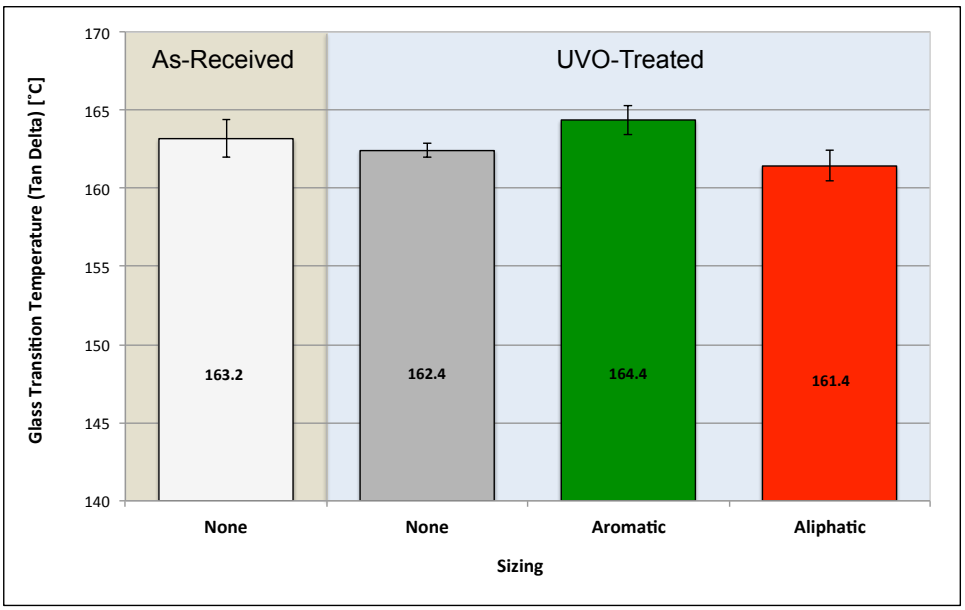

Figure 3.18: Glass transition temperature of unidirectional AS4-12k carbon fiber composites with different fiber surface treatments and fiber sizing as determined from the maximum of the Tan δ function from DMA

As shown in Figure 3.18, there is no significant influence of the fiber surface treatment and fiber sizing on the glass transition temperature (alpha-relaxation) as determined from the Tan δ function, with all differences being within 1%. Representative Tan δ curves from each composite are shown in Figure 3.19.

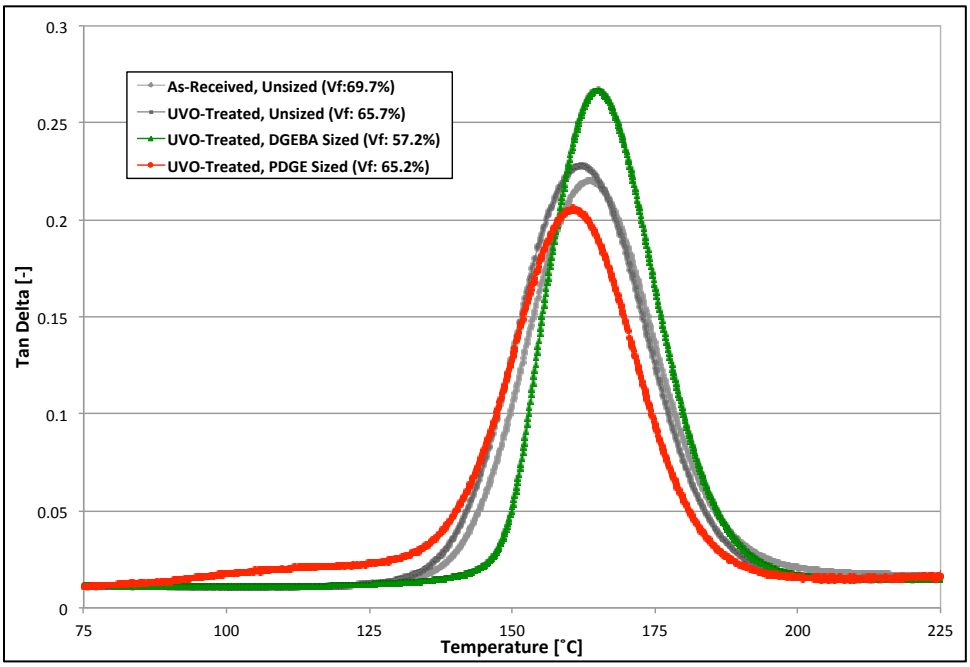

Figure 3.19: Tan δ function of unidirectional AS4-12k carbon fiber composites with different fiber surface treatments and fiber sizing as determined from DMA

Both unsized fiber composites (as-received and UVO) have similar peak heights, indicating similar dampening behaviors. The aromatic sized fiber composite shows the highest peak height. This may however be due to the lower fiber volume fraction. This is consistent with what has been reported in the literature, that a reduction in Tan δ peak height with increasing fiber volume fraction due to the greater restriction of polymer chain movement by the reinforcing fibers [3], [25], [26]. The aliphatically sized fiber composite shows two distinct features: first, it has the lowest peak height, indicating a more elastic response compared to the other composites. The lower modulus of the aliphatic sizing may be a contributing factor here; second, there is a shoulder that is formed at a lower temperature range (110-125˚C) that is not present in the other composites. This may be an indication of the beginning of the formation of a second

phase having a lower T_g. Based on the low modulus of the aliphatic epoxy sizing, this is probably in the vicinity of the fiber/matrix interface.

3.5 Conclusion

Interfacial engineering of the fiber-matrix interphase by optimizing the fiber surface treatment and sizing has been shown to be able to toughen carbon fiber-reinforced epoxy composites without significantly reducing other static-mechanical properties such as flexural properties and glass transition temperature, of the composites. Based on the enhancement of oxygen groups on the fiber surface, the UVO-treatment of AS4 carbon fiber shows significant increases (+23%) in Mode I fracture toughness due to better fiber/matrix adhesion. The addition of an epoxy fiber sizing increased the Mode I fracture toughness by 50% and 84% for aromatic and aliphatic epoxies respectively over the as-received, unsized fiber composite.

The influence of toughening the aromatic epoxy matrix of the composite with a 1wt% aliphatic epoxy copolymer will be discussed in an upcoming paper.

BIBLIOGRAPHY

BIBLIOGRAPHY

[1] U. S. EPA, OAR, O. O. T. A. A. Quality, and A. A. S. Division, “EPA and NHTSA Set Standards to Reduce Greenhouse Gases and Improve Fuel Economy for Model Years 2017-2025 Cars and Light Trucks,” pp. 1–10, Aug. 2012.

[2] M. J. Rich, E. Drown, P. Askeland, and L. T. Drzal, “Surface Treatment Of Carbon Fibers By Ultraviolet Light+Ozone: Its Effect On Fiber Surface Area And Topography,” *The 19th International Conference On Composite Materials*, pp. 1196–1204, Jul. 2013.

[3] S. Dong and R. Gauvin, “Application of dynamic mechanical analysis for the study of the interfacial region in carbon fiber/epoxy composite materials,” *Polym. Compos.*, vol. 14, no. 5, pp. 414–420, 1993.

[4] M. S. Madhukar and L. T. Drzal, “Fiber-matrix adhesion and its effect on composite mechanical properties: I. Inplane and interlaminar shear behavior of graphite/epoxy composites,” *Journal of Composite Materials*, vol. 25, pp. 932–957, 1991.

[5] M. Sharma, S. Gao, E. Mäder, H. Sharma, L. Y. Wei, and J. Bijwe, “Composites Science and Technology,” *Composites Science and Technology*, vol. 102, no. C, pp. 35–50, Oct. 2014.

[6] L. G. Tang and J. L. Kardos, “A review of methods for improving the interfacial adhesion between carbon fiber and polymer matrix,” *Polym. Compos.*, vol. 18, no. 1, pp. 100–113, Feb. 1997.

[7] L. T. Drzal, M. J. Rich, M. F. Koenig, and P. F. Lloyd, “Adhesion of graphite fibers to epoxy matrices: II. The effect of fiber finish,” *The Journal of Adhesion*, vol. 16, pp. 133–152, 1983.

[8] Z. Dai, F. Shi, B. Zhang, M. Li, and Z. Zhang, “Applied Surface Science,” *Applied Surface Science*, vol. 257, no. 15, pp. 6980–6985, May 2011.

[9] H. L. Cox, “The elasticity and strength of paper and other fibrous materials,” *British Journal of Applied Physics*, vol. 3, no. 3, pp. 72–79, Mar. 1952.

[10] P. S. Theocaris, *The Mesophase Concept in Composites*, 1st ed. New York: Springer Science & Business Media, 1987.

[11] T. F. Cooke, “High Performance Fiber Composites with Special Emphasis on the Interface A Review of the Literature,” *Journal of Polymer Engineering*, vol. 7, no. 3, pp. 197–254, 1987.

[12] V. B. Gupta, L. T. Drzal, C. C. Lee, and M. J. Rich, “The temperature-dependence of some mechanical properties of a cured epoxy resin system,” *Polym Eng Sci*, vol. 25, no. 13, pp. 812–823, 1985.

[13] T. Kamae and L. T. Drzal, “Composites: Part A,” *Composites Part A*, vol. 43, no. 9, pp. 1569–1577, Sep. 2012.

[14] W. Qin, F. Vautard, L. T. Drzal, and J. Yu, “Mechanical and electrical properties of carbon fiber composites with incorporation of graphene nanoplatelets at the fiber–matrix interphase,” *Composites Part B: Engineering*, vol. 69, pp. 335–341, Feb. 2015.

[15] C. H. Zhang, H. G. Wei, Y. Y. Liu, H. F. Tan, and Z. Guo, “Enhanced toughness and shape memory behaviors of toughed epoxy resin,” *High Performance Polymers*, vol. 24, no. 8, pp. 702–709, Nov. 2012.

[16] T. Misaki, T. Hirohata, M. Yoshii, and T. Hamasaki, “Properties of networks obtained by internal plasticization of epoxy resin with aromatic and aliphatic glycidyl compounds,” *J. Appl. Polym. Sci.*, vol. 37, no. 9, pp. 2617–2625, 1989.

[17] S.-J. Park, T.-J. Kim, and J.-R. Lee, “Cure behavior of diglycidylether of bisphenol A/trimethylolpropane triglycidylether epoxy blends initiated by thermal latent catalyst,” *J. Polym. Sci. B Polym. Phys.*, vol. 38, pp. 2114–2123, Aug. 2000.

[18] M. A. Downey and L. T. Drzal, “Toughening of aromatic epoxy via aliphatic epoxy copolymers,” *Polymer*, vol. 55, no. 26, pp. 6658–6663, Dec. 2014.

[19] L. T. Drzal, M. J. Rich, and P. F. Lloyd, “Adhesion of Graphite Fibers to Epoxy Matrices: I. The Role of Fiber Surface Treatment,” *J Adhes*, vol. 16, no. 1, pp. 1–30, Jan. 1983.

[20] D. R. Cox and N. Reid, “Chapter 6: Factorial designs: further topics,” in *The Theory of the Design of Experiments*, no. 6, CRC Press, 2000, pp. 1–42.

[21] P. Ross, *Taguchi Techniques for Quality Engineering: Loss Function, Orthogonal Experiments, Parameter and Tolerance Design*, 1st ed. New York: McGraw-Hill, 1988.

[22] J. Li, “Interfacial studies on the O3 modified carbon fiber-reinforced polyamide 6 composites,” *Applied Surface Science*, vol. 255, no. 5, pp. 2822–2824, Dec. 2008.

[23] Handbook-MIL-HDBK, *17-1F: Composite Materials Handbook, Volume 1- Polymer Matrix Composites: Guidelines for Characterization of Structural Materials*. Department of Defence, 2002.

[24] K. Friedrich, S. Fakirov, and Z. Zhang, *Polymer Composites*. Springer, 2005.

[25] D. Romanzini, A. Lavoratti, H. L. Ornaghi Jr, S. C. Amico, and A. J. Zattera, “Influence of fiber content on the mechanical and dynamic mechanical properties of glass/ramie polymer composites,” *Materials and Design*, vol. 47, no. C, pp. 9–15, May 2013.

[26] M. Idicula, S. K. Malhotra, K. Joseph, and S. Thomas, “Dynamic mechanical analysis of randomly oriented intimately mixed short banana/sisal hybrid fibre reinforced polyester composites,” *Composites Science and Technology*, vol. 65, no. 7, pp. 1077–1087, Jun. 2005.

Chapter 4: Toughed Carbon Fiber-Reinforced Aromatic Epoxy Polymer Composite Matrices Using Low Concentrations of Aliphatic Copolymers

4.1 Abstract

This chapter demonstrates an approach to enhancing the toughness of aromatic epoxy matrix based carbon fiber-reinforced composites using 1wt% addition of aliphatic epoxy copolymer. As discussed in Chapter 2, this toughening approach has been shown to greatly improve (up to 60%) the impact toughness of the diglicidyl ether of bisphenol A/ meta-phenylenediamine (DGEBA/mPDA) base matrix without detrimentally affecting other static-mechanical properties. The influence of the UVO fiber surface treatment as well as the aromatic and aliphatic fiber sizing, which were discussed in Chapter 3, on the toughening potential of 1wt% aliphatically toughened aromatic matrix are investigated. The aliphatic toughening of the matrix is shown to improve the Mode I fracture toughness of the composite in most cases. The magnitude of increase is dependent on the initial toughness of the composite, i.e. toughness using a neat DGEBA matrix: at low initial toughness (as-received, unsized fiber) the increase is 35%, at intermediate initial toughness (UVO-treated, unsized and UVO-treated, aromatic sized fiber) the increase is 13 to 17%. At high toughness (UVO-treated, aliphatic sized) a reduction of the fracture toughness is seen (-30%). The high effectiveness of the matrix toughening at low initial toughness is attributed to the higher toughness of the matrix, which requires more energy for fracture and would play a more dominant roll in the low toughness system. As fiber/matrix bonding improves with UVO fiber surface treatment and aromatic fiber sizing, the strength of the fiber/matrix bond contributes

more to the fracture toughness and the improved toughness of the 1wt% aliphatic toughened matrix is not as important. The reduction in fracture toughness for the UVO-treated, aliphatically sized fiber composite is due to the changed diffusion behavior of the aliphatic sizing when aliphatic copolymer is added to the matrix. Less diffusion of the aliphatic copolymer from the fiber surface will result in an interphase that has a lower modulus and higher amount of cure shrinkage. The result is a reduction of the fracture toughness and transverse flexural properties, which are fiber dominated.

4.2 Introduction

The reduction of vehicle weight is becoming the focus of many industries in the transportation sector, including the aerospace and automotive industries, in an effort to improve fuel efficiency and reduce emissions. Modern airliners, such as the Boeing 787 and Airbus A350, are being made with increasingly larger percentages of composites materials. The automotive industry is looking to lightweighting approaches using carbon fiber-reinforced composite to meet the US EPA CAFÉ standards by 2025. [1]

Carbon fiber-reinforced composites usually consist of two major components: First, the reinforcing fiber, which is the load bearing component; second is the epoxy matrix that holds the carbon fibers together, transfers the applied load between the fibers and gives the part its final shape. An important, but often overlooked third component, is the fiber-matrix interphase which consists of a fiber surface treatment and a very thin 30-100 nm sizing (coating) applied to the fiber for adhesion enhancement and fiber handling purposes. Good fiber/matrix adhesion is needed to yield a tough composite. [2] In Chapter 3, the impact of fiber surface treatment and

epoxy fibersizing, both aromatic and aliphatic, was discussed. This current chapter focuses on toughening the aromatic matrix of the composite by the addition of low concentrations of a di-functional aliphatic copolymer. The impact of the aliphatic matrix toughening approach in conjunction with different fiber surface treatments, UVO-treatment and epoxy fiber sizing both aromatic and aliphatic, is examined.

The use of aliphatic epoxy copolymers has traditionally been as viscosity reducers for better processing. [3] Compared to the aromatic epoxy like DGEBA with a ridged and bulky backbone containing, the more flexible backbone of the aliphatic epoxy should be able to absorb more energy when cross-linked into the network. This could increase the amount of energy absorbed by the network prior to fracture. As shown in Figure 4.1 both the aromatic (DGBEA) and aliphatic (PDGE) epoxies are di-functional and will undergo the same reaction with the curing agent during network formation.

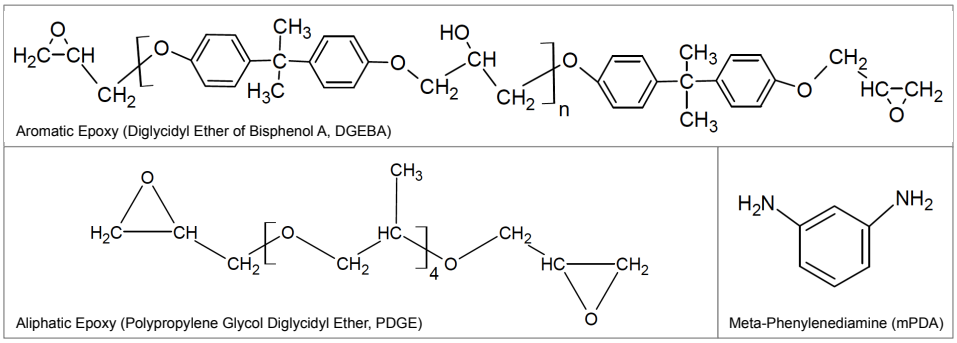

Figure 4.1: Structure of aromatic and aliphatic epoxies as well as curing agent

The toughening of aromatic epoxies using di- and tri-functional aliphatic epoxies has been shown a number of studies. Most of the studies looked at high concentrations of aliphatic copolymers (~10 to 100wt%). [4]-[6] While considerable increases in toughness (70 to 120%) were achieved, they were associated with reductions in static-mechanical properties, such as flexural modulus (30 to 40%) and glass transition

temperature (up to 65%), both of with are important when a composite is considered for structural applications. Low concentrations (1wt%) of aliphatic copolymers have also been shown to substantially improve the impact toughness (~60%) of the DGEBA/mPDA system, without detrimentally affecting the static-mechanical properties. [7] These properties were discussed in Chapter 2.

With any toughening approach, the composite properties need to be viewed as a whole. The optimization of a single property, in this work toughness, is usually fairly straightforward but may cause a reduction of other mechanical properties, e.g. reducing static strength. This paper will discuss the promising effects of toughening the composite matrix with 1wt% aliphatic copolymer in conjunction with a novel fiber surface treatment and fiber sizing without significant reductions of the other composite mechanical properties. Curing kinetics and cure shrinkage of the aromatic and aliphatic epoxies and their mixtures are also discussed.

4.3 Materials and Methods

Materials, sample production and testing procedures are identical to those listed in Chapter 3.2, with the only difference being in the preparation of the 1wt% aliphatically toughened matrix, which is described below.

A disruption in the supply of the curing agent meta-Phenylenediamine (mPDA) at Sigma-Aldrich necessitated the change to procuring the mPDA from Acros Organics. To check the influence of the change in curing agent supplier on the mechanical properties of the base matrix, both neat and 1wt% toughened, a large number of tests were

conducted. Mechanical properties, as well as ASTM specifications or test methods on bases of which tests were conducted are shown in Table 4-1:

Table 4-1: Testing methods or ASTM specifications on basis of which mechanical properties of base matrix both neat and 1wt% aliphatically toughened were determined

Property	Test Method or ASTM Specification
Flexural	D 790
Glass Transition Temperature	Dynamic Mechanical Analyser (DMA)
Noched Izod Impact Strength	D 256
Fracture Toughness	D 5045
Strain Energy Release Rate	D 5045
Compression Strength (0.2% Offset)	D 695
Linear Coefficient of Thermal Exansion	Thermalmechanical Analyzer (TMA)

4.4 Production of Aliphatically Toughened Matrix

The toughened matrix was prepared by blending 1wt% of aliphatic epoxy copolymer into the aromatic epoxy. The epoxy blend was mixed with a magnetic stir bar while heating to about 70˚C until homogeneous (~15min). The stoichiometric amount (14.5phr) of mPDA curing agent was melted in a convection oven and mechanically mixed with the epoxy blend.

4.4.1 Curing Kinetics of Aromatic and Aliphatic Epoxy Cured with mPDA Curing Agent

Differential scanning calorimetry (DSC) was used to evaluate the curing kinetics of the aromatic and aliphatic epoxy as well as the mixtures of the two epoxies. A TA Instruments model Q2000 DSC was operated in isothermal mode at 75˚C. Uncured samples of epoxy and curing agent were prepared by the methods previously described. Aliquots of 8-9mg were placed in hermetically sealed DSC pans, ramped (15˚C/min) to the curing temperature of 75˚C and held there for 5h.

4.4.2 Determination of Cure Shrinkage

The shrinkage of the epoxy blends (neat and 1wt% aliphatically toughened at 14.5phr mPDA), aromatic and aliphatic fiber sizing (9phr mPDA) resins, as well as several mixtures of aromatic and aliphatic epoxies to cover the concentration range for fiber sizing, was determined using a Micromeritics AccuPyc II gas pycnometer. A similar method has been previously described by Schoch *et al.* [8] The empty volumes of disposable 3.3cc sample cups were determined, giving each cup a distinct identity. The mass of each cup was measured with an analytical balance. The epoxy and the appropriate ratio of mPDA curing agent was weight out using 14.5phr for the standard matrix compositions and 9phr for the fiber sizing composition. Following melting in a convection oven at 75˚C, the curing agent was homogenized by hand in the heated epoxy and degassed for about 5min until all entrained air was released. The 3.3cc sample cup was filled up to about 1mm below the rim and again degassed to eliminate air bubbles. The mass of the liquid epoxy/curing agent sample was determined and the sample was placed in the measurement chamber of the pycnometer. The volume of the sample was determined over 20 cycles. The liquid sample was then removed from the pycnometer, placed into a pre-heated convection oven and cured at the standard curing cycle of 75˚C and 125˚C for 2h each. After cooling to room temperature, the mass of the cured samples was determined and the samples were re-measured in the pycnometer. The volume of the sample and cup was again determined over 20 cycles. The unstable volume data from the first 5 cycles was discarded and final 15 measurements were averaged to determine the sample volume. The volume of the 3.3cc sample cup, which

was previously determined, was subtracted from each average value. The amount of cure shrinkage was calculated using the following equation:

$$Cure\ Shrinkage = \left(1 - \left(\frac{V_{Cured\ Sample+Cup} - V_{Cup}}{V_{Liquid\ Sample+Cup} - V_{Cup}}\right)\right) * 100 \qquad (1)$$

Three samples of each composition were measured to determine the average and standard deviation.

The main limitation of this approach is that the pycnometer is only able to determine the volumes at ambient temperatures; hence no in-situ measurement of shrinkage during curing is possible. [9]

4.5 Results and Discussion

4.5.1 Mechanical Properties of Neat and 1wt% Aliphatically Toughened Matrix

The toughening behavior of di- and tri-functional aliphatic epoxies up to 20wt% was discussed in Chapter 2. At a concentration of 1wt% of di-functional aliphatic epoxy, a significant increase (~56%) in notched Izod impact toughness was seen without reducing other static-mechanical properties. Based on these results, this concentration was chosen to toughen the matrix of the high-fiber volume fraction composite.

The results are shown Table 4-2 and the results normalized to the value of the neat matrix are shown in Figure 4.2:

Table 4-2: Mechanical and static-mechanical properties of neat DGEBA and 1wt% aliphatically toughened matrix

Property	Neat DGEBA	DGEBA+ 1wt% Aliphatic
Flexural Modulus [MPa]	3160 +/- 14	3152 +/- 44
Flexural Strength [MPa]	125 +/- 0.2	124 +/- 2
Glass Transition Temperature [˚C]	156.5 +/- 1.0	155.7 +/- 0.8
Noched Izod Impact Strength [J/m]	28.3 +/- 3.8	34 +/- 1.6
Fracture Toughness [MPa/m^0.5]	1.45 +/- 0.26	1.51 +/- 0.26
Strain Energy Release Rate [J/m^2]	407 +/- 91	369 +/- 81
Compression Strength (0.2% Offset) [MPa]	59.5 +/- 3.7	56.1 +/- 1.8
Linear Coefficient of Thermal Exansion Below Tg [µm/(m*˚C)]	76.3 +/- 0.4	76.5 +/- 2.4
Linear Coefficient of Thermal Exansion Above Tg [µm/(m*˚C)]	174 +/- 2.2	170.7 +/- 2.9

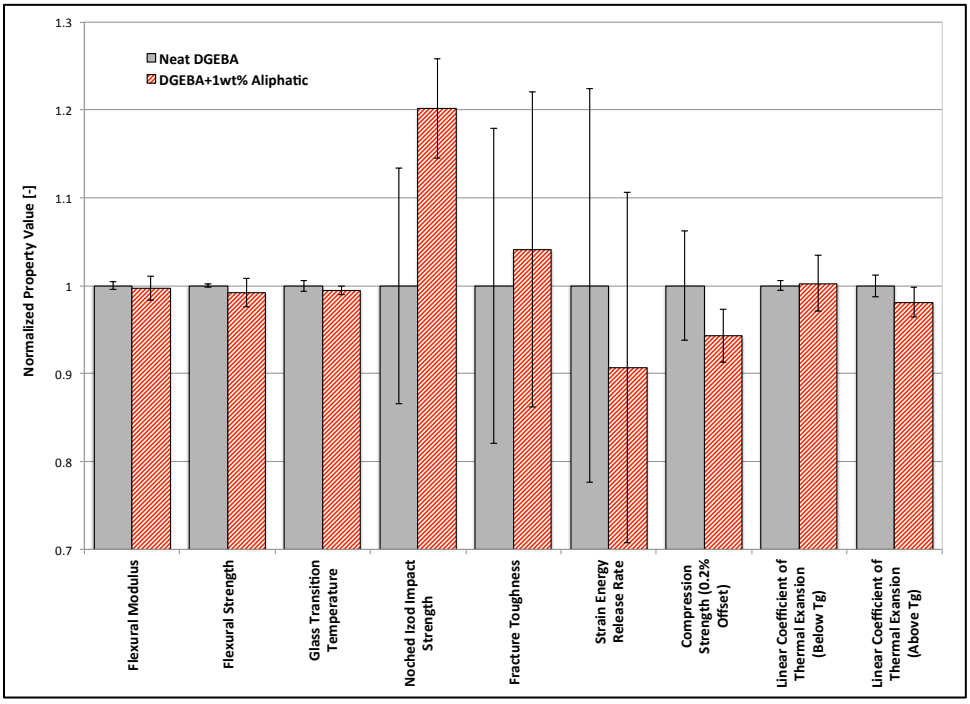

Figure 4.2: Mechanical and static-mechanical properties of neat DGEBA (solid grey) and 1wt% aliphatically toughened matrix (red hatched). Property values are normalized to value of neat DGEBA

As can be seen in Figure 4.2, almost all of the mechanical properties of the neat and 1wt% toughened matrices are statistically equivalent. While strain energy release rate, compressive strength and thermal expansion above T_g are lower for the toughened matrix, the scatter of the measurements makes them statistically the same. The exception is the notched Izod impact strength, which is 20% higher for the toughened

matrix. This is consistent with the results presented in Chapter 2. However, the enhancement in notch Izod impact strength is lower than was previously determined. The Acros Organics mPDA appears to yield a higher base notched Izod impact toughness for the neat matrix than the Sigma Aldrich mPDA. With the value of the 1wt% toughened matrix staying statistically equivalent, the higher impact toughness of the baseline reduces the effectiveness of the toughening at 1wt% di-functional aliphatic. A comparison of the two matrices cure with the different mPDA suppliers is show in Figure 4.3:

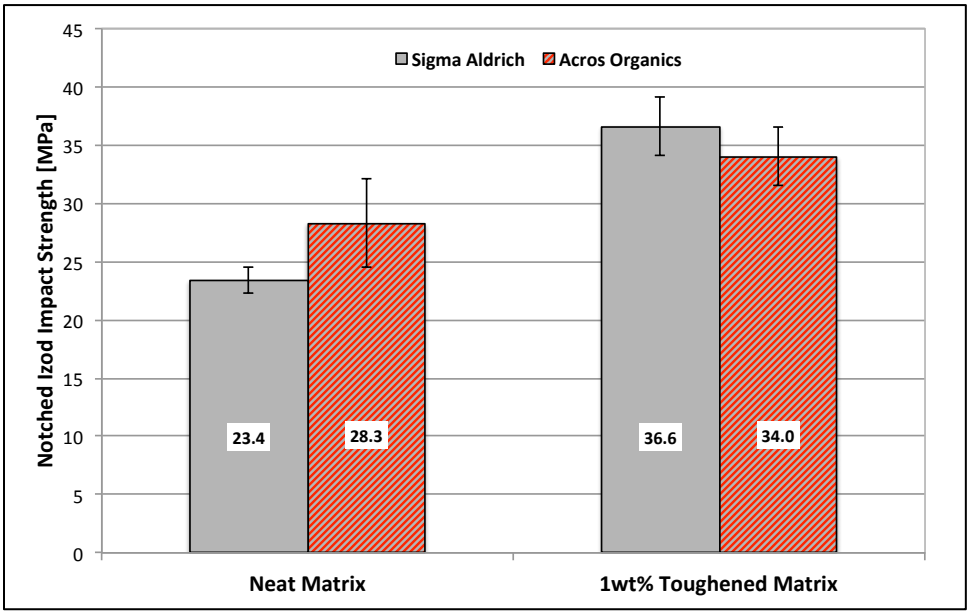

Figure 4.3: Comparison of neat and 1wt% toughened matrices cured with Sigma Aldrich (gray) and Acros Organics (hashed) meta-Phenylenediamine

The main reason behind this higher baseline toughness may be rooted in the higher amount of ortho- and para-Phenylenediamine (o-PDA & p-PDA) that is allowed in the Acros Organics mPDA. For o-PDA and p-PDA these values are 100ppm and 200ppm for the Acros Organics and 26ppm and 29ppm for the Sigma Aldrich mPDA. P-PDA has a melting temperature of about 137˚C, while m-PDA has a melting

temperature of about 66˚C. This is supported by the slightly higher glass transition temperature of the Sigma Aldrich and Acros Organics mPDA cured neat and toughened matrix samples. The T_g of the neat and toughened matrix samples is shown in Figure 4.4:

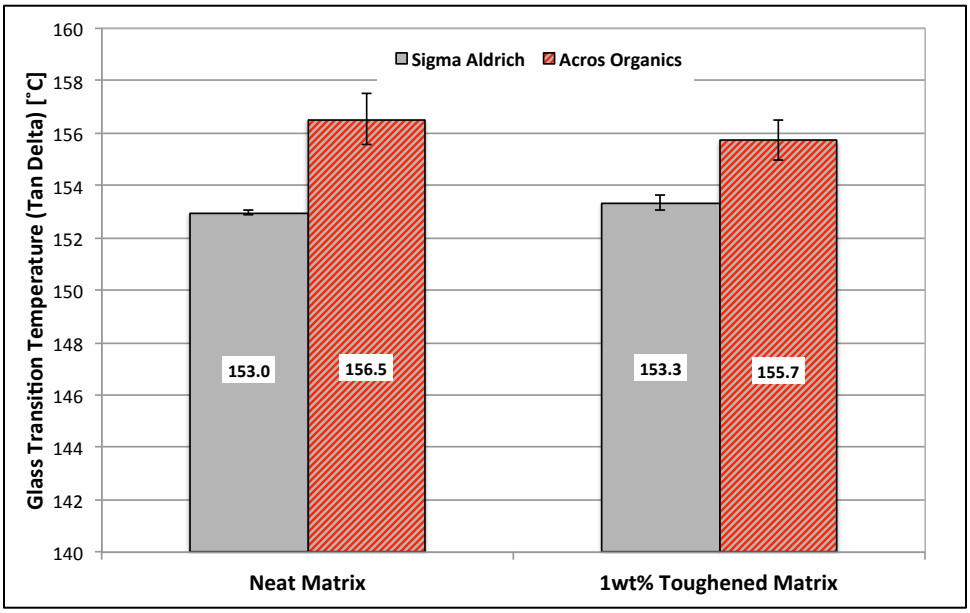

Figure 4.4: Glass transition temperature determined from the maximum of the Tan δ peak from DMA measurements (Frequency: 1Hz; amplitude: 20μm) of neat and 1wt% aliphatically toughened matrix samples cured with Sigma Aldrich (gray) and Acro Organics (hashed) mPDA

Additional, the difference orientation of the amine groups on the benzene ring relative to each other could influence the mechanical properties of the DGEBA/mPDA network. Krunoskin showed that the gel time of an diglycidyl ether epoxy cured with Phenylenediamine decreased in the order of ortho > meta > para, indicating that p-PDA had a higher reactivity than m-PDA. [10] Other factors such as surface coatings or surfactant additions may also play a roll but according to Acros Organics, no other additives are present in the mPDA. The smaller increase in notched Izod impact strength with the Acros Organics mPDA may limit the enhancement of toughness in the

high fiber volume fraction composite that can be achieved with the 1wt% aliphatic addition.

4.5.2 Composite Production and Handling

The process of manufacturing the toughened matrix composite was the same in every respect to the process of manufacturing composites with the neat matrix. The epoxies were found to be fully miscible and readily formed transparent mixtures. No additional production parameters needed to be adjusted for the toughened matrix.

4.5.3 Curing Kinetics of Aromatic and Aliphatic Epoxy Cured with mPDA Curing Agent

While being held at 75˚C for 5h, the liquid epoxy/curing agent mixtures undergo crosslinking by an exothermic reaction. The heat flow into the sample pan to maintain the constant 75˚C temperature was monitored. The speed of the reaction kinetics in an isothermal DSC scan is related to the time at which the maximum reaction isotherm occurs. Slower reaction kinetics are indicated by a reaction exotherm at a later time in the curing cycle [11], [12]. The results of the isothermal DSC scans of the two sizing compositions are shown in Figure 4.5 and those of the two matrix material compositions are shown in Figure 4.6.

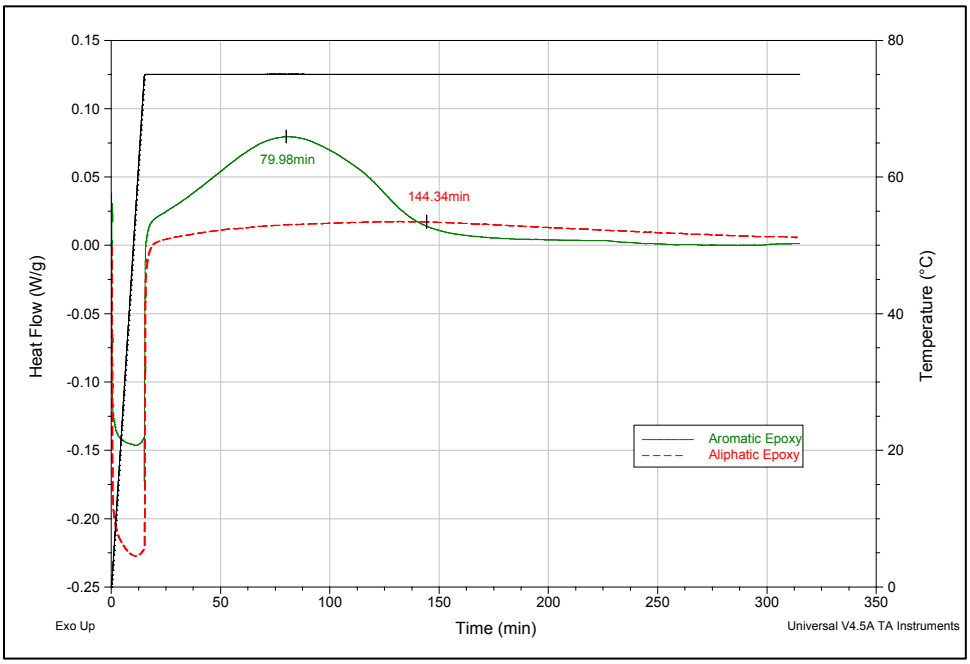

Figure 4.5: Isothermal DSC scans at 75˚C for 5h of aromatic and aliphatic epoxy at 9phr mPDA curing agent concentration (sizing composition)

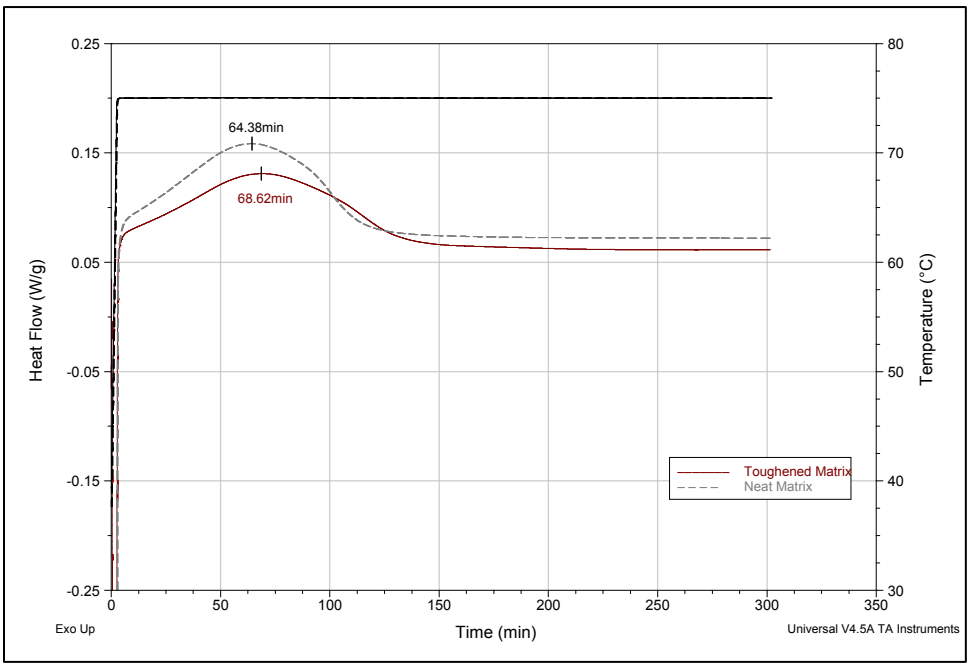

Figure 4.6: Isothermal DSC scans at 75˚C for 5h of neat DGEBA matrix and DGEBA+1wt% aliphatic matrix at 14.5phr mPDA curing agent concentration (matrix composition)

The two compositions used for the matrix, DGEBA+14.5phr mPDA and DGEBA+1wt% PDGE+14.5phr mPDA, show maximum reaction exotherm at similar times in the isothermal scan (Figure 4.5). The toughened matrix material has a reaction exotherm about 7% later (68.2 vs 64.4 min), indicating slightly slower reaction kinetics; however, the decreased reaction kinetics is not expected to have a significant effect on matrix properties. Based on the results of the pure aliphatic epoxy (Figure 4.6), the slower reaction kinetics is attributed to the 1wt% addition of aliphatic epoxy to the DGEBA epoxy. The pure epoxies used for fiber sizing show maximum reaction exotherm at different times in the isothermal DSC scan (Figure 4.6). The aliphatic epoxy has a reaction exotherm that is about 80% later than the aromatic epoxy (80 vs 144 min). This indicates that the aliphatic epoxy has slower reaction kinetics that the aromatic epoxy. This implicates that the aliphatic epoxy will stay mobile longer as the system is cured, potentially into the 125˚C post cure.

4.5.4 Cure Shrinkage of Epoxies at Matrix and Sizing Compositions

The curing process of the epoxy/amine system was discussed in Chapter 1.4. The epoxy/amine system undergoes shrinkage during the curing process, due to the conversion of Van der Waals bonds to shorter but stronger covalent bonds. [13] This shrinkage could have significant influence of the properties of a high fiber volume fraction composite due to the restriction of the polymer between the fibers. The results of the cure shrinkage study, for the matrix compositions is shown in Figure 4.7:

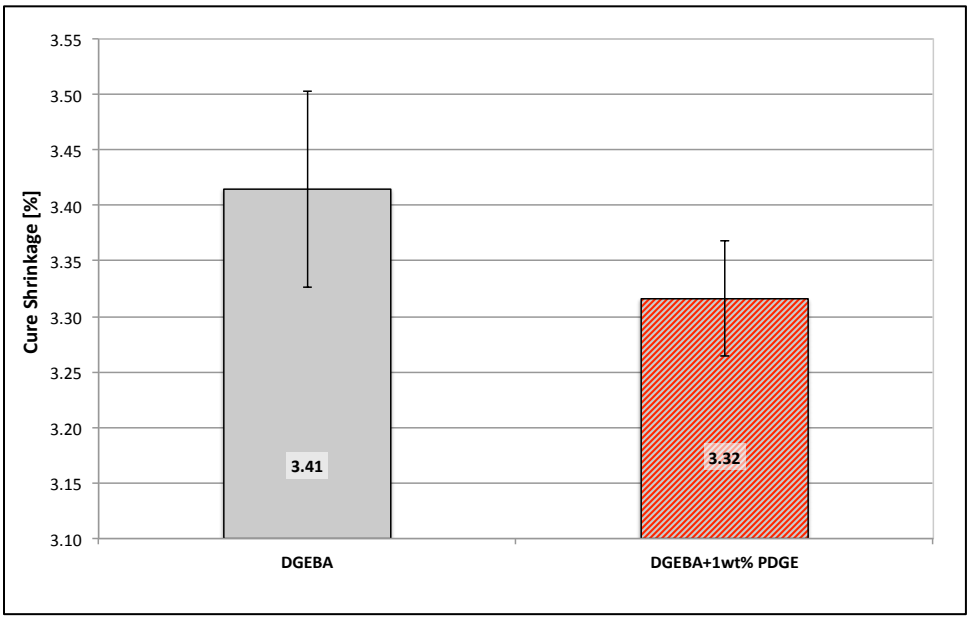

Figure 4.7: Cure shrinkage of neat and 1wt% aliphatically toughened aromatic epoxy at 14.5phr mPDA used as matrix in high fiber volume fraction composites

The cure shrinkage behavior of the neat and 1wt% aliphatically toughened matrices are similar at around 3.4%. This value agrees well with those published in literature for the DGEBA/mPDA system. [14] [8] While the 1wt% aliphatically toughened matrix shows 3% lower cure shrinkage compared to the neat matrix, the change is within the scatter of the data. The small concentration of aliphatic epoxy, which is homogeneously distributed in the matrix, does not appear to significantly influence the cure shrinkage. This implies that no significant differences in mechanical properties based on the cure shrinkage are expected in the high fiber volume composite.

The cure shrinkage behavior of the pure aromatic and aliphatic epoxies as well as mixtures of the two epoxies at 60% stoichiometry (9phr) are presented in Figure 4.8:

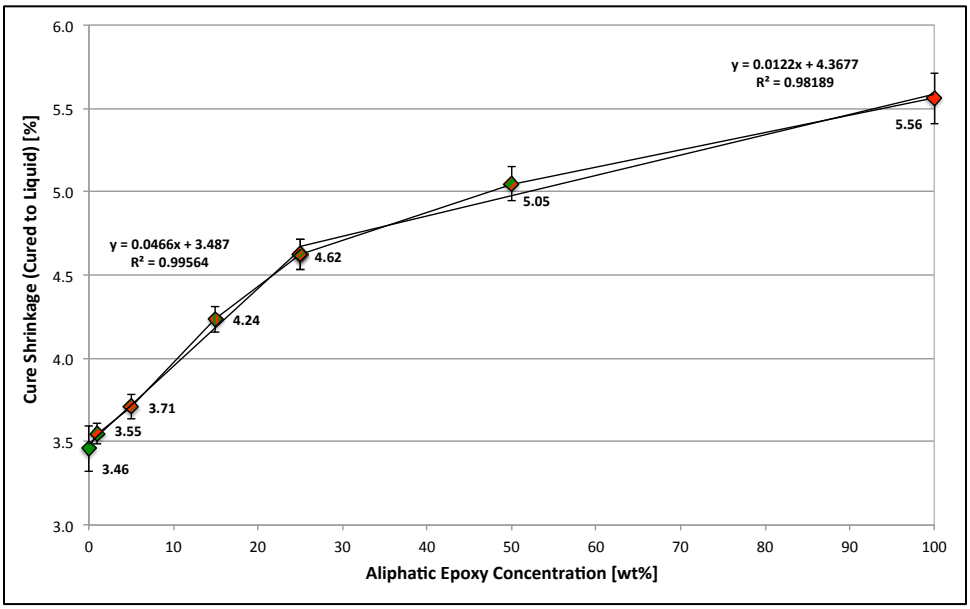

Figure 4.8: Cure shrinkage of aromatic and aliphatic epoxy as well as their mixtures at 9phr mPDA (60% stoichiometry) as used for fiber sizing in high fiber volume fraction composite

The pure aromatic epoxy at 60% stoichiometry (sizing composition) shows similar cure shrinkage to that of the aromatic epoxy at 100% stoichiometry (matrix composition). In fact the values are within the scatter of the measurements. This implies that there should be little difference in shrinkage between the matrix and the fiber sizing during composite consolidation. The cure shrinkage rapidly increases with the addition of aliphatic copolymer. As shown in Figure 4.8, there is a linear increase in cure shrinkage up to 25wt% aliphatic epoxy. Above 25wt% the increase is also linear but with less slope. In the aliphatic concentration range of 5wt% and above, the averages are statistically different. This implies that that small increases in the concentration of aliphatic copolymer could lead to higher shrinkage and higher stresses at the fiber/matrix interphase. The pure aliphatic epoxy at 60% stoichiometry shows significantly more cure shrinkage (+61%) than the pure aromatic epoxy. Compared to the ridged backbone of the aromatic epoxy, the higher flexibility of the aliphatic

backbone appears to allow the epoxy to contract more during curing, resulting in higher cure shrinkage. The high shrinkage of the aliphatic sizing could potentially lead to high stresses at the fiber/matrix interphase in a high fiber volume fraction composite. However, this is not supported by the significantly improved mechanical properties that probe the fiber/matrix bonding (transverse flexural properties and Mode I fracture toughness) that were discussed in Chapter 3. Diffusion of the vitrified aliphatic fiber sizing away from the fiber surface during composite consolidation appears to establish a gradient of aliphatic epoxy in the interphase that mitigates the issue of high cure shrinkage at higher concentrations of aliphatic epoxy.

The results discussed above are for the pure matrix and sizing compositions. During the curing of the high fiber volume fraction composite, diffusion of the partially vitrified sizing is expected, leading to a composition gradient at the fiber matrix interphase. While this will change the cure shrinkage behavior in the interphase, high shrinkage could still be expected at the fiber surface. Lower shrinkage is also expected in the fiber-reinforced composite due to hindrance by the fibers. [15], [16]

4.5.5 Interfacial Shear Strength

The influence of fiber surface treatment and fiber sizing on the interfacial shear strength (IFSS) in both neat matrix and aliphatically toughened matrix as determined by single-fiber fragmentation test is shown in Figure 4.9:

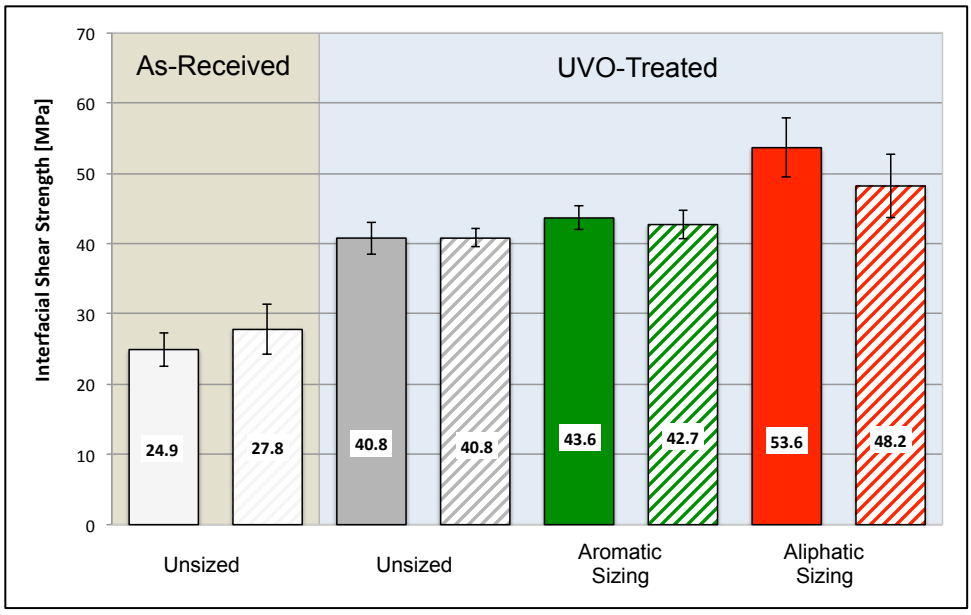

Figure 4.9: Interfacial shear strength of AS4-12k carbon fiber with different fiber surface treatments and fiber sizing in either neat matrix (solid) or aliphatically toughened matrix (hashed)

The changes in IFSS are analogous to the neat matrix. The details were described in Chapter 3.3.3. This section will focus on the differences in interfacial properties between the neat and toughened matrices.

Comparing the IFSS between the neat matrix and the toughened matrix shows interesting behavior. For the as-received, unsized fiber, the IFSS of the aliphatically toughened matrix is about 12% greater. The scatter in the two data sets overlaps considerably, making if difficult to determine if the increase in IFSS is statistically significant. The matrix toughening appears most effective on this lowest toughness fiber/matrix system of the materials evaluated in this study. Since no changes were made to the fiber surface, the toughening mechanism must be rooted in the matrix. With the addition of 1wt% aliphatic epoxy copolymer, the matrix in the vicinity of the fiber may be better at resisting crack initiation as shown with the higher notched Izod impact strength of the 1wt% aliphatically toughened matrix were discussed in Chapter 2.3. As

this may be only a weak effect in a low loading rate test, it only manifests itself in the lowest toughness system and is obscured by the enhancements of fiber/matrix adhesion seen in the other systems to be discussed. Within error both the UVO-treated, unsized and UVO-treated, aromatic sized fibers show the same IFSS between the neat and toughened matrices. The toughness of both these fiber/matrix systems is similar, 40.8 and 43.7 MPa respectively. In the case of the UVO-treated, unsized fiber, the enhancement of surface oxygen groups and reduction of surface defects improves the fiber/matrix adhesion over the as-received fiber, not allowing the same enhancement with the toughened matrix as was seen with as-received fiber. A similar line of argumentation goes for the UVO-treated, aromatic sized samples, which would have the same benefits of the UVO-surface treatment. The sizing is the same aromatic epoxy as the matrix, however with an under-stoichiometric amount (60%) of curing agent. During composite consolidation, a stoichiometry gradient is formed which in turn leads to a stiffer fiber/matrix interphase. With the application of the aliphatic fiber sizing, the IFSS of the toughened matrix is actually about 10% lower that of the neat matrix. As the fiber/matrix system toughness is the highest of those investigated in this study, the matrix toughening appears to reduce the IFSS. An enrichment of aliphatic epoxy at the fiber/matrix interphase could explain this behavior. With the addition of 1wt% aliphatic epoxy to the bulk matrix, the concentration gradient from the fiber surface to the bulk matrix is different than in the composite with the neat matrix. Additionally, the slower curing kinetics of the aliphatic epoxy compared to the aromatic epoxy discussed above supports the idea of an enrichment of aliphatic epoxy at the fiber matrix interphase. A higher concentration of aliphatic epoxy at the fiber surface could have several

consequences: First the lower modulus of the aliphatic epoxy compared to the aromatic epoxy (8 vs. 3200 MPa at full stoichiometry respectively) may lead to a lower modulus interphase, which would in turn reduce the fiber/matrix bond strength as predicted by the Cox equation (see discussion in Chapter 3). Secondly, as was discussed in Chapter 4.5.1 , higher concentration of aliphatic epoxy at the fiber surface would lead to larger differences in cure shrinkage between matrix and fiber sizing and higher stresses in the fiber/matrix interphase during composite consolidation.

The birefringence patters from the single-fiber fragmentation test are shown in Figure 4.10:

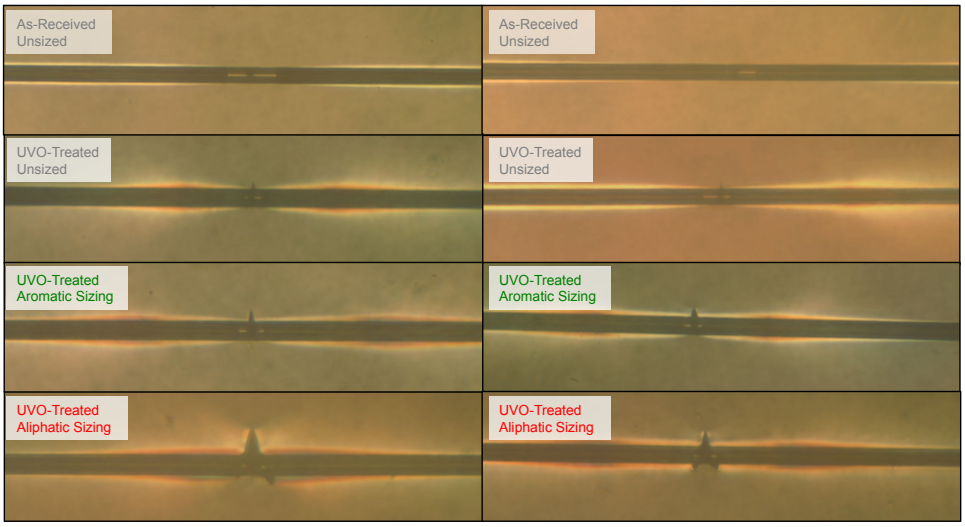

Figure 4.10: Birefringence patters with photoelastic stress patterns of AS4 carbon fiber with different fiber surface treatments and fiber sizing in neat matrix (left) and toughened matrix (right)

There is very little visual difference between the fracture morphology of the samples with neat and toughened matrices. With the fiber UVO-treatment, the fracture morphology shifts from a low strength fracture to an intermediate strength fracture. The intermediate strength fracture morphology is similar when the fibers are sized with

aromatic epoxy. However, the aliphatic sized fibers present a change to high strength fracture exhibiting a 45˚ shear failure matrix crack in the interphase. The similarity in interphase failure mechanisms between the neat and toughened matrix suggest that the changes in IFSS are due to toughening effects in the bulk matrix rather than material property changes the fiber/matrix interphase. One difference is that the birefringence patterns of the toughened matrix samples do not appear to be as concentrated around the fiber fracture. This difference is most noticeable with the aliphatic fiber sizing and supports the hypothesis discussed above that with the addition of aliphatic epoxy copolymer to the matrix results in an enrichment of aliphatic concentration at the fiber/matrix interphase.

4.5.6 Mechanical Properties of the High Fiber Volume Fraction Composite

The fiber volume fraction (V_f) of the different composites had some variation as shown in Figure 4.11:

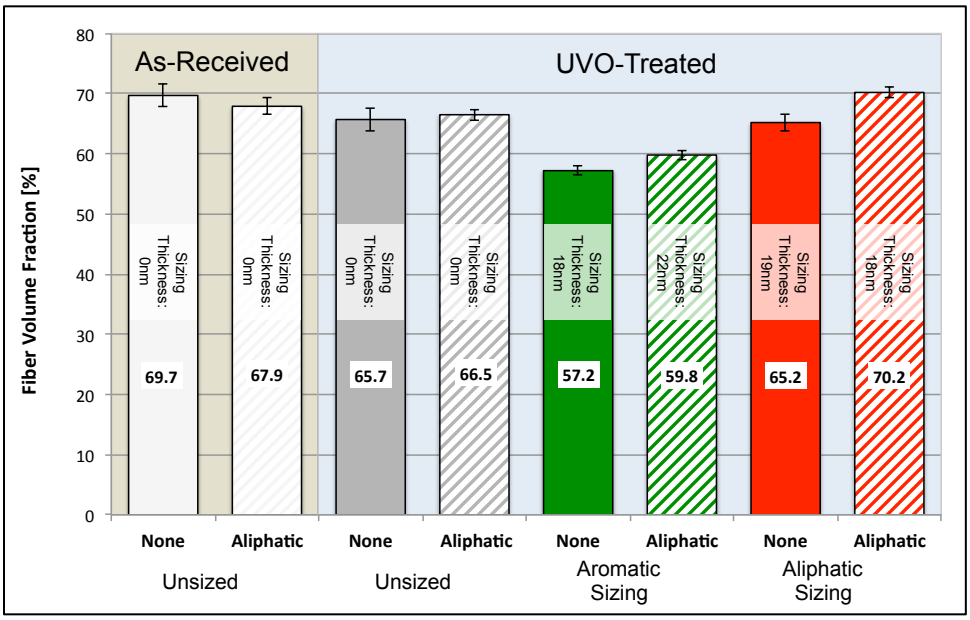

Figure 4.11: Fiber volume fraction and estimated sizing thickness of unidirectional AS4-12k carbon fiber composites with different fiber surface treatments and fiber sizing in neat matrix (solid) and aliphatically toughened matrix (hashed)

For the unsized fiber samples, both as-received and UVO-treated, the matrix toughening does not appear to have a significant impact on Vf, as the difference in V_f is within the scatter of the data. For both of the sized UVO-treated fiber sample sets, the samples with the toughened matrix appear to have a slightly higher V_f, 5% higher for aromatic sizing and 8% higher for aliphatic sizing. The high V_f of the aliphatically sized fiber with a toughened matrix could also be rooted in the cure shrinkage behavior. As the aliphatic sizing exhibits significantly higher shrinkage, the addition of aliphatic epoxy to the matrix may reduce the diffusion away from the fiber surface, compared to the neat matrix. The toughened matrix would then have a higher aliphatic epoxy concentration at the fiber surface or a steeper concentration gradient of aliphatic epoxy at the fiber/matrix interphase. Either case could contribute to higher shrinkage during curing and a higher V_f. The higher V_f of the samples with sized fibers may be an indication of enhanced diffusion at the fiber/matrix interface during composite curing. If

the increase in fiber volume fraction is truly due to the toughening of the matrix, variations of the manufacturing process or a combination of both is a point that requires further investigation.

Due to the variation of V_f, longitudinal flexural modulus and strength were normalized to a V_f of 65% by the method described in Chapter 3.4.3. [17] The unadjusted longitudinal data is presented in the appendix. The transverse properties are challenging to adjust based on the complex stress distributions that are present in the transverse direction. For this reason, the transverse properties are presented as-measured with reference to the actual fiber volume fraction for each composite.

The void volume of all composites, as determined from representative SEM micrographs using digital image editing software, was well below the 1% threshold as has been established in the literature, below which no effect on mechanical properties is expected. [18]

The flexural properties of the unidirectional composite were investigated in both the longitudinal (0˚) and the transverse (90˚) fiber direction. The longitudinal direction is dominated by the fiber properties, while the transverse direction is more sensitive to fiber/matrix adhesion. The flexural modulus, both longitudinal and transverse, is shown in Figure 4.12:

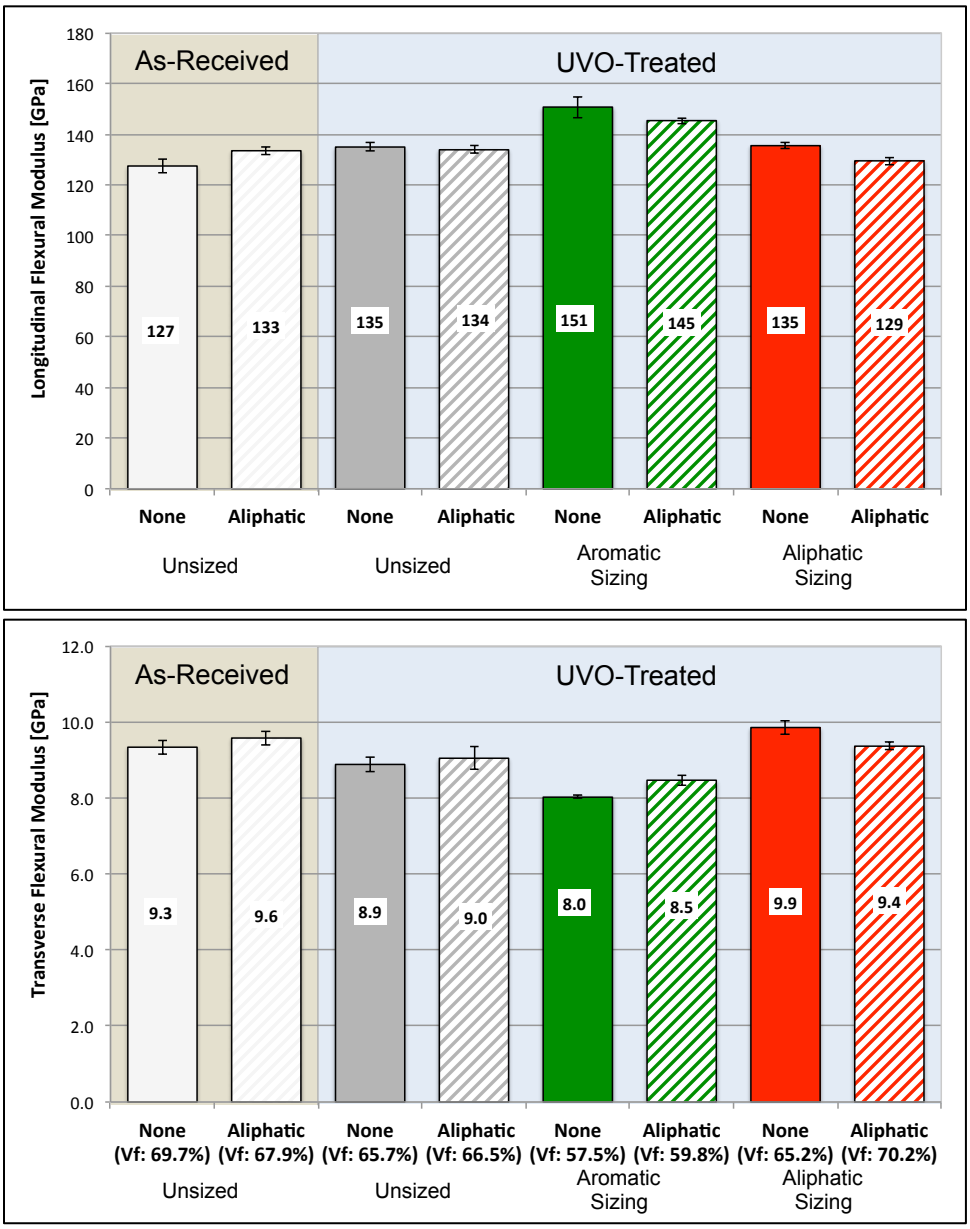

Figure 4.12: Flexural modulus (top: longitudinal, adjusted V_f:65%; bottom: transverse, as-measured) of unidirectional AS4-12k carbon fiber composites with different fiber surface treatments and fiber sizing in neat matrix (solid) and aliphatically toughened matrix (hashed)

Toughening of the matrix does not have a significant influence on the longitudinal modulus. The differences between the neat and toughened matrix for the as-received, unsized samples is 5% higher, which may be a manifestation of the weak toughening mechanism seen in the interfacial shear strength results discussed above. For the UVO-

treated, unsized samples the longitudinal modulus is equivalent. Both of the sized samples sets, aromatic and aliphatic epoxy sized, have 4% lower longitudinal moduli with the toughened matrix. For the UVO-treated, aromatic sized fiber composite, the high scatter of the neat matrix samples make it difficult to interpret if the averages are statistically different. The slight reduction in modulus of the UVO-treated, aliphatic sized composite may be a consequence of the lower interfacial shear strength discussed in the previous section.

In the transverse direction, the data trend follows that of the interfacial shear strength discussed above. (Section 4.5.5) This is consistent, as both tests interrogate fiber/matrix adhesion. The as-received, unsized samples show a 3% increase in modulus. The UVO-treated, unsized samples has identical modulus for the neat and toughened matrices. The UVO-treated, aromatic sized samples show a 6% higher modulus, which may be related to the stiffer interphase, expected from the under-stoichiometric curing agent concentration. The UVO-treated, aliphatic sized samples have a 12% decrease in modulus, analog to the interfacial shear strength results. As discussed above, there is probably an enrichment of aliphatic epoxy at the fiber/matrix interphase, leading to a lower modulus interphase and a reduced global modulus.

The flexural strength, both longitudinal and transverse, is shown in Figure 4.13:

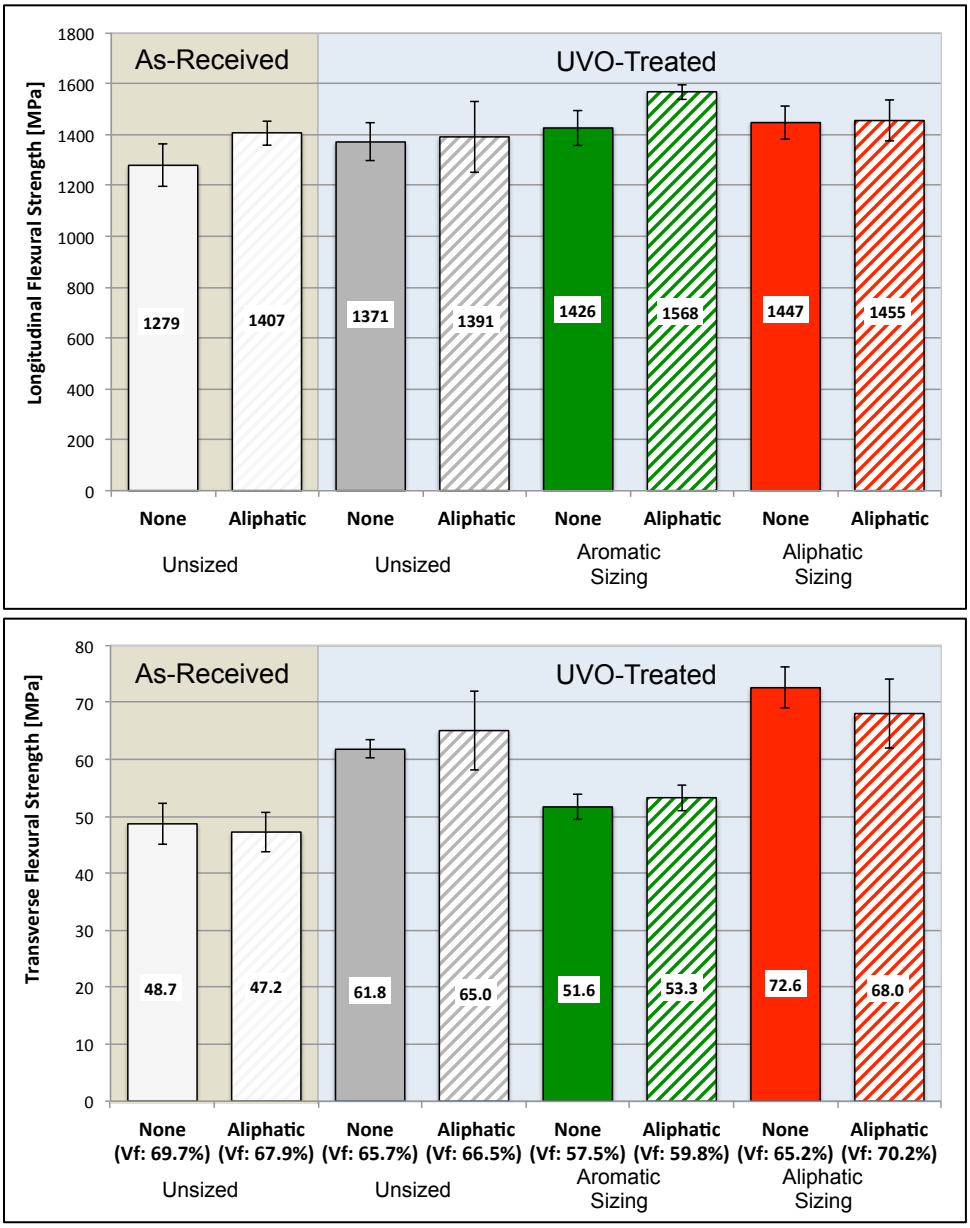

Figure 4.13: Flexural strength (top: longitudinal, adjusted V_f:65%; bottom: transverse, as-measured) of unidirectional AS4-12k carbon fiber composites with different fiber surface treatments and fiber sizing in neat matrix (solid) and aliphatically toughened matrix (hashed)

The longitudinal strength of the UVO-treated, unsized and UVO-treated, aliphatic sized sample sets is statistically similar. The as-received, unsized and UVO-treated, aromatic sized sample sets shows a 10% higher strength with the aliphatically

toughened matrix. For the as-received, unsized samples the overlap of the error bars makes it challenging to judge if the increase is statistically significant.

For the transverse flexural strength, toughening the matrix does not appear to have any effect, with all samples sets having statistically similar averages. The exception is the aliphatically toughened sample set, where a 13% reduction with the aliphatically toughened matrix is seen. As discussed above, an enrichment of aliphatic epoxy at the fiber/matrix interphase may not only lead to a lower modulus (Figure 4.12) but also lower strength interphase. The toughening of the matrix does not appear to enhance the fiber/matrix adhesion, which is the attribute that dominates the properties in the transverse direction. This behavior is also seen in the interfacial shear strength, (Figure 4.9) with the exception of the as-received, unsized fiber composite which does not show the increase with the toughened matrix.

It should also be pointed out that the toughening of the matrix does not have a negative effect on the flexural properties of the composite having different combinations of fiber surface treatment and fiber sizing. All properties are equal to or better than the neat matrix composite. The exception is the aliphatic fiber sizing composite.

The effect of toughening of the matrix for the different fiber surface treatments and sizing on the Mode I fracture toughness is shown in Figure 4.14:

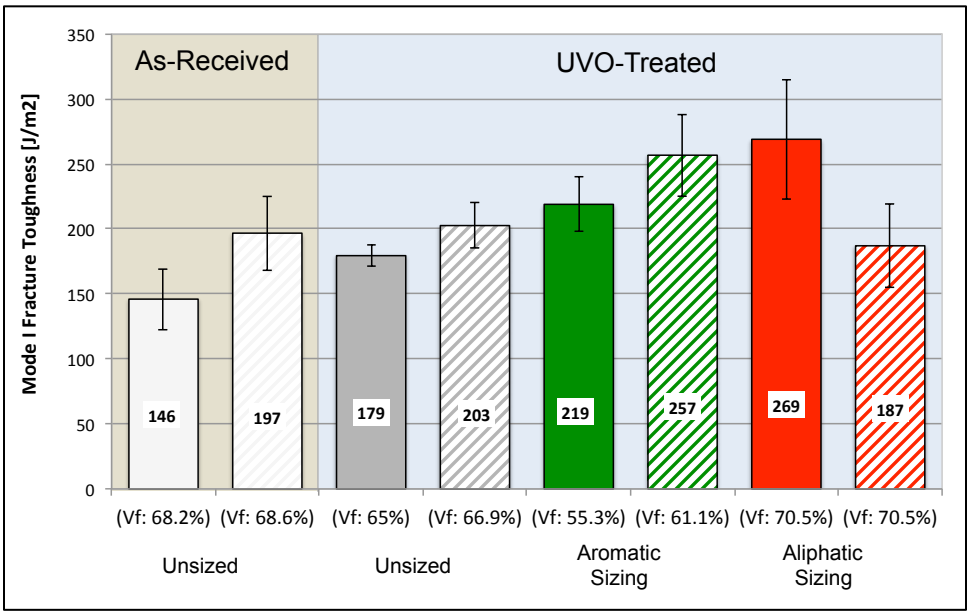

Figure 4.14: Mode I fracture toughness of unidirectional AS4-12k carbon fiber composites with different fiber surface treatments and fiber sizing in neat matrix (solid) and aliphatically toughened matrix (hashed)

The fracture toughness of the toughened matrix behaves analogously to the interfacial shear strength results shown in Figure 4.9. The lower toughness system of as-received, unsized shows the largest increase of 34%. The enhanced toughness of the aliphatically toughened matrix appears to be more dominant in the Mode I test, where the facture of the epoxy matrix also plays a role, as opposed to the single fiber fragmentation test. As system toughness increases for the UVO-treated, unsized system, the increase in fracture toughness is about 13%. A similar increase of about 17% is evident for the UVO-treated, aromatic sized samples. There are overlapping error bars on the average values of fracture toughness due to scatter. The Mode I fracture toughness of the UVO-treated, aliphatically sized sample set is lower than the neat matrix by about 30%. This mirrors all the previously discussed tests that are influenced by fiber/matrix adhesion (interfacial shear strength, transverse flexural

strength). Broadly speaking, all properties of the toughened matrix composites are better than the baseline as-received, unsized composite system.

These results are supported by the scanning electron microscope images of the longitudinal flexural fracture surfaces shown in Figure 4.15:

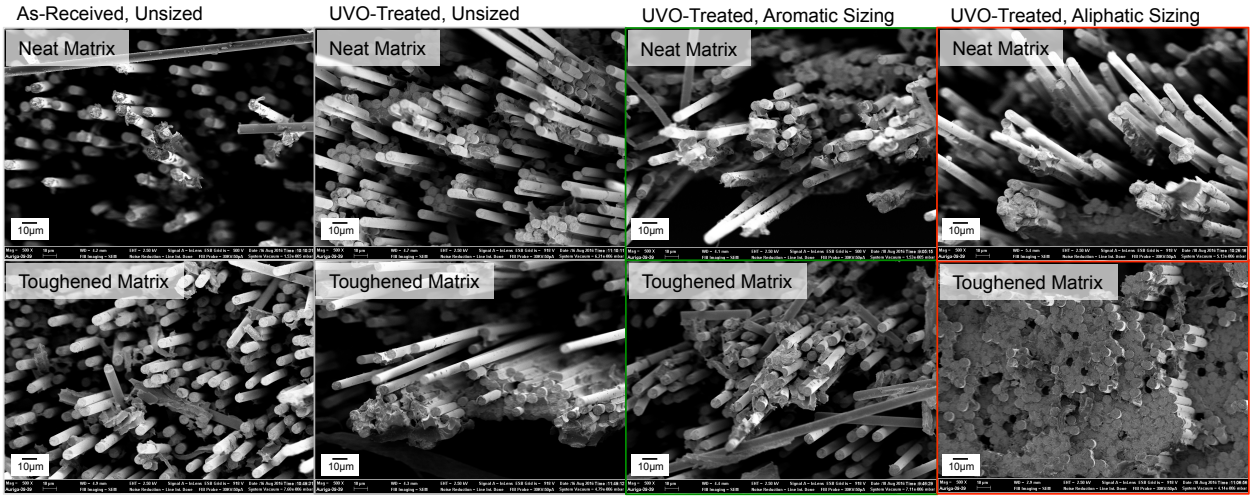

Figure 4.15: Scanning electron micrographs of longitudinal flexural fracture surfaces of unidirectional AS4-12k carbon fiber composites with different fiber surface treatments and fiber sizing in neat matrix (top row) and aliphatically toughened matrix (bottom row) taken at the tension side of the coupon

The as-received, unsized fiber sample has little indication of residual matrix on the fiber surfaces, a qualitative indicator of a low adhesion system. Significantly more matrix material is visible on the fiber surface of the UVO-treated, unsized fiber samples. This is an indication of the improved fiber/matrix adhesion. The UVO-treated, aromatic sized fiber samples show similar levels of residual matrix on the fiber surface as the UVO-treated, unsized fiber samples. There are minor differences in the fracture morphology of the neat versus toughened matrices. The UVO-treated, aliphatically sized fiber sample with neat matrix show a similar morphology to the other UVO-treated fiber samples with neat matrix. The aliphatically sized fiber sample with the toughened matrix on the other hand shows very different fracture morphology. Here the fibers are

still held together by the matrix, suggestive of fiber pullout from the matrix. As was reported by Madhukar *et al.* [19] this fracture morphology suggests a matrix dominated failure. This result would be consistent with the results from both the transverse flexural strength (Figure 4.13) and Mode I fracture toughness (Figure 4.14) that indicate lower strength and fracture toughness. With a more compliant and lower strength fiber/matrix interphase, the matrix properties will dominate the failure.

The interlaminar shear strength (ILSS) as determined by the short beam shear test is shown in Figure 4.16:

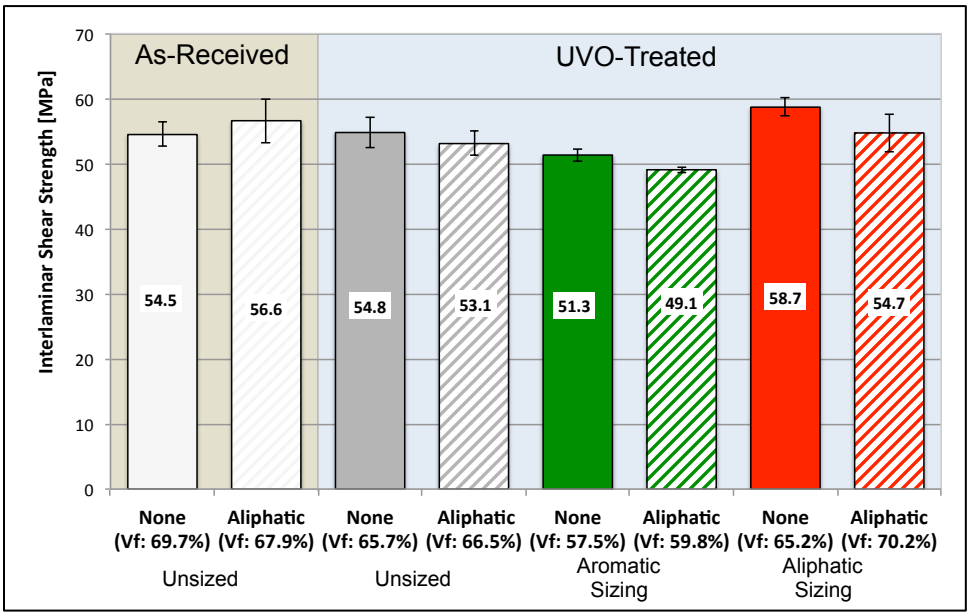

Figure 4.16: Interlaminar shear strength of unidirectional AS4-12k carbon fiber composites with different fiber surface treatments and fiber sizing in neat matrix (solid) and aliphatically toughened matrix (hashed) as determined by the short beam shear test

Looking at the behavior of the samples with toughened matrix (hashed bars in Figure 4.16), both the unsized sample sets, as-received and UVO-treated, have statistically similar averages with overlapping error bars between the neat and toughened matrices. The two sized sample sets, aromatic and aliphatic, on the other hand, show lower ILSS values for the toughened matrix, with 4% and 7% reductions

respectively. When the sample sets with toughened matrices (hashed bars) are compared, there does not appear to be a statistically significant difference between any of the fiber surface treatments and sizing, with the exception of the aromatic sized fiber composite. There may be several different mechanisms responsible for the overall behavior of the ILSS with the toughened matrix. It was proposed by Madhukar *et al.*, [20] that when the fiber/matrix adhesion was already utilized to the maximum extent, the matrix would dominate the ILSS behavior. If the toughened matrix was to be enhanced with the addition of 1wt% aliphatic epoxy, fiber/matrix adhesion be the limiting factor. This would be consistent as both the unsized fiber samples, as-received and UVO-treated, show statistically similar ILSS between neat and toughened matrices. For the aromatic sized fiber sample the lower shear strain to failure expected from the under-stoichiometric may be leading to a reduced ILSS. The softer, lower strength interphase of the aliphatic sized fiber in the toughened matrix may also be reducing the ILSS, as was shown in transverse flexural strength (Figure 4.13) and Mode I fracture toughness (Figure 4.14). The slightly lower ILSS of the toughened matrix may be rooted in that the toughening mechanism using low concentrations of aliphatic copolymer may be mainly an increase in damage initiation toughness during high impact events. If the toughened matrix mainly enhanced the materials ability to absorb energy during high loading rate events, it may not have an advantage during slow loading rate events (flexural or interlaminar shear strength) or tests that start with a crack that is already initiated (Mode I fracture toughness). This hypothesis is supported by the work previously published, [7] showing that the notched Izod impact strength (high loading rate event) of a 1wt% aliphatically toughened aromatic epoxy matrix was significantly increase (~50%) while

no effect on the flexural properties (low loading rate event) was seen. This would represent a limitation of this toughening approach when applied to carbon fiber-reinforced composites.

As shown in Figure 4.17, there is no significant influence of the toughened matrix on the glass transition temperature regardless of the fiber surface treatment and fiber sizing, with all differences being within 1%. The slight decreases in T_g for the toughened matrix samples within this narrow band may be due to the slightly higher fiber volume fractions of the samples with toughened matrices (see Figure 4.11). The polymer chain motion would be more restricted by higher fiber volume fraction that will have less space between fibers. This is supported by the peak heights of the Tan δ function that are shown in Figure 4.18:

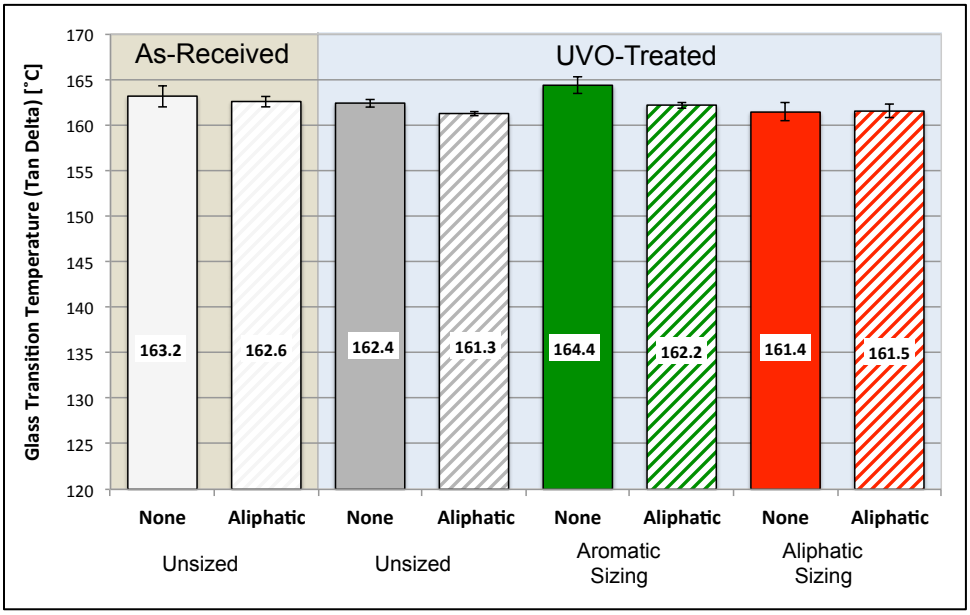

Figure 4.17: Glass transition temperature of unidirectional AS4-12k carbon fiber composites with different fiber surface treatments and fiber sizing in neat matrix (solid) and aliphatically toughened matrix (hashed) as determined from the maximum of the Tan δ function from DMA

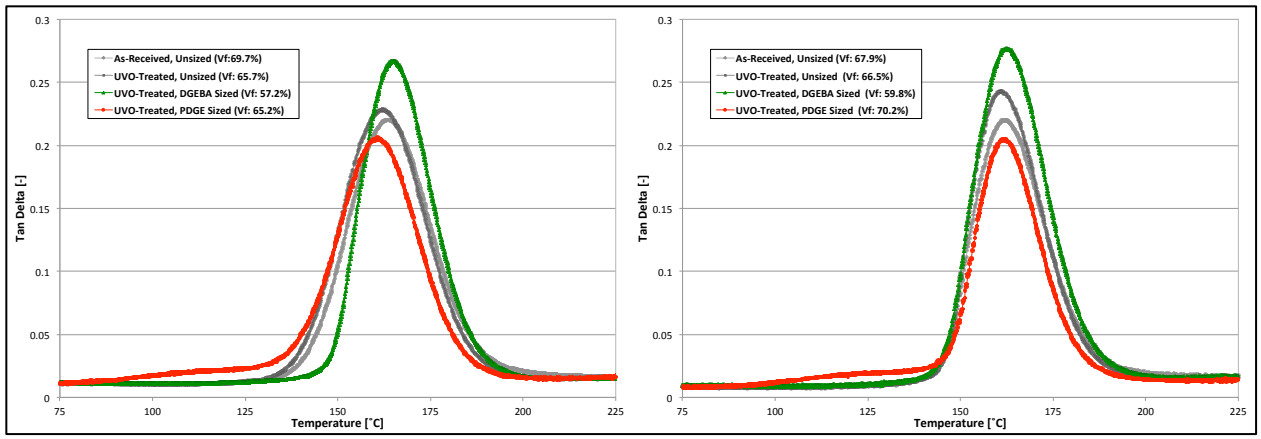

Figure 4.18: Tan δ function of unidirectional AS4-12k carbon fiber composites with different fiber surface treatments and fiber sizing as determined from DMA in neat matrix (left) and aliphatically toughened matrix (right)

The peak height of the Tan δ function for the toughened matrix samples is slightly higher than for those of the neat matrix, which may be due to the marginally higher fiber volume fraction of the toughened matrix composites. The shape of the Tan δ does not significantly change for any of the fiber surface treatment/fiber sizing combinations when applying aliphatic matrix toughening.

4.6 Conclusion

The influence of matrix toughening using 1wt% aliphatic copolymer on the mechanical properties of unidirectional carbon fiber reinforced composites in conjunction with UVO fiber surface treatment and fiber sizing was demonstrated. Improvements in Mode I fracture toughness were manifested and the improvement being most effective for the systems possessing low baseline toughness. This is attributed to the toughening effect in the matrix dominating the fiber/matrix adhesion. The toughening effect becomes less pronounced as fiber/matrix adhesion increases. Combining aliphatic fiber sizing with an aliphatic toughened matrix reduces the Mode I

fracture toughness and the transverse flexural properties. The addition of the aliphatic copolymer to the matrix leads to a reduced concentration gradient and reduced diffusion away from the fiber/matrix interphase. This leads to an enrichment of aliphatic copolymer and a more compliant, lower strength interphase.

All improvements in fracture toughness were achieved without significant reductions in other static-mechanical properties.

APPENDIX

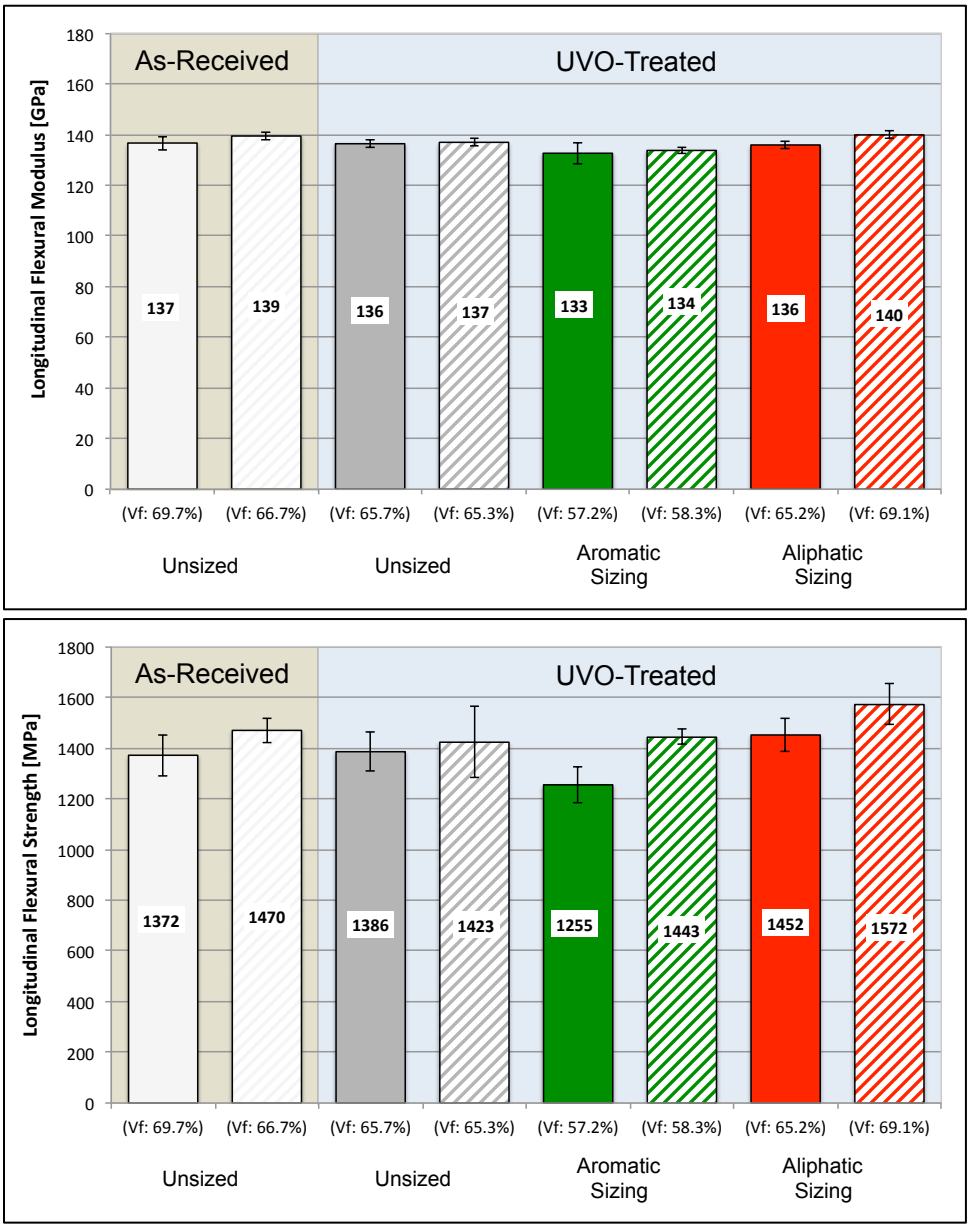

Figure 4.19:Longitudinal flexural composite properties as measured, neat matrix (solid) and aliphatically toughened matrix (hashed): modulus (top), strength (bottom)

BIBLIOGRAPHY

BIBLIOGRAPHY

[1] U. S. EPA, OAR, O. O. T. A. A. Quality, and A. A. S. Division, “EPA and NHTSA Set Standards to Reduce Greenhouse Gases and Improve Fuel Economy for Model Years 2017-2025 Cars and Light Trucks,” pp. 1–10, Aug. 2012.

[2] S. Dong and R. Gauvin, “Application of dynamic mechanical analysis for the study of the interfacial region in carbon fiber/epoxy composite materials,” *Polym. Compos.*, vol. 14, no. 5, pp. 414–420, 1993.

[3] S.-J. Park, T.-J. Kim, and H.-Y. Kim, “Thermal and mechanical properties of diglycidylether of bisphenol A/ trimethylolpropane triglycidylether epoxy blends cured with benzylpyrazinium salts,” *Polym. Int.*, vol. 51, no. 5, pp. 386–392, 2002.

[4] C. H. Zhang, H. G. Wei, Y. Y. Liu, H. F. Tan, and Z. Guo, “Enhanced toughness and shape memory behaviors of toughed epoxy resin,” *High Performance Polymers*, vol. 24, no. 8, pp. 702–709, Nov. 2012.

[5] S.-J. Park, T.-J. Kim, and J.-R. Lee, “Cure behavior of diglycidylether of bisphenol A/trimethylolpropane triglycidylether epoxy blends initiated by thermal latent catalyst,” *J. Polym. Sci. B Polym. Phys.*, vol. 38, pp. 2114–2123, Aug. 2000.

[6] T. Misaki, T. Hirohata, M. Yoshii, and T. Hamasaki, “Properties of networks obtained by internal plasticization of epoxy resin with aromatic and aliphatic glycidyl compounds,” *J. Appl. Polym. Sci.*, vol. 37, no. 9, pp. 2617–2625, 1989.

[7] M. A. Downey and L. T. Drzal, “Toughening of aromatic epoxy via aliphatic epoxy copolymers,” *Polymer*, vol. 55, no. 26, pp. 6658–6663, Dec. 2014.

[8] K. F. Schoch Jr., P. A. Panackal, and P. P. Frank, “Real-time measurement of resin shrinkage during cure,” *Thermochimica Acta*, vol. 417, no. 1, pp. 115–118, Jul. 2004.

[9] D. U. Shah and P. J. Schubel, “Evaluation of cure shrinkage measurement techniques for thermosetting resins,” *Polymer Testing*, vol. 29, no. 6, pp. 629–639, Sep. 2010.

[10] A. V. Kurnoskin, “Polymers based on epoxy oligomers and hardeners. Chelates of metals with aromatic and heterocyclic amines,” *Ind. Eng. Chem. Res.*, no. 31, pp. 524–529, 1992.

[11] D. Puglia, L. Valentini, I. Armentano, and J. M. Kenny, “Effects of single-walled carbon nanotube incorporation on the cure reaction of epoxy resin and its detection by Raman spectroscopy,” *Diamond and Related Materials*, vol. 12, no. 3, pp. 827–832, Mar. 2003.

[12] A. Allaoui, “How carbon nanotubes affect the cure kinetics and glass transition temperature of their epoxy composites? – A review,” *expresspolymlett*, vol. 3, no. 9, pp. 588–594, Aug. 2009.

[13] C. Billotte, F. M. Bernard, and E. Ruiz, “Chemical shrinkage and thermomechanical characterization of an epoxy resin during cure by a novel in situ measurement method,” *European Polymer Journal*, vol. 49, no. 11, pp. 3548–3560, Nov. 2013.

[14] H. Lee and K. Neville, “Aromatic Primary Amines As Curing Agents,” in *Handbook Of Epoxy Resins*, First. no. 8, New York: McGraw-Hill, 1967.

[15] Y. Nawab, P. Casari, N. Boyard, and F. Jacquemin, “Characterization of the cure shrinkage, reaction kinetics, bulk modulus and thermal conductivity of thermoset resin from a single experiment,” *J Mater Sci*, vol. 48, no. 6, pp. 2394–2403, Nov. 2012.

[16] Y. Nawab, F. Jaquemin, P. Casari, N. Boyard, and V. Sobotka, “Evolution of chemical and thermal curvatures in thermoset-laminated composite plates during the fabrication process,” *Journal of Composite Materials*, vol. 47, no. 3, pp. 327–339, Jan. 2013.

[17] Handbook-MIL-HDBK, *17-1F: Composite Materials Handbook, Volume 1- Polymer Matrix Composites: Guidelines for Characterization of Structural Materials*. Department of Defence, 2002.

[18] K. Friedrich, S. Fakirov, and Z. Zhang, *Polymer Composites*. Springer, 2005.

[19] M. S. Madhukar and L. T. Drzal, “Fiber-matrix adhesion and its effect on composite mechanical properties: II. Longitudinal (0) and transverse (90) tensile and flexure behavior of graphite/epoxy …,” *Journal of Composite Materials*,

1991.

[20] M. S. Madhukar and L. T. Drzal, “Fiber-Matrix Adhesion and Its Effect on Composite Mechanical Properties. III. Longitudinal (0) Compressive Properties of Graphite/Epoxy Composites,” *Journal of Composite Materials*, vol. 26, no. 3, pp. 310–333, Jan. 1992.

Chapter 5: Toughening of Aromatic Epoxy Using Amine-Grafted Graphene Nanoplatelets

5.1 Abstract

Graphene nanoplatelets can be utilized to toughen the DGEBA/mPDA epoxy system. The toughening potential was demonstrated with different grades of graphene nanoplatelets (GnP), which had different edge areas and aspect ratios. Amine groups were grafted to the GnP edges via reaction with tetraethylenepentamine (TEPA) to enhance filler/matrix adhesion using different grafting schemes, including processing via 3-roll milling.

GnP C750, which has the smallest platelet diameter (1-2μm) and largest edge area, was found to be best at enhancing the flexural properties (+1 to +5%) while not having any impact on the fracture toughness. TEPA-grafting improved the filler/matrix adhesion as indicated by improved flexural strength.

GnP M5 improved fracture toughness of DGEBA/mPDA by +22% to +31%. TEPA-grafting lead to smaller reductions in flexural strength, while additional reaction of the TEPA-grafted GnP M5 with DGEBA almost negated the reductions in flexural properties.

GnP M25 improved the fracture toughness (+32 to +43%) of DGEBA/mPDA based on the large aspect ratio that has been shown to be superior in crack deflection. Improvements in flexural modulus were in the +6% to +9% range. Flexural strength was reduced by about 15%. TEPA-grafting did not significantly influence the nano-composite properties, probably due to the small amount of edge area that the TEPA can graft to.

Small reductions in the improvement of nano-composite properties are seen with additional processing that are probably based on reductions in platelet diameter.

All of the GnP grades reduced the notched Izod impact strength of DGEBA/mPDA, regardless of TEPA-grafting. During the high loading rate event of the impact test, the stiff inclusion of GnP within the matrix probably acted as stress concentrators.

5.2 Introduction

One of the main challenges with epoxy polymers that needs to be addressed is the brittle nature of the material. [1]-[3] Since they have no natural crack retention mechanism, any cracks forming in the material will propagate uninhibited. Different approaches have been proposed to toughen epoxies. Toughening with low concentrations of aliphatic epoxy was discussed in Chapter 2 in order to enhance the amount of absorbed energy prior to fracture. A different approach is to disperse nano-scale filler materials throughout the matrix to act as crack arresting agents. On a per volume basis nano-scale filler materials will have a much larger surface area than a filler material on the micro-scale, enhancing the contact area between filler and matrix. [4] The nano-scale size of the filler material will also allow for finer distribution of the filler within the matrix. With a homogeneous distribution of the filler material, any crack growing through the matrix would intersect a particle. As was discussed in the introduction, several nano-scale toughening mechanisms are proposed, including crack bridging, crack pinning, and crack deflection. [5]

Nano-fillers can be roughly divided into two categories: inorganic and organic. The inorganic nano fillers include clays [6] and alumina [7]; organic are carbon based,

including graphene and carbon nanotubes, which have garnered much of the current research effort in the past decade. [8]

Graphene, which was first reported 2004 [9], consists of a single layer of sp^2-hybridized carbon atoms. In the single layer form, graphene has some of the highest mechanical properties ever measured for any material. [10] However in its single layer form, graphene is challenging to use based on production cost and processing. Graphene nanoplatelets (GnP) are stacks of graphene layers and is a material that can be commercially made at a reasonable cost compared to other carbon-based fillers like single-walled carbon nanotubes. [11], [12] The use of GnP is also beneficial on the basis of their platelet-type structure. This structure has two-dimensions (2D) on the micrometer scale with a third on the nanometer scale. The high aspect ratio of 2D nano-fillers occupy a large area and are superior at intersecting cracks compared to 1D nano-fillers such as carbon nano tubes. [13]

Filler/matrix adhesion is a key aspect in toughening with nano fillers. Only with strong bonding between the matrix and the filler can the load be effectively transferred between the two. Weakly bonded fillers will act as stress concentrators within the matrix and potentially reduce the mechanical properties. The graphene layers, which make up the GnP, will in general have pristine basal planes made of sp^2-hybridized carbons. Without disruption of the sp^2-hybridized carbon network, as in the formation of graphene oxide [14], no reaction will take place on the basal plane. Oxygen containing functional groups like hydroxyl, ester, or carboxylic acid, will only be present at defects in the basal plane and around the platelet edge. These are the areas where bonding between the GnP and matrix can take place. Reacting these existing functional groups with a large

molecule containing multiple amine groups will increase the possibility of the GnP bonding with the epoxy groups in the matrix and increasing the mechanical properties. Initially reported by Pittman *et al.*, tetraethylenepentamine (TEPA) was reacted with reactive groups on the surface of carbon fiber was used to enhance surface functionality. [15], [16] Oxidizing the carbon fiber surface with nitric acid was used to increased the amount of reactive surface groups. TEPA has subsequently also been used to add amine functionality to graphene nanoplatelets [17] and graphene oxide. [18]

In this study, no initial acid oxidation of the GnP was done before the TEPA reaction. The oxygen groups present on the edges of the GnP from the production process were used to graft TEPA molecules to the GnP. Three grades of GnP having significantly different amounts of platelet edge area were investigated for their impact on the mechanical properties of the DGEBA/mPDAsystem

5.3 Materials and Methods

5.3.1 Materials

The aromatic epoxy, diglycidyl ether of bisphenol A (Epon 828, DGEBA), with an epoxy equivalent weight (EEW) of 185-195, was purchased from Hexion Inc. The curing agent meta-Phenylenediamine (mPDA) was purchased from Acros Organics. The ACS-grade 2-propanol (IPA) and acetone were purchased from J.T. Baker. Tetraethylenepentamine (TEPA) was provided by the Huntsman Corporation. All chemicals were used as received. The structures of the epoxies and the amines are shown in Figure 5.1:

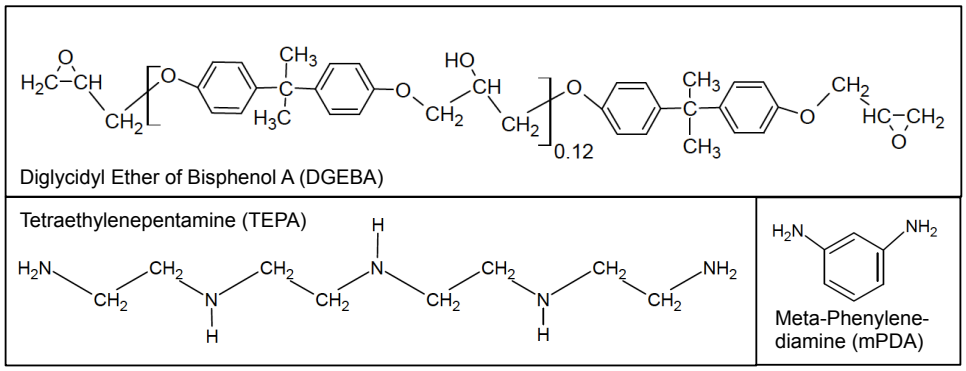

Figure 5.1: Structure of epoxy and amines

Graphene nanoplatelets (GnP) were provided by X.G. Sciences. Three different grades of GnP were used: C750, M5 and M25. Some nominal material properties are shown in Table 5-1:

Table 5-1: Physical and mechanical properties of graphene nanoplatelets [19], [20]

	GnP Grade		
	C750	**M5**	**M25**
Nominal Platelet Diameter [μm]	1-2	5	25
Nominal Surface Area [m2/g]	750	130-150	130-150

All GnP was heat-treated in a muffle furnace at 400˚C for 1h in air prior to use to remove of any residuals from the production process.

5.3.2 Amine-Grafting of Graphene Nanoplatelets

Tetraethylenepentamine (TEPA) was used to add amines to the GnP following a method adapted from Pittman *et al*. [16] The GnP was dispersed in TEPA at a 1:30 (GnP:TEPA) mass ratio. The GnP-TEPA mixture was sonicated at 200W for 30min (10s on/ 5s off) in a dry ice bath with agitation on a stir plate using a Virsonic 750 sonication

probe. After sonication, the GnP-TEPA mixture was heated to 200˚C and reacted for 5h at temperature under agitation in an oil bath. The reacted GnP-TEPA mixture was filtered over a 0.22μm PTFE filter membrane and washed with reverse-osmosis water until the pH reached that of the wash water. The TEPA-grafted GnP (GnP C750HT-TEPA or M25HT-TEPA) was dried overnight in a vacuum oven at ~100˚C to remove the residual water.

To improve the grafting of TEPA to the M-grade GnP, a processing step with an Exact 80E 3-roll mill was also investigated. This calendaring technique has been shown to be very effective at dispersing and separating/exfoliating nano-fillers. [21], [22] The high shear forces generated in the 3-roll mill should help exfoliate the GnP, reducing the number of platelets in the GnP stacks. Additionally, the platelets could be fractured at weaker defect sites, leading the formation of new edges that would be highly reactive to the surrounding TEPA. As described above, a 1:30 (GnP:TEPA) mass ratio mixture was sonicated, after which the mixture was processed on the 3-roll mill at 400rpm with 5 passes at 20μm and 10μm nip gaps and 10 passes at 5μm nip gap. After 3-roll milling the GnP-TEPA mixture was reacted and processed the same way as described above. This yielded GnP M5HT-3R-TEPA and M25HT-3R-TEPA.

The GnP M5HT that was processed with the 3-roll mill prior to TEPA-grafting was also further reacted with DGEBA. The amine groups grafted to the GnP would undergo a reaction with the DGEBA to provide bonding to the matrix. GnP M5HT-3R-TEPA was added into DGEBA to make a 7wt% GnP solution and dispersed using a Flaktec mixer for 3min at 3000rpm. The DGEBA/GnP mixture was subsequently processed in the 3-roll mill at 250rpm with 2 passes at 20μm, 3 passes at 10μm, and 5 passes at 5μm nip

gap. The processed mixture was reacted at 150˚C for 2h under stirring in an oil bath. After reaction the mixture was filtered through a 0.22μm PTFE filter membrane and washed with acetone 3 times to remove excess DGEBA. Then the GnP was dried in a vacuum oven overnight at 60˚C, yielding GnP M5HT-3R-TEPA-3R-DGEBA.

5.3.3 Manufacturing of DGEBA-GnP Nano-Composite

The epoxy-GnP nano-composites were manufactured using a solvent blending technique. GnP were dispersed in acetone at a concentration of 10wt% and sonicated at 180W for 30min (10s on/ 5s off) in a dry ice bath with magnetic stirring on a stir plate using a Virsonic 750 sonication probe. DGEBA was added to the sonicated acetone/GnP solution to make a 3wt% DGEBA/GnP mixture. The acetone/DGEBA/GnP solution was further sonicated at 180W for 15min (10s on/ 5s off) in a dry ice bath with agitation on a stir plate. After sonication, the acetone was removed by heating to ~60˚C overnight and agitation on a stir plate. The DGEBA-GnP mixture was then processed on the 3-roll mill. The mill was operated at 250 rpm and the nip gap was successively reduced throughout the milling process. The 3-roll milling parameters are shown in Table 5-2:

Table 5-2: Processing parameters for 3-roll mill for different GnP grades

	M5	**M25**	**C750**
Mill Speed [RPM]	250	250	250
Passes at 20μm Nip	5	5	5
Passes at 10μm Nip	5	5	5
Passes at 5μm Nip	15	15	15

After 3-roll milling, the DGEBA-GnP mixture was degassed at ~70˚C under vacuum for 1h to remove the entrained air. The appropriate amount of mPDA curing agent for a 14.5phr stoichiometry was melted at 75˚C and added to the DGEBA-GnP mixture. The mixture was homogenized by hand and degassed for about 15min to remove entrained air. The DGEBA-GnP-mPDA mixture was poured into silicone molds and cured at 75˚C for 2h and post-cured at 125˚C for 2h in a convection oven.

5.3.4 Mechanical Properties

The cured samples were polished on a Struers Abramin polisher with 320, 600, 1200 and 4000 grit paper to yield a smooth sided sample prior to mechanical testing.

All mechanical properties were tested on the bases of at least 4 samples. The flexural properties were determined on the basis of ASTM D790 using a United Testing Systems SFM-20 load frame with a 100lbf load cell. The flexural samples had dimensions of 75x12.5x3mm. The support span width to thickness ratio was taken at 16:1 and the crosshead speed was calculated per ASTM D790-10. The notched Izod impact properties were determined using a TMI pendulum impact tester on the basis of ASTM D256 using a 1 ft-lbf hammer. The notched Izod impact samples used a molded pre-notch and had dimensions of 63.5x12.5x12.5mm. The fracture toughness was determined on the basis of ASTM D5045-99 using the compact tension sample configuration and a crosshead speed of 10 mm/min. The pre-crack was made by tapping a fresh razor blade into the molded pre-notch. The thermo-mechanical properties were determined using a TA Instruments Q800 dynamic mechanical analysis

(DMA) instrument using a single-cantilever beam setup in air from room temperature to 250˚C at a ramp rate of 3˚C/min at an amplitude of 20μm and a frequency of 1Hz.

The scanning electron microscopy investigation of the fracture surfaces were done using a Zeiss LS25 EVO SEM under high vacuum. The samples were sputter coated with a 1nm thick layer of tungsten prior to observation.

Surface analysis by XPS was conducted using a Physical Electronics PHI 5400 ESCA system. Samples were pumped to a pressure of less than 10^{-7} Torr and irradiated with a non-monochromatic Mg X-Ray with K-alpha 1,2 combined at an energy of 1254.6 eV. The take-off angle was 45 deg. Data analysis was performed using the Multipak version 8.0 by Physical Electronics.

5.4 Results and Discussion

5.4.1 Estimation of Graphene Nanoplatelet Edge Area

The sp^2-hybridisation of the carbon atoms that form the basal plane of graphene yields the planar structure of graphene. [23] Graphene nanoplatelets (GnP) are stacks of graphene layers (Figure 5.2) that have different number of graphene layers, held together by π-π stacking. [24] The morphologies of the GnP C- and M-grades are very different, with the C-grade having a ball-like structure and the M-grade being much more platelet like. The main contribution to the surface area comes from the basal plane of the top and bottom most graphene layer. The edge area of the individual graphene layers will not contribute significantly to the total surface area. With the sp^2-hybridization, reactive groups that are able to form covalent bonds are only available at

defect sites on the basal plane or at the edge of the platelet. This gives the edge area of the GnP considerable importance, as this is where the formation of covalent bonds occur. Based on the theoretical surface area of 2600 m^2/g, [25] an estimated number of graphene layers and their approximate edge area for each GnP-grade can be calculated. This estimation represents a theoretical maximum, as not all edge area may be populated with reactive groups that can undergo reaction with the matrix. An estimation of the nominal edge area for the three GnP grades is shown in Table 5-3:

Table 5-3: Estimation of GnP edge area

	C750	M5	M25
Nominal Surface Area [m2/g]	750	130-150	130-150
# of Platletes Per Stack [-]	3.5	20	20
Nominal Platlete Diameter [µm]	1	5	25
Basel Plane Area [m2]	1.57E-12	3.93E-11	9.82E-10
# of Platelet Stacks [Platelet Stacks/g]	4.77E+14	3.31E+12	1.32E+11
Platelete Circumference [m]	3.14E-06	1.57E-05	7.85E-05
Platelet Thickness [m]	3.35E-10	3.35E-10	3.35E-10
Platelet Edge Area [m2]	1.05E-15	5.26E-15	2.63E-14
Edge Area [m2/g]	*1.742*	*0.348*	*0.070*

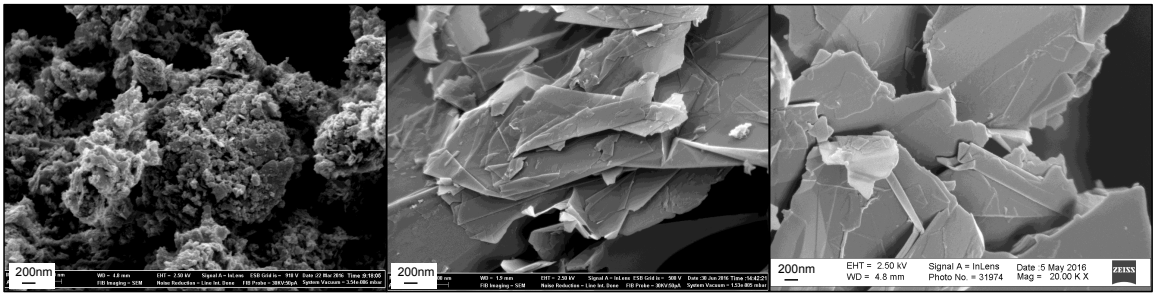

Figure 5.2: Morphology of heat-treated GnP; C750 (left), M5 (middle) and M25 (right)

5.4.2 TEPA-Grafting to Graphene Nanoplatelets

5.4.2.1 C750

The C-grade GnP has the smallest platelet diameter and the largest surface area of the GnP grades investigated in this study. This also gives the C750 the highest edge area as shown in Table 5-3 and the highest potential for grafting of amines. The XPS spectrum of the carbon 1s and oxygen 1s peaks for GnP C750HT-TEPA are shown in Figure 5.3:

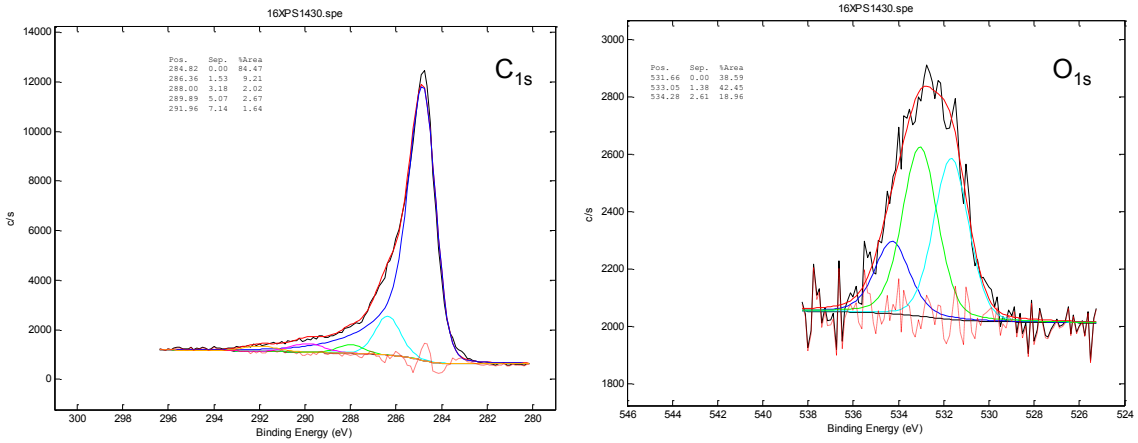

Figure 5.3: XPS spectra of C_{1s} (left) and O_{1s} (right) peaks for GnP C750HT-TEPA

Both peaks are a composite of several different peaks, representing the different bonding energies of the carbon and oxygen atoms. The peaks have been curve fit to de-convolute the different binding energies. The shift in binding energy comes from differences in electronegativity between two atoms that are bonded together. The large peak in the C_{1s} spectrum represents carbon-carbon bonds. When carbon atoms are bonded to oxygen atoms, the kinetic energy of photoemitted electrons will be reduced due to the higher electronegativity of the oxygen atom that will draw the bonding electrons toward it. The peak for that carbon atom will appear at a higher binding energy. The more oxygen atoms the carbon atom is bonded to, the higher the binding

energy will be. In addition, the surface (3-8nm) atomic concentration of carbon, oxygen and nitrogen can be determined from XPS. These are presented in a tabular form for all the GnP grades and treatments. The changes to the heat-treated C750 after TEPA-grafting is shown in Table 5-4:

Table 5-4: Influence of TEPA-grafting on atomic concentrations of carbon, nitrogen and oxygen on GnP C750 as determined by XPS

Atomic Concentration [%]	C750HT	C750-TEPA
C1s	87.7	88.6
N1s	0.0	6.6
O1s	12.3	4.8

In the heat-treated condition (C750HT), the C750 shows a significant concentration of oxygen. With TEPA-grafting (C750HT-TEPA) this oxygen concentration is reduced by about two-thirds, indicating that some reaction of the TEPA with the edge groups has taken place. This is further supported by changes to the nitrogen signal. In the heat-treated condition, no detectable nitrogen surface concentration. The grafting with TEPA increases the nitrogen content on the C750 significantly from 0 to 6.6%. This indicates that there nitrogen containing groups are bonded to the GnP, which are probably TEPA.

SEM images of the GnP C750 (Figure 5.4) show that the morphology of the GnP has not significantly change with TEPA-grafting. The TEPA-grafted GnP does however appear to show more small platelets with platelet diameters in the sub 1µm range.

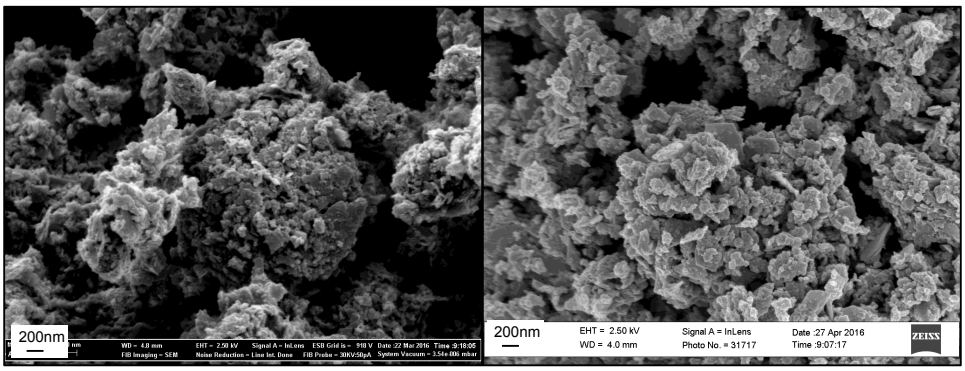

Figure 5.4: SEM images of GnP C750, heat-treated only (left) and TEPA-grafted (right)

5.4.2.2 M5

GnP M5 was processed in TEPA via 3-roll milling. The further processing and reaction of TEPA-grafted M5 in DGEBA should lead to a GnP that is very compatible with the polymer matrix. The changes to the surface chemistry for both processing steps is shown in Table 5-5:

Table 5-5: Influence of TEPA-grafting via 3-roll mill and further reaction of TEPA-grafted GnP M5HT with DGEBA

Atomic Concentration [%]	M5HT	M5HT-3R-TEPA	M5HT-3R-TEPA-3R-DGEBA
C1s	93.7	90.7	83.7
N1s	0.0	1.6	1.1
O1s	6.3	7.7	15.3

The surface oxygen concentration of the heat-treated GnP M5 (M5HT) is lower than measured on the GnP C750 due to the lower edge area. No nitrogen signal is detected. After TEPA-grafting via 3-roll mill (M5HT-3R-TEPA) the oxygen concentration is slightly higher (+22%), probably due to the formation of new edge surfaces from plates fracturing at weak spots during 3-roll milling. A 1.6% nitrogen signal is also seen, indicating that grafting of TEPA has taken place. Further reacting the M5HT-3R-TEPA

with DGEBA results in a -32% reduction in nitrogen concentration, indicating that some of the amine groups have reacted. The significant increase in surface oxygen concentration is probably due to the hydroxyl and ether groups present on the DGEBA molecules that were bonded to the GnP.

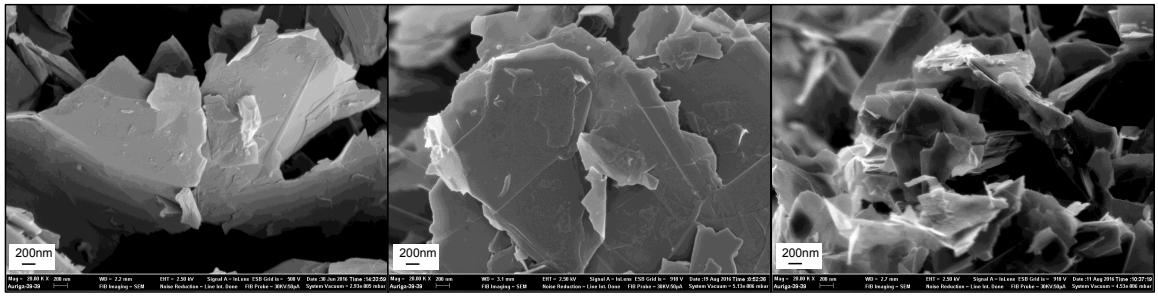

Figure 5.5: Influence of TEPA-grafting via 3-roll mill and further DGEBA reaction on morphology of GnP M5; M5HT (left), M5HT 3-roll mill TEPA-grafted (middle) and M5HT 3-roll mill TEPA-grafted DGEBA reacted

5.4.2.3 M25

The GnP M25 represents the highest aspect ratio platelet investigated in this study. However, it also has the lowest edge area as seen in Table 5-3, limiting the amount of TEPA that can be grafted. The influence of TEPA-grafting with and without 3-roll milling is shown in Table 5-6:

Table 5-6: Influence of TEPA-grafting with and without 3-roll milling on atomic concentrations of carbon, nitrogen and oxygen on GnP M25 as determined by XPS

Atomic Concentration [%]	M25HT	M25HT-TEPA	M25HT-3R-TEPA
C1s	96.2	93.2	90.4
N1s	0.0	1.1	1.2
O1s	3.8	5.7	8.4

The heat-treated only GnP (M25HT) shows a small amount of oxygen groups and no measureable amount of nitrogen groups. This is consistent with the results from the

GnP C750HT. With the TEPA-grafting (M25HT-TEPA) the concentration of both the oxygen and nitrogen groups present on the GnP increases. The oxygen concentration increases by about 50% with the nitrogen increasing from 0 to 1.1%. The increase in surface oxygen groups may be rooted in the formation of new edges if the GnP was to fracture at defect sites during the reaction with TEPA, which was done under atmospheric conditions. The smaller increase in surface nitrogen groups compared to C750HT is probably due to the smaller amount of edge area. The increase in oxygen concentration is even more pronounced (+120%) in the M25HT that was processed in the 3-roll mill with TEPA (M25HT-3R-TEPA). The expectation here is that the high shear forces generated in the 3-roll mill will not only exfoliate the GnP but also fracture some of the platelets, leading to the formation of new edges that can react either the TEPA or the oxygen from the surrounding atmosphere. A higher concentration of nitrogen surface groups is also detected. Compared to the TEPA-grafting only, the processing of the GnP M25HT with the 3-roll mill results in a 14% increase in surface nitrogen groups and a 45% increase in surface oxygen groups.

The morphology of the GnP M25 as shown in Figure 5.6, is significantly different from the C750 (Figure 5.4). The high aspect ratio of the M-grade GnP is clearly seen as well as the stacks of graphene layers. The grafting of TEPA to the M25 appears to leave a slight residue on the surface of the GnP. While no significant difference between the GnP that was processed with and without 3-roll milling can be seen, the average platelet diameter is challenging to qualify.

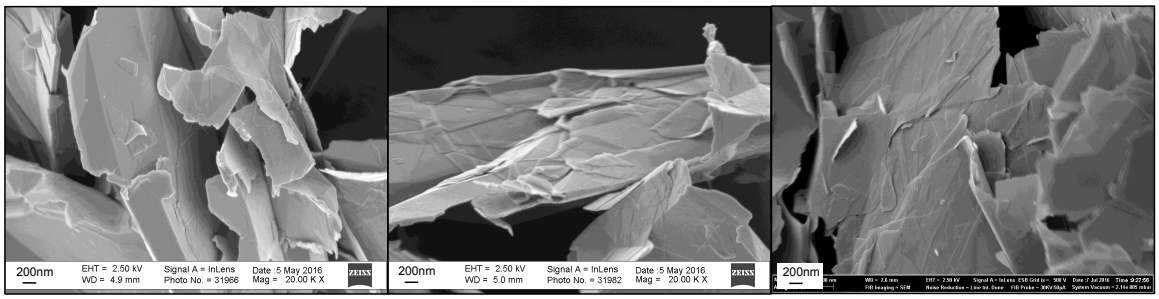

Figure 5.6: Morphology of GnP M25 heat-treated only (left), TEPA-grafted (middle) and 3-roll mill TEPA-grafted (right)

As discussed above the functional groups on the GnP are located mainly around the edges of the GnP. This implies that the concentration of surface oxygen should be related to the amount of edge area in the GnP. A plot of the surface oxygen concentration as a function of calculated edge area is shown in Figure 5.7. A linear relationship is clearly visible (R^2 close to unity), with GnP M25 having the lowest edge area also showing the lowest surface oxygen concentration. The GnP C750, with the highest calculated edge area also shows the highest surface oxygen concentration.

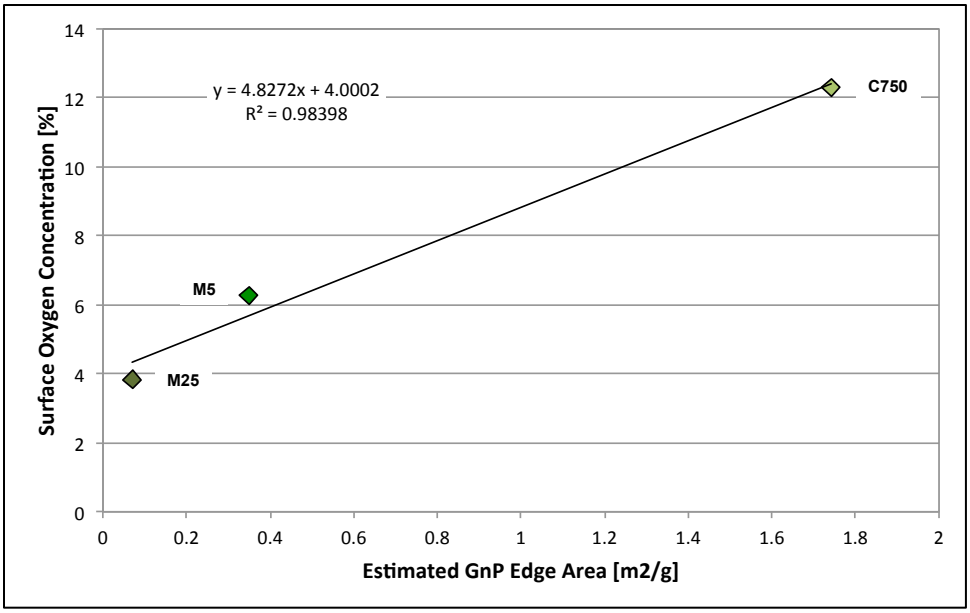

Figure 5.7: Surface oxygen concentrations from XPS as a function of estimated GnP edge area for different GnP grades in heat-treated condition

It follows that since the grafting of TEPA will take place at the edges and surface functional groups, a similar relationship should exist. As shown in Figure 5.8, this is indeed the case, if at a lower level than the oxygen surface functional groups.

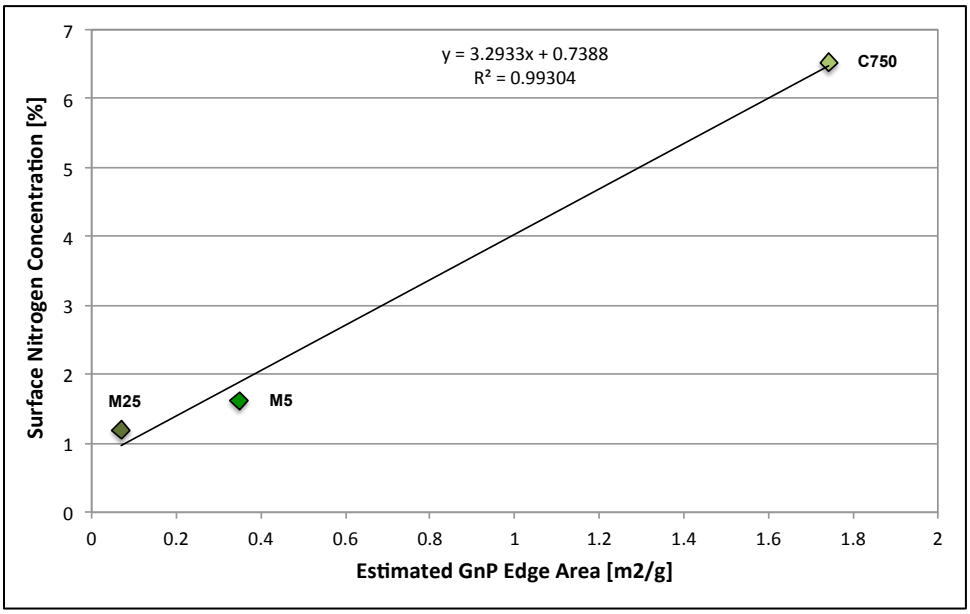

Figure 5.8: Surface nitrogen concentrations from XPS as a function of estimated GnP edge area for different GnP grades after TEPA grafting

5.4.3 Mechanical Properties of DGEBA/GnP/mPDA Nano-Composite

5.4.3.1 GnP C750: Influence of TEPA Grafting

The dispersion of GnP in the nano-composite as investigated by SEM is shown in Figure 5.9:

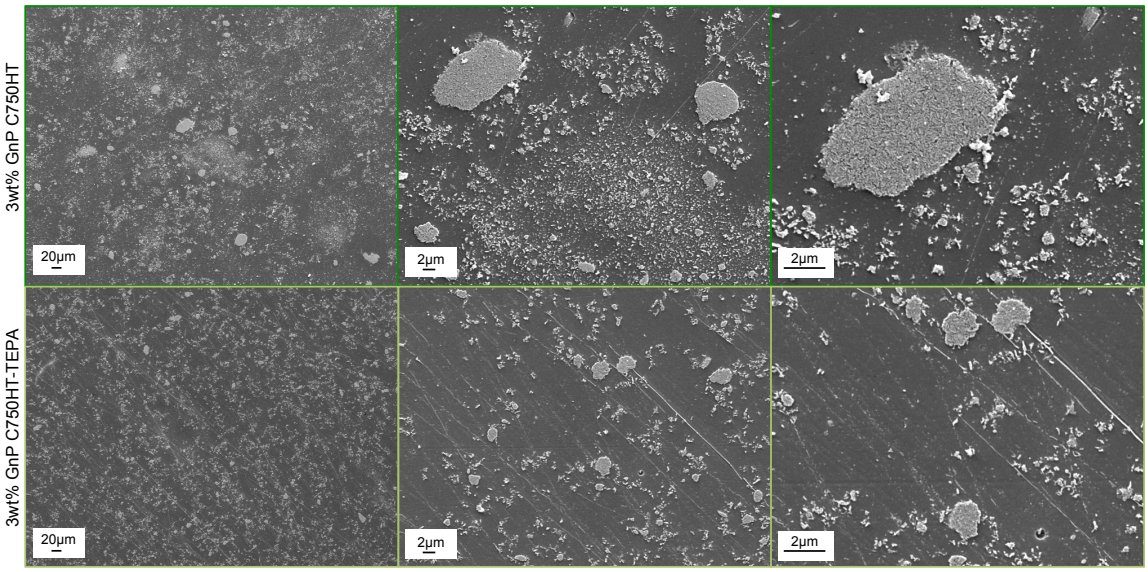

Figure 5.9: GnP dispersion in cross-section of DGEBA/3wt% GnP C750 nano-composite. GnP C750HT (top) and GnP C750HT-TEPA (bottom)

No indications of GnP settling in the form of differences in GnP dispersion or concentration between top and bottom of samples were seen in either nano-composite. The heat-treated GnP composite showed some large agglomerates of GnP throughout the cross-section, which are 5-6µm in size. Visible are also clusters of particles, which are smaller than the nominal GnP C750 platelet diameter of 1-2µm. These smaller particles are present in the uncompounded, heat-treated GnP shown in Figure 5.4. These clusters indicate that concentrations of small particles establish within the cross-section. The dispersion of the TEPA-grafted GnP appears to be more uniform. The visible particles are similar in size to the nominal GnP C750 diameter of 1-2µm. There is also less evidence of small particle clusters. The TEPA-grafting has improved the exfoliation of the GnP, probably due to the TEPA molecules grafted to the platelet edge reducing the re-agglomeration of the GnP after exfoliation during 3-roll milling with DGBEA. However, the dispersion of the GnP C750 could still be further improved.

The mechanical properties of GnP C750 in both the heat treated only and TEPA-grafted condition are shown in Figure 5.10:

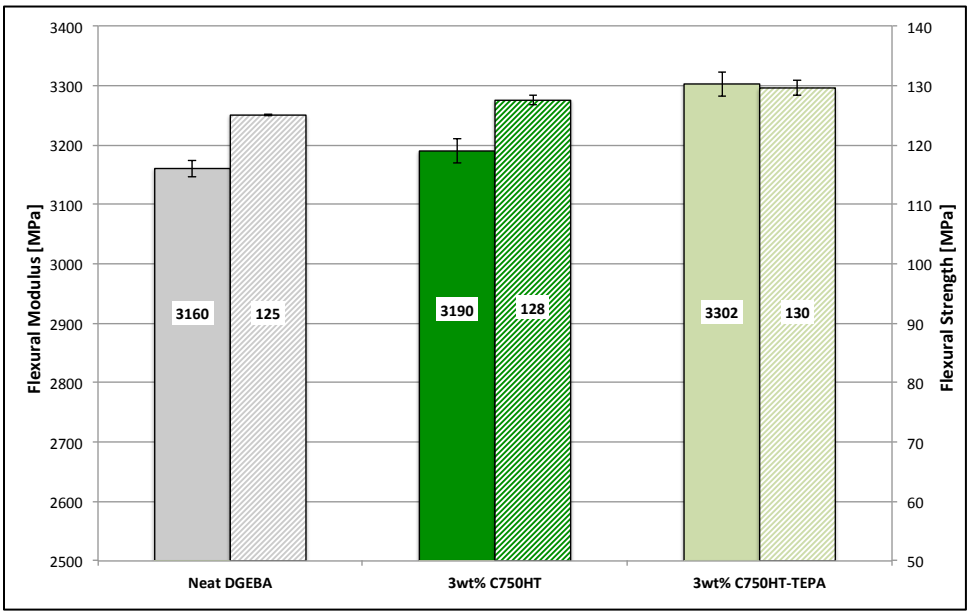

Figure 5.10: Influence of TEPA grafting on flexural strength (solid) and modulus (hashed) of DGEBA/GnP C750HT nano-composite at 3wt% GnP loading

The addition of the higher modulus GnP is expected to increase the modulus of the DGEBA/GnP nano-composite. The GnP C750HT shows a minor increase (+1%) in modulus. However, this increase is not statistically significant. This may indicate marginal GnP/matrix bonding. A slight increase in strength (+2%) supports this. The high amount of edge area may be providing some bonding of the GnP into the matrix. Improvements in flexural properties are seen with the GnP C750HT-TEPA. The increased modulus (+4.5%) and strength (+3.7%) indicate better GnP/matrix adhesion. Observing the fracture surfaces of the flexural samples (Figure 5.11) on the tension side of the coupons supports the trends discussed above.

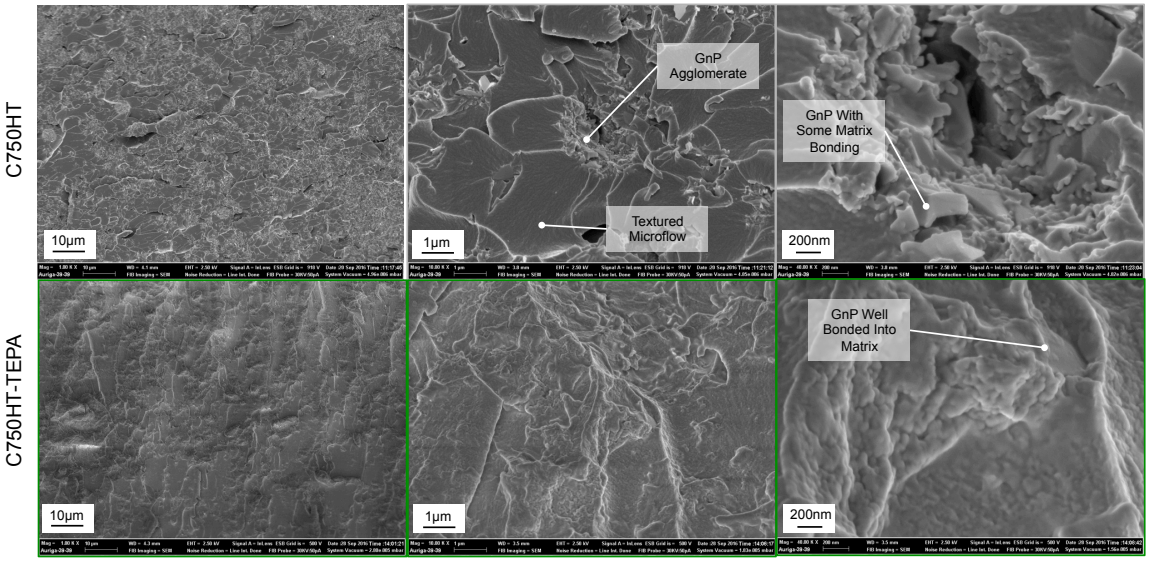

Figure 5.11: Fracture surfaces of DGEBA/GnP/mPDA nano-composite with 3wt% GnP. GnP C750HT (top) and GnP C750HT-TEPA (bottom) from tension side of flexural test samples

Both nano-composite fracture surfaces show increased surface roughness, which indicates that some additional energy has been used during fracture. Additionally, there are indications of GnP agglomerates surrounded by areas of neat matrix for both GnP treatments. This may indicate that while the processing of the DGEBA/ GnP C750 via the 3-roll mill yields good mechanical results, the GnP dispersion could be further improved. The GnP C750HT-TEPA appears to be more integrated into the fracture surface, indicating better GnP/matrix adhesion from the amine groups grafted to the edges of the GnP. The better integration is probably based on the shape of the GnP C750, which is more particle-like than the platelet-like M-grade GnP discussed next.

The impact of TEPA-grafting on the notched Izod impact strength of the DGEBA/GnP C750/mPDA nano-composite is shown in Figure 5.12:

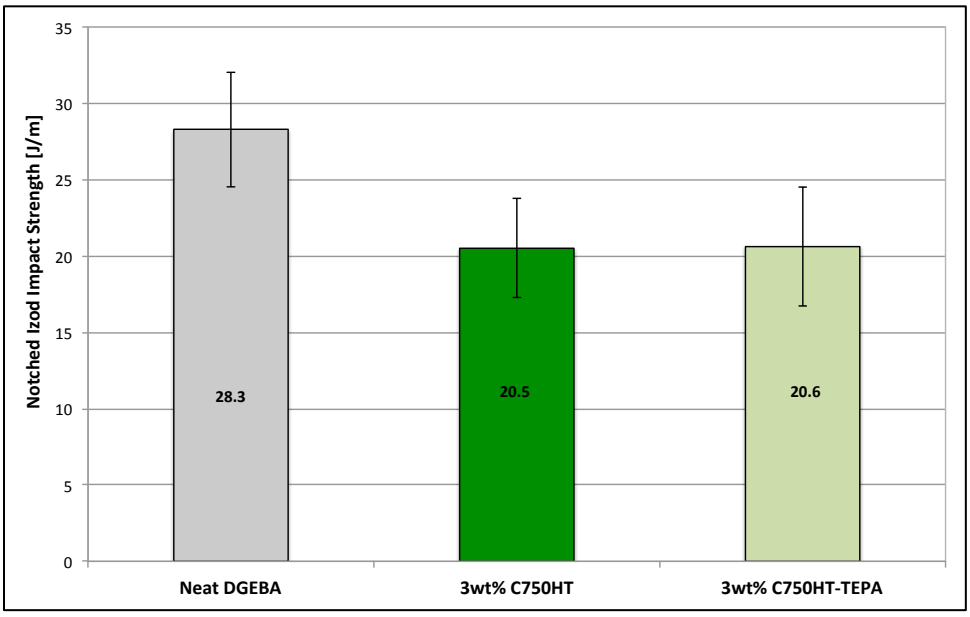

Figure 5.12: Influence of TEPA grafting on notched Izod impact strength of DGEBA/GnP C750HT nano-composite at 3wt% GnP loading

The notched Izod impact strength of the GnP C750 nano-composite is significantly reduced (-28%) irrespective of TEPA-grafting. The high loading rate of the notched Izod impact test, the GnP C750 represents more of a void within the DGEBA matrix, reducing the impact strength. This is in contrast to the flexural test with a slow loading rate that showed slight improvements in strength with the addition of GnP C750. (Figure 5.10) The improved bonding of the GnP C750HT-TEPA does not appear to be of benefit.

The fracture toughness of the DGEBA/GnP C750/mPDA nano-composite (Figure 5.13) is not statistically affected by TEPA-grafting. The C750HT has a lower average fracture toughness (-6%), while the C750HT-TEPA is slightly higher (+2%), compared to the neat DGEBA baseline. The C750 does not appear to be effective in toughening the composite via crack deflection due to the low aspect ratio of the C-grade GnP. Similar findings have been reported by Chong *et al.* [26], who also determined no

improvements in fracture toughness a DGEBA/GnP C750 nano-composite up to a GnP concentration of 2wt%.

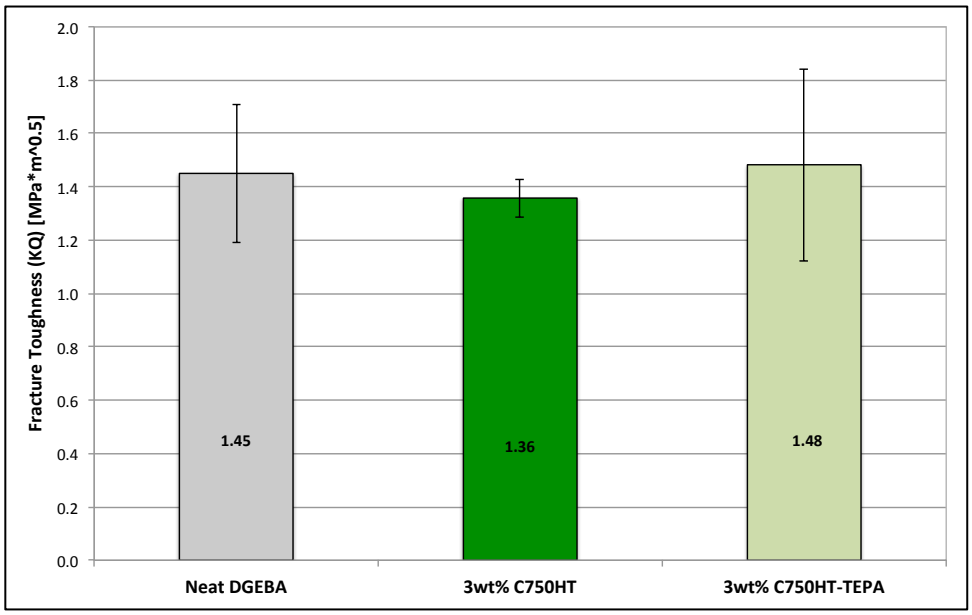

Figure 5.13: Influence of TEPA grafting on fracture toughness of DGEBA/GnP C750HT nano-composite at 3wt% GnP loading

The fracture surface morphology shown in Figure 5.14 changes significantly with the addition of 3wt% GnP C750.

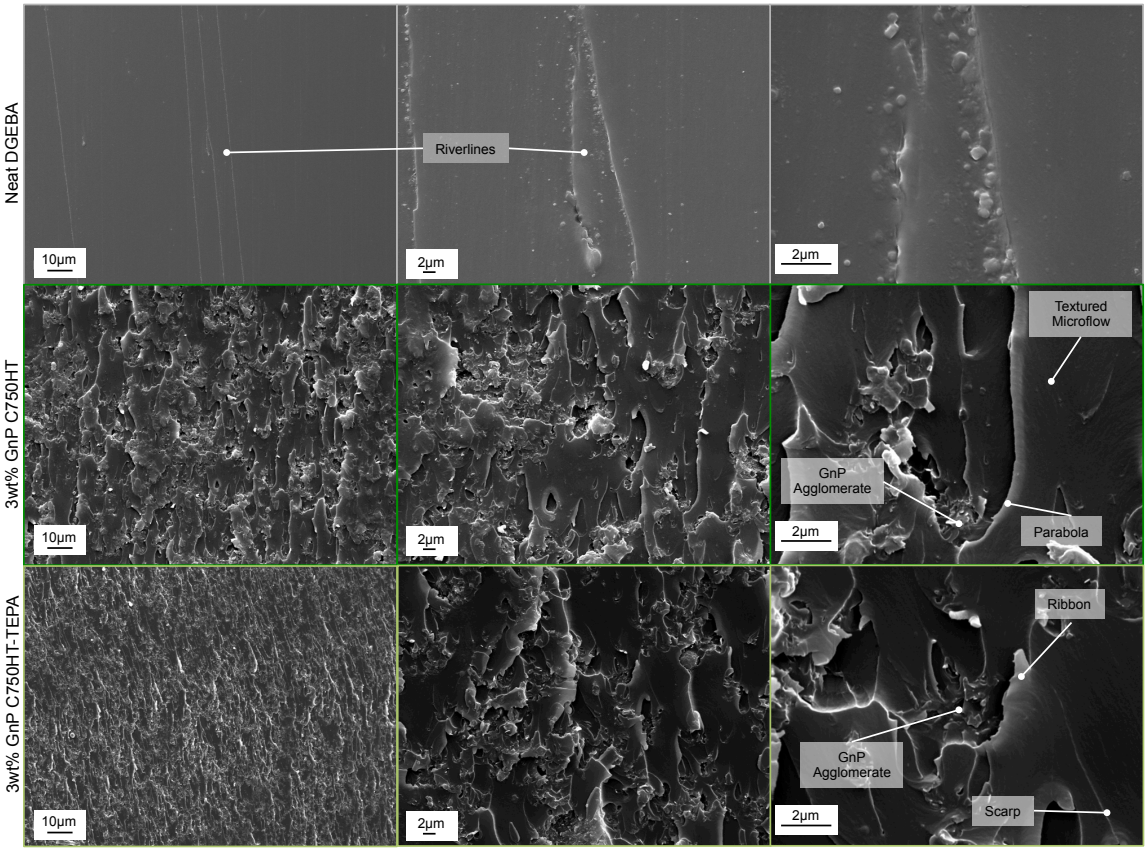

Figure 5.14: Fracture surfaces of fracture toughness samples (compact tension) as observed by SEM. Neat DGEBA (top); DGEBA+3wt% GnP C750HT (middle); DGEBA+3wt% GnP C750HT-TEPA (bottom). Crack propagation direction is from bottom to top of image

The neat DGEBA fracture surface shows typical brittle fracture morphology. The surface appears very smooth with little surface roughness. The main visible features on the fracture surface are riverlines, regions where cracks growing in two different planes intersect and combine. These riverlines are oriented parallel to the direction of crack propagation. With the addition of 3wt% GnP C750 into the DGEBA matrix, the fracture surface morphology becomes much rougher. The formation of parabolas is visible, where an agglomerate of GnP acts as an inhomogeneity ahead of the advancing crack front. Along the crack front multiple cracks appear to have advanced on different planes that merge at somewhere across the fracture surface as indicated by the formation of

scarps and ribbons. Similar to the fracture surfaces from the flexural samples shown in Figure 5.11 regions of matrix are visible, which don't appear to have GnP in them. Textured microflow aligned in the fracture direction, which is prevalent in brittle epoxy systems, is visible in these regions at higher magnification.

The addition of GnP C750 increases the glass transition temperature (T_g) of the DGEBA/GnP C750/mPDA nano-composite by about +4%. (Figure 5.15) Improvement of T_g is usually an indication of good filler/matrix adhesion. The impact of TEPA-grafting on the glass transition temperature is minimal, with the C750HT-TEPA showing a slightly higher T_g. The Tan δ curves shown in Figure 5.16 show a single peak, indicating a single phase. The Tan δ peak height is the same for the neat DGEBA and the nano-composites, indicating similar dampening behavior.

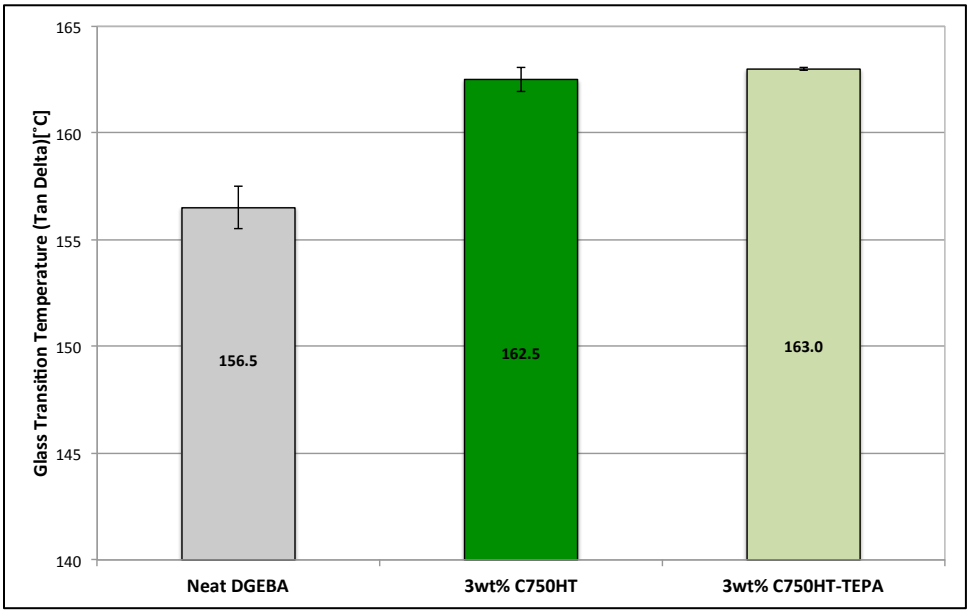

Figure 5.15: Influence of TEPA grafting on glass transition temperature determined from maximum of Tan delta curve of DGEBA/GnP C750HT nano-composite at 3wt% GnP loading

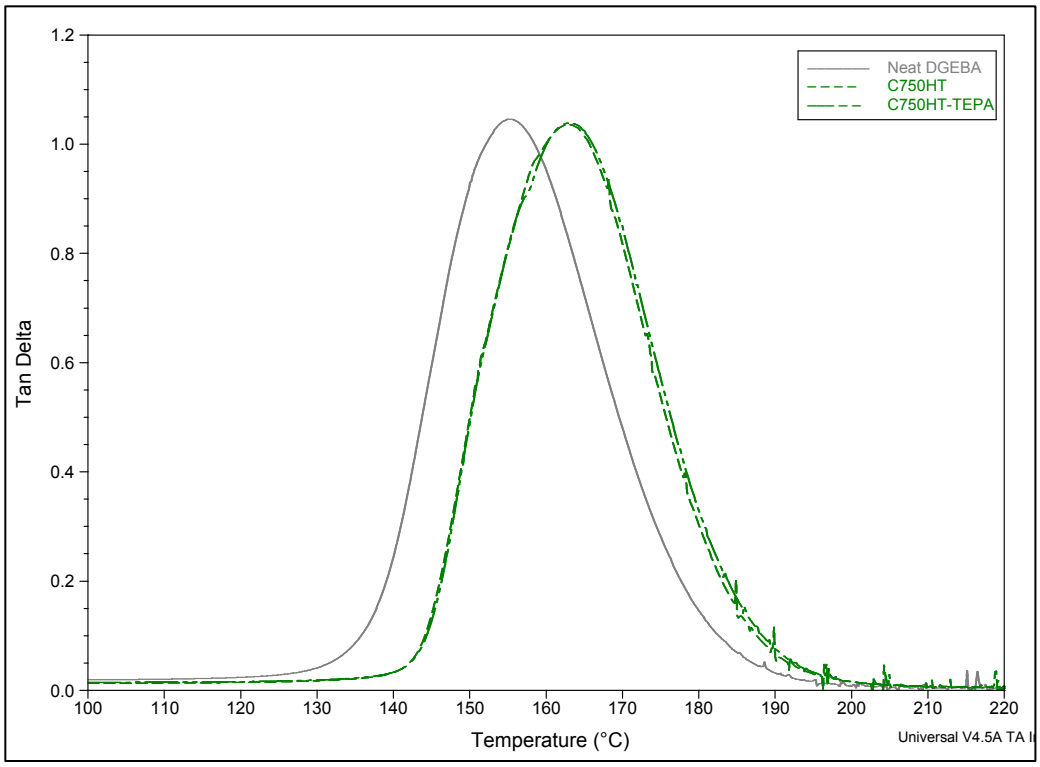

Figure 5.16: DMA Tan δ curves of 3wt% GnP C750/DGEBA nano-composites as determined at 20μm amplitude and 1Hz frequency

5.4.3.2 GnP M5: Influence of TEPA-Grafting and Reaction with DGEBA

The dispersion of GnP in the nano-composite as investigated by SEM is shown in Figure 5.17:

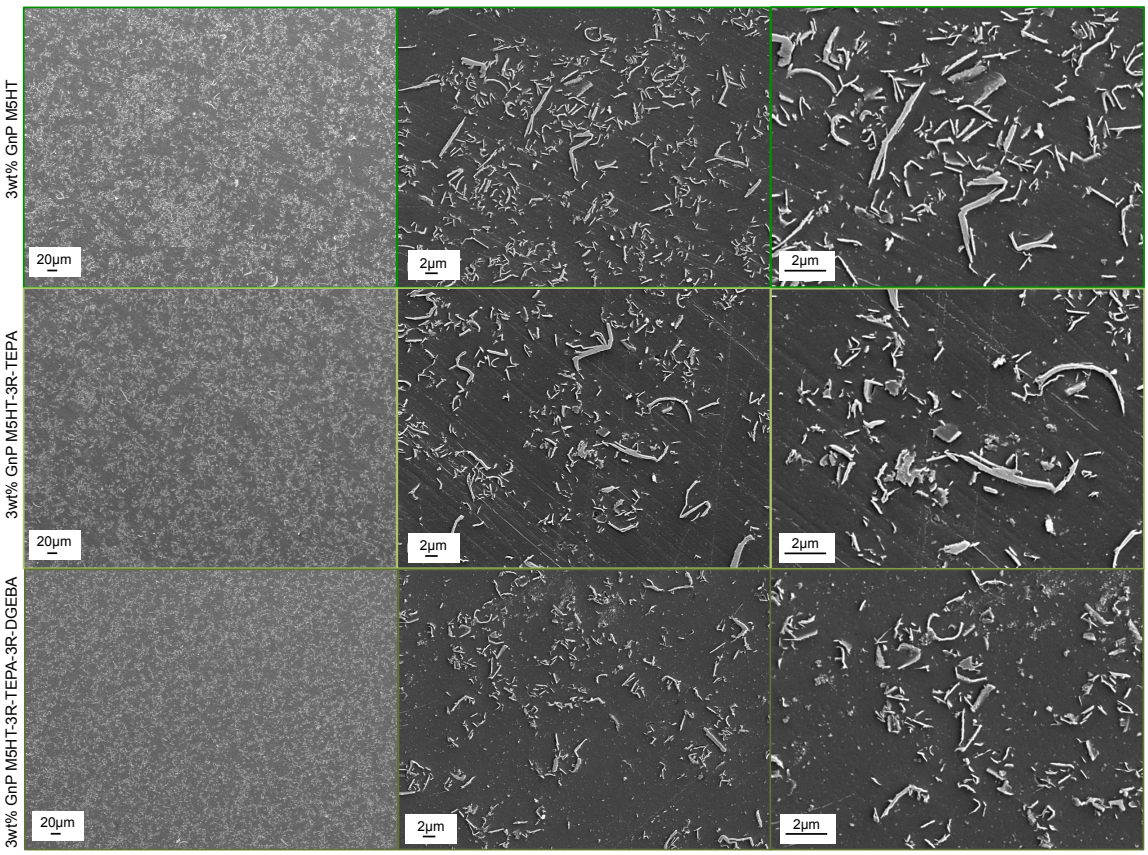

Figure 5.17: GnP dispersion in cross-section of DGEBA/3wt% GnP M5 nano-composite. GnP M5HT (top), GnP M5HT-3R-TEPA (middle), and GnP M5HT-3R-TEPA-3R-DGEBA (bottom)

No indications of GnP settling in the form of differences in GnP dispersion or concentration between top and bottom of samples were seen in any nano-composite. The dispersion of GnP M5 appears to be fairly uniform within the sample cross-section. The GnP M5HT and M5HT-3R-TEPA show similar amounts of resin rich areas in the cross-section. The M5HT may have slightly more large GnP agglomerates (5-6µm) than the M5HT-3R-TEPA. The GnP M5HT-3R-TEPA-3R-DGEBA exhibits the best dispersion of GnP within the sample cross-section and the size of the resin-rich areas appears to be smaller. The platelet size, at 2-4µm, also appears to be smaller than for the M5HT and M5HT-3R-TEPA. This is probably an indication of the additional processing of the

GnP in the 3-roll mill seen by the M5HT-3R-TEPA-3R-DGEBA, which was processed with the 3-roll mill three times. Higher shear forces should be generated when processing the GnP in DGEBA, which has a higher viscosity that TEPA.

The mechanical properties of GnP M5HT in both the heat treated only and TEPA-grafted condition are shown in Figure 5.18:

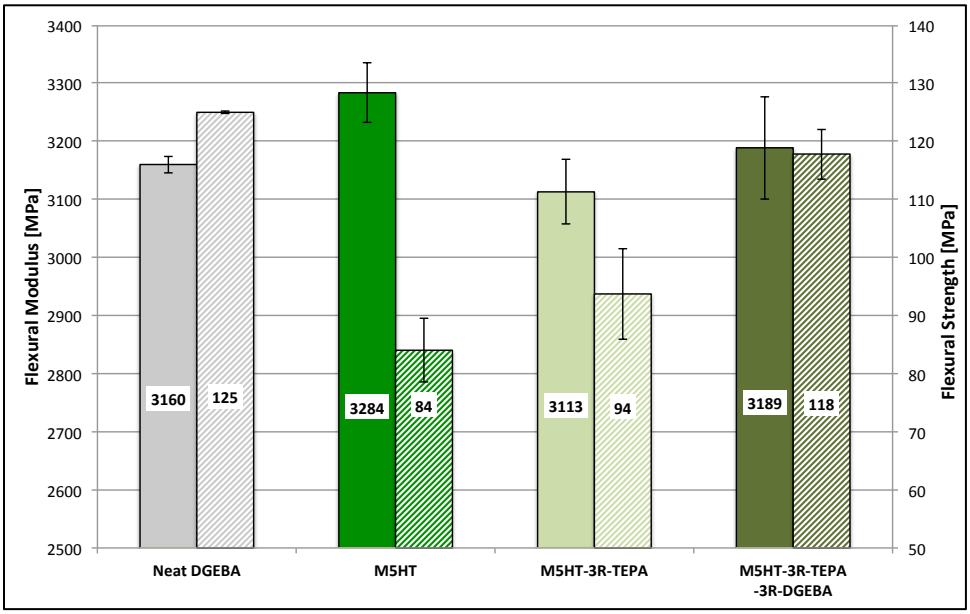

Figure 5.18: Influence of TEPA-grafting and TEPA-grafting with further DGEBA reaction on flexural strength and modulus of DGEBA/GnP M5HT nano-composite at 3wt% GnP loading

The heat-treated only M5 increases the modulus (+4%). With the 3-roll milling of the GnP M5 in TEPA and the further reaction of the TEPA-grafted GnP M5 with DGEBA, the modulus is equal to the neat DGEBA within data scatter. A reduction in platelet size is possible with high shear processing in the 3-roll mill, leading to marginal influences on the flexural modulus. The flexural strength also decreases with the addition of GnP M5, analogous to GnP M25. While the heat-treated only GnP M5 reduces the strength by 33%, grafting TEPA to the GnP M5HT lowers the reduction to 25% below the neat DGEBA. Further reacting the TEPA-grafted GnP M5 with DGEBA

mitigates the reduction in flexural strength to 6%, very close to neat DGEBA. Improved bonding between the platelet edges and the matrix are probably the main causes of improved flexural strength.

The investigation of the fracture surfaces of the flexural samples support the reasoning above (Figure 5.19):

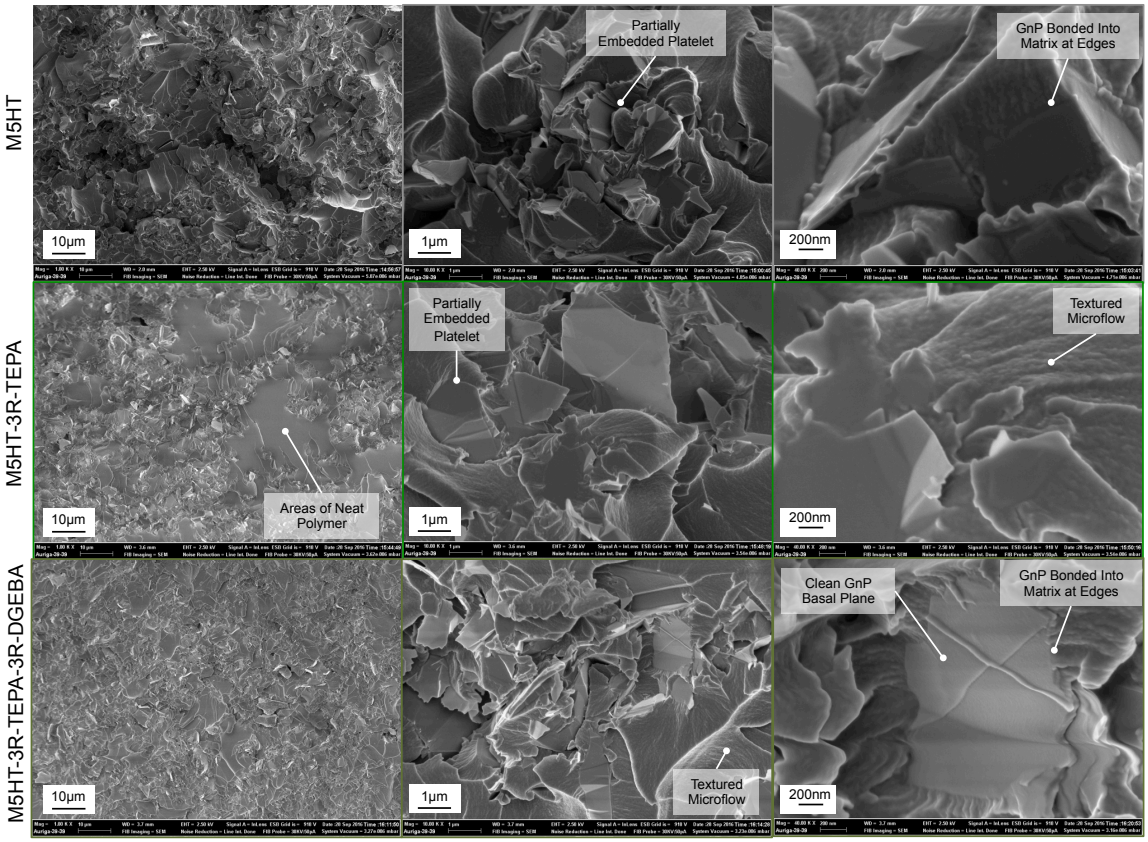

Figure 5.19: Fracture surfaces of DGEBA/GnP/mPDA nano-composite with 3wt% GnP M5 heat treat only (top) and GnP M5HT-3R-TEPA (middle), and GnP M25HT-3R-TEPA-3R-DGEBA (bottom) from tension side of flexural test samples

With heat-treatment alone there is some bonding at the platelet edges. There is some indication of GnP that is partially imbedded into the matrix with the other side protruding from the matrix. This implies two potential toughening mechanisms: first, there is pullout of the GnP from the matrix. This toughening would be limited to the covalent bonds around the GnP edges; second is the mechanism of crack bridging,

where the GnP is spans the width of the propagating crack, holding it together and reducing the stress intensity at the crack tip, slowing crack growth. Which of these mechanisms it predominant is challenging to identify. The GnP edge-bonding into the matrix visually increases with TEPA-grafting and further with DGEBA reaction, indicating improved filler/matrix bonding with TEPA-grafting and further reaction with DGEBA. In all cases any exposed basal planes are very clean, indicating that while the platelets were bonded with the matrix, the failure happened between the graphene layers within the GnP stack, that are only held together by weaker π-π interactions. Covalent bonding between platelets or total GnP exfoliation would be needed to address this issue.

Analogous to the GnP C750 previously discussed, the addition of GnP M5 reduces the notch Izod impact strength significantly compared to neat DGEBA/mPDA. (Figure 5.20) The reductions in impact strength for the GnP M5 range from 33 to 39% but are all statistically similar. The M5HT-3R-TEPA shows a slightly lower average reduction than the M5HT (-37% vs -39%) with the M5HT-3R-TEPA-3R-DGEBA being slightly above that (-33%). As consistently seen, the very stiff GnP nano-filler does not appear to be a good toughening agent for high loading rate events.

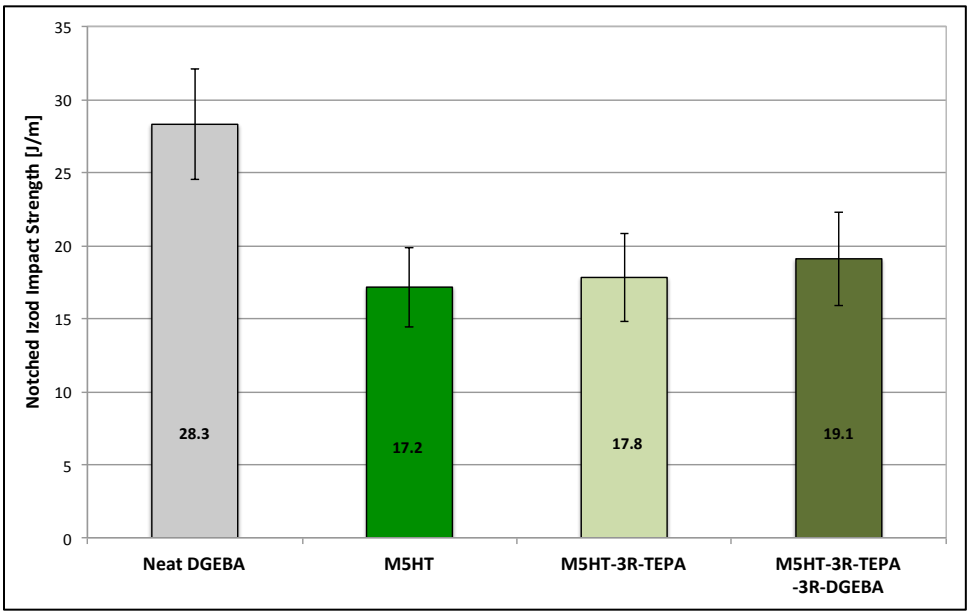

Figure 5.20: Influence of TEPA-grafting and TEPA-grafting with further DGEBA reaction on notched Izod impact strength of DGEBA/GnP M5HT nano-composite at 3wt% GnP loading

GnP M5HT shows the highest increase of +31% compared to neat DGEBA/mPDA. Both M5HT-3R-TEPA and M5HT-3R-TEPA-3R-DGEBA show lower improvements over neat DGEBA/mPDA of +22% and +24%, respectively. The improved GnP/matrix bonding that was shown in the flexural strength is probably mitigated by the reduction in the platelet size from the high shear processing in the 3-roll mill as shown in Figure 5.17, which decreased the effectiveness for toughening by crack deflection.

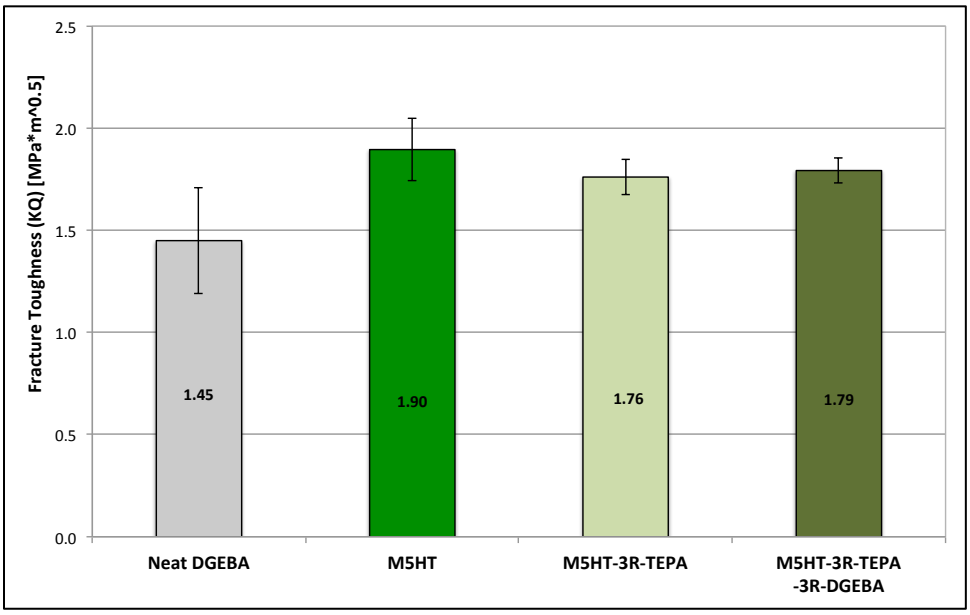

Figure 5.21: Influence of TEPA-grafting and TEPA-grafting with further DGEBA reaction on fracture toughness of DGEBA/GnP M5HT nano-composite at 3wt% GnP loading

The morphology of the fracture toughness fracture surfaces shown in Figure 5.22 change significantly with the addition of 3wt% GnP M5. The overall roughness of the fracture surface is significantly higher compared to neat DGEBA and even to the 3wt% C750HT fracture surfaces (Figure 5.14). This indicates significantly more crack deflection and increased energy dissipation during fracture, which is seen in the increased fracture toughness. Fracture surface features like textured microflow, ribbons, and scarps are visible. With the higher aspect ratio GnP M5 there are also platelets that are partially embedded in the fracture surface, indicating potential for toughening via crack bridging. [5] Analog to the flexural fracture surfaces (Figure 5.19), there is indication of bonding around the GnP platelet edges, especially for the M5HT-3R-TEPA. The clean basal plane surface indicates that the failure occurred between the GnP layers or at the outer GnP layer. The fracture surfaces of the DGEBA reacted GnP

(M5HT-3R-TEPA-3R-DGEBA) are similar to those of the TEPA-reacted GnP. This is consistent given their statistically identical fracture toughness.

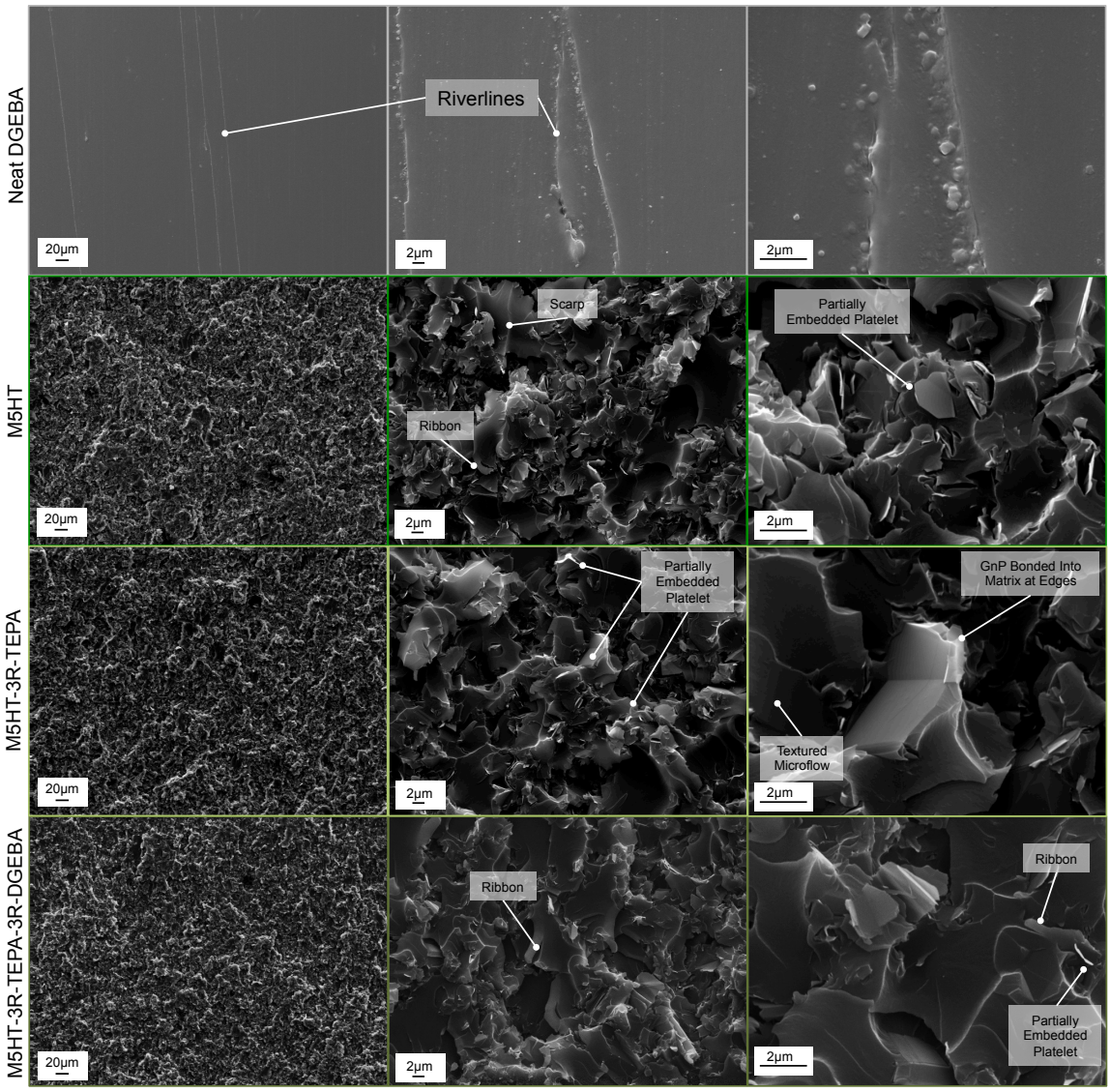

Figure 5.22: Fracture surfaces of fracture toughness samples (compact tension) as observed by SEM. Crack propagation direction is from bottom to top of image. Neat DGEBA (top); DGEBA+3wt% GnP M5HT (top, middle); DGEBA+3wt% GnP M5HT-3R-TEPA (bottom, middle); DGEBA+3wt% GnP M5HT-3R-TEPA-3R-DGEBA (bottom)

The glass transition temperature (T_g) of the DGBEA/GnP M5/mPDA nano-composite is slightly increased (+1.2% to +1.7%) over neat DGEBA/mPDA. All T_g of the nano-composites are within a half percent of one another, indicating a minor impact of

TEPA-grafting and further DGEBA reaction. This is further supported by the shape and height of the Tan δ curves shown in Figure 5.24, which do not change significantly.

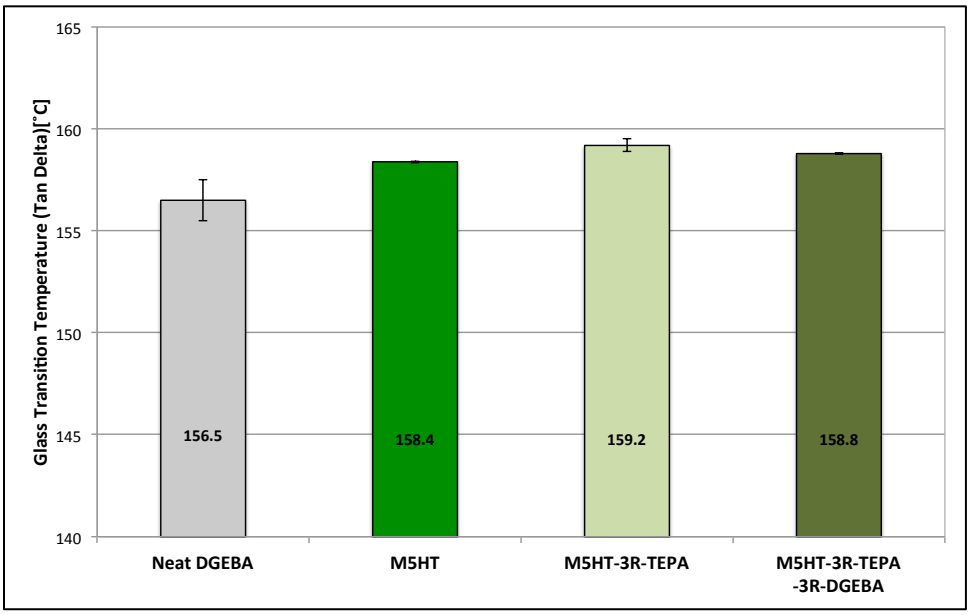

Figure 5.23: Influence of TEPA-grafting and TEPA-grafting with further DGEBA reaction on glass transition temperature as determined from maximum of Tan delta curve of DGEBA/GnP M5HT nano-composite at 3wt% GnP loading

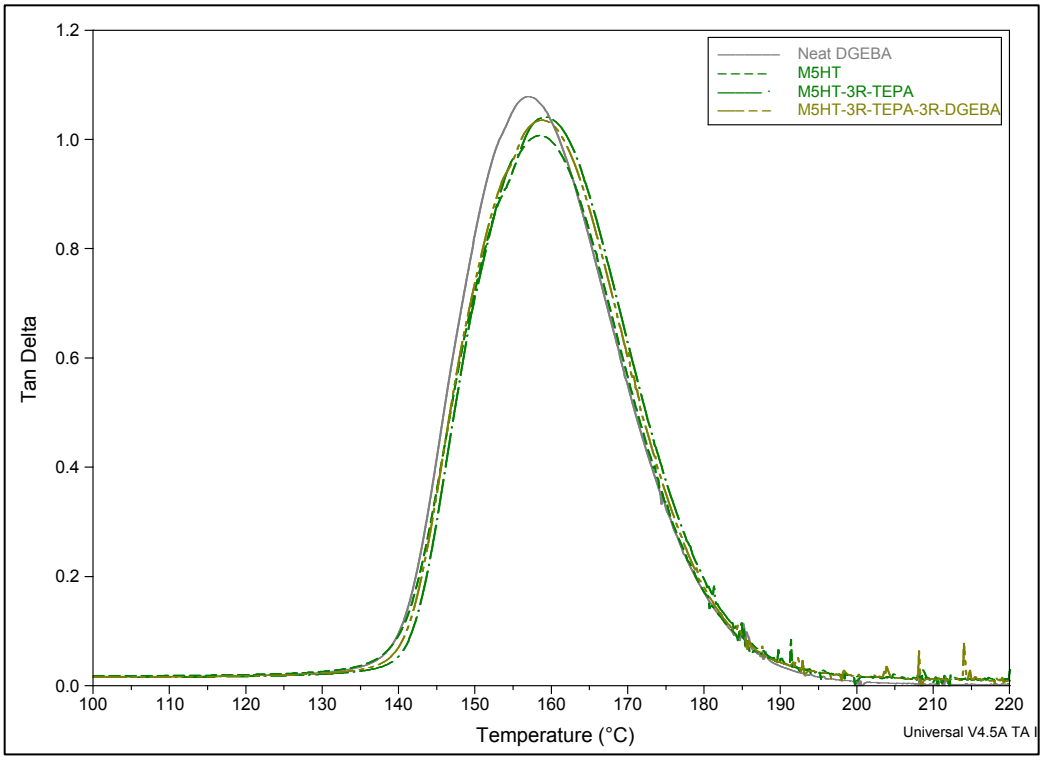

Figure 5.24: DMA Tan δ curves of 3wt% GnP M5/DGEBA nano-composites as determined at 20μm amplitude and 1Hz frequency

5.4.3.3 GnP M25: Influence of TEPA-Grafting With and Without 3-Roll Milling

The dispersion of GnP in the nano-composite as investigated by SEM is shown in Figure 5.25:

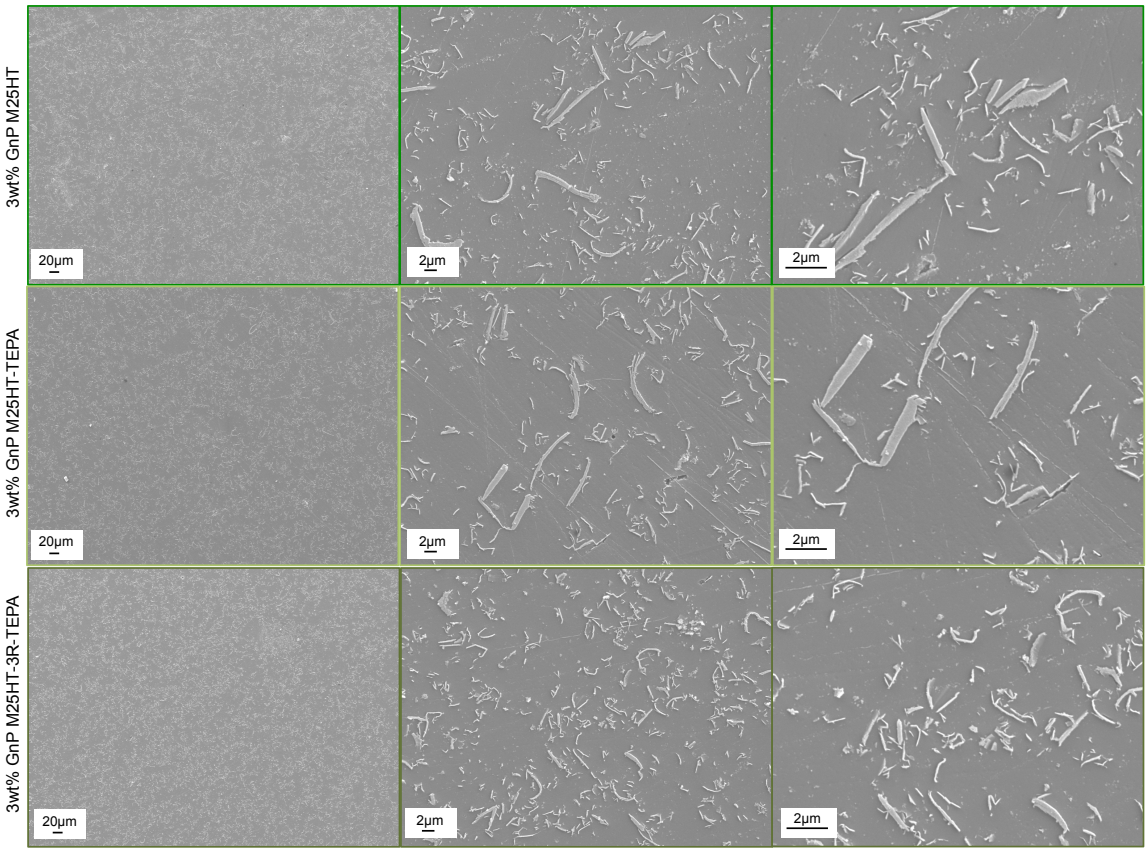

Figure 5.25: GnP dispersion in cross-section of DGEBA/3wt% GnP M25 nano-composite. GnP M25HT (top), GnP M25HT-TEPA (middle), and GnP M25HT-3R-TEPA (bottom)

No indications of GnP settling in the form of differences in GnP dispersion or concentration between top and bottom of samples were seen in either nano-composite. The dispersion of GnP M25 appears to be fairly uniform within the sample cross-section. All the DGBEA/GnP M25HT nano-composites appear to have similar GnP dispersions, regardless of TEPA-treatment. Both the GnP M25HT and M25HT-TEPA appear to have the similar GnP agglomerates (10-15µm size), indicating that for M25 the TEPA-treatment alone does not improve exfoliation. The platelet size below the nominal diameter of 25µm may indicate an effect of the high shear processing in DGEBA in the 3-roll. The GnP M25HT-3R-TEPA, which was twice processed in the 3-roll mill, shows smaller size GnP agglomerates (5-6µm).

The mechanical properties of GnP M5HT in both the heat treated only and TEPA-grafted condition are shown in Figure 5.26:

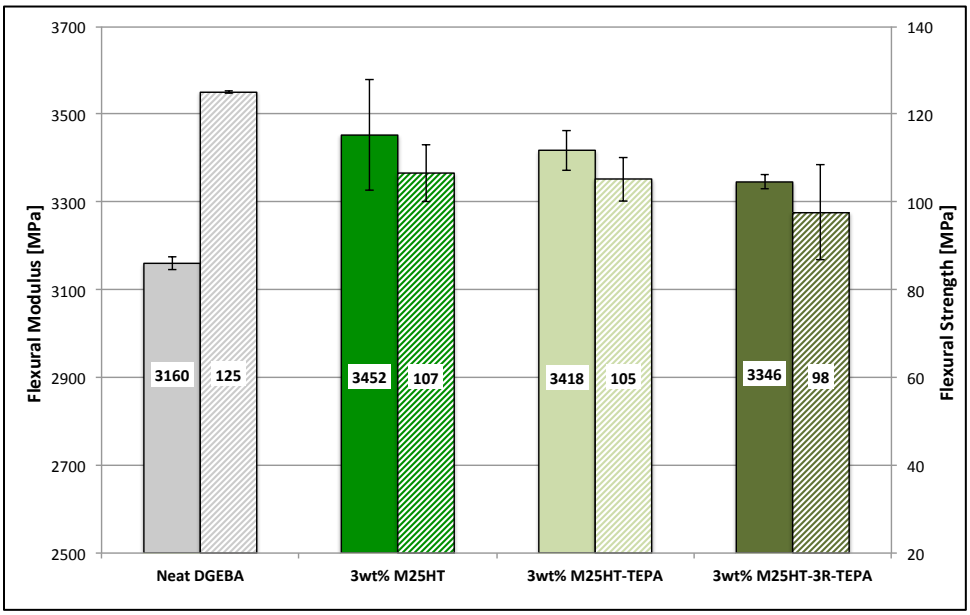

Figure 5.26: Influence of TEPA grafting with and without 3-roll milling on flexural strength (solid) and modulus (hashed) of DGEBA/GnP M25HT nano-composite at 3wt% GnP loading

The changes in flexural modulus with the addition of GnP M25HT mirror the trends seen with the GnP M5HT. The addition of 3wt% GnP M25 increases the modulus of the nano-composite regardless of TEPA-grafting. Both the heat-treated only M25 and the TEPA-grafted M25 show similar increase in modulus (+8 to 9%). An increase in modulus is expected due to the stiffer GnP dispersed throughout the DGEBA matrix. The M25 that was processed in the 3-roll mill shows slightly smaller increase (+6%) in modulus. This could be due to reductions in platelet size from the high shear forces generated during 3-roll milling that may break down the GnP. The flexural strength of all three M25 GnP nano-composites is similar within the data scatter and below that of the neat DGEBA (-15 to -22%). The enhanced bonding by TEPA-grafting, which takes place around the edges of the GnP stacks, does not appear to improve the flexural strength. A

possible explanation may be the weak Van der Waals forces of the π-electron interactions that hold the GnP layers together. At about 2 kcal/mol, these Van der Waals forces are considerable weaker than the covalent bonds formed between the functional groups on the edges of the GnP platelet and the DGEBA matrix, which are estimated about 84 kcal/mol for a carbon-carbon bond. Estimating that the GnP stack consists of about 20 GnP layers (Table 5-3), a strong covalent bond between the platelet edge and the matrix would be of limited benefit if the platelet stack were subjected to a shear that mainly relied on the Van der Waals bonds between GnP layers.

This explanation is supported by the investigation of the fracture surfaces of the flexural samples shown in Figure 5.27:

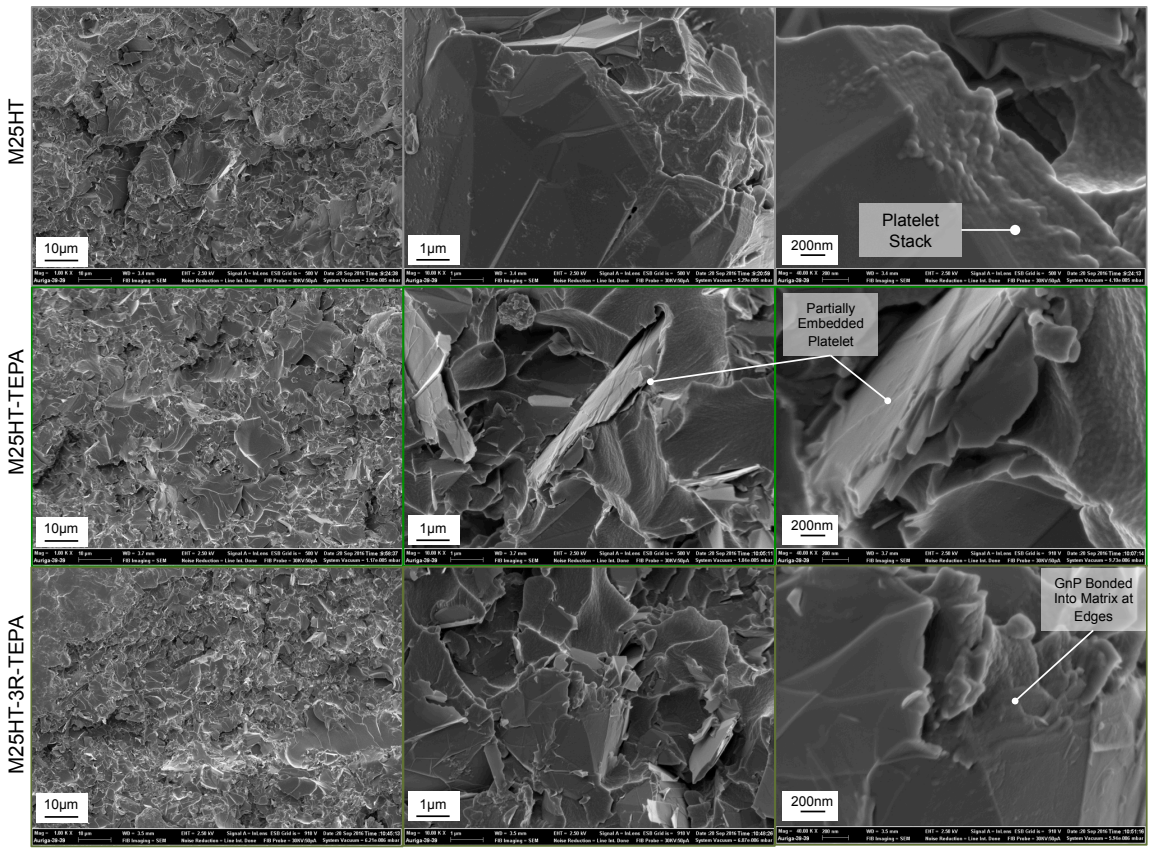

Figure 5.27: Fracture surfaces of DGEBA/GnP/mPDA nano-composite with 3wt% GnP M25 heat treat only (top) and GnP M25HT TEPA-grafted (middle), and GnP M25HT-3R-TEPA (bottom) from tension side of flexural test samples

The morphologies of the facture surfaces are very similar to those of the GnP M5 samples. The M25HT shown in the top row above, shows the edge of a GnP platelet stack. The edges of the GnP layers are visible with some limited material bonded to the platelet edges. The basal plane of the GnP shows some indication of material attached to the surface but does not point to substantial bonding into the matrix. With TEPA-grafting (middle images) the bonding around the edges of the GnP appears to improve. Basal planes of the GnP appear to be fairly clean and there are gaps between the platelet surface and the surrounding matrix. Both of these facts indicate that while the edges are well bonded into the matrix, the weaker Van der Waals forces between the graphene layers are the weak point. Very similar fracture surface morphologies are

evident with the GnP M5 that was TEPA-grafted after 3-roll milling; evidence of bonding at the GnP platelet edges and fairly clean basal planes. There may have been a reduction in platelet diameters during the high shear of the 3-roll milling.

The addition of GnP M25 to the reduces the notched Izod impact strength of DGEBA/mPDA. (Figure 5.28) For the M25HT the reduction is the largest at about 50%. TEPA-grafting appears to mitigate the reduction to -36% with M25HT-TEPA and additional processing via 3-roll mill to -31%. While the improved filler/matrix bonding may be playing a beneficial roll, the main reason for the lower reduction is probably the smaller platelet size of the TEPA-grafted M25. Sonication of the M25HT in TEPA prior to reaction at elevated temperature could be exfoliating some of the GnP. The additional processing of the M25HT via 3-roll mill before TEPA-grafting has probably also reduced the platelet diameter to a certain degree.

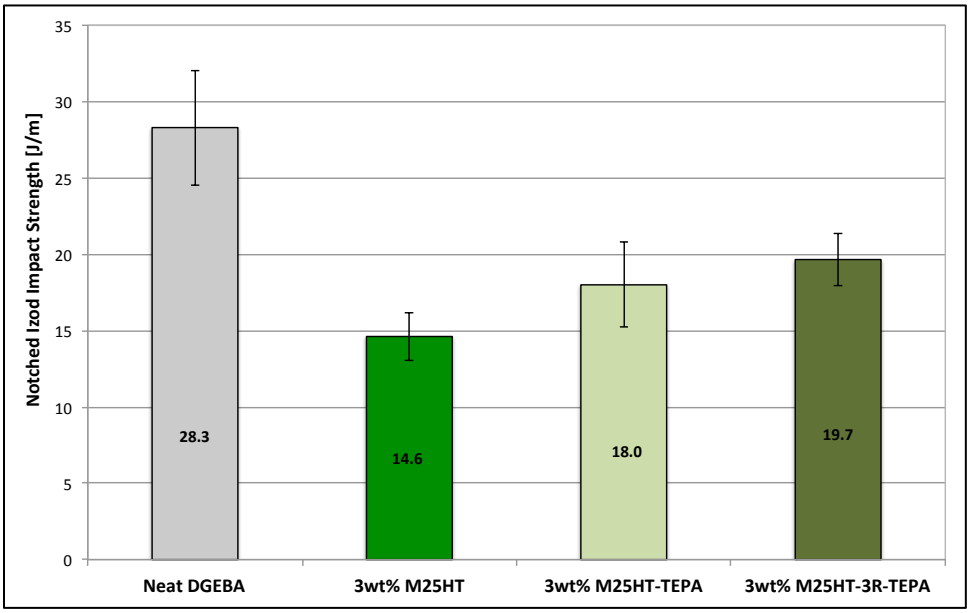

Figure 5.28: Influence of TEPA grafting with and without 3-roll milling on notched Izod impact strength of DGEBA/GnP M25HT nano-composite at 3wt% GnP loading

The fracture toughness of the DGEBA/GnP M25/mPDA nano-composite (Figure 5.29) is significantly improved over neat DGEBA/mPDA and mirrors that of GnP M5 discussed above. GnP M25HT shows the largest increase of 43%. The large aspect ratio of the M25HT appears to be most effective at toughening the DGEBA/mPDA system via crack deflection. This is again consistent with the results published by Chong *et al.* [26], where GnP M25 showed a +37% increase in fracture toughness. M25HT-TEPA shows lower average fracture toughness than the M25HT but the data scatter overlaps the error bars. The fracture toughness is higher than neat DGEBA/mPDA by +33%. While the TEPA-grafting should improve the filler/matrix adhesion, a reduction in platelet size could be the cause of the lower average. M25HT-3R-TEPA improves the fracture toughness by 32% over neat DGEBA/mPDA. Compared to M25HT the average fracture toughness is statistically lower by about 8%. The additional processing of the M25HT in TEPA via 3-roll milling has probably reduced the platelet diameter and aspect ratio, reducing the effectiveness of the GnP to deflect cracks. The GnP M25HT-3R-TEPA nano-composite has a similar fracture toughness of the GnP M5HT nano-composite, which may be rooted in the similar platelet diameters.

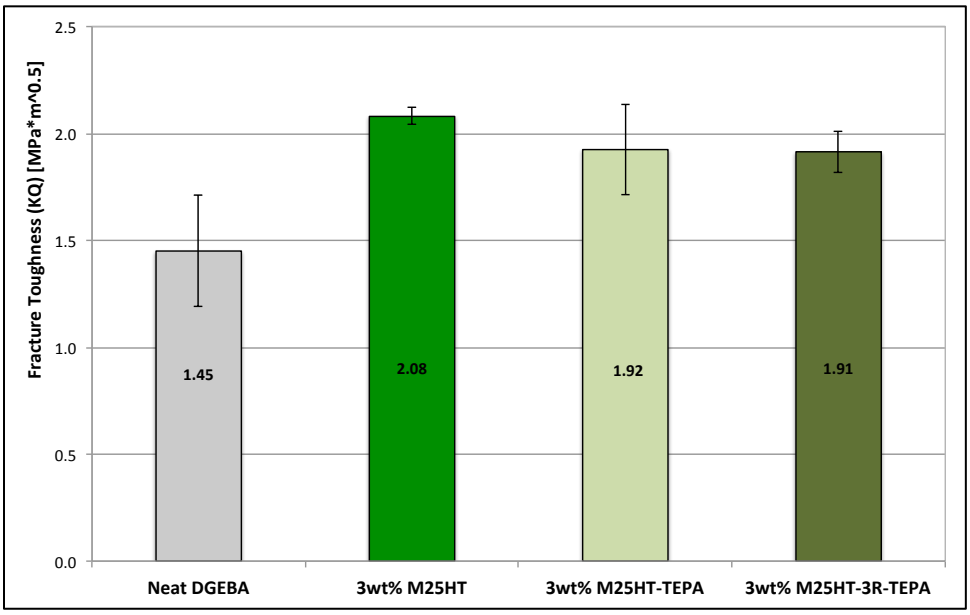

Figure 5.29: Influence of TEPA grafting with and without 3-roll milling on fracture toughness of DGEBA/GnP M25HT nano-composite at 3wt% GnP loading

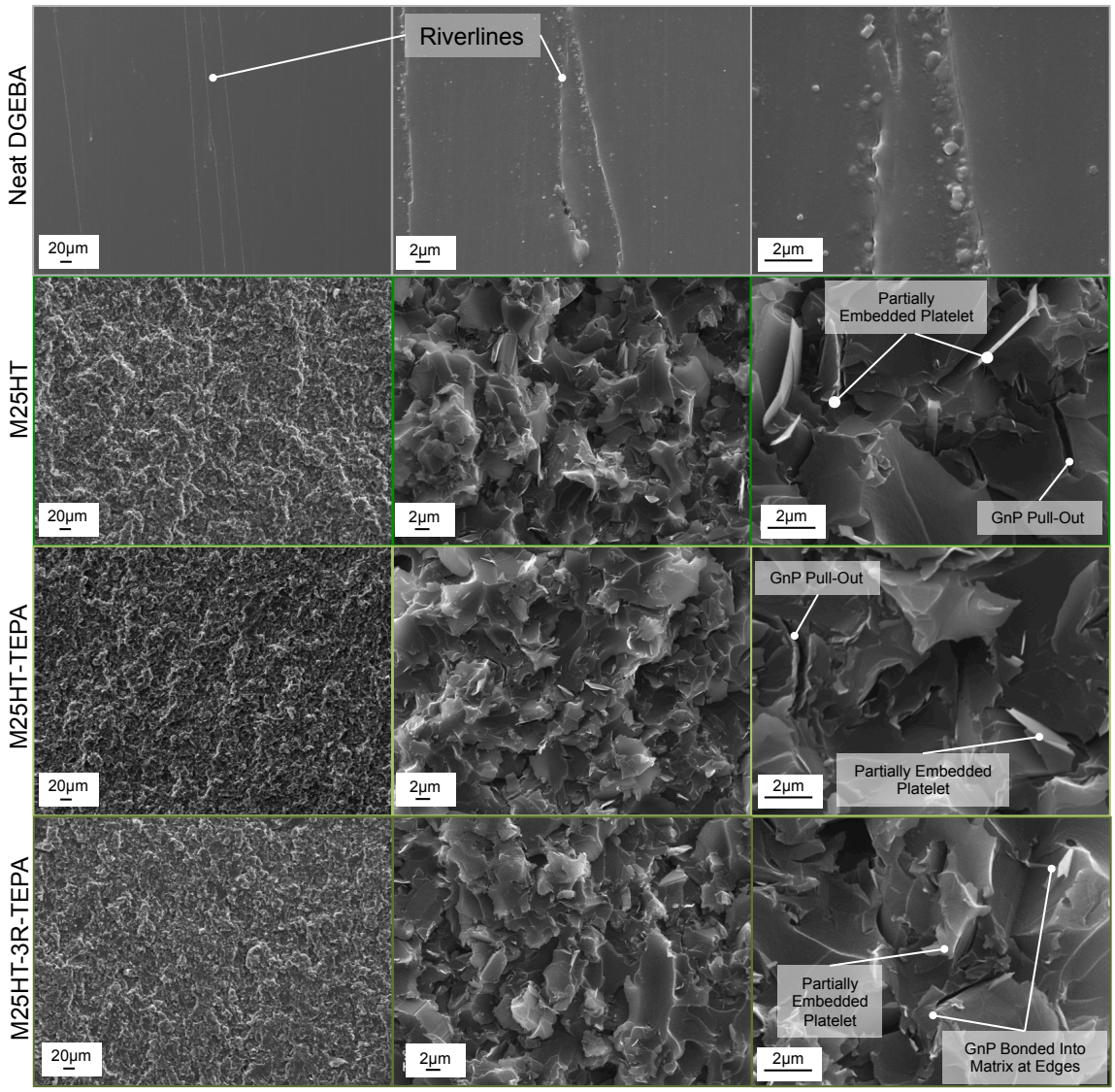

Figure 5.30: Fracture surfaces of fracture toughness samples (compact tension) as observed by SEM. Crack propagation direction is from bottom to top of image. Neat DGEBA (top); DGEBA+3wt% GnP M25HT (top, middle); DGEBA+3wt% GnP M25HT-TEPA (bottom, middle); DGEBA+3wt% GnP M25HT-3R-TEPA (bottom)

The fracture surfaces of the GnP M25 toughened are significantly rougher than the neat DGEBA fracture surface. This is an indication of crack deflection from the high aspect ratio platelets. All fracture surfaces show significant indications of GnP partially embedded into the fracture surface and some holes in the fracture surface where a GnP was probably pulled out. As discussed about, this indicates toughening via crack

bridging and GnP pullout. There is some indication of GnP bonded into the matrix at the platelet edge for the M25HT-3R-TEPA. Based on the limited edge area of the GnP M25, the mechanical exfoliation of the 3-roll milling is needed to improve the TEPA grafting.

An increase in glass transition temperature (T_g) is seen with the addition of GnP M25. (Figure 5.31) The differences in T_g of the heat-treated only and the TEPA-grafted GnP nano-composites are within a half percent band. The M25 processed by 3-roll mill shows a smaller increase in T_g. Since both the TEPA-grafted M25 samples have similar surface nitrogen concentrations, the difference is probably due to the additional processing in the 3-roll mill. The high shear forces from the 3-roll milling process may have led to smaller platelet sizes and more GnP stacks. With a limited amount of TEPA-grafted to the GnP, the additional bonding may not be able to overcome the higher number of platelets. The shape and height of the tan delta curves shown in Figure 5.32 do not change significantly.

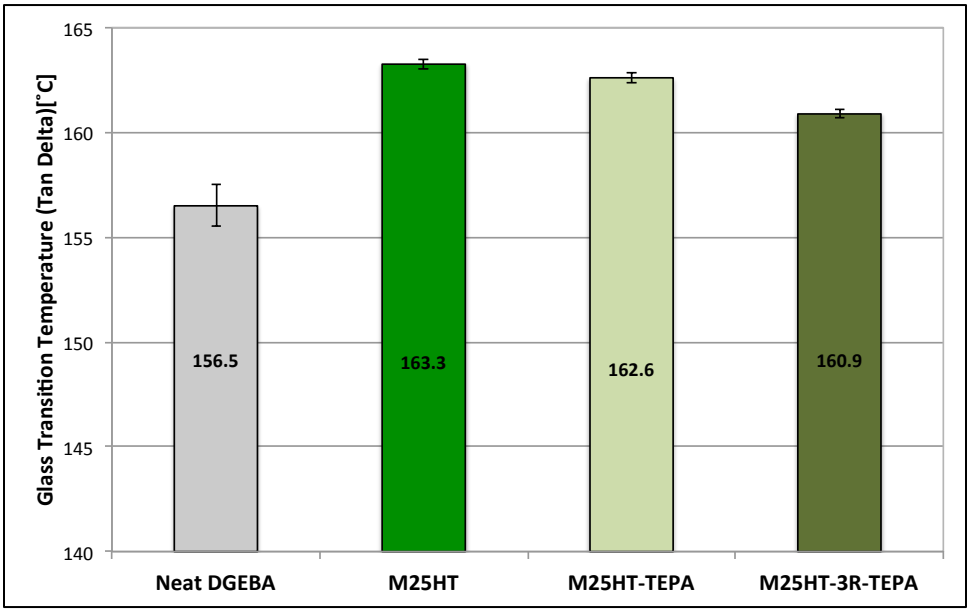

Figure 5.31: Influence of TEPA grafting with and without 3-roll milling on glass transition temperature as determined from maximum of Tan delta curve of DGEBA/GnP M25HT nano-composite at 3wt% GnP loading

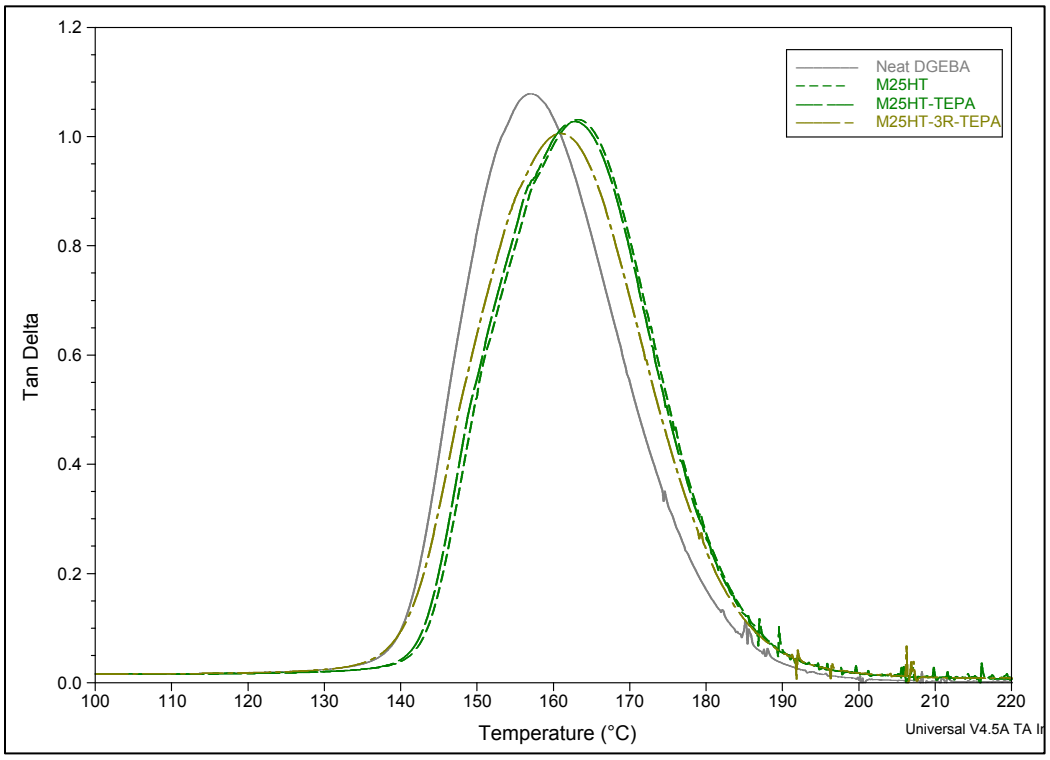

Figure 5.32: DMA Tan δ curves of 3wt% GnP M25/DGEBA nano-composites as determined at 20μm amplitude and 1Hz frequency

5.5 Down Selection of GnP Grade for Carbon Fiber Sizing

From the discussions in the sections above, the TEPA-treatment has shown potential for improving filler/matrix adhesion, most of the illuminated mechanical properties benefit from TEPA-grafting.

To explore the potential of using TEPA-grafted GnP to toughen the interphase of high fiber volume fraction composites, which will be discussed in Chapter 7, three different GnP grades could be added to the fiber sizing. Sizing the carbon fiber with an epoxy/mPDA sizing solution, containing GnP will lock the GnP into place at the fiber surface when the sizing partly vitrifies. As discussed in Chapter 4, when the sizing swells during composite consolidation, the GnP will also diffuse away from the fiber

surface and be present at the fiber/matrix interphase, increasing the modulus and acting as crack arresting/ crack deflection agents.

The GnP C750, with a small aspect ratio, has the highest edge area and also shows the highest concentration of nitrogen surface groups after TEPA-grafting. This should allow for improved GnP/matrix bonding, which is supported by similar flexural properties compared to neat DGEBA. While having the smallest decrease in notched Izod impact strength, there is no positive impact on the fracture toughness. The small aspect ratio of the C750 does not allow it to be a good crack deflection agent. Prioritizing a crack deflection/ crack arresting toughening mechanism for use in the high-fiber volume fraction composite, the C750 would not appear to be a good choice.

GnP M25 shows reductions in flexural strength and notched Izod impact strength, with only limited mitigation through TEPA-grafting. The root is the small amount of edge area of M25, which limits the amount of TEPA that can be grafted to platelet edge, reducing the benefit of TEPA-grafting on the mechanical properties of the nano-composite. Very good increases in fracture toughness are seen, with the best results coming with the least processed GnP, indicating good crack deflection with large aspect ratio GnP platelets. However, the carbon fiber that will be used for the high fiber volume fraction composite is AS4-12k, an aerospace-grade PAN-based fiber, with a nominal fiber diameter of 7.1μm. [27] While the 3-roll milling may decrease the platelet diameter to a certain degree, the large platelet diameter (~25μm) compared to the fiber diameter (~7.1 μm) remains a challenge for fibersizing.

The GnP M5 appears to be the best compromise for fibersizing applications. Some of the reduction in flexural strength and notched Izod impact strength can be

mitigated with TEPA-grafting. The fracture toughness is not increased quite as high as with GnP M25 (+22% vs +32% over neat DGEBA) due to the smaller aspect ratio. The smaller platelet diameter allows the GnP M5HT-3R-TEPA to be used for fiber sizing of AS4-12k carbon fiber. The additional benefit on the flexural strength of additionally DGEBA reacting the M5HT-3R-TEPA needs to be weighed against the additional effort of this processing step.

5.6 Conclusion

The potential of using GnP as toughening agents for the DGEBA/mPDA system were illuminated. The three investigated GnP grades, all exhibiting very different aspect ratios, were shown to enhance different mechanical properties depending on their filler/matrix bonding and crack deflection potential. The GnP C750 enhanced the flexural modulus and strength based on its large edge area leading to better filler/matrix bonding but did not change the fracture toughness due to the small aspect ratio. The M-grade GnP showed reductions in flexural strength due to poor filler/matrix adhesion but good improvements in fracture toughness due to the crack deflection potential of the high-aspect ratio plates. The higher increase in fracture toughness was seen with the large aspect ratio GnP M25 compared to the smaller GnP M5. This specificity of improved properties indicates that a different grade of GnP need to be selected depending on the mechanical properties of interest.

To enhance the filler/matrix adhesion, amine groups were added by treatment of GnP with tetraethylenepentamine (TEPA). The amount of TEPA that could be grafted to the GnP was shown to be dependent on the edge area of the GnP, as that is where the

reactive groups are present. A linear dependence of the surface oxygen for heat-treated GnP on calculated edge area was determined. This linear dependence was also found for the surface nitrogen concentration after TEPA-grafting, indicating that reaction is indeed taking place at the platelet edges.

Some improvements in the mechanical properties with TEPA-grafted GnP were seen by virtue of better filler/matrix adhesion. The GnP C750 in the heat-treated form showed some improvements in flexural properties that were further enhances with TEPA-grafting. For GnP M25 with low edge area showed only slight improvements in mechanical properties due to the limited TEPA-grafting potential. GnP M5 appears to gain the most benefit from TEPA-grafting. Further reaction of GnP M5HT-3R-TEPA with DGEBA to react with the grafted amine groups was effective in reducing the negative impact on the flexural properties.

When applied to fibersizing, GnP M5HT-3R-TEPA represents the best compromise between improved fracture toughness and platelet diameter that is compatible with the ø7μm AS4-12k carbon fiber.

BIBLIOGRAPHY

BIBLIOGRAPHY

[1] Le Hoang Sinh, B. T. Son, N. N. Trung, D.-G. Lim, S. Shin, and J.-Y. Bae, "Improvements in thermal, mechanical, and dielectric properties of epoxy resin by chemical modification with a novel amino-terminated liquid-crystalline copoly(ester amide)," *REACTIVE AND FUNCTIONAL POLYMERS*, vol. 72, no. 8, pp. 542–548, Aug. 2012.

[2] A. C. Garg and Y.-W. Mai, "Failure mechanisms in toughened epoxy resins—A review," *Composites Science and Technology*, vol. 31, no. 3, pp. 179–223, Jan. 1988.

[3] N. Domun, H. Hadavinia, T. Zhang, T. Sainsbury, G. H. Liaghat, and S. Vahid, "Improving the fracture toughness and the strength of epoxy using nanomaterials – a review of the current status," *Nanoscale*, vol. 7, no. 23, pp. 10294–10329, 2015.

[4] B. Wetzel, F. Haupert, and M. Qiu Zhang, "Epoxy nanocomposites with high mechanical and tribological performance," *Composites Science and Technology*, vol. 63, no. 14, pp. 2055–2067, Nov. 2003.

[5] R. A. Pearson and A. F. Yee, "Toughening mechanisms in thermoplastic-modified epoxies: 1. Modification using poly (phenylene oxide)," *Polymer*, vol. 34, no. 17, pp. 3658–3670, 1993.

[6] Y. Kojima, A. Usuki, M. Kawasumi, A. Okada, Y. Fukushima, T. Kurauchi, and O. Kamigaito, "Mechanical properties of nylon 6-clay hybrid," *J. Mater. Res.*, vol. 8, no. 5, pp. 1185–1189, May 1993.

[7] S. Zhao, L. S. Schadler, H. Hillborg, and T. Auletta, "Improvements and mechanisms of fracture and fatigue properties of well-dispersed alumina/epoxy nanocomposites," *Composites Science and Technology*, vol. 68, no. 14, pp. 2976–2982, Nov. 2008.

[8] H. H. T. Z. T. S. G. H. L. S. V. N Domun, "150605_GE_Update_Mtg_Rev0," *Nanoscale*, vol. 7, pp. 10294–10329, May 2015.

[9] A. H. Castro Neto, "Drawing Conclusions from Graphene," *American Physical Society*, p. 1002, Oct. 2007.

[10] C. Lee, X. Wei, J. W. Kysar, and J. Hone, “Measurement of the Elastic Properties and Intrinsic Strength of Monolayer Graphene,” *Science*, vol. 321, no. 5887, pp. 385–388, Jul. 2008.

[11] K. Kalaitzidou, H. Fukushima, and L. T. Drzal, “Multifunctional polypropylene composites produced by incorporation of exfoliated graphite nanoplatelets,” *Carbon*, vol. 45, no. 7, pp. 1446–1452, Jun. 2007.

[12] Y. Li, J. Zhu, S. Wei, J. Ryu, L. Sun, and Z. Guo, “Poly(propylene)/Graphene Nanoplatelet Nanocomposites: Melt Rheological Behavior and Thermal, Electrical, and Electronic Properties,” *Macromol. Chem. Phys.*, vol. 212, no. 18, pp. 1951–1959, Jul. 2011.

[13] M. A. Rafiee, J. Rafiee, Z. Wang, H. Song, Z.-Z. Yu, and N. Koratkar, “Enhanced Mechanical Properties of Nanocomposites at Low Graphene Content,” *ACS Nano*, vol. 3, no. 12, pp. 3884–3890, Dec. 2009.

[14] J. Guerrero-Contreras and F. Caballero-Briones, “Graphene oxide powders with different oxidation degree, prepared by synthesis variations of the Hummers method,” *Materials Chemistry and Physics*, vol. 153, pp. 209–220, Mar. 2015.

[15] C. U. Pittman, G. R. He, B. Wu, and S. D. Gardner, “Chemical modification of carbon fiber surfaces by nitric acid oxidation followed by reaction with tetraethylenepentamine,” *Carbon*, 1997.

[16] C. U. Pittman, Z. Wu, W. Jiang, G. R. He, B. Wu, and W. Li, “Reactivities of amine functions grafted to carbon fiber surfaces by tetraethylenepentamine. Designing interfacial bonding,” *Carbon*, 1997.

[17] H. Fukushima, “Graphite Nanoreinforcements in Polymer Nanocomposites,” Michigan State University, 2003.

[18] H. Ribeiro, W. M. da Silva, J. C. Neves, H. D. R. Calado, R. Paniago, L. M. Seara, D. das Mercês Camarano, and G. G. Silva, “Polymer Testing,” *Polymer Testing*, vol. 43, no. C, pp. 182–192, May 2015.

[19] X. G. Sciences, “XGnP Graphene Nanoplatelets - Grade C -Technical Data Sheet,” pp. 1–1, Jun. 2012.

[20] X. G. Sciences, “xGnP Graphene Nanoplatelets - Grade M - Technical Data Sheet,” pp. 1–1, Apr. 2011.

[21] F. Wang, L. T. Drzal, Y. Qin, and Z. Huang, “Enhancement of fracture toughness, mechanical and thermal properties of rubber/epoxy composites by incorporation of graphene nanoplatelets,” *Composites Part A: Applied Science and Manufacturing*, vol. 87, pp. 10–22, Aug. 2016.

[22] P.-C. Ma, N. A. Siddiqui, G. Marom, and J.-K. Kim, “Dispersion and functionalization of carbon nanotubes for polymer-based nanocomposites: A review,” *Composites Part A*, vol. 41, no. 10, pp. 1345–1367, Oct. 2010.

[23] R. Saito, M. Hofmann, G. Dresselhaus, A. Jorio, and M. S. Dresselhaus, “Raman spectroscopy of graphene and carbon nanotubes,” *Advances in Physics*, vol. 60, no. 3, pp. 413–550, Jun. 2011.

[24] S. Chatterjee, F. Nafezarefi, N. H. Tai, L. Schlagenhauf, F. A. Nüesch, and B. T. T. Chu, “Size and synergy effects of nanofiller hybrids including graphene nanoplatelets and carbon nanotubes in mechanical properties of epoxy composites,” *Carbon*, vol. 50, no. 15, pp. 5380–5386, Dec. 2012.

[25] J. R. Potts, D. R. Dreyer, C. W. Bielawski, and R. S. Ruoff, “Graphene-based polymer nanocomposites,” *Polymer*, vol. 52, no. 1, pp. 5–25, Jan. 2011.

[26] H. M. Chong, S. J. Hinder, and A. C. Taylor, “Graphene nanoplatelet-modified epoxy: effect of aspect ratio and surface functionality on mechanical properties and toughening mechanisms,” *J Mater Sci*, vol. 51, no. 19, pp. 8764–8790, Jul. 2016.

[27] Hexcel, “HexTow AS4 Carbon Fiber.” Hexcel Corporation, pp. 1–2, 15-Mar-2013.

Chapter 6: Toughening of Carbon Fiber-Reinforced Epoxy Composites Using Amine-Grafted Graphene Nanoplatelets

6.1 Abstract

In this chapter, toughening of aromatic epoxy matrix based carbon fiber composites with graphene nano-platelets (GnP) in the fibersizing is discussed. Aromatic and aliphatic epoxy based fibersizing are further enhanced with TEPA-grafted GnP M5HT (M5HT-3R-TEPA) at different concentrations (0.1wt% and 0.5wt%). A composite with 0.5wt% heat-treated only GnP was also made to illuminate the benefits of adding amine groups to GnP via TEPA-grafting.

The flexural properties of all aromatic sized composites with GnP are similar or better than the neat aromatic sized composite. The fiber/matrix bonding dominated transverse flexural strength was constant with heat-treated GnP and improved by +22% to +26% with TEPA-grafted GnP. In conjunction with the aliphatic sizing, the 0.5wt% TEPA-grafted GnP reduced all the flexural properties of the composite compared to the neat aliphatic sized composite.

Mode I fracture toughness was significantly enhanced with the addition of GnP to the aromatic fibersizing. The 0.5wt% heat-treated only GnP increased the fracture toughness by +61%, based on the superior crack deflection of the large aspect ratio GnP. The TEPA-grafted GnP showed fracture toughness increases of +23% at 0.1wt% and +37% at 0.5wt% GnP sizing bath concentration. The better exfoliation and reduced platelet size of the more heavily processed TEPA-grafted GnP reduces the crack deflection ability and lowers the increase in fracture toughness.

Changes in glass transition temperature with the addition of GnP into the fibersizing are within a range of -1.7% to +0.1% compared to the neat epoxy sized fiber.

6.2 Introduction

The importance of carbon fiber-reinforced composites in many different industries has been well established and enhancing the toughness of fiber-reinforced epoxy composites is a topic that much effort has been invested in over the past few decades. In the previous chapters of this dissertation several areas have been identified that can be improved in order to enhance the overall composite toughness: The epoxy matrix, the fiber/matrix interphase, and the fiber surface.

The high stiffness and strength of epoxy polymers have made them a popular choice as matrix materials for structural applications. However, the brittle nature of the epoxy matrix material has been the focus of improving the composite toughness. [1] These approaches include toughening with rubbers [2], aliphatic amines [3], aliphatic epoxies [4], [5], and suspended nano-filler materials [6]. Of the listed approaches rubber toughening and the toughening with aliphatic epoxies and amines have made it to commercial distribution in toughened epoxy systems.

The matrix toughening approach on the basis of nano-particles usually relies on suspending these in the epoxy matrix via a number of the different methods, such as sonication, high-shear mixing or calendaring. For production of a carbon fiber-reinforced composite, the challenge lies in achieving a homogeneous distribution of nano-particles in the matrix around the reinforcing fibers. For a pre-preg process this means infiltrating and surrounding the fiber tow or fiber weave with the liquid matrix material containing

the suspended nano-particles during pre-preg production. In a resin-transfer type manufacturing procedure like vacuum-assisted resin transfer molding (VARTM) were a fiber-layup needs to be infiltrated, the resin needs to flow through fairly restricted spaces between the fibers. Suspended nano-filler particles in the resin may get filtered out, leading to a non-uniform distribution of filler, negating any potential benefit. An alternate approach is to add the nano particle into the fugitive fibersizing, rather than suspending it in the matrix material. The partially vitrified sizing will fix the nano particles at the fiber surface putting them in place at the fiber/matrix interphase. If the nano-filler is already in place on the fiber, a neat resin can be injected into the layup for VARTM or during pre-pregging. As discussed in Chapter 3, the sizing will swell allowing the nano-filler to diffuse away from the fiber surface during composite consolidation and toughening the fiber/matrix interphase.

Multiple studies have applied different nano particles to the fiber (both glass and carbon fiber) surface in an effort to enhance composite toughness: Clay [7], silicon dioxide [8], Carbon nanotubes (CNT) [9]-[11], and graphene nanoplatelets (GnP) [12]-[15]. Based on the reasonable production cost [16], [17] and better aspect ratio for crack deflection when compared to CNT, GnP will be the nano-filler investigated in this chapter.

Applied to the fiber/matrix interphase, toughening the epoxy via the addition of a graphene nano-platelets, two main factors will contribute to improving the fiber/matrix bond strength: first, by adding a stiffer nano-filler material, the modulus at the fiber/matrix interphase will increase. As discussed in Chapter 3, the application of the Cox equation to a single fiber in a cylindrical matrix indicates that the fiber/matrix bond

strength will depend mainly on the shear strain-to-failure and the modulus at the fiber matrix interface. [18]-[20] Assuming good filler/matrix adhesion, the stiff GnP platelets should increase the modulus and the fiber/matrix adhesion. Secondly, the 2D-structure of the GnP should be superior at deflecting cracks away from the fiber/matrix interface and into the bulk matrix. This increased energy needed for crack propagation should enhance the Mode I facture toughness.

Several lessons learned on toughening a fiber-reinforced epoxy composite can be taken from the previous chapters of this dissertation. In Chapter 4, improved fiber/matrix adhesion through UVO-fiber surface treatment and epoxy fibersizing, especially aliphatic epoxy, was shown to enhance composite Mode I fracture toughness. Chapter 6 illuminated the increase in fracture toughness of DGEBA/mPDA system using GnP. The importance of improving filler/matrix adhesion by grafted amine groups to the GnP M5HT were clearly visible. The improvement of fracture toughness rooted in good crack deflection of the high aspect ratio GnP M5 is expected to transfer to the fiber-reinforced composite by deflecting the crack away from the fiber/matrix interphase. In this chapter the effect of using GnP M5HT-3R-TEPA in conjunction with aromatic and aliphatic fibersizing on composite properties is investigated.

6.3 Materials and Methods

6.3.1 Materials

Material used to produce high fiber volume fraction composites are the same as those described in Chapter 3.

The TEPA-grafted GnP M5HT was made by the same procedure using the 3-roll mill as described in Chapter 5. Enough GnP M5HT-3R-TEPA was made to yield one composite set at 0.1wt% and two composite sets at 0.5wt% GnP from the same batch.

6.3.2 Manufacturing of High-Fiber Volume Fraction Composite With GnP M5HT-3R-TEPA Based Fiber Sizing

The procedure of manufacturing the composite with GnP based fibersizing was analogous to those described in Chapter 3 for pre-pregging, layup, and autoclave. The sizing solution was prepared by dissolving the appropriate amount of epoxy (aromatic or aliphatic) in isopropanol (IPA) using mechanical stirring and mild sonication (~50W) to make a 1wt%(epoxy+9phr mPDA) solution. The appropriate amount of mPDA curing agent was then added and also dissolved by stirring and mild sonication. GnP, either M5HT or M5HT-3R-TEPA, were added to the IPA/DGEBA/mPDA solution to make a 0.1wt% or 0.5wt% GnP concentration and stirred for 5min. The mixture was transferred to the recirculation tank and placed in a dry ice bath with strong magnetic stirring. The solution was sonicated in a Sonics medium volume continuous flow cell sonicator for 2h at 100W. The solution was circulated through the flow cell at about 6 l/h (100ml/min set point), corresponding to a residence time in the flow cell of 30 sec. (Figure 6.1)

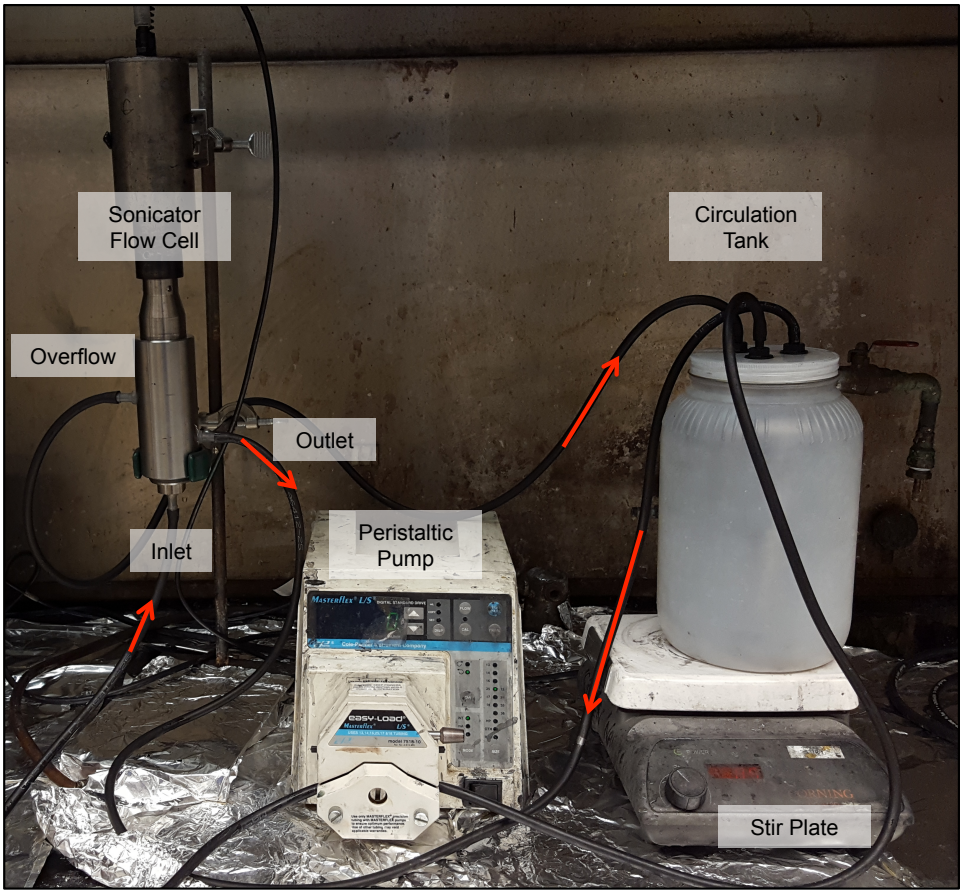

Figure 6.1: Sonics medium volume flow cell sonicator with circulation system (pump and tank). Solution flow direction indicated by arrows. Dry ice bath is not shown in this image

After 2h the circulation tank was moved to the sizing tower and strong agitation via magnetic stir bar in both the sizing bath and circulation tank keeping the GnP suspended during sizing. Identical processing parameters were used to those described in Chapter 3. The sizing parameters were as described in Chapter 3.4.3, composite prepregging in Chapter 3.4.4, and composite layup, autoclave, and mechanical testing in Chapter 3.4.5. One adjustment made for prepregging was the addition of 0.076mm shims between the slit die blocks in order to widen the slit die gap. The wider slit die gap reduced the possibility of the GnP sizing to be removed from the fiber tow. One consequence was that, the prepregs had higher resin content, than with the standard

die configuration (~55% vs 40% resin). The higher amount of resin is expected to be removed during composite consolidation in the autoclave.

To investigate the void volume and GnP dispersion within the composite, pieces of the cured composite were mounted in Leco room temperature cure epoxy and polished using a Struers Abramin polisher with 320, 600, 1200 and 4000 grit paper. Subsequently the samples were polished with 1μm alumina slurry and then with 0.05μm alumina slurry in a Vibromet polisher for 18h. The polished cross-sections were etched with oxygen plasma for 30min at 275W using a plasma reactor to increase the contrast between the matrix and carbon fiber and GnP.

Cross-sections and sized AS4-12k-UVO fiber tows were investigated using a Zeiss EVO LS25 scanning electron microscope under high-vacuum. Samples were coated with a 1 nm thick layer of tungsten prior to observation.

6.3.3 Mechanical Properties

The methods to determine the composite mechanical properties were described in detail in Chapter 3.

6.4 Results and Discussion

6.4.1 Determination of Sizing Level and Quality

The sizing level is dependent on GnP sizing bath concentration and GnP treatment (Figure 6.2). At a sizing bath concentration of 0.5wt% GnP M5HT shows higher amounts of sizing pickup as well as the highest scatter at 3.7wt%. This compares to the GnP M5HT-3R-TEPA at 2.5%. This is probably due to better dispersion and exfoliation

of the TEPA-grafted GnP compared to the heat-treated only GnP. The sizing level is fairly similar, regardless if an aromatic or aliphatic epoxy is used for the fiber sizing, mirroring the trend in the neat epoxy sizing that also showed similar sizing level between aromatic and aliphatic epoxies. There is also a linear increase in sizing level with GnP M5HT-3R-TEPA sizing bath concentration as shown in Figure 6.3.

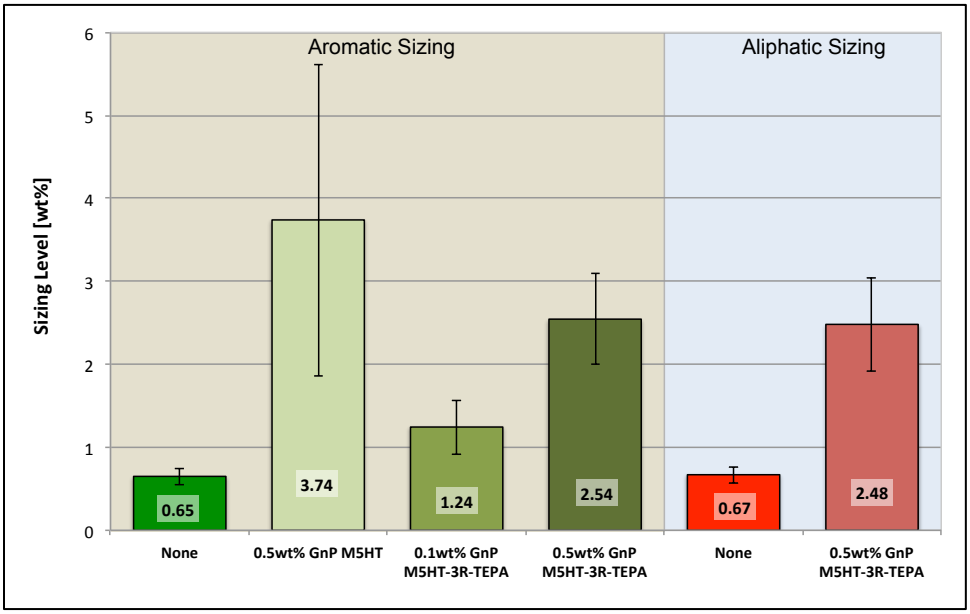

Figure 6.2: Sizing level of AS4-12k-UVO carbon fiber tow with aromatic or aliphatic fibersizing at 9phr mPDA with different GnP M5 sizing bath concentrations and GnP treatments

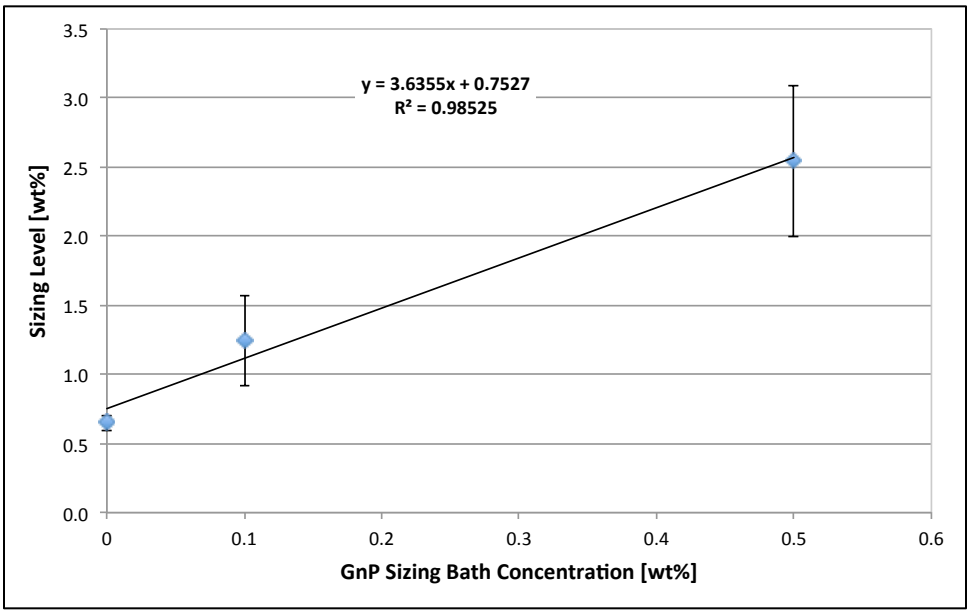

Figure 6.3: Dependence of sizing level on GnP sizing bath concentration for GnP M5HT-3R-TEPA in IPA with 1wt%(DGEBA+9phr mPDA) epoxy concentration

The visual quality of the sizing on the AS4-12k-UVO carbon fiber tow as imaged by SEM after processing on the sizing tower system is shown in Figure 6.4:

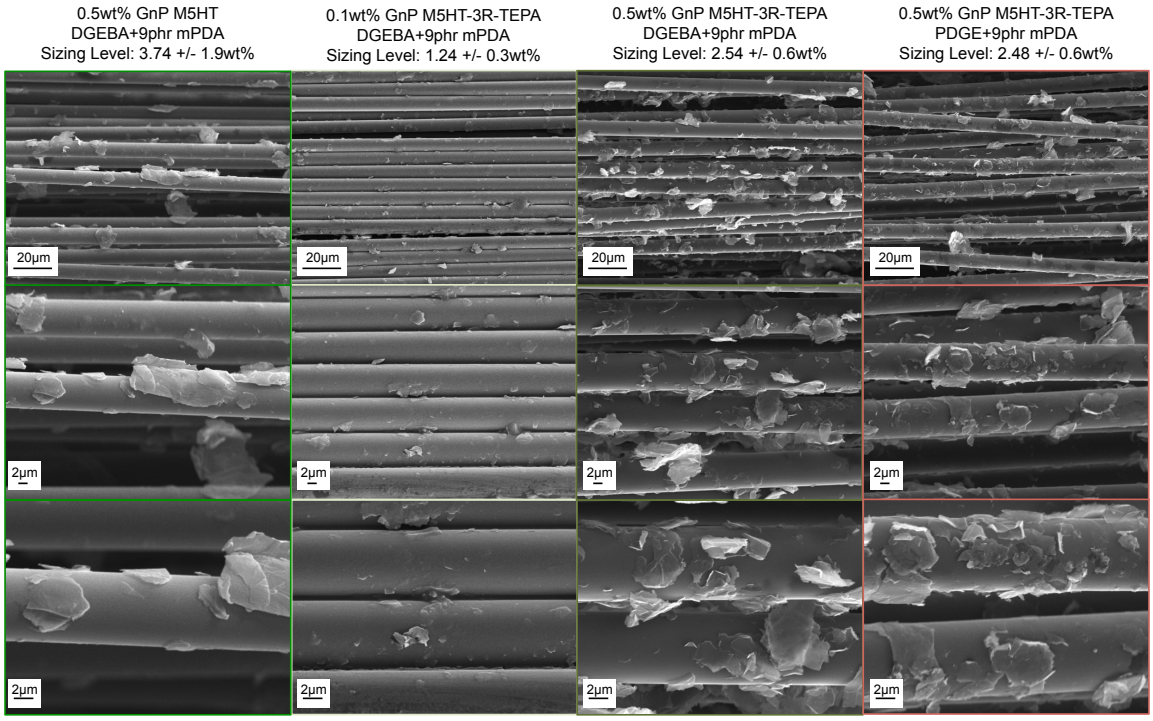

Figure 6.4: Sizing quality and level of AS4-12k-UVO fiber tow processed on fiber sizing tower system with different GnP M5 concentrations and treatments in 1wt% aromatic or aliphatic epoxy at 9phr mPDA

The visual sizing quality of the GnP M5HT sized fiber tow is consistent with the sizing level previously shown. There appear to be larger agglomerates of GnP present on the fiber tow, which would account for the high sizing level and high scatter. At 0.1wt% GnP sizing bath concentration, the coverage of GnP is significantly lower. While less GnP agglomerates are visible, the coverage is fairly light. Both the aromatic and aliphatic epoxy sizing at 0.5wt% GnP M5HT-3R-TEPA show similar sizing quality, which is expected based on the similar sizing levels. Compared to the M5HT, the GnP agglomerates on the M5HT-3R-TEPA sized fiber tows are smaller and the GnP coverage is more uniform. The additional processing and grafting of TEPA to the edges of the graphene platelets appear to have improved the exfoliation of the GnP. At 0.5wt% the GnP coverage is much better compared to 0.1wt% for aromatic sizing. Further

optimization of the sizing quality, especially uniform GnP coverage and better exfoliation should be achieved.

6.4.2 Mechanical Properties of High-Fiber Volume Fraction Composite

The distribution of the GnP within the composite was investigated in the SEM using polished and plasma etched cross-sections and is shown in Figure 6.5:

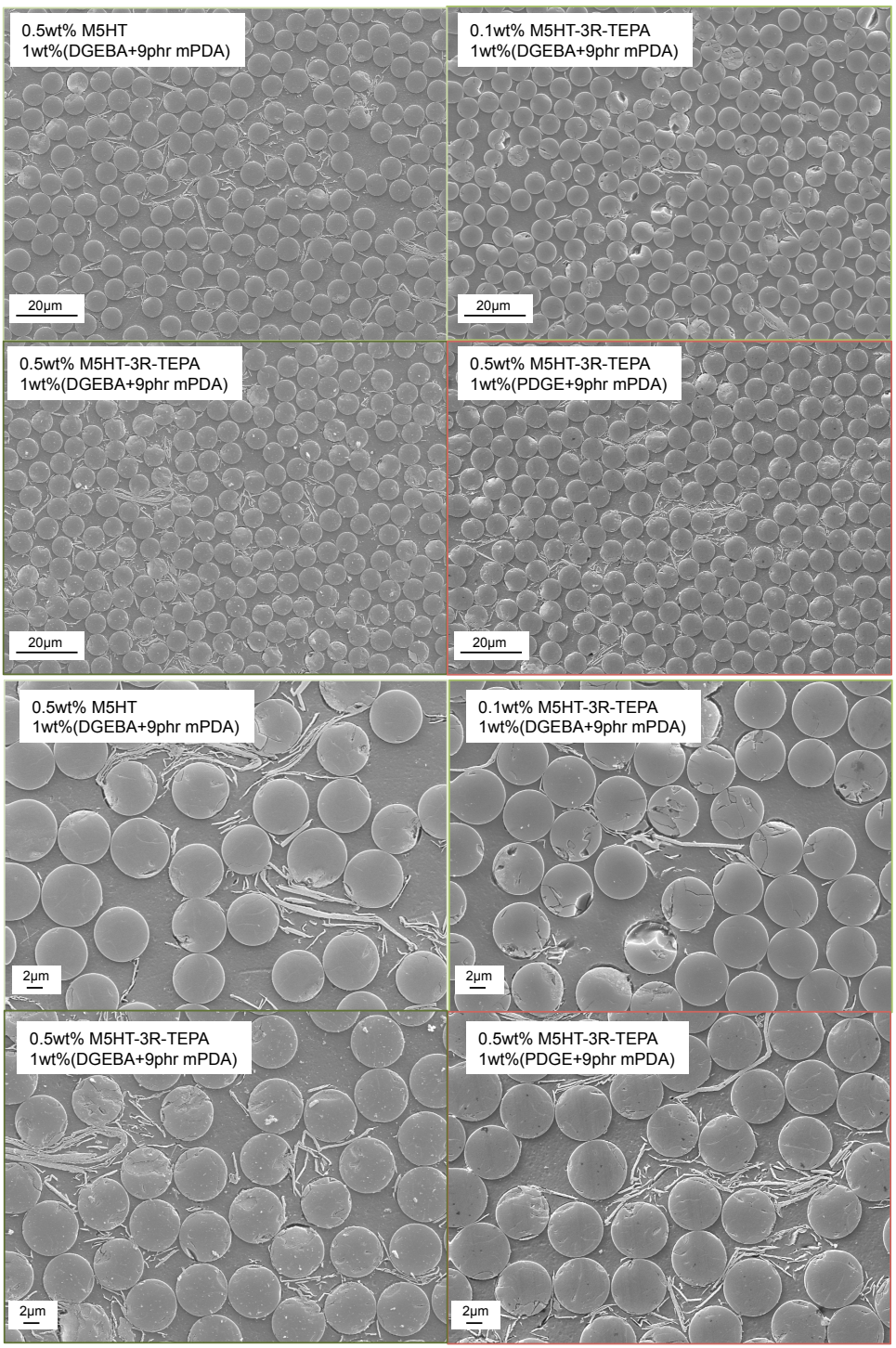

Figure 6.5: Polished and plasma etched cross-section of AS4-12k-UVO composite with heat-treated and TEPA-grafted GnP in aromatic and aliphatic fibersizing (top: 2000x; bottom: 5000x)

The dispersion of the GnP within the cross-section appears to be marginal for all GnP treatments and concentrations with some areas not showing any evidence of GnP. These trends are similar to the sizing quality of the fiber tows previously shown. The 0.1wt% GnP M5HT-3R-TEPA composite especially shows little evidence of GnP dispersion, indicating that the concentration of GnP may have been too low. The higher sizing bath concentrations at 0.5wt% GnP show stronger evidence of GnP throughout the cross-section. As shown in the high magnification of Figure 6.5 there is also evidence of GnP agglomerates for all composites. The TEPA-grafted GnP appears to have slightly smaller agglomerates compared to the heat-treated GnP as also seen on the sized fiber tow. Sizing the fiber tow with GnP has succeeded in introducing GnP into the composite. However, the overall appearance of the cross-sections in terms of the GnP agglomerates and GnP distribution implies that additional effort is needed to improve the dispersion and exfoliation of the GnP M5.

The fiber volume fraction (Vf) of the different fibersizing combinations varied somewhat as shown in Figure 6.6:

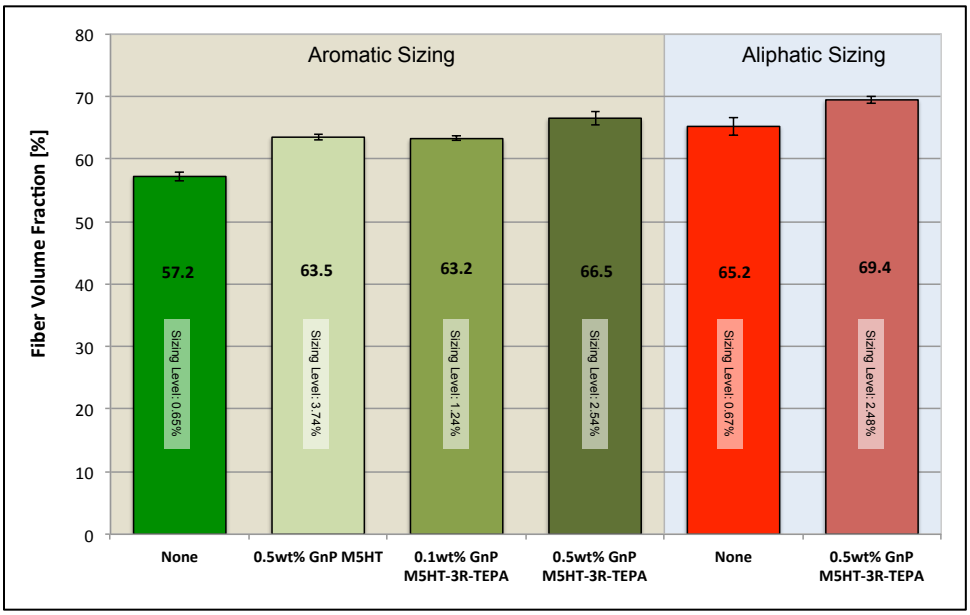

Figure 6.6: Fiber volume fraction and sizing level of AS4-12k-UVO carbon fiber composites with heat treated and TEPA-grafted GnP in aromatic and aliphatic fibersizings

The addition of GnP appears to increase the Vf, independent of TEPA-grafting. Adding higher amounts of GnP appears to further increase the Vf.

To better compare the mechanical properties of all the composites, longitudinal flexural modulus and strength were normalized to 65% fiber volume fraction as described in Chapter 3.4.3. [21] The unadjusted longitudinal data is presented in the appendix. The transverse properties are challenging to adjust based on the complex stress distributions that are present in the transverse direction. For this reason, the transverse properties are presented as-measured with reference to the actual fiber volume fraction for each composite.

The void volume of all composites was determined from SEM micrographs using digital image editing software (Adobe Photoshop CS6). The void volume was well below the 1% threshold as has been established in the literature, below which no effect on mechanical properties is expected. [22]

The flexural moduli, both longitudinal and transverse, are shown in Figure 6.7:

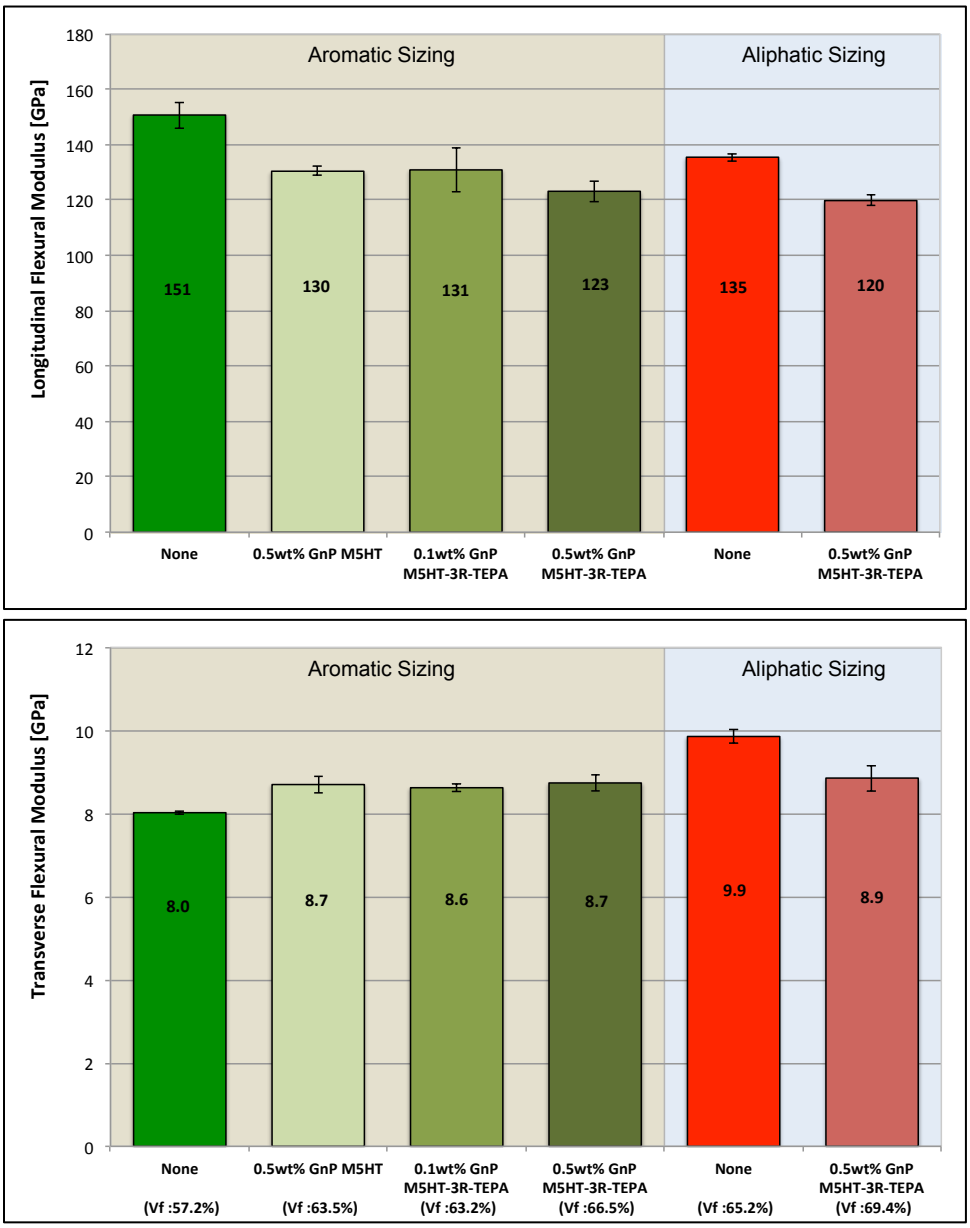

Figure 6.7: Influence of heat treated and TEPA-grafted GnP on the flexural modulus of AS4-12k-UVO carbon fiber composites with aromatic and aliphatic fiber sizing (top: longitudinal, adjusted V_f:65%; bottom: transverse, as-measured)

With the exception of the neat DGEBA sized fiber composite, all composite moduli are on a similar level. The GnP sized fiber composites have a statistically similar

modulus, with the 0.5wt% TEPA-grafted GnP composite being slightly lower than the 0.5wt% heat-treated GnP fiber composite. Since it has the lowest fiber volume fraction of all composites, the high modulus value of the neat DGEBA sized fiber composite may be an artifact of the normalization procedure. For the as-measured data, shown in the appendix, all composites have a statistically similar longitudinal modulus.

In the fiber/matrix bonding dominated transverse flexural modulus, the aromatic, GnP based fiber composites show a higher modulus than the neat aromatic sized composite. This may be a consequence of the stiffer GnP platelets present at the fiber/matrix interphase increasing the composite modulus. With aliphatic sizing the addition of GnP reduces the both the longitudinal and transverse modulus, indicating a significant influence of the TEPA-grafted GnP. Additional cross-linking from the amine groups introduced on the TEPA-grafted GnP may be a contributing factor. The additional cross-linking may reduce the diffusion of the aliphatic epoxy away from the fiber surface, leading to a more compliant interphase, analog to the aliphatic sizing in conjunction with the 1wt% aliphatically toughened matrix. (Chapter 5) The greater reduction in flexural modulus appears to support this explanation.

The flexural strength both longitudinal and transverse are shown in Figure 6.8:

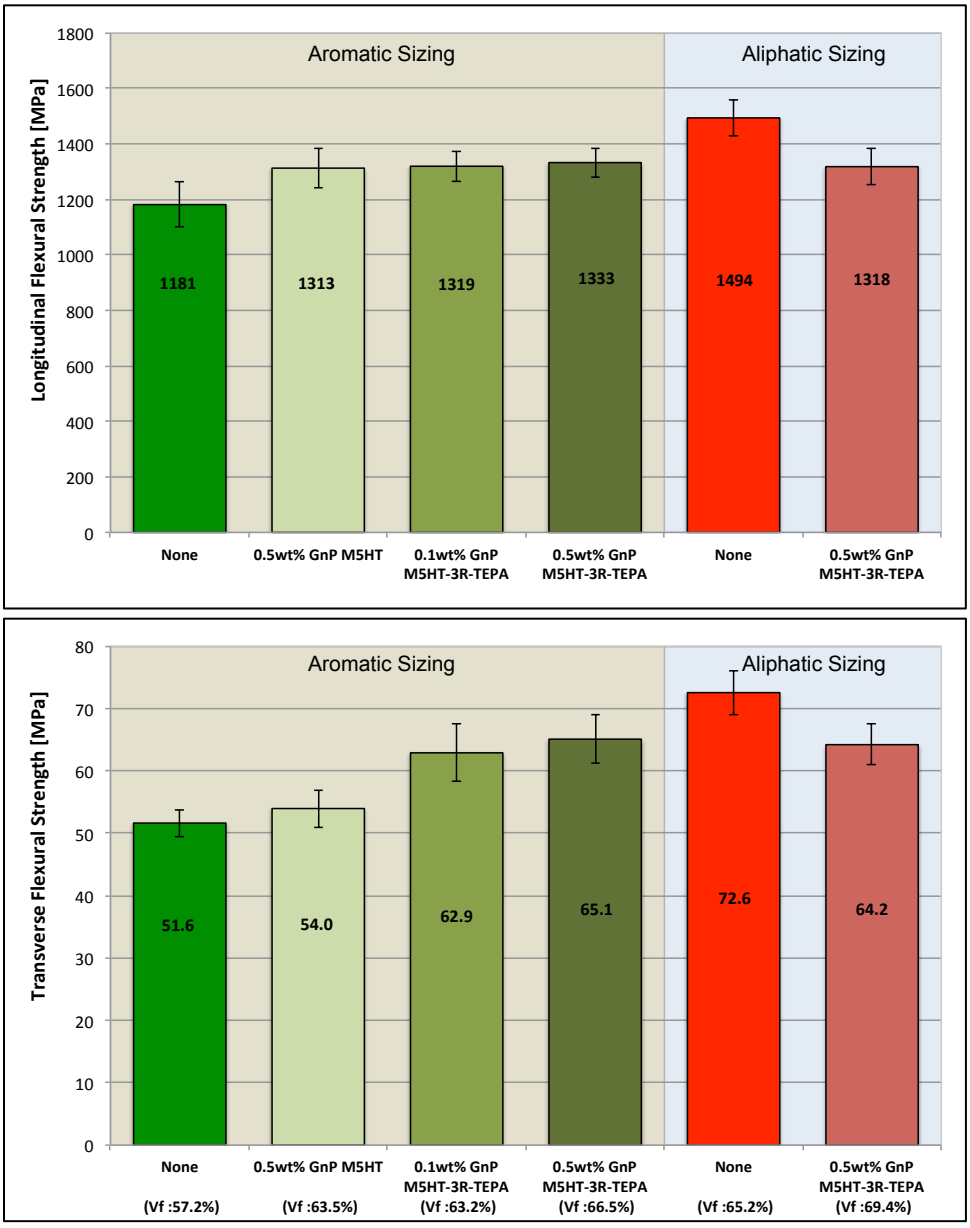

Figure 6.8: Influence of heat-treated and TEPA-grafted GnP on the flexural strength of AS4-12k-UVO carbon fiber composites with aromatic and aliphatic fiber sizing (top: longitudinal, adjusted V_f:65%; bottom: transverse, as-measured)

The longitudinal strengths of all aromatic GnP sized composites are statistically similar and about +12% higher than the neat aromatic sized fiber composite. For the transverse flexural strength, which is dominated by fiber/matrix adhesion, the 0.5wt% GnP M5HT composite shows statistically similar strength to the neat DGEBA sized

composite. This may be further evidence of the GnP/matrix bonding of the heat-treated M5 needing further improvement. The 0.1wt% and 0.5wt% GnP M5HT-3R-TEPA both show higher transverse flexural strength by +22% and +26% respectively, compared to the neat DGEBA composite. Better GnP/matrix adhesion at the fiber/matrix interphase, allowing better stress transfer compared to the GnP M5HT may be the cause. The 0.5wt% GnP M5HT-3R-TEPA in conjunction with the aliphatic fibersizing appears to reduce the transverse flexural strength by about -11% compared to the PDGE sized composite. Based on the lower modulus values shown in Figure 6.6, this could again be a case of reduced diffusion of the aliphatic fibersizing away from the fiber surface. Since there is an amine content on the GnP, similar argumentation to Chapter 5 may apply where an aliphatically toughened matrix in conjunction with aliphatic fibersizing showed reductions in fiber/matrix bonding dominated properties.

The addition of GnP to the fibersizing has a positive influence on the Mode I fracture toughness for the aromatic sized composite as shown in Figure 6.9:

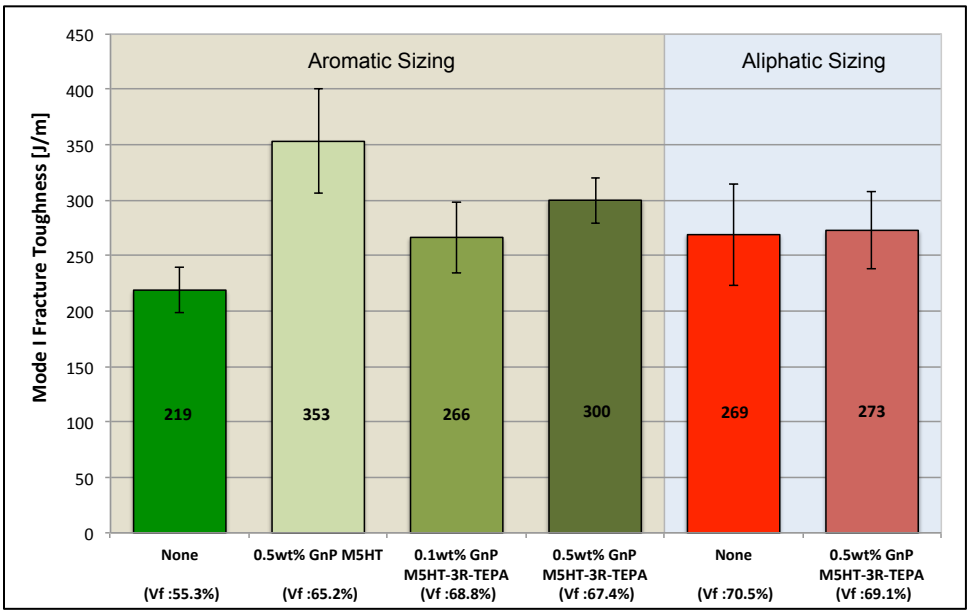

Figure 6.9: Influence of heat treated and TEPA-grafted GnP on the Mode I fracture toughness of AS4-12k-UVO carbon fiber composites with aromatic and aliphatic fiber sizing

The 0.5wt% GnP M5HT shows to largest increase in fracture toughness over the neat DGEBA sized composite. (+61%) The large platelet diameter allows the GnP to be a good crack deflection agent. This had been discussed in Chapter 5.4.3, where 3wt% GnP M5HT showed a +31% increase in fracture toughness over the neat DGEBA/mPDA matrix. The 0.1wt% GnP M5HT-3R-TEPA showed a +22% increase over the neat DGEBA sized composite but the scatter in the data makes for overlapping error. A statistically significant increase of +37% is seen with the 0.5wt% GnP M5HT-3R-TEPA. At the same GnP concentration, the TEPA-grafted GnP shows a smaller increase in fracture toughness compared to the heat-treated only GnP. This is again consistent with the results seen in the base DGEBA/mPDA matrix (Chapter 5.4.3) where the M5HT showed a +31% increase compared to the +22% increase of the GnP M5HT-3R-TEPA. The additional processing of the GnP in the 3-roll mill may have reduced the platelet size, reducing the effectiveness as a crack deflection agent. There

does appear to be an influence of the GnP concentration on the fracture toughness increase as is when comparing the 0.1 and 0.5wt% GnP M5HT-3R-TEPA composite results at +22% and +37% over neat DGEBA sized composite respectively. In conjunction with the aliphatic fibersizing, the 0.5wt% GnP M5HT-3R-TEPA does not show any increase in fracture toughness. As discussed above, the additional amine groups present in the TEPA-grafted GnP may be reacting with the aliphatic epoxy and leading to additional vitrification of the sizing. The toughening effect of the GnP may be offsetting the reduction in fracture toughness from the more compliant interphase, leading to equal fracture toughness.

Fracture surfaces of the Mode I fracture toughness samples as observed by SEM are shown in Figure 6.10 for aromatic sizing. The neat DGEBA sized composite shows indications of fiber/matrix bonding. With the addition of 0.5wt% heat-treated GnP M5 (M5HT) the fracture surface roughness increases, indicating crack deflection. Significantly more matrix material is present around the fibers indicating that the GnP is deflecting the propagating cracks away from the fiber/matrix interphase into the matrix. At higher magnification, GnP at the fiber/matrix interphase is clearly visible both on the exposed fracture surface and in-between fibers. At 0.1wt% TEPA-grafted GnP (M5HT-3R-TEPA), the fracture surface shows more roughness than the neat DGEBA composite but not as much as with the higher concentrations of GnP. Increasing the GnP M5HT-3R-TEPA concentration to 0.5wt%, the fracture surface roughness visibly increases over 0.1wt% GnP, indicating further crack deflection with increased GnP presence. There is little visual difference between the fracture surfaces of the heat-treated and the TEPA-grafted GnP composites at 0.5wt% concentration. This mirrors

the result from the DGEBA/mPDA systems discussed in Chapter 5, where the best increase in fracture toughness was seen with heat-treated GnP, compared to TEPA-grafted GnP. At higher magnification the exposed basal planes of the GnP embedded in the fracture surface are clean, without any indication of residual matrix material attached. As had been discussed in Chapter 5, the GnP/matrix bonding predominantly takes place around the platelet edges. As a crack propagates around the GnP, the GnP is sheared apart between the layers, which are only held together by π-π bonding.

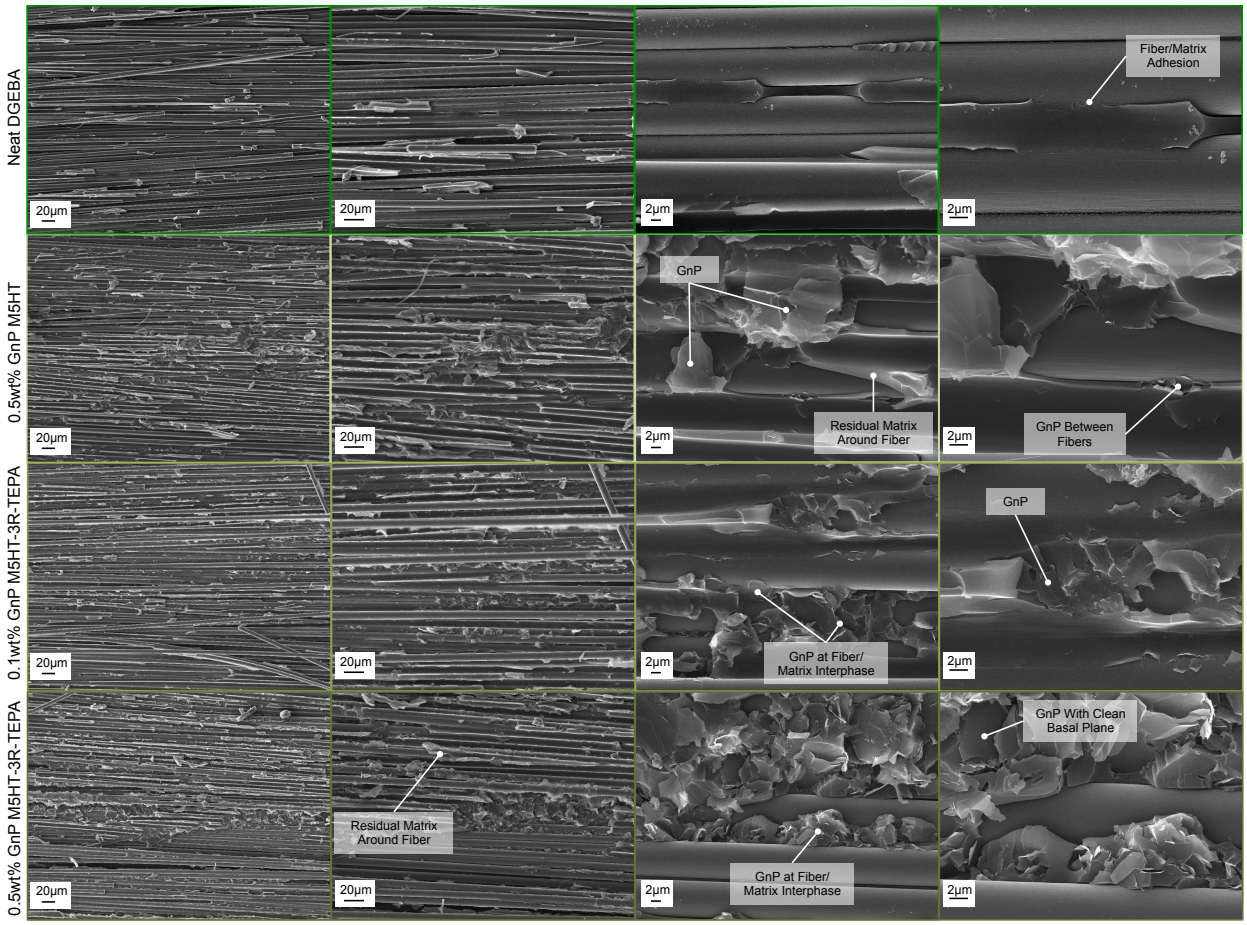

Figure 6.10: Fracture surface morphology of Mode I fracture toughness samples with aromatic epoxy sizing: neat DGEBA (top), 0.5wt% GnP M5HT (top, middle), 0.1wt% GnP M5HT-3R-TEPA (bottom, middle), 0.5wt% GnP M5HT-3R-TEPA (bottom). Direction of fracture is left to right across the image

Figure 6.11 shows the facture surface morphology of Mode I fracture toughness samples with aliphatic epoxy fibersizing. The changes in fracture surface morphology are analog to those seen with the aromatic fibersizing discussed above. The neat PDGE sized composite shows indications of good fiber/matrix adhesion. The addition of 0.5wt% GnP M5HT-3R-TEPA significantly increases the roughness of the fracture surface, indicating crack deflection from the ridged GnP. Visible GnP embedded in the fracture surface also exhibits clean basal planes, implying that there has been separation between graphene layers in the GnP stack.

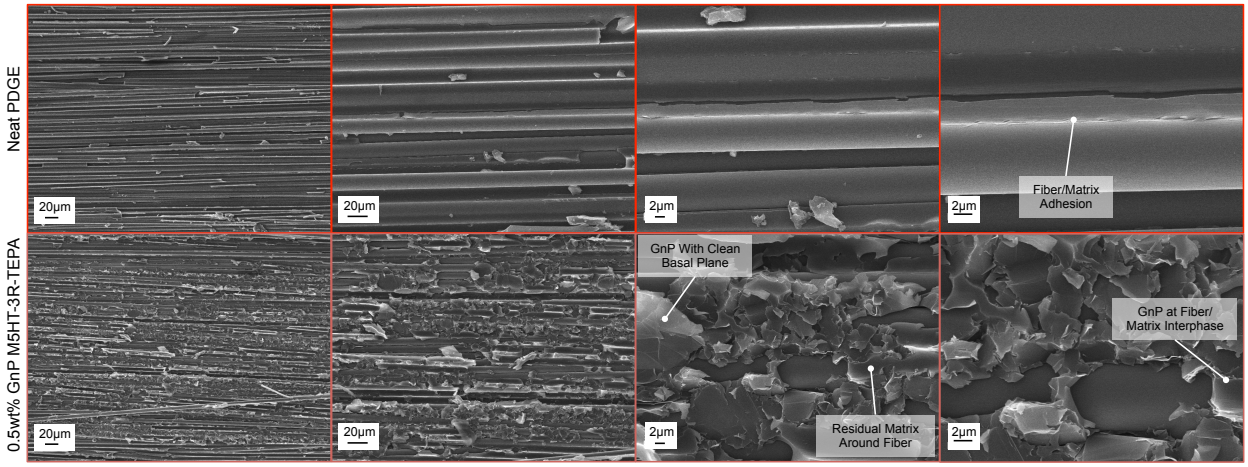

Figure 6.11: Fracture surface morphology of Mode I fracture toughness samples with aliphatic epoxy sizing: neat PDGE (top), 0.5wt% GnP M5HT-3R-TEPA (bottom). Direction of fracture is left to right across the image

The impact of adding GnP to the fibersizing on the glass transition temperature (Tg) is shown in Figure 6.12. All changes in Tg appear to be minor (<2%):

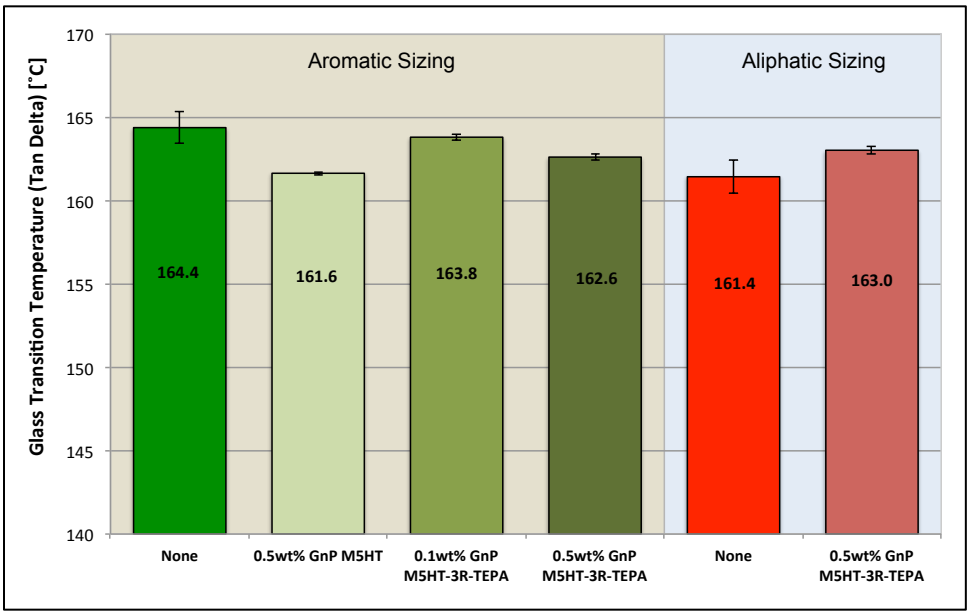

Figure 6.12: Influence of heat-treated and TEPA-grafted GnP on the glass transition temperature of AS4-12k-UVO carbon fiber composites with aromatic and aliphatic fiber sizing as determined from the maximum of the Tan δ peak from DMA (1 Hz frequency, 20μm amplitude)

The addition of 0.5wt% GnP M5HT shows a slight decrease (-1.7%) in T_g compared to the neat DGEBA composite. Poor GnP/matrix adhesion may be the cause. Both the 0.1wt% and 0.5wt% GnP M5HT-3R-TEPA composites show similar or only slightly lower T_g of 0.3% and 1.1%, respectively. The improved GnP/matrix adhesion of the edge grafted TEPA may be the root cause. The 0.5wt% GnP M5HT-3R-TEPA with aliphatic sizing has a slightly higher T_g (+1.4%) compared to the aliphatically sized composite.

The Tan δ curves from the DMA measurements of the aromatic and aliphatic sized composites are shown in Figure 6.13. The height of the Tan δ peaks as the average of three measurements is shown in Figure 6.14:

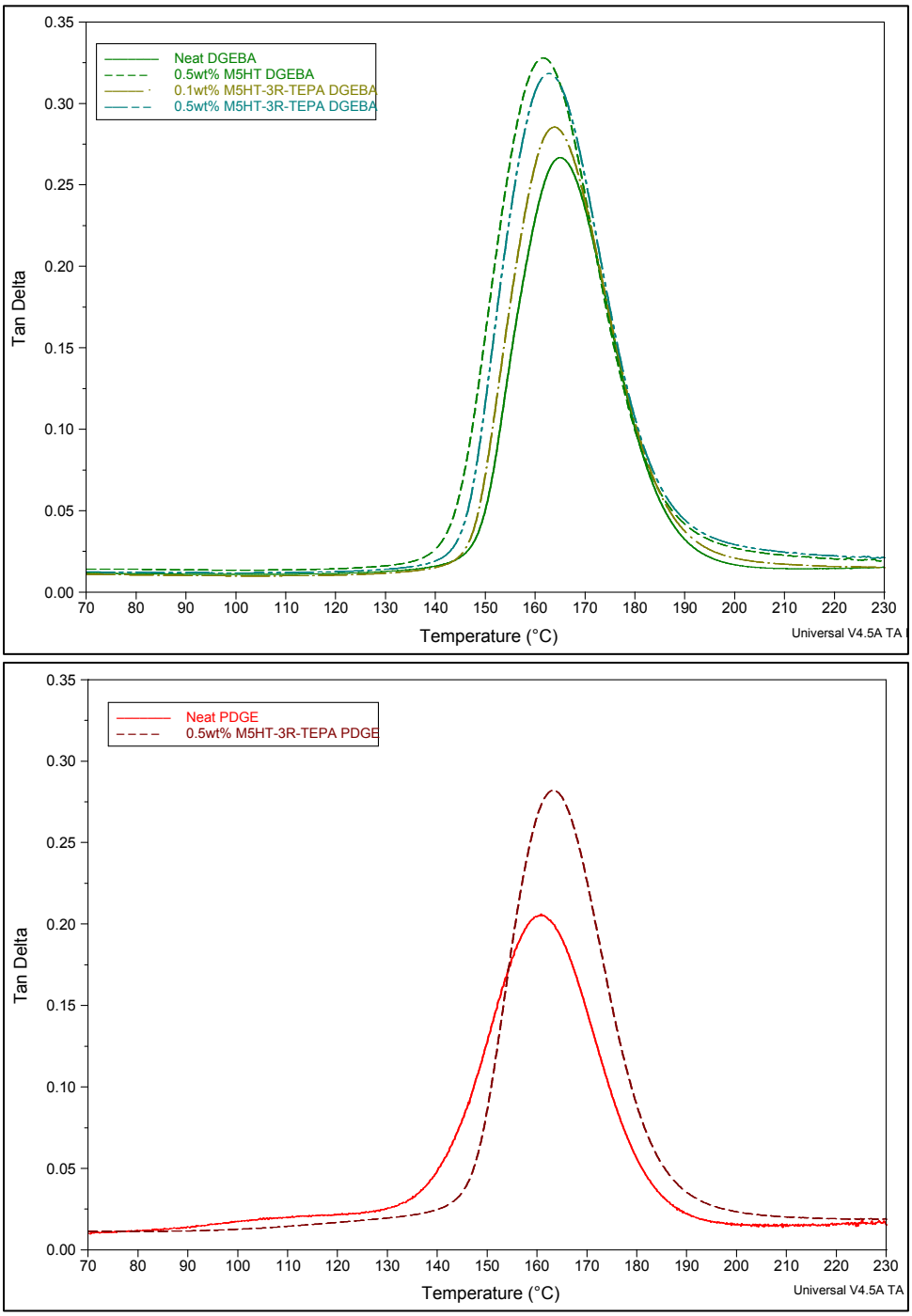

Figure 6.13: Tan δ signal of AS4-12k-UVO carbon fiber composites with heat-treated and TEPA-grafted GnP in aromatic (top) and aliphatic (bottom) fiber sizing as determined by DMA (1 Hz frequency, 20μm amplitude)

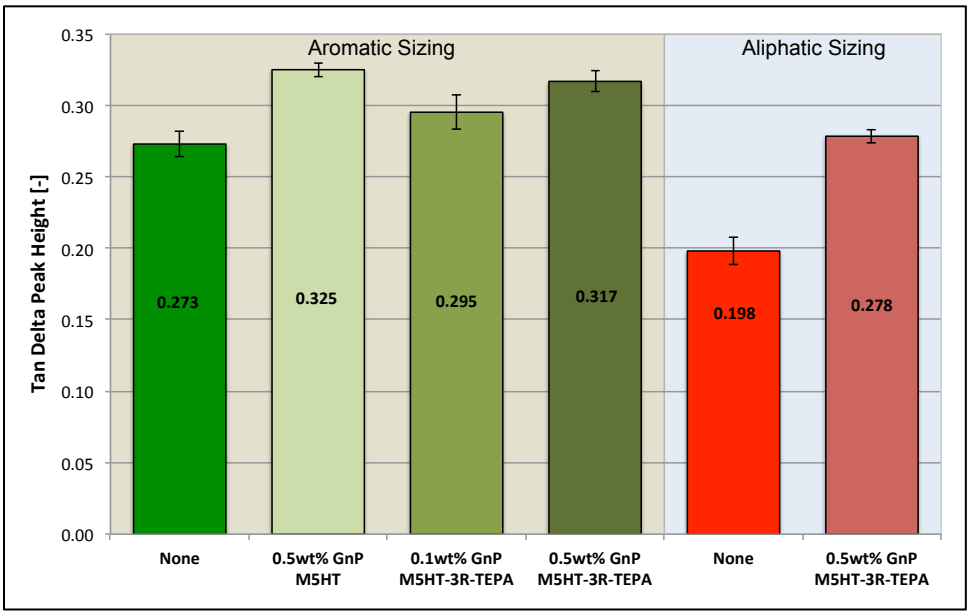

Figure 6.14: Influence of heat-treated and TEPA-grafted GnP on the Tan d peak height of AS4-12k-UVO carbon fiber composites with aromatic and aliphatic fiber sizing as determined from the average of three DMA measurements (1 Hz frequency, 20μm amplitude)

The aromatic sized composites show a single peak that increases in peak height with the addition of GnP. The peak height increases with GnP M5HT-3R-TEPA concentration. Since the Tan δ function is the ratio of the loss to the storage modulus, the implication may be an increased energy loss from the increasing number of GnP/matrix interfaces from 0.1wt% to 0.5wt% GnP. The 0.5wt% GnP M5HT appears to have a slightly higher peak height than the GnP M5HT-3R-TEPA composite. However, when the average of three measurements is taken, the peak height for both is within the scatter of the data (Figure 6.14). The aliphatically sized fiber composite shows the lowest peak height, which indicates the most elastic response of all the composites. Based on the low modulus of the aliphatic epoxy, this is to be expected. As discussed in Chapter 4, the Tan δ function also shows the formation of a shoulder in the lower temperature area (100-130˚C). The addition of GnP to the fibersizing significantly

increases the Tan δ peak height, indicating an interphase with more GnP/matrix interfaces. The shoulder, that may indicate the beginning of a second, lower Tg phase forming within the composite, is still present with the addition of GnP. However, it is not as pronounced with the GnP as with the neat epoxy fibersizing.

6.5 Conclusion

The addition of GnP to the fibersizing has shown good potential of enhancing the Mode I fracture toughness. Based on the good crack deflection, the heat-treated GnP (M5HT) shows the highest increase in fracture toughness (+60%), which mirrors the previously results discussed in Chapter 5 from GnP toughening of the base matrix. With the same 0.5wt% GnP concentration, TEPA-grafted GnP (M5HT-3R-TEPA) also improved the fracture toughness but to a lesser extent (+37%), probably based on the reduced platelet size from processing. For the TEPA-grafted GnP, a definite dependence of the fracture toughness on the GnP concentration was seen, with an increase in Mode I fracture toughness from 0.1wt% to 0.5wt%. For the aliphatic epoxy sizing, the 0.5wt% addition of TEPA-grafted GnP did not improve the fracture toughness.

The addition of GnP to the aromatic fibersizing did not appear to have a significant impact on the flexural properties of the composite. Both longitudinal and transverse flexural properties were statistically the same or better. For aliphatic fibersizing, the addition of GnP reduced all the flexural properties by -10% to -15%. This reduction is caused by higher concentration of aliphatic epoxy at the fiber surface, resulting in a more compliant interphase.

The dispersion and agglomeration of the GnP as seen in the composites cross-sections indicates that more effort needs to be put into improving the dispersion and exfoliation of the GnP when applying it to fibersizing of AS4-12k-UVO composites.

APPENDIX

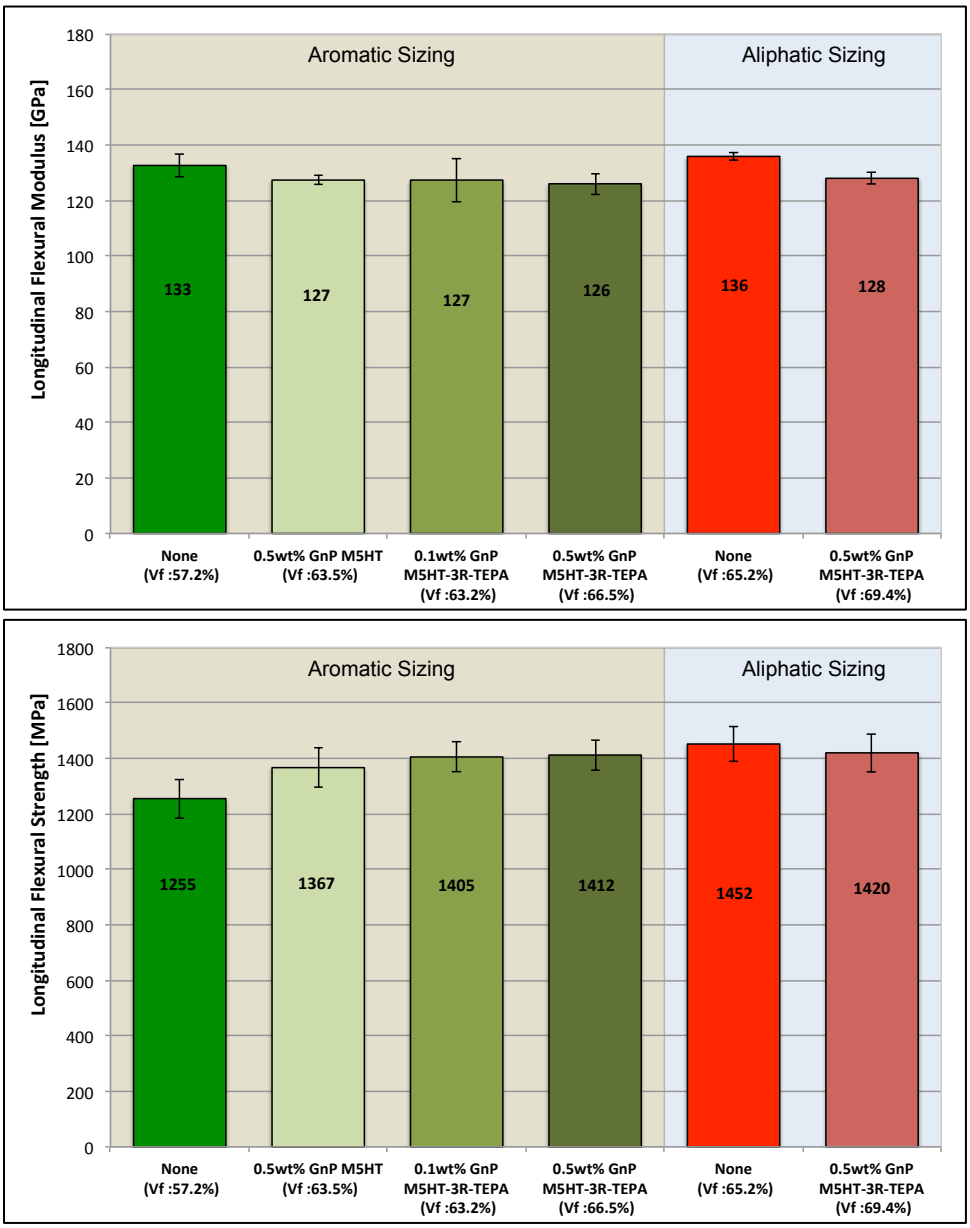

Figure 6.15: Longitudinal flexural composite properties as-measured; modulus (top), strength (bottom)

BIBLIOGRAPHY

BIBLIOGRAPHY

[1] P. Mohan, “A Critical Review: The Modification, Properties, and Applications of Epoxy Resins,” *Polymer-Plastics Technology and Engineering*, vol. 52, no. 2, pp. 107–125, 2013.

[2] R. Bagheri, B. T. Marouf, and R. A. Pearson, “Rubber-toughened epoxies: a critical review,” *Journal of Macromolecular …*, 2009.

[3] F. G. Garcia, B. G. Soares, V. J. R. R. Pita, R. Sánchez, and J. Rieumont, “Mechanical properties of epoxy networks based on DGEBA and aliphatic amines,” *J. Appl. Polym. Sci.*, vol. 106, no. 3, pp. 2047–2055, 2007.

[4] C. H. Zhang, H. G. Wei, Y. Y. Liu, H. F. Tan, and Z. Guo, “Enhanced toughness and shape memory behaviors of toughed epoxy resin,” *High Performance Polymers*, vol. 24, no. 8, pp. 702–709, Nov. 2012.

[5] T. Misaki, T. Hirohata, M. Yoshii, and T. Hamasaki, “Properties of networks obtained by internal plasticization of epoxy resin with aromatic and aliphatic glycidyl compounds,” *J. Appl. Polym. Sci.*, vol. 37, no. 9, pp. 2617–2625, 1989.

[6] N. Domun, H. Hadavinia, T. Zhang, T. Sainsbury, G. H. Liaghat, and S. Vahid, “Improving the fracture toughness and the strength of epoxy using nanomaterials – a review of the current status,” *Nanoscale*, vol. 7, no. 23, pp. 10294–10329, 2015.

[7] A. Dorigato, S. Morandi, and A. Pegoretti, “Effect of nanoclay addition on the fiber/matrix adhesion in epoxy/glass composites,” *Journal of Composite Materials*, vol. 46, no. 12, pp. 1439–1451, May 2012.

[8] W. Qin, F. Vautard, P. Askeland, J. Yu, and L. T. Drzal, “Incorporation of silicon dioxide nanoparticles at the carbon fiber-epoxy matrix interphase and its effect on composite mechanical properties,” *Polym. Compos.*, pp. n/a–n/a, Jul. 2015.

[9] Y. Zhu, C. E. Bakis, and J. H. Adair, “Effects of carbon nanofiller functionalization and distribution on interlaminar fracture toughness of multi-scale reinforced polymer composites,” *Carbon*, vol. 50, no. 3, pp. 1316–1331, Mar. 2012.

[10] D. C. Davis and B. D. Whelan, “An experimental study of interlaminar shear fracture toughness of a nanotube reinforced composite,” *Composites Part B*, vol. 42, no. 1, pp. 105–116, Jan. 2011.

[11] D. C. Davis, J. W. Wilkerson, J. Zhu, and D. O. O. Ayewah, “Improvements in mechanical properties of a carbon fiber epoxy composite using nanotube science and technology,” *Composite Structures*, vol. 92, no. 11, pp. 2653–2662, Oct. 2010.

[12] W. Qin, F. Vautard, L. T. Drzal, and J. Yu, “Modifying the carbon fiber–epoxy matrix interphase with graphite nanoplatelets,” *Polym. Compos.*, 2014.

[13] N. T. Kamar, M. M. Hossain, A. Khomenko, M. Haq, L. T. Drzal, and A. Loos, “Composites: Part A,” *Composites Part A*, vol. 70, no. C, pp. 82–92, Mar. 2015.

[14] R. J. Zaldivar, J. P. Nokes, and H. I. Kim, “The effect of surface treatment on graphite nanoplatelets used in fiber reinforced composites,” *J. Appl. Polym. Sci.*, pp. n/a–n/a, Oct. 2013.

[15] F. Yavari, M. A. Rafiee, J. Rafiee, Z.-Z. Yu, and N. Koratkar, “Dramatic increase in fatigue life in hierarchical graphene composites.,” *ACS Appl. Mater. Interfaces*, vol. 2, no. 10, pp. 2738–2743, Oct. 2010.

[16] Q. Meng, J. Jin, R. Wang, H.-C. Kuan, J. Ma, N. Kawashima, A. Michelmore, S. Zhu, and C. H. Wang, “Processable 3-nm thick graphene platelets of high electrical conductivity and their epoxy composites,” *Nanotechnology*, vol. 25, no. 12, p. 125707, Feb. 2014.

[17] K. Kalaitzidou, H. Fukushima, and L. T. Drzal, “Multifunctional polypropylene composites produced by incorporation of exfoliated graphite nanoplatelets,” *Carbon*, vol. 45, no. 7, pp. 1446–1452, Jun. 2007.

[18] H. L. Cox, “The elasticity and strength of paper and other fibrous materials,” *British Journal of Applied Physics*, vol. 3, no. 3, pp. 72–79, Mar. 1952.

[19] P. S. Theocaris, *The Mesophase Concept in Composites*, 1st ed. New York: Springer Science & Business Media, 1987.

[20] T. F. Cooke, “High Performance Fiber Composites with Special Emphasis on the

Interface A Review of the Literature," *Journal of Polymer Engineering*, vol. 7, no. 3, pp. 197–254, 1987.

[21] Handbook-MIL-HDBK, *17-1F: Composite Materials Handbook, Volume 1- Polymer Matrix Composites: Guidelines for Characterization of Structural Materials*. Department of Defence, 2002.

[22] K. Friedrich, S. Fakirov, and Z. Zhang, *Polymer Composites*. Springer, 2005.

Chapter 7: Summary and Future Work

7.1 Summary

The research discussed in this dissertation outlines methods of toughening aromatic epoxy polymers and aromatic epoxy based carbon fiber-reinforced composites without detrimentally affecting other static-mechanical properties. Several different areas of the composite were enhanced to toughen the overall composite (neat matrix, fiber sizing, composite with modified matrix and composite with modified matrix and modified sizing). All materials and chemicals used in the dissertation are commodity chemicals and none of the production methods needed to be significantly adjusted.

Chapter 2 discussed toughening the DGEBA/mPDA system using di- and tri-functional aliphatic epoxy. 1wt% aliphatic copolymer enhanced the notched Izod impact toughness by 60% for the di-functional and 80% for the tri-functional aliphatic. No reductions in flexural properties or glass transition temperature were seen at 1wt% aliphatic.

Chapter 3 discussed toughening epoxy based carbon fiber-reinforced composites by fiber surface treatment and fiber sizing. UV-Ozone treatment of the carbon fiber enhanced the Mode I fracture toughness by 23% over the as-received fiber by increasing the amount of surface oxygen groups. Adding an aromatic fiber sizing to the UVO-treated fiber further enhances the Mode I fracture toughness by 50% over the as-received fiber. An aliphatic fiber sizing increases the fracture toughness by 84% over the as-received fiber by enhancing the strain-to-failure and increasing the toughness at the fiber/matrix interphase as indicated by enhanced transverse flexural strength. All

improvements in fracture toughness were achieved without reducing other static-mechanical properties.

Chapter 4 illuminated combining the 1wt% di-functional aliphatic matrix toughening discussed in Chapter 2, with the fiber surface treatment and fiber sizing discussed in Chapter 3. The 1wt% aliphatic toughening of the matrix was shown to transfer to the high fiber volume fraction composite, without detrimentally affecting the static-mechanical properties. The enhancement in Mode I fracture toughness was most effective (+35% compared to the neat matrix composite) in low toughness system where the fracture toughness of the matrix plays a more important roll. With improvements to the fiber/matrix bonding, UVO fiber surface treatment and UVO-treatment with aromatic fiber sizing, the enhancement of the Mode I fracture Toughness was lower (+13% and +17% compared to the neat matrix composite, respectively). In conjunction with the aliphatic fiber sizing, the matrix toughening reduced the composite fracture toughness by -30%. This reduction is hypothesized to be due to reduced diffusion of the aliphatic sizing away from the fiber/matrix interphase, leading to a more compliant and lower strength interphase.

Toughening of the DGEBA/mPDA system using graphene nanoplatelets (GnP) was the topic of Chapter 5. Three different grades of GnP were investigated at a concentration of 3wt%. The GnP was also modified by grafting tetraethylenepentamine (TEPA) to the edges of the GnP in order to improve the GnP/matrix adhesion. Since reactive groups are predominantly present around the edges of the GnP, the amount of TEPA grafted to the GnP was found to be linearly dependent on the edge area of the GnP. All GnP grades reduced the notched Izod impact strength, as the stiff platelet

appear to act as stress concentrators in the high loading rate event. Each grade of GnP was found to improve a different material property, which needs to be considered for each application.

GnP C750, with the largest edge area and smallest aspect ratio, was found to enhance the flexural properties (+1 to +5%) but have no impact on the fracture toughness. TEPA-grafting improved the filler/matrix adhesion as indicated by improved flexural strength.

GnP M5, with a significantly higher aspect ratio, improved fracture toughness by +22 to +31%. The additional processing of the GnP via 3-roll mill reduced the enhancement of fracture toughness, probably due to a reduction in platelet diameter and aspect ratio. Reductions in flexural strength were almost negated by additional reaction of the TEPA-grafted M5 with DGEBA. TEPA-grafted M5 was selected for sizing AS4-12k carbon fibers due to the combination of improvements in fracture toughness and the 5μm platelet diameter being compatible with the 7μm diameter fiber.

GnP M25, with the largest aspect ratio, showed the largest enhancements in fracture toughness of +32% to +41%. Increases in flexural modulus were in the range of +6% to +9% but reductions of -15% were seen in flexural strength. TEPA-grafting did not significantly improve the mechanical properties which is probably due to the small edge area available for TEPA-grafting.

Chapter 6 showed the ability of a TEPA-grafted GnP M5 based fiber sizing to improve carbon fiber-reinforced composite Mode I fracture toughness at low GnP concentrations. The highest enhancement of +61% was achieved with 0.5wt% heat-treated GnP due to the GnP ability for crack deflection. 0.1wt% and 0.5wt% TEPA-

grafted GnP showed +22% and +37% enhancements in fracture toughness, respectively in addition to improving the transverse flexural strength by +8 to +10%. With the aliphatic fiber sizing, a 0.5wt% addition of TEPA-grafted GnP did change the fracture toughness and showed a -17% reduction in transverse flexural strength. These tends are probably due to enrichment of aliphatic epoxy at the fiber surface, leading to a lower strength and more compliant interphase. Other static-mechanical properties were fairly constant.

7.2 Future Work

7.2.1 Base Matrix Toughening

Toughening of the aromatic matrix with 1wt% di- and tri-functional aliphatic epoxy copolymer was shown to be successful with reducing other material properties. A more in-depth investigation of the network topology at a concentration range below 1wt% may be informative in developing a more detailed understanding of the system behavior.

Illuminating the toughening behavior of the system using an aliphatic amine could also vastly enhance the understanding of the toughening mechanism. A linear aliphatic curing agent added to the same aliphatic content could yield insight into toughening using aliphatic epoxies vs aliphatic amines.

7.2.2 Fiber Surface Treatment and Fibersizing

Measuring the diffusion of the fiber sizing away from the fiber surface during composite consolidation would be a significant contribution to the field of composites. One approach to this issue could be using scanning probe microscopy to probe the

mechanical properties radially around the fiber surface. The magnitude of the changes in mechanical properties (increases in modulus) moving away from the fiber surface could be used to infer the diffusion distance of the sizing. This approach should be particularly useful for the aliphatic fiber sizing, where there are very large differences in the modulus of the epoxy materials. A second approach would be to use a DGEBA epoxy for the fiber sizing that is marked with a specific atomic group that would only appear in conjunction with that molecule. A brominated DGEBA could be used and the concentration profile of bromine at the fiber/matrix interphase could be mapped using EDS or XPS techniques. Given a robust experimental design, a model of the sizing diffusion could also be developed.

The potential of using the tri-functional aliphatic epoxy for fiber sizing is an area that warrants more investigation. Since the tri-functional epoxy copolymer showed higher potential for enhancements of impact properties in the base matrix, better improvements of fracture toughness could also be expected.

7.2.3 Composite Matrix Toughening

The toughening of the composite matrix with 1wt% di-functional aliphatic copolymer was shown to be most effective at low system toughness. A more pronounced toughening effect could be possible at slightly higher aliphatic copolymer concentrations such as 2 to 5wt%. As is the central idea of this research work, the toughening of the matrix must be balanced against the other composite properties.

As a better understanding of the diffusion of the fiber sizing away from the fiber surface is developed, the issue of the reduced mechanical properties when an aliphatic

fiber sizing is combined with an aliphatically toughened matrix should be revisited. Looking at combining the di-functional aliphatic fiber sizing with a different aliphatic copolymer (tri-functional) in the matrix may yield some insight into the toughening behavior.

The potential of the tri-functional aliphatic copolymer should also be explored as it showed very good improvements of the base matrix material.

7.2.4 Base Matrix Toughening With Amine-Grafted GnP

Grafting TEPA to the GnP was demonstrated as a straight-forward approach leading to improved filler/matrix adhesion. The main limitation was the availability of reactive groups to react with the TEPA, which were only present at the platelet edges. Further reactive sites could be created by oxidation of the GnP with acid prior to reaction with TEPA. The amount of oxidation needs to be controlled in order to find a balance between preserving the GnP structure and mechanical strength and creation of additional reactive surface groups.

An additional improvement could be to increase the length of the poly-amine used for grafting to the GnP. A longer poly-amine such as polyetheramine, with 3 primary amines, (Jeffamine T-5000) or branched polyethylenimine (PEI), with many amine groups could reduce the re-agglomeration of the graphene platelets due to the steric hindrance of the large molecule grafted to the GnP.

A combination of a matrix toughened with low concentrations of aliphatically copolymer with GnP nano-filler could yield a superior toughened system. The improved

energy absorption of the aliphatically toughened matrix may offset some of the reductions seen by the addition of GnP into the matrix for high loading rate event.

7.2.5 Toughening of Carbon-Fiber Reinforced Composite With Amine-Grafted GnP Based Fibersizing

The two greatest improvements necessary for this research are the dispersion and the functionalization of GnP. For the dispersion, the optimization of the solvent used to size the carbon fiber tow with the GnP will have the greatest impact on the sizing quality. The solvent will need to be very good at dispersing and reducing the re-agglomeration of the GnP. The solvent will also have to be easily removable from the fiber tow after sizing and not introduce any unwanted side reactions with the DGEBA/mPDA system. Depending on the functionalization of the GnP, the choice of solvent may be different.

Functionalizing the GnP can serve two purposes: first, the added functional groups should improve the filler/matrix adhesion by covalently bonding between the GnP and the matrix; secondly, functionalization can improve the exfoliation of the GnP, if the functional groups are located on the basal plane. Controlled disruption of the basal plane could enhance the amount of functional groups available for reaction, without significantly reducing mechanical strength.